TECHNICAL REPORT STANDARD TITLE PAGE

1. Report No.	2. Government Accession No.	3. Recipient's Catalog No.
FHWA/TX-87/70+437-3F		

4. Title and Subtitle	5. Report Date
APPLICATIONS AND LIMITATIONS OF THE SPECTRAL-ANALYSIS-OF-SURFACE-WAVES METHOD	November 1986
	6. Performing Organization Code

7. Author(s)	8. Performing Organization Report No.
Jiun-Chyuan Sheu, Kenneth H. Stokoe, II, Jose M. Roesset, and W. Ronald Hudson	Research Report 437-3F

9. Performing Organization Name and Address	10. Work Unit No.
Center for Transportation Research The University of Texas at Austin Austin, Texas 78712-1075	11. Contract or Grant No. Research Study 3-8-85-437
	13. Type of Report and Period Covered
12. Sponsoring Agency Name and Address Texas State Department of Highways and Public Transportation; Transportation Planning Division P. O. Box 5051 Austin, Texas 78763-5051	Final
	14. Sponsoring Agency Code

15. Supplementary Notes

Study conducted in cooperation with the U. S. Department of Transportation, Federal Highway Administration. Research Study Title: "Utilization of Surface Wave System for Measuring Moduli of Pavements"

16. Abstract

The Spectral-Analysis-of-Surface-Waves (SASW) method is an in situ seismic method for nondestructively determining the modulus profiles of geotechnical, pavement, and structural systems. This method requires no boreholes and is performed entirely from the surface of the system being tested. Measurements are made at strains below 0.001 percent where elastic properties of the materials are independent of strain amplitude. The versatility and relatively easy deployment of this method represent two of the strengths of the method. By generating and measuring surface waves in the field, a dispersion curve, a plot of surface wave velocity versus wavelength, is constructed. This dispersion curve is then inverted in the office. Inversion is an analytical process for reconstructing the shear wave velocity profile from the field dispersion curve. Layering and the Young's modulus of each layer are readily obtained from the shear wave velocity profile.

Due to the complex nature of surface wave propagation, a half space with infinite lateral extent was assumed in the past for most theoretical analyses. As a result, the existence of reflected waves from any reflecting boundary was neglected. To understand the impact from the existence of reflecting boundaries in the real world such as joints or edges in a pavement system, a simplified model was developed. Field experiments were then performed to verify this model. Based on the results from both model and field studies, remedial measures for minimizing the effects of reflections in SASW testing are recommended. Several case studies are presented to illustrate the versatility of the SASW method, and a MASSCOMP minicomputer was introduced in an attempt to automate the SASW method.

17. Key Words	18. Distribution Statement
spectral analysis of surface waves, SASW, seismic method, modulus profiles, dispersion curve, inversion, case studies	No restrictions. This document is available to the public through the National Technical Information Service, Springfield, Virginia 22161.

19. Security Classif. (of this report)	20. Security Classif. (of this page)	21. No. of Pages	22. Price
Unclassified	Unclassified	306	

Form DOT F 1700.7 (8-69)

APPLICATIONS AND LIMITATIONS OF THE SPECTRAL-ANALYSIS-OF-SURFACE-WAVES METHOD

by
Jiun-Chyuan Sheu
Kenneth H. Stokoe, II
Jose M. Roesset
W. Ronald Hudson

Research Report Number 437-3F

Utilization of Surface Wave System for
Measuring Moduli of Pavements
Research Project 3-8-85-437

conducted for

Texas State Department of Highways
and Public Transportation

in cooperation with the
U.S. Department of Transportation
Federal Highway Administration

by the

CENTER FOR TRANSPORTATION RESEARCH
BUREAU OF ENGINEERING RESEARCH
THE UNIVERISTY OF TEXAS AT AUSTIN

November 1986

The contents of this report reflect the views of the authors, who are responsible for the facts and the accuracy of the data presented herein. The contents do not necessarily reflect the official views of policies of the Federal Highway Administration. This report does not constitute a standard, specification, or regulation.

There was no invention or discovery conceived or first actually reduced to practice in the course of or under this contract, including any art, method, process, machine, manufacture, design or composition of matter, or any new and useful improvement thereof, or any variety of plant which is or may be patentable under the patent laws of the United States of America or any foreign country.

PREFACE

This report is the third report in a series of five reports on the Spectral-Analysis-of-Surface-Waves (SASW) method. The first report is published under Research Report 368-1F and is a detailed description of the practical aspects of the SASW method. The second report is published under Research Report 437-2 and is a detailed discussion of the theoretical aspects of the SASW method. The fourth and fifth reports will be published under Research Project 1123. The fourth report will present a new analytical formulation for surface waves in layered systems which accounts for all wave types. The fifth report will consist of a manual for an interactive computer program called INVERT1. This program is essential for determining the stiffnesses of the different layers from the in situ data. In this volume, the results of analytical and experimental investigations of the most important variables affecting SASW testing are presented. These variables include: source and receiver types, source/receiver configurations, natural frequencies of the coupled receiver-pavement system, body and surface wave reflections from discontinuities in the pavement system, and impact stress levels used to generate the surface waves.

The division of the reports on Projects 368, 437 and 1123 was necessary so that readers with different levels of knowledge and interest could easily access the required material. This division of reports also results from a natural development of the SASW method. This report has been prepared in a manner that permits variables involved in the SASW method to be understood without referring to the other reports.

The authors extend their sincere gratitute to personnel of the Texas Department of Highways and Public Transportation for their continuous support and enthusiasm throughout the course of this study.

Jiun-Chyuan Sheu
Kenneth H. Stokoe, II
Jose M. Roesset
W. Ronald Hudson

November 1986

LIST OF REPORTS

Report No. 437-1, "Dynamic Interpretation of Dynaflect and Falling Weight Deflectometer Tests," by Ko-Young Shao, J.M. Roesset, and K.H. Stokoe, II, presents the results of analytical studies of the dynamic effects on measurements made with the Dynaflect and Falling Weight Deflectometer methods, based on the consideration of wave propagation including body waves (P- and S-waves) and Rayleigh (surface) waves.

Report No. 437-2, "In Situ Determination of Elastic Moduli of Pavement Systems by Spectral-Analysis-of-Surface-Waves Method (Theoretical Aspects)," by Soheil Nazarian and K.H. Stokoe, II, presents the pertinent theoretical aspects of wave propagation in a layered system (such as a pavement system) as they apply to the SASW method.

Report No. 437-3F, "Applications and Limitations of the Spectral-Analysis-Surface-Waves Method," by Jiun-Chyuan Sheu, Kenneth H. Stokoe, II, Jose M. Roesset and W. Ronald Hudson presents the results of experimental and analytical studies of variables, such as source and receiver types, source/receiver configurations, natural frequencies in the measurement system, and body and surface wave reflections, that affect modulus measurements by the Spectral-Analysis-of-Surface-Waves (SASW) Method.

ABSTRACT

The Spectral-Analysis-of-Surface-Waves (SASW) method is an in situ seismic method for nondestructively determining the modulus profiles of geotechnical, pavement, and structural systems. This method requires no boreholes and is performed entirely from the surface of the system being tested. Measurements are made at strains below 0.001 percent where elastic properties of the materials are independent of strain amplitude. The versatility and relatively easy deployment of this method represent two of the strengths of the method. By generating and measuring surface waves in the field, a dispersion curve, a plot of surface wave velocity versus wavelength, is constructed. This dispersion curve is then inverted in the office. Inversion is an analytical process for reconstructing the shear wave velocity profile from the field dispersion curve. Layering and the Young's modulus of each layer are readily obtained from the shear wave velocity profile.

Due to the complex nature of surface wave propagation, a half space with infinite lateral extent was assumed in the past for most theoretical analyses. As a result, the existence of reflected waves from any reflecting boundary were neglected. To understand the impact from the existence of reflecting boundaries in the real world such as joints or edges in a pavement system, a simplified model was developed. Field experiments were then performed to verify this model. Based on the results from both model and field studies, remedial measures for minimizing the effects of reflections in SASW testing are recommended.

A comprehensive investigation of variables affecting modulus measurements in the field by the SASW method was conducted. Variables such as receiver types and combinations, impact stress level, natural frequency of the receiver and resonant frequency of the coupled receiver/pavement system were studied experimentally. A source capable of generating high-frequency impulses, the "V" meter, was employed. With this source, measurements of near-surface properties at pavement sites have been greatly simplified and a "quick and easy" method for accessing the material properties in the near-surface region has been developed.

Several case studies are presented to illustrate the versatility of the SASW method. A MASSCOMP minicomputer was introduced in an attempt to automate the SASW method. Its capability, architecture, current operating level, and recommended future software enhancement are discussed.

SUMMARY

An investigation of variables affecting measurements by the Spectral-Analysis-of-Surface-Waves (SASW) method is presented herein. The SASW method is used to determine the shear wave velocity and elastic modulus profiles of pavement sections and soil sites. With this method, a transient vertical impulse is applied to the surface, and a group of surface waves with different frequencies are generated in the medium. These waves propagate along the surface with velocities that vary with frequency and the properties of the different layers comprising the medium. Propagation of the waves is monitored with two receivers a known distance apart at the surface. By analysis of the phase information of the cross power spectrum and by knowing the distance between receivers, phase velocity, shear wave velocity and moduli of each layer are determined.

This report contains a comprehensive investigation of variables affecting these modulus measurements. Variables such as receiver types, source/receiver configurations, natural frequencies of the coupled receiver-pavement system, and body and surface wave reflections from discontinuities in the pavement system were studied experimentally. Most of the experimental work was conducted at the rigid pavement test facility at Balcones Research Center of The University of Texas at Austin. Analytical studies were also performed. These studies included modelling of body and surface wave reflections and analyzing the rigid body dynamics associated with receivers attached to pavements.

IMPLEMENTATION STATEMENT

The Spectral-Anlysis-of-Surface-Waves (SASW) method has many applications in material characterization of pavement systems. With this method, elastic moduli and layer thicknesses of pavement systems can be evaluated in situ. The method can be utilized as a tool for quality control during construction and during regular maintenance inspections.

The method can be implemented to evaluate the integrity of flexible and rigid pavements. Reduction of the experimental data collected in the field is fully automated. The inversion process is not automated, as yet. The method has been employed at more than 35 pavement sites to study the precision and reliability of the method. From this and previous studies, it can be concluded that the thicknesses of different layers are generally within about ten percent of those measured from boreholes and the moduli are, on the average, within 20 percent of moduli measured with other independent methods employing in situ seismic techniques. For accurate moduli measurements in the upper 2 inches of the concrete or asphalt pavement, surface waves with frequencies in the range from 30 to 70 kHz should be used and testing can be performed within about one wavelength of the source.

TABLE OF CONTENTS

LIST OF TABLES

LIST OF FIGURES

Figure **Page**

Figure **Page**

Figure **Page**

Figure **Page**

Figure **Page**

Figure **Page**

Figure **Page**

Figure **Page**

CHAPTER ONE

INTRODUCTION

1.1. PROBLEM STATEMENT

Shear moduli of engineering materials such as soil, rock, concrete, and asphalt are important in characterizing the mechanical behavior of these materials under many different types of loading. In geotechnical engineering, low-amplitude shear moduli are employed in designing facilities such as vibrating machine foundations, as reference levels for evaluating liqufaction potential during earthquake shaking, and for in situ evaluation of hard-to-sample natural soil deposits like gravels and cobbles. In transportation engineering, Young's moduli of pavement systems can be determined from the shear moduli of the systems by the simple relationship between Young's moduli and shear moduli. Young's moduli are utilized in characterizing materials for initial pavement design, in evaluating structural adequacy of existing pavements, and in delineating zones of pavement deterioration. Because the velocities of seismic waves are directly related to the properties of the materials through which they propagate, it is possible to measure seismic wave velocities and then derive material properties, such as shear modulus and Young's modulus, from the measured wave velocities. This is the basic idea behind the use of seismic methods to assess in situ material properties.

The stiffness of geotechnical and pavement materials can be measured either in situ or in the laboratory with intact samples. Seismic methods, such as the crosshole method and seismic reflection methods, have been employed frequently as in situ methods in the past for this type of measurement. However, seismic refraction is not applicable in the situation where stiff material is underlain by soft material, such as is the case in a pavement system. The crosshole method can be used to determine accurate and detailed stiffness profiles of pavment systems, but use of this method requires boreholes (destructive) and is labor intensive. Laboratory tests, on the other hand, are less expensive than field tests, but they usually suffer from problems such as sample disturbance, non-representative samples, and alteration of stress states. As a result, in situ tests are preferable for stiffness profiling but, because of costs, are generally used frugally.

One field seismic method that has undergone significant advancement in the past few years is the Spectral-Analysis-of-Surface-Waves (SASW) method . In this method, both the source and receivers are placed on the ground surface. Surface waves are generated by applying a vertical impulse to the pavment or ground surface. The propagation of these waves along the

surface is monitored. From the velocities of propagation, the stiffness profile of the site is calculated. The method is easy to use, requires no boreholes which makes it nondestructive, and has the possibility for full automation.

A significant effort has been devoted to the development and improvement of the SASW method at The University of Texas at Austin. Over the past five years, this effort has been directed towards improvement of field testing procedures, data processing techniques, and analytical solutions as well as development of an understanding of the variables that affect the results, and the initial steps toward automation of the method. Rewards from these efforts have been very encouraging. The method has been applied to many soil and pavement sites with great success. While problems are being solved, new challenges are arising. For example, in applying the SASW method at various sites, particularly pavements, difficulties have been encountered with reflected waves, with coupling between the receivers and the pavement surface, and with the inability to generate adequate energy at high frequencies (above 30 kHz). It is clear that there are still a lot of parameters which need to be studied and room exists for improvement in this method.

To automate this testing method, a device which is capable of performing high speed data acquisition and rapid numerical computations is required. For this study, a MASSCOMP MC5500 minicomputer has been employed. The intention is to use this computer for both field data acquisition and numerical computation. The final goal for the deployment of this computer is that testing time can be reduced to a minimum (say five minutes), and the stiffness profile can be determined and reviewed at the test site in "real" time.

1.2 OBJECTIVES

Although the SASW method is a well established method, the influence of several parameters on testing pavements are not fully understood. The influence of reflected surface and body waves, field test procedures and equipment arrangement, impact stress level, high-frequency generation, and natural frequencies of receiver and coupled receiver/pavement systems remain to be studied. Therefore, the main objective of this study is to investigate the influence of these parameters on the SASW tests and to provide methods of resolving possible problems. In addition, several new applications of the method are also explored as a second objective.

The third objective of this study is to begin to automate the SASW method. A minicomputer was purchased for data collection and processing. The funds for this equipment were obtained from the U.S. Air Force Office of Scientific Research and the College of Engineering at The Univeristy of Texas at Austin. A MASSCOMP MC5500 computer was

selected to serve as the heart of the automation system. This attempt was not totally completed, but the capacity and current operating level is presented.

1.3. ORGANIZATION

A brief overview of the SASW method is presented in Chapter Two. Since more detailed discussions of both the theoretical and field aspects of this method can be found elsewhere (Nazarian and Stokoe, 1985, 1986), only the very basic ideas and field procedure are outlined so that it is possible for readers to proceed to the following chapters comfortably and without referring to other articles.

In Chapter Three, a simplified analytical model to investigate the effects of reflected surface waves and direct and reflected body waves on a field dispersion curve based on the assumption of only direct surface waves is presented. (The field dispersion curve can be considered the "raw data" collected in SASW testing as discussed in Chapter Two.) Reflecting boundaries such as edges or joints of a pavement system or the interface between the pavement layers are considered. An example is presented to demonstrate the use and validity of this method. Additional analytical and experimental studies on this subject are presented in Chapter Four for reflected surface waves and Chapter Five for reflected and direct body waves. All experimental studies were conducted at the rigid pavement research facility at Balcones Research Center of The University of Texas at Austin. A MASSCOMP minicomputer was used intensively for the analytical part of the study presented in these chapters and for preparation of the graphical presentation of results.

A few data processing techniques for improving data quality are presented in Chapter Six. Both time domain and frequency domain approachs are discussed. The main purpose of these techniques is to smoothen the field dispersion curve and possible remove some of the adverse effects from any wave arrivals other than direct surface waves. At the end of this chapter, a data processing procedure for typical SASW testing is recommended. This procedure, however, serves more as a guidline than a standard.

In Chapter Seven, some practical problems associated with the field testing procedure, such as natural frequencies of the accelerometers and of the coupled accelerometer/pavement system are studied. Also, the impact stress level, and accelerometer attachment methods are discussed. Suggestions are made for avoiding or reducing some adverse effects from these problems.

A new source, the "V" meter, was found to be an excellent source in generating high-frequency signals. This new source is very easy to use and made the measurement of material properties in the near-surface extremely effective. A big part of Chapter Eight is dedicated to the discussion of the use of this new source. A quick and easy method in assessing the material stiffness in the near-surface region using the "V" meter is presented. This method represents a significant advance for in-situ nondestructive testing. Other subjects such as the repeatibility of the SASW method, and estimation of maximum aggregate size by the SASW method are also presented in this chapter.

Two applications of the SASW method, other than regular existing pavement testing, are selected and discussed in Chapter Nine. The first application is use of the SASW method for stiffness profiling of the BRC facility during construction. The other one is use of SASW method for monitoring the stiffness change of concrete during the curing process. This application illustrates the effectiveness in assessing the material properties and the nondestructive nature of the SASW method.

In Chapter Ten, use of the MASSCOMP MC5500 minicomputer is reviewed. Its capability, software, and hardware configurations are briefly outlined. The current operating level and future prospects for development are also discussed.

In Chapter Eleven, summary and conclusions are presented for this study. Recommendations for future research are also presented.

CHAPTER TWO

BRIEF OVERVIEW OF THE SASW METHOD

2.1. Introduction

There is a reasonably short history of researchers and practitioners who have tried to use the surface wave method for engineering applications. Jones (1962) and Henkelom and Klomp (1962) were some of the first researchers to use surface waves to try to investigate pavement systems. Henkelom and Klomp (1962) used steady-state vibrations to perform surface wave tests on pavement systems. They tried to measure changes in surface wave velocity and to relate these changes to variations in the water content of the subgrade. Jones (1962) performed experimental and mathematical studies on the use of surface wave velocity to monitor changes in properties of pavement sections. Unfortunately, no theoretically correct solution existed in either of these studies. Therefore, the researchers were unsuccessful in their efforts.

The use of steady-state surface waves to determine elastic modulus profiles of geotechnical and pavement systems in the field has also been studied extensively at the U. S. Army Engineers Waterways Experimental Station (WES) by Ballard (1964), Fry (1965), Maxwell and Fry (1967), Ballard and Casagrande (1967), Cunny and Fry (1973), and Ballard and Chang (1973) to cite a few studies. This work was most successfully applied to soil and dam sites. However, the method never gained much acceptance because of the effort and equipment required to perform the tests and because of the lack of a theoretically correct analysis procedure.

The researchers cited above are just a few of those people who shared the same idea of assessing the in situ stiffness profile from the ground surface. In these studies, steady-state vibration sources were used, and data were collected in the time domain. This field approach handicapped the researchers. In addition, no proper analytical model of the system was used. (All of them, except Jones, correlated sampling depth with wavelength by an empirical factor.) As a result, the most successful applications of the surface wave method were limited to soil sites (no need for a high-frequency source and associated data acquisition equipment) with relatively uniform stiffness profiles. The lack of variation in the stiffness profiles resulted in tolerable errors which were introduced by not using a proper mathematical model and made this shortcoming rather unnoticeable.

With the development of portable sophisticated electronics, it has become possible to perform accurate, high-frequency data acquisition and complex mathematical manipulations

rapidly in the field. As a result, application of the surface wave method has begun a new era Heisey (1982) and Heisey et al (1982) used the new generation of electronics (the HP5423A Structural Dynamics Analyzer) and started experimental studies on the surface wave method. Nazarian (1984) developed an analytical model for the surface wave method which brought the method from a purely empirical stage to the theoretically sound level at which it is today. Sanchez-Salinero (1987) and Sanchez-Salinero et al (1987) further enhanced the theoretical study by using an even more complex mathematical approach. Currently, efforts with this surface wave method are devoted to automation, exploration of new applications, and some refinements such as data smoothing and filtering.

In this chapter a brief overview of the background and operation of the SASW method is presented. Practical aspects of the SASW method are discussed in detail in Nazarian and Stokoe (1985). Theoretical aspects of the SASW method are presented in Nazarian and Stokoe (1986).

2.2. GENERAL BACKGROUND OF THE SASW METHOD

The SASW method is an in situ seismic method which is used for near-surface profiling of geotechnical and pavement sites. The general arrangement of the source, receivers (vertical sensors), and recording equipment is shown schematically in Fig. 2.1. In the field, this method is performed in such a way that both the source and receivers are placed on the ground/pavement surface. As no boreholes are required, the method is nondestructive. The simplest and most effective source is a transient vertical impact, usually delivered by a hammer, which generates a group of surface waves with various frequencies. The surface waves travel along the surface in all directions from the source. Two vertical receivers, usually geophones or accelerometers, are placed on the surface in a linear array and are used to monitor the propagation of surface wave energy. By analyzing the phase of the cross power spectrum determined between the two receivers, surface wave velocities over the frequency range generated are determined. The shear wave velocity profile is then obtained from the surface wave velocities, and finally elastic moduli profiles are determined.

2.2.1. Surface Waves

The surface wave (Rayleigh wave) problem was first solved by Rayleigh (1887). This wave exists in a system with a free surface like a pavement or geotechnical site. Particle motion for this type of wave is confined to the near-surface region because the amplitude of particle motion attenuates rapidly with respect to depth below the free surface.

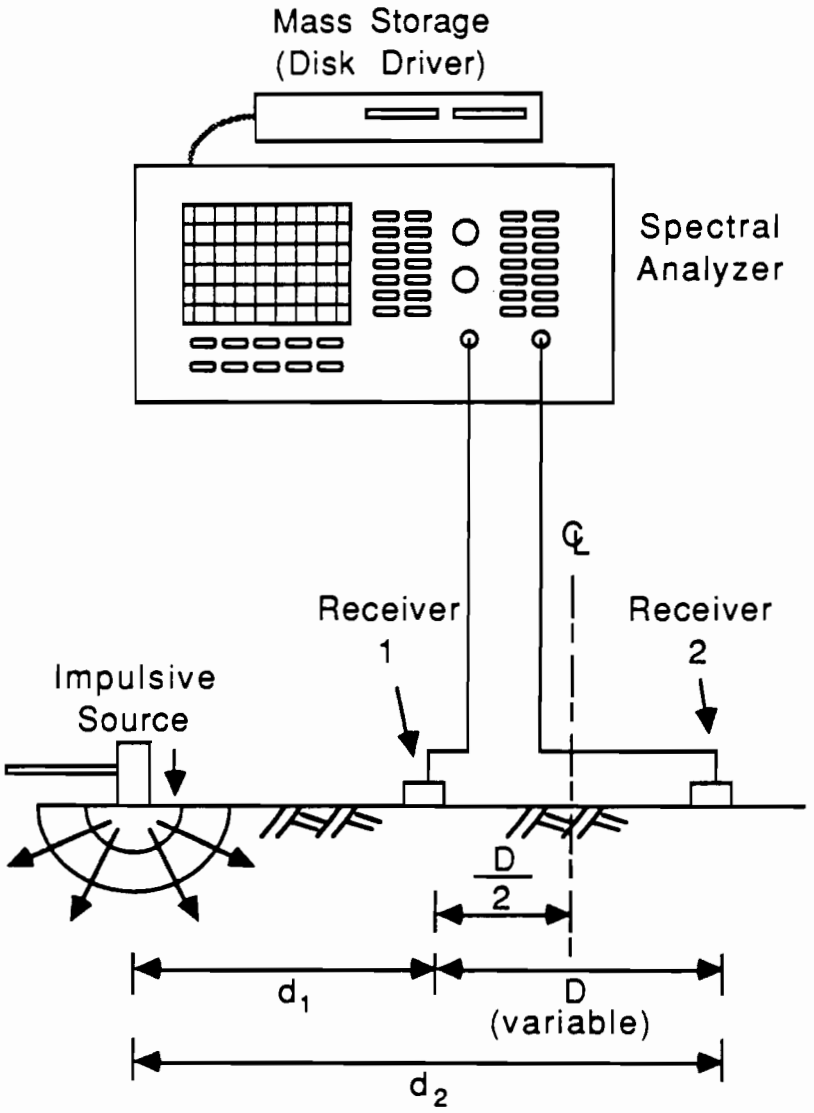

Fig. 2.1. Field Arrangement of Source, Receivers, and Recording Equipment for Typical SASW Testing.

There are several different terminologies used in the past for defining the surface wave velocity such as phase velocity, group velocity, and apparent wave velocity. Since this study does not focus on the theoretical development of the SASW method, these terminologies are used loosely. The "apparent wave velocity" or "surface wave velocity" are used to represent the surface wave velocity in either the formulation or measurements in the field.

The essence of SASW testing is the generation and detection of surface waves. Surface wave velocity, V_R, is constant in a homogeneous half-space and independent of frequency. Each frequency, f, has a corresponding wavelength, L_R, according to:

$$V_R = f \times L_R \tag{2.1}$$

Once V_R is determined, shear wave velocity can be determined from the relationship between surface wave and shear wave velocities (which are related by Poisson's ratio). In an isotropic, elastic half-space, the ratio of surface-wave-to-shear-wave velocity increases as Poisson's ratio increases. This ratio varies from 0.87 to 0.96 for values of Poisson's ratio ranging from 0.0 to 0.5.

2.2.2. Dispersive Characteristic of Surface Waves

Suppose the stiffness of a site varies with depth. The velocity of the surface wave will then vary and become a function of wavelength (or frequency). The variation of surface wave velocity with respect to wavelength (frequency) is called dispersion, and a plot of surface wave velocity versus wavelength (frequency) is called a dispersion curve.

The dispersion curve is derived from the phase of the cross power spectrum. This phase provides the relative time lag (travel time) between two signals detected by a pair of receivers. The time lag can be obtained at every frequency over the frequency span excited in an SASW test. For a travel time equal to one period of the surface wave at a particular frequency, the phase difference is 360 degrees. Thus, for each frequency, the travel time between receivers can be calculated by:

$$t(f) = \phi(f)/(360 \times f) \tag{2.2}$$

where:

f = frequency, Hz,
t(f) = travel time for a given frequency, and
ϕ(f) = phase difference (phase of the cross power spectrum) in degrees for a given frequency.

The distance between the two receivers, D, is a known parameter. Therefore, surface wave velocity at a given frequency, $V_R(f)$, can be calculated by:

$$V_R(f) = D/t(f) \tag{2.3}$$

and the corresponding wavelength, $L_R(f)$, can be calculated from:

$$L_R(f) = V_R(f)/f \tag{2.4}$$

By repeating the procedure outlined by Eqs. 2.2 through 2.4 for every frequency, the surface wave velocity corresponding to each wavelength (frequency) can be evaluated, and the resulting dispersion curve can be determined.

2.2.3. Data Interpretation and the Dispersion Curve

Among all of the types of frequency domain data that can be collected in the field for a typical SASW test, two spectra represent the key measurements. They are the phase of the cross power spectrum and the coherence function. Wave velocities are extracted from the phase of the cross power spectrum, and the coherence function reflects the quality of data.

A typical example of field data in terms of phase of the cross power spectrum and the coherence function are shown in Fig. 2.2. It is favorable, and generally necessary, to have high values (nearly 1.0) in the coherence function all across the sampling bandwidth because low values (say less than 0.9) in the coherence function imply that the data may be contaminated by noise. In the example in Fig. 2.2, the coherence function is low in the frequency range from about 0 to 500 Hz, and the associated phase curve in this range is quite rough compared to the remainder of the phase curve. Data in this range are not used because they are, most likely, not representative of the site.

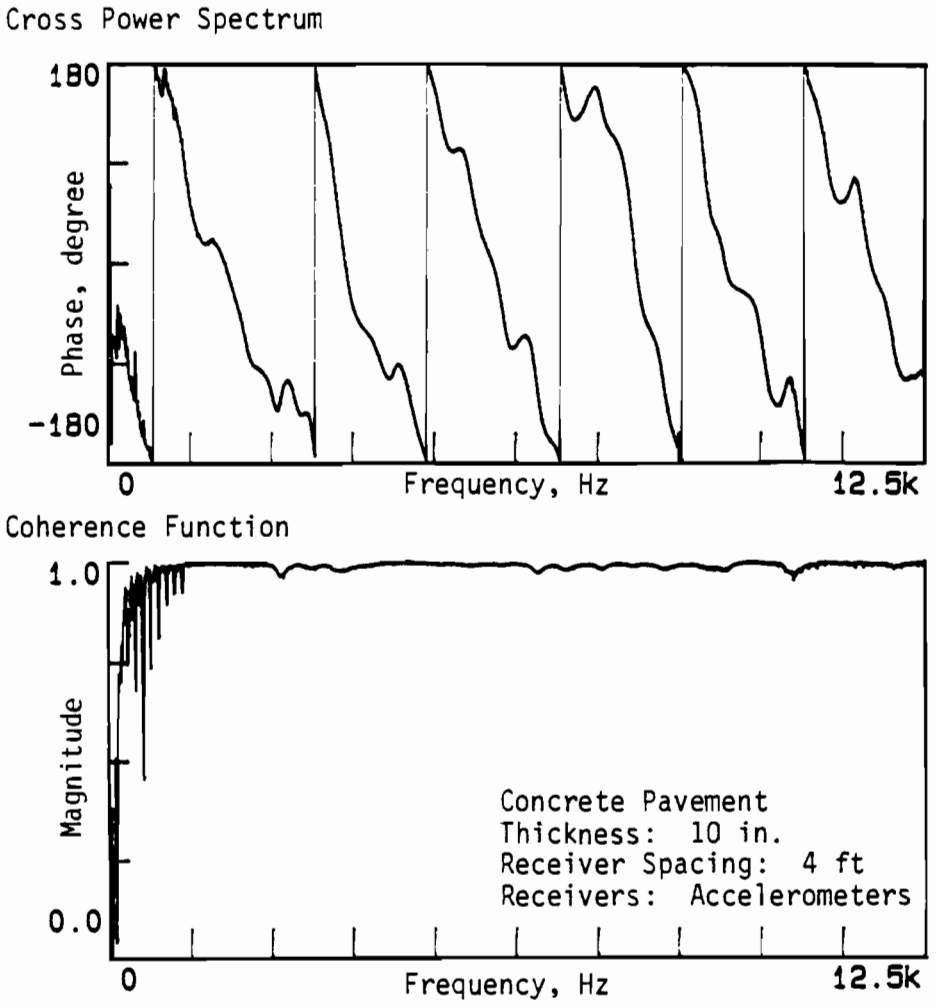

Fig. 2.2 Typical Phase of the Cross Power Spectrum and Coherence Function Recorded in the Field During SASW Testing.

The phase of the cross power spectrum shown in Fig. 2.2 is actually a "folded phase" because the phase of the cross power spectrum is shown as ranging between +180 degrees and -180 degrees. As a result, it is necessary to unfold the phase before wave velocities can be calculated. To unfold the phase, each section of the phase jump going from -180 to +180 degrees (or +180 to -180 degrees) is patched back to its proper location as illustrated in Fig. 2.3. The unfolded phase is also shown in Fig. 2.4. Notice that the sign of phase has been changed from minus to plus between Figs. 2.3 and 2.4. This sign change is usually done because the recovered phase always bears a minus sign. (A positive phase implies negative wave velocity.) However, the minus sign is omitted for convenience.

By knowing the phase and the distance between the receivers (4 ft or 1.3 m in this example), the wavelength and wave velocity corresponding to each frequency can then be calculated using Eqs. 2.2 through 2.4. With frequency, wavelength, and velocity, a dispersion curve can be constructed. There are several ways of presenting dispersion curves. One way of plotting the curve is to plot wave velocity versus frequency as shown in Fig. 2.5. However, wavelength is generally more significant than frequency in typical SASW testing because wavelength relates directly to sampling depth. Therefore, the dispersion curve is often presented by plotting wave velocity versus wavelength as shown in Fig. 2.6. The wavelength axis in Fig. 2.6 can be thought of as the depth axis except that the scale has to be divided by a factor which depends on the layering at the site. For a typical site without drastically different stiffnesses between layers, this factor ranges from about 2 to 3.

Because a major part of this study is devoted to testing pavements using high frequencies in the near-surface range (depths less than about 1 ft (0.3 m)), the behavior of dispersion curves in the short-wavelength range is a major concern. Therefore, most dispersion curves are presented in this study by plotting wave velocity versus the logarithm of wavelength as shown in Fig. 2.7. In this case, the behavior of the dispersion curve corresponding to shallow depths is magnified. Upon comparison of Figs. 2.6 and 2.7, it is clear that trends in the dispersion curve in the short-wavelength range (say in the range of 0.5 ft to 2 ft (15 cm to 30 cm)) are better displayed in Fig. 2.7 than in Fig. 2.6.

As an aside, data in the high-frequency range correspond to wave velocities at shallow depths (the right hand side of the curve shown in Fig. 2.5). Data in the short-wavelength range (left hand side of the dispersion curves shown in Figs. 2.6 and 2.7) correspond to wave velocity at shallow depths. It is important to recognize that in Fig. 2.5, the sampling depth decreases along the X axis (as frequency increases) while in Figs. 2.6 and 2.7, sampling depth increases

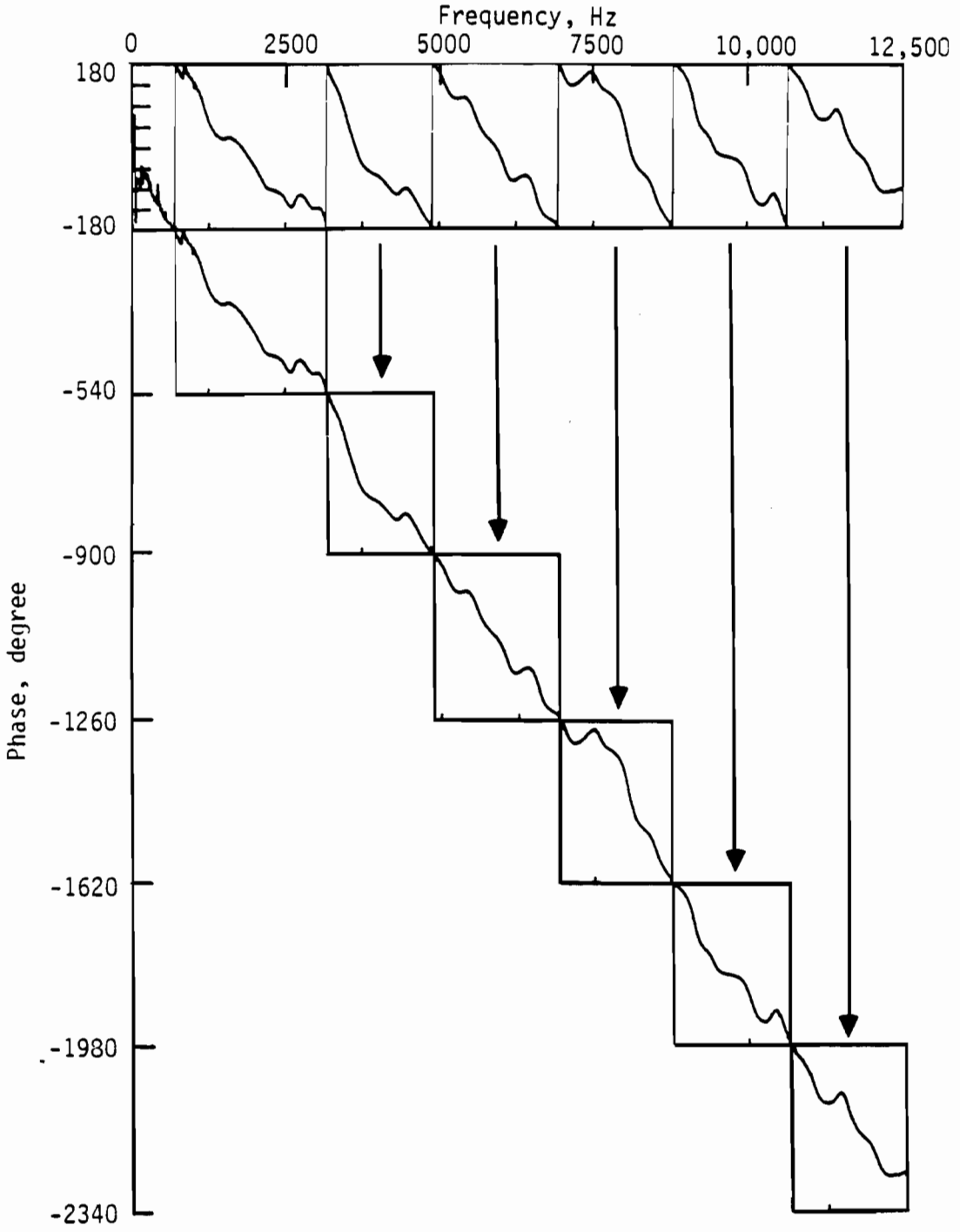

Fig. 2.3. Illustration of the Unfolding Process Applied to the Phase of the Cross Power Spectrum.

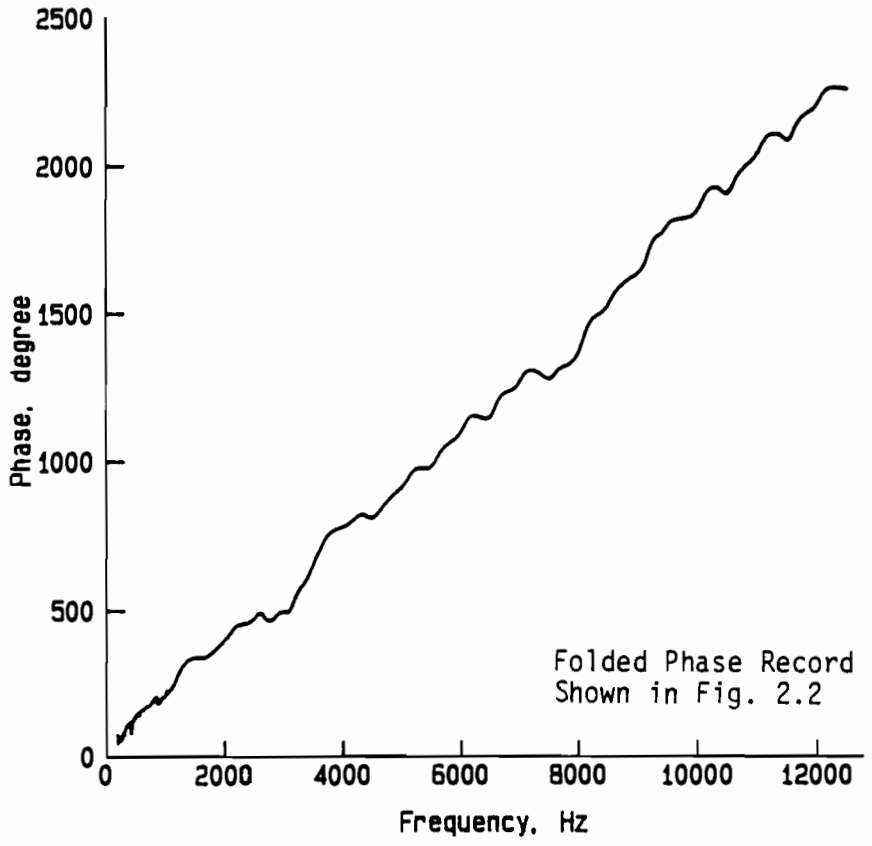

Fig. 2.4. Phase of the Cross Power Spectrum After Being Unfolded and Changed in Sign.

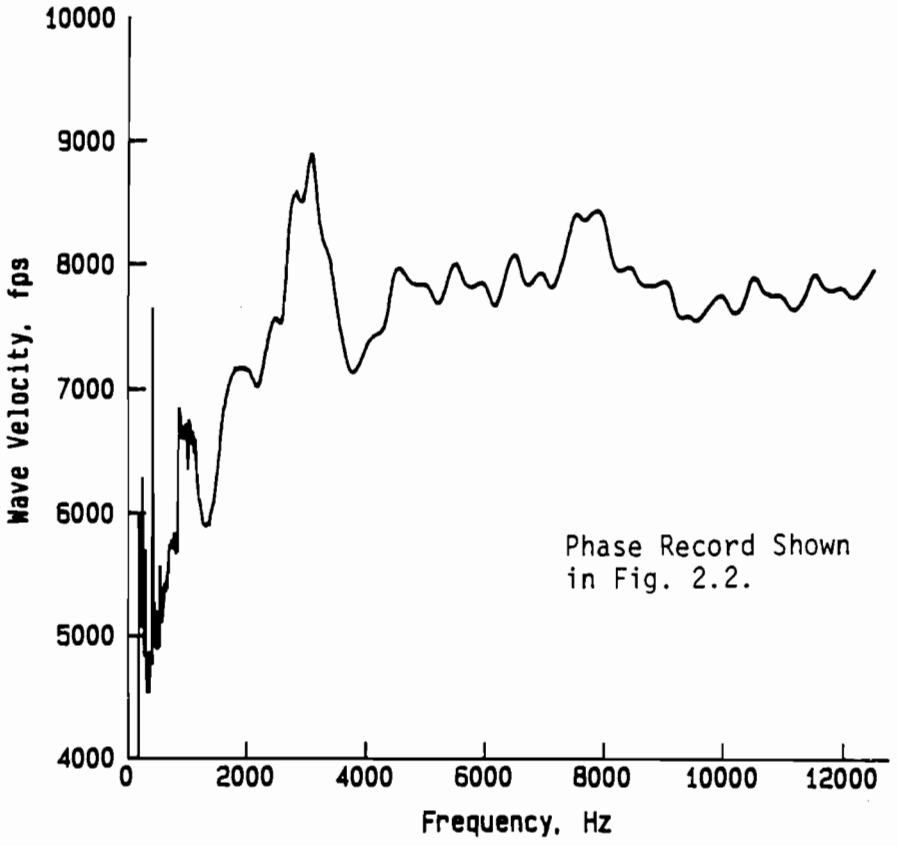

Fig. 2.5. Dispersion Curve In Terms of Wave Velocity Versus Frequency.

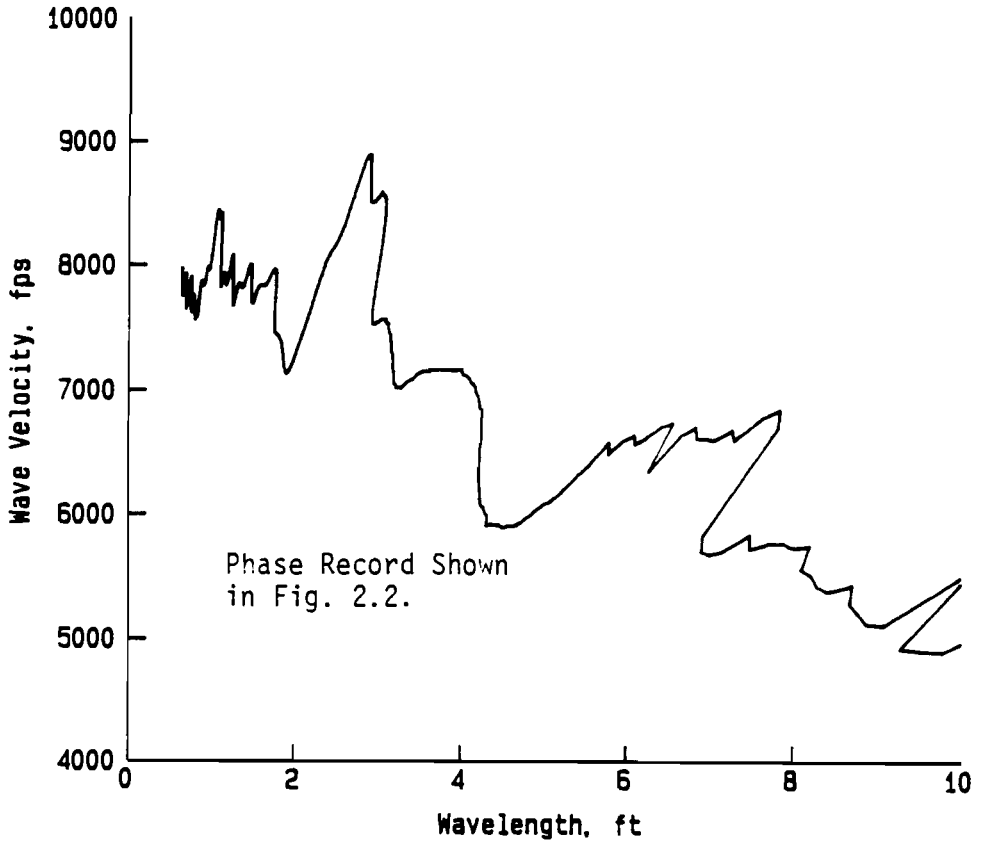

Fig. 2.6. Dispersion Curve In Terms of Wave Velocity Versus Wavelength.

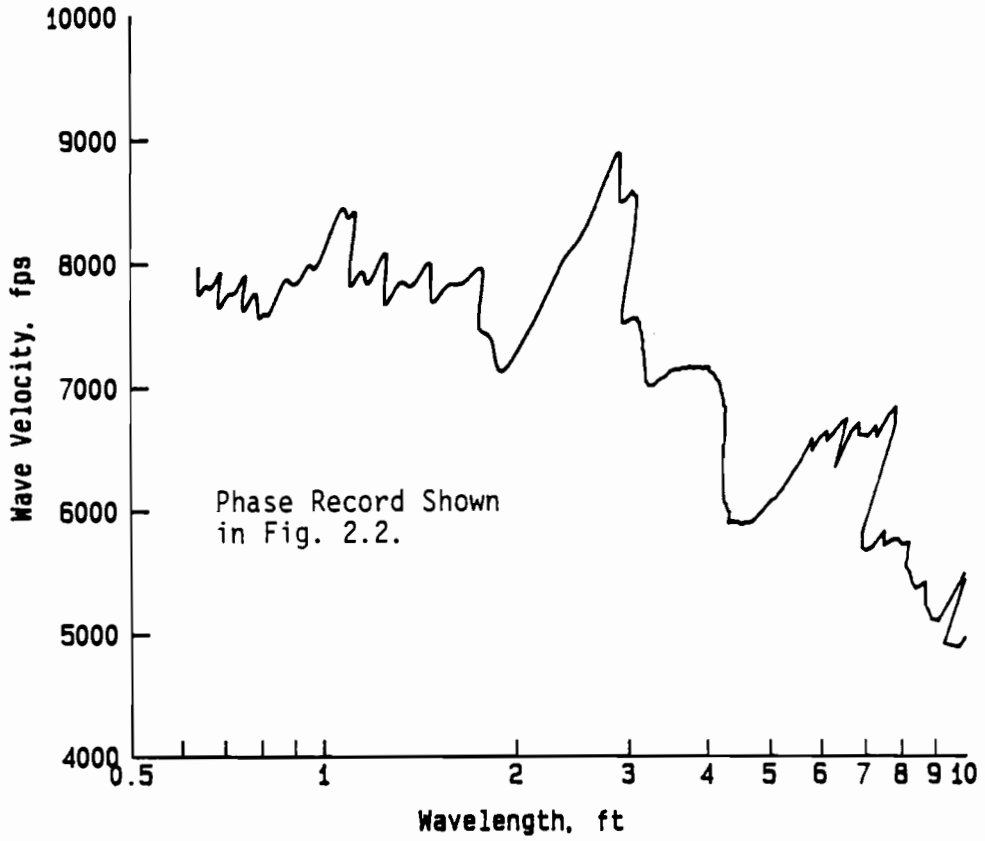

Fig. 2.7. Dispersion Curve In Terms of Wave Velocity Versus the Logarithm of Wavelength.

along the X axis (as wavelength increases). The dispersion curves in Figs. 2.5 and 2.7 actually present exactly the same information. The difference is that they are, more or less, a mirror image of each other with respect to the wave velocity axis.

It is also interesting to notice that, in Fig. 2.5, wave velocity is a single-valued function of frequency. In Fig. 2.6, however, wave velocity is not a single-valued function of wavelength. That is, there may be more than one wave velocity corresponding to one particular wavelength. This multiple-valued phenomenon is caused solely by transforming the X-axis from frequency to wavelength. If one tries to perform mathematical manipulations, such as curve fitting,on the V_R-L_R curve, mathematical difficulties occur because of the multiple values of V_R for a given L_R. Therefore, some mathematical manipulations, such as curve fitting, are performed in the frequency domain. In fact, a particular frequency can be represented by a straight line passing through the origin in Fig. 2.6. This point is further illustrated in Fig. 2.8. In Fig. 2.8, straight lines passing through origin are shown with different frequencies. While transforming the X axis from frequency (Fig. 2.5) to wavelength (Fig. 2.6), the frequency axis becomes a polar-like coordinate (Fig. 2.8) with frequency increasing from 0 Hz to ∞ Hz for counterclockwise rotation in the first quadrant. If this polar-like coordinate is used, wave velocity is still a single-valued function of frequency because only one wave velocity is associated with a particular frequency (represented by a straight line passing through the origin).

2.2.4. Criteria for Data Filtering

Since phase information corresponding to low values in the coherence function may be contaminated by noise, this phase information may not be representative of the site. As a result, the first step in data filtering is almost always elimination of phase of the cross power spectrum corresponding to low values in the coherence function. Based on past experience, a small drop of the coherence function (say less than 0.95) usually corresponds to large fluctuations in the phase. These fluctuations are easy to identify and eliminate during construction of the dispersion curve.

It is, however, very common to have the situation when the values of the coherence function are high (say more than 0.98), and yet the corresponding phase of the cross power spectrum has to be eliminated to construct the correct dispersion curve. It is also not uncommon that at some particular sites, the values of the coherence function in certain frequency ranges cannot be improved by any possible means such as changing the source or improving the receiver/ground coupling, and, from time to time, the phase of the cross power spectrum in this frequency range is vital and also seems to be reasonable. While there is no better alternative, data

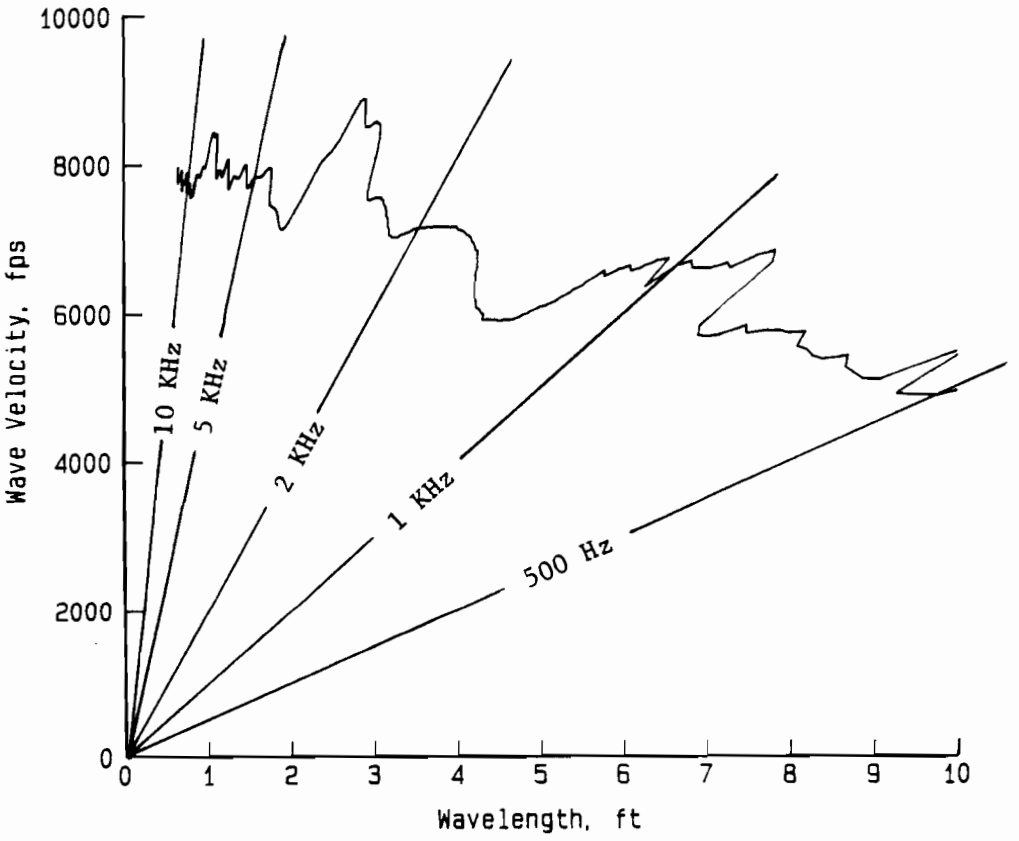

Fig. 2.8. Illustration of Relationship Between Wave Velocity, Wavelength, and Frequency in a Velocity-Wavelength Dispersion Curve.

corresponding to low values in the coherence function were still accepted with the knowledge that these data may not be correct. These exceptions, when the coherence function does not seem to serve as the data quality indicator, usually demand an experienced operator to make decisions and hence increase the difficulty of data interpretation. As a result, the relationship between the coherence function and the phase of the cross power spectrum in general SASW testing requires more study so that the criteria for accepting or rejecting the phase of the cross power spectra in any frequency range can be better defined.

In addition to the rejection of data corresponding to low values in the coherence function (below about 0.95), there are also restrictions for the acceptable range of wavelengths generated in the field. Heisey et al (1981), based on studies at several soil sites, suggested that the distance between receivers, D, should be less than two times the sampling wavelength and greater than one third of the sampling wavelength. This relationship can be expressed as:

$$L_R/3 < D < 2L_R \tag{2.5}$$

As the velocities of different layers are unknown before testing, it is difficult to know if these limits are satisfied. Practically speaking, it is more appropriate to test with various distances between receivers in the field and then evaluate in the laboratory the range of wavelengths over which reliable measurements were made. The relationship between receiver spacing and wavelength is then better expressed as:

$$D/2 < L_R < 3D \tag{2.6}$$

The upper limit (< 3D) is based on the thought that the sampling waves can not be fully developed to a depth beyond 3D since the impact is on the surface and certain spacing must be allowed between the source and first receiver so that the surface waves are fully developed when they reach the first receiver. The lower limit (D/2 <) is related to the accuracy of the measuring equipment.

The filtering criteria outlined by Eq. 2.6 were used for most field tests in the past, except that the lower limit (D/2<) was removed because its validity was found to be unjustified with the newer equipment in use (HP 3562A). Recently, a very detailed theoretical study has been performed to ascertain the best source/receivers configuration (Sanchez-Salinero et al, 1987). Imagine a field test with the source/receiver configuration shown in Fig. 2.1. Let the distance

between the source and near receiver be d_1 and the distance between the source and far receiver be d_2. Sanchez-Salinero et al concluded that it is desirable to have:

$$d_2/d_1 \geq 2 \tag{2.7}$$

and the useful range of signals are those which have a wavelength less than d_1. This relationship can be expressed as:

$$L_R < d_1 \tag{2.8}$$

In the past, the distance between the source and near receiver has usually been equal to the distance between the two receivers (Nazarian et al, 1983). This source/receiver arrangement can be expressed as:

$$d_2/d_1 = 2 \tag{2.9}$$

As a result, the distance between the two receivers, D, will be:

$$D = d_2 - d_1 = d_1 \tag{2.10}$$

Thus, as opposed to Eq. 2.6, the new criterion requires that:

$$L_R < D \tag{2.11}$$

In addition, no lower limit for L_R is imposed. Field data (presented in Chapter Seven), however, show that this new criterion may be too conservative and suggest that the upper limit of the old criterion:

$$L_R < 3D \tag{2.12}$$

seems to provide reasonably good results.

To impose these criteria, the procedure is to select a spacing between receivers, perform the test, and reduce the data to determine the wavelengths and velocities. Finally, eliminate all data points that do not satisfy Eq. 2.11 (or Eqs. 2.12 or 2.6).

Due to the existence of these filtering criteria (Eqs. 2.6, 2.11, and 2.12), it is necessary to justify that data collected in the field are satisfying the filtering criteria while the data are being collected. An easy method was found as follows. The cycle number (multiples of 360 degrees) of the phase of the cross power spectrum is inversely proportional to wavelength by the factor of distance between the two receivers. This statement in equation form is:

$$\text{Wavelength} = \frac{\text{Receiver Spacing}}{\text{Number of Cycles}} \tag{2.13}$$

Therefore, enforcement of the criteria described by Eqs. 2.6, 2.11, or 2.12 becomes simple and is illustrated in Fig. 2.9. The filtering criteria described by Eq. 2.6 is illustrated in Fig. 2.9a. The upper limit (< 3D) requires that only data corresponding to more than 1/3 of a cycle is accepted, and the lower limit (D/2 >) requires that only data corresponding to less than 2 cycles is accepted. By the same token, the usable range of data in the phase of the cross power spectrum based on Eqs. 2.11 and 2.12 can be found as illustrated in Figs. 2.9b and 2.9c, respectively.

2.2.5. Shear Wave Velocity Profiles from Inversion

The dispersion curve measured by the surface wave method is only the relation between surface wave velocity and wavelength. When the medium consists of layers with different stiffnesses (in terms of shear wave velocities or elastic moduli), the relationship between the shear wave velocity profile and dispersion curve becomes quite complex. As a result, development of the shear wave velocity profile from a known dispersion curve is one of the key steps in the SASW method. The process, which back-calculates the shear wave velocity profile for the corresponding dispersion curve, is called inversion of the dispersion curve (or in short, inversion). The method currently used to back-calculate the shear wave velocity profile is actually a forward modeling method, however, the term "inversion" is still used herein.

To reduce the complexity of the wave propagation problem to a reasonable level, the soil or pavement system is presumed to consist of horizontal layers as shown in Fig. 2.10. Each layer is assumed to be homogeneous, linearly elastic, and to have constant material properties. (Hence, the wave velocity of each layer is assumed to be constant.) Inversion consists of

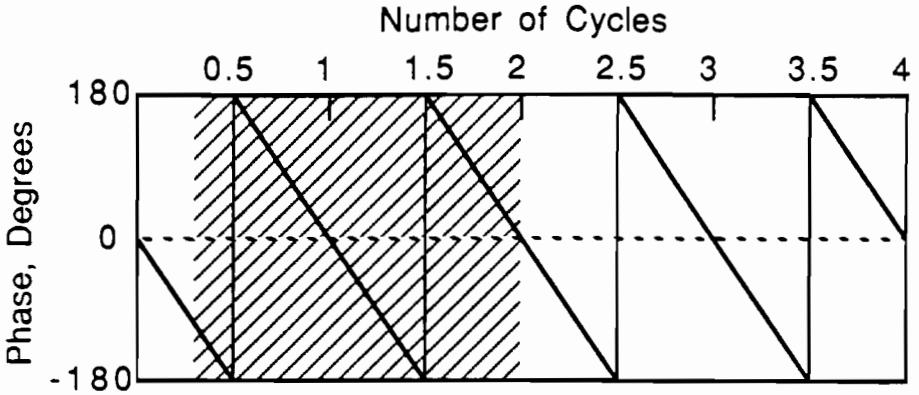

a. Usable Range of Data (Hatched Area) Based on Eq. 2.6.

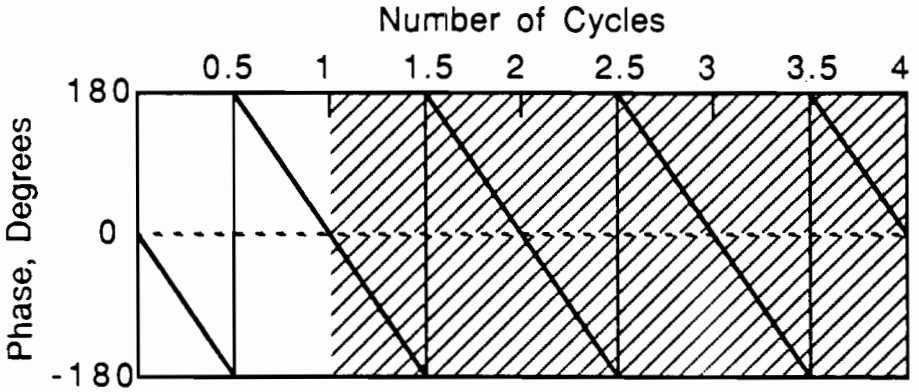

b. Usable Range of Data (Hatched Area) Based on Eq. 2.11.

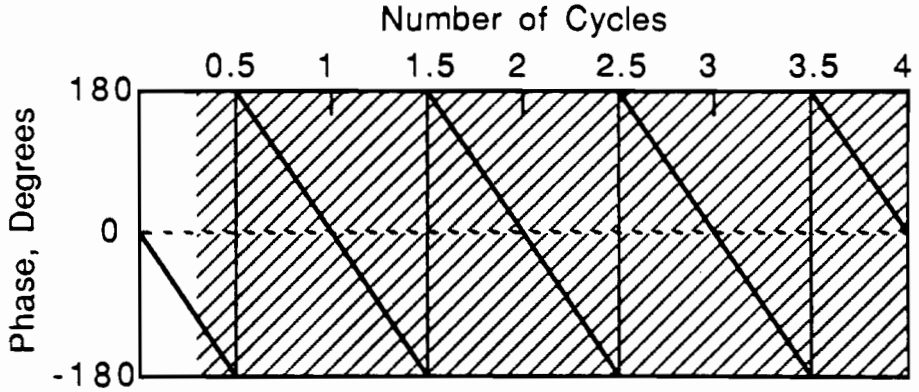

c. Usable Range of Data (Hatched Area) Based on Eq. 2.12.

Fig. 2.9. Usable Range of Phase Data Defined by Filtering Criteria Expressed by Eqs. 2.6, 2.11, and 2.12.

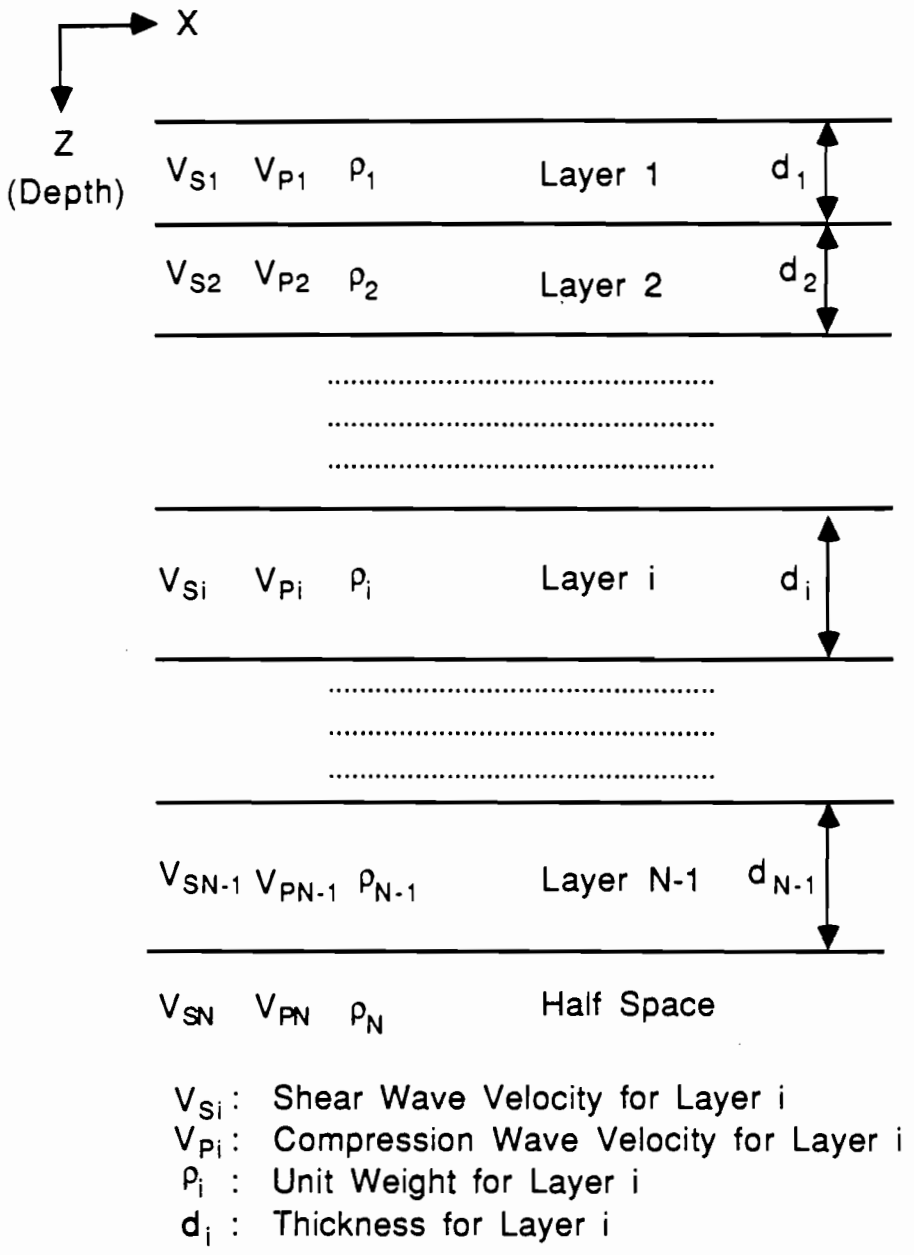

Fig 2.10. Layering System Assumed for the Inversion (Forward Modelling) Process in the SASW Method.

determination of the depth, thickness, and the actual shear wave velocity of each layer from the dispersion curve (apparent surface wave velocity versus wavelength).

Based upon a modified version of Thomson's (1950) and Haskell's (1953) matrix solution for elastic surface waves in a layered solid media , this process is carried out in an iterative fashion. A shear wave velocity profile is initially assumed in the beginning of the iterative process, a theoretical dispersion curve is calculated based on this assumed shear wave velocity profile and the layered model. The theoretical dispersion curve is compared against the field dispersion curve. Proper adjustments in the assumed profile (typically the shear wave velocity or the thickness of several layers) to possibly compensate for discrepancies between the field and modeled dispersion curves are made. A second dispersion curve is then generated based on the newly adjusted shear wave velocity profile. This new dispersion curve is compared against the field dispersion curve, and adjustments in the assumed shear wave velocity profile are again made. This process is repeated until the two curves (experimental and theoretical dispersion curves) match within a reasonable tolerance.

Once the shear wave velocity profile is determined, it is possible to calculate shear and Young's moduli by the following equations:

$$G = \rho V_S^2 \tag{2.14}$$

and

$$E = 2G(1 + \nu) \tag{2.15}$$

where:

- G = shear modulus,
- E = Young's modulus,
- ρ = mass density (total unit weight divided by the acceleration of gravity), and
- ν = Poisson's ratio.

2.3. FIELD PROCEDURE

For typical SASW tests, accelerometers are used as receivers for close receiver spacings (usually 4 ft (122 cm) and less). Accelerometers are used because they exhibit a better response

(than geophones) to high-frequency signals, and high-frequency signals are of most concern for these short-spacing measurements. Geophones are usually used as receivers for larger spacings (greater than 4 ft (122 cm)) because they can better respond to low-frequency signals which are of the most concern for these larger spacings. In addition, the wave signals are frequently too small to be measured by accelerometers at the large spacings.

Geophones used in the past have been made by Mark Products, Houston, Texas. These geophones have natural frequencies ranging from 1 Hz to about 8 Hz. Accelerometers which are manufactured by PCB, Depew, New York, have been used. These accelerometers have the sensitivities ranging from 10 mV/g to 1 V/g and natural frequencies from 5 KHz to 70 KHz. Obviously, the larger the output of any receiver, the easier it is to use as long as it performs properly over the frequency range measured.

The common receivers midpoint (CRMP) geometry (Nazarian et al, 1983) is used for the source/receiver arrangement in most SASW testing. This testing sequence is illustrated in Fig. 2.11. With this test sequence, the two receivers are moved away from an imaginary centerline located midway between the receivers at an equal pace. The source is moved in such a way that the distance between the source and near receiver is equal to the distance between the two receivers. In addition, the location of the source is reversed for each receiver spacing so that forward and reverse profiling are performed.

At pavement sites, spacings between receivers of 0.5, 1, 2, 4, and 8 ft (15, 30, 61, 122, and 244 cm) are typically used. Larger receiver spacings are used at most soil sites and generally start from 1 or 2 ft (30 or 61 cm) and end with 64 or 128 ft (19.5 or 39 m). Even larger spacings are necessary for detecting material at deep depths (depths of the order of 75 to 200 ft (23 to 61 m)) and are used at some soil sites. However, generation and measurement of signals for such large spacings are always a problem, and research is needed to explore this problem.

Surface wave energy must be generated over a wide range of frequencies. To develop such energy, different sources are used. For close receiver spacings (about 2 ft (61 cm) or less), a 4-oz (114 gm) or smaller hammer is used for generating frequencies specifically in the high-frequency range (up to about 30 KHz). A "V" meter (discussed in Chapter Eight) was found to be extremely useful on pavement sites for high-frequency generation (up to about 100 KHz). For intermediate distances [between about 2 to 8 ft (61 to 244 cm)], hammers with weights of about 20 oz (568 g) are employed which generate frequencies in the range (several hundred Hz to several KHz). Sledge hammers (with weights up to about 15 lb (6.8 Kg)) or even bigger weight

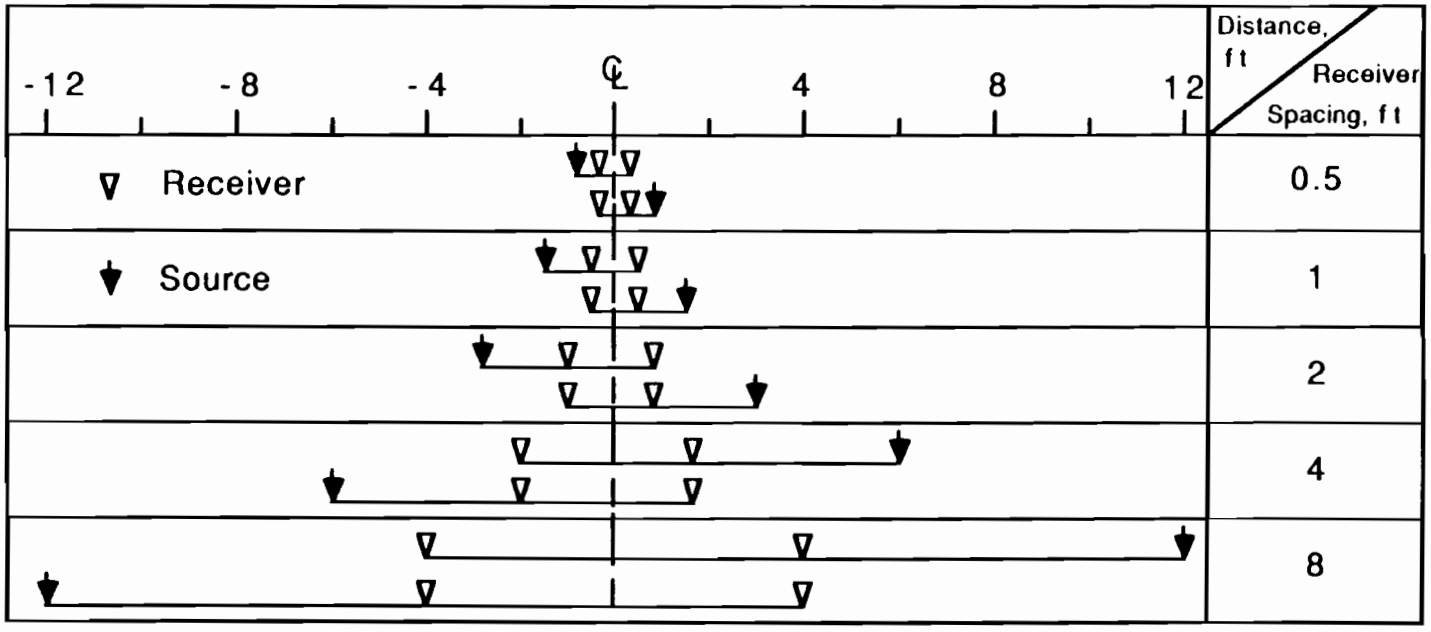

Fig. 2.11. Common Receivers Midpoint (CRMP) Geometry Used in Typical SASW Testing (after Nazarian et al, 1983).

drops are used for most soil sites to generate energy in the low-frequency range (less than 200 Hz).

In most seismic tests, people tend to record time domain data in the field and then perform all data analyses in the office after finishing the field test. This kind of operation is not suitable for typical SASW testing for one major reason. Frequency domain information is critical to proper testing. It is a necessity to examine the data in the frequency domain right after the data have been taken in the field. As a result, proper actions, such as accepting or rejecting the data, identifying the source of noise, or changing the frequency range of the source, can be taken promptly in the field to assure the quality of data. Therefore, spectral analyzers are used in all field tests for data recording and immediate processing.

A spectral analyzer is a digital oscilloscope with the capability of carrying out waveform analysis and some complex mathematical manipulations (such as Fast Fourier Transformation) on sampled data. This kind of equipment has not only speeded up the field testing process but has also helped to assure the quality of field data. The availability of this equipment is one of the major reasons for the advancement of the SASW method.

2.4. SUMMARY

A general overview of the SASW method is given in this chapter. The history, field procedure, and data reduction process are briefly outlined. It appears that the advancement of this method has hinged upon both the theoretical development of an analysis procedure and advancement in electronic data acquisition equipment. It was possible to perform data acquisition in the field and then carry out waveform analyses with a digital computer in the laboratory before portable spectral analyzers were available. However, little field testing was performed because this process was too cumbersome and time consuming. With the development of the portable spectral analyzer, which integrates both data acquisition and waveform analysis into one unit, it became possible to perform numerous field tests in a short period of time.

With the help of Thomson's and Haskell's matrix solution for a layered system, the surface wave method now resides on a firm analytical foundation, and reliable shear wave velocity and elastic moduli profiles can be developed. Modification of the Thomson's (1950) and Haskell's (1953) formulation by Nazarian (1984) made it possible to model a pavement system properly. A pavement system is difficult because the top layer is the stiffest layer in the layered model, as opposed to a soil system where the half-space is often the stiffest layer in the model.

This advancement widened application of the SASW method and made the method a possible technique for routine testing in the pavement industry.

The surface wave method is now theoretically sound and possible to deploy from a practical stand point. Yet, through modern technology, there is still ample room for improvement of the method in terms of speed and ease of deployment. One of the optimum goals is automation of this method which may be incorporated with advanced computer technology and artificial intelligence science.

CHAPTER THREE

SIMPLIFIED MATHEMATICAL MODEL FOR EVALUATING THE EFFECT OF DIRECT AND REFLECTED WAVES ON DISPERSION CURVES

3.1. INTRODUCTION

Due to the complex nature of wave propagation problems, most analytical models are based on the assumption that waves propagate in a layered half space or full space with no additional boundaries or interfaces. As a result, reflected surface waves created by boundaries of a finite space are not included in most analytical solutions. It is obvious that a system without boundaries does not exist in the real world. In fact, whenever a system is tested using a wave propagation method, such as the SASW method, reflected waves from discontinuities such as edges, joints, or cracks are inevitably generated. A pavement system is a good example of a system with numerous reflecting boundaries. However, the key reflecting boundaries are nearly always those in the top layer such as the concrete layer in a rigid pavement.

The existence of reflected surface waves is not considered in the analytical model used to analyze (invert) SASW dispersion curves (Nazarian and Stokoe, 1986). Therefore, it is important to investigate how and to what extent reflected waves influence field results so that errors derived from neglecting their existence are not accidentally overlooked. It is then possible to either avoid or reduce the influence of reflected waves by adjusting the field test procedure or in-house data reduction process.

In addition, only plane surface waves are assumed to exist in the inversion process used in the SASW method. However, when the test is carried out in the field, surface waves are generated by applying a point load (impact) on the surface. As a result, body waves are generated simultaneously with the surface waves. These body waves may propagate directly from the source to the receivers (direct body waves) or they may be reflected, just like surface waves, by those discontinuities in the system and then reach the receivers (reflected body waves). The effect of direct and reflected body waves on the dispersion curve is not known and needs to be studied. Sanchez-Salinero (1987) initiated a formulation which incorporates all waves in the system. However, more work is necessary before this formulation can be easily used.

A mathematical model which is capable of simulating the effect of direct and reflected waves on dispersion curves is presented in this chapter. Use of this model is further explained

with an example. More detailed exploration of reflected and direct waves by both model and field studies are presented in Chapter Four for reflected surface waves and Chapter Five for reflected and direct body waves.

3.2. FIELD TEST FACILITY AND EQUIPMENT

Most field data referred to in this and following chapters are from tests performed on the rigid concrete pavement at the research facility at Balcones Research Center (BRC), The University of Texas at Austin. This research facility (referred to as the BRC facility herein) was designed for the study of nondestructive pavement evaluation methods such as the SASW, Dynaflect, and Falling Weight Deflectometer methods (White et al, 1986). A schematic of the BRC facility is shown in Fig. 3.1. (The material profile is presented in Chapter Nine.)

A Hewlett Packard model 3562A Dynamic Signal Analyzer and an Hewlett Packard model 5423A Structural Dynamics Analyzer were used in the field for data collection (mainly phase of the cross power spectrum and coherence functions). Most data were collected with the model 3562A. Detailed field procedures can be found in Nazarian and Stokoe (1985) and are outlined in Chapter Two.

Different types of accelerometers and geophones were used to monitor motions on the pavement surface. Most field data, however, were collected using PCB model 308B02 accelerometers as motion monitoring devices. Field data (phases of cross power spectra) were transferred to a MASSCOMP model MC5500 minicomputer through a general purpose interface bus (GPIB) for further processing. With the MASSCOMP computer, the researcher is able to: filter out low quality and questionable phase information acquired in the field, calculate the dispersion curves from the filtered phase information, average the dispersion curves from different receiver spacings to find the final (averaged) dispersion curves, and perform other miscellaneous plotting and numerical manipulations. The final dispersion curves were then transferred from the MASSCOMP computer to the University's Dual Cyber System through a telephone line to perform inversion and to evaluate the material property profiles. The MASSCOMP computer has the capability of running the inversion program, but the speed is relatively slow compared to the Dual Cyber System (about 10 times slower compared to the gross speed of the Cyber System operating in a multi-user mode during regular hours) and was not used. The MASSCOMP minicomputer is discussed in Chapter Ten.

Locations of the SASW tests at the BRC facility are shown in Fig. 3.2. Location 1 is on the movable concrete slab, locations 2 through 6 are on the fixed concrete slab, and location 7 is

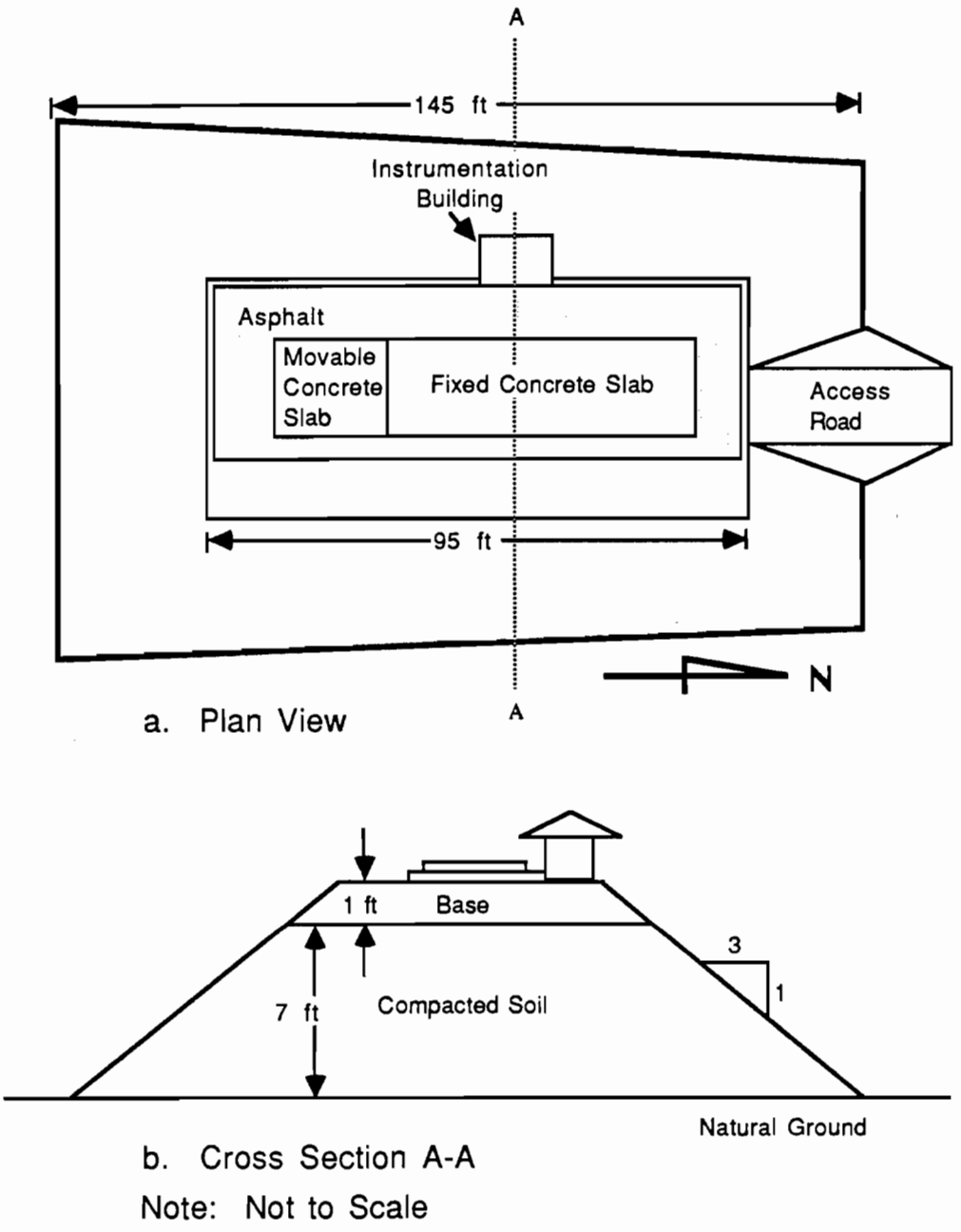

Fig. 3.1. Plan and Cross-Sectional Views of BRC Pavement Facility.

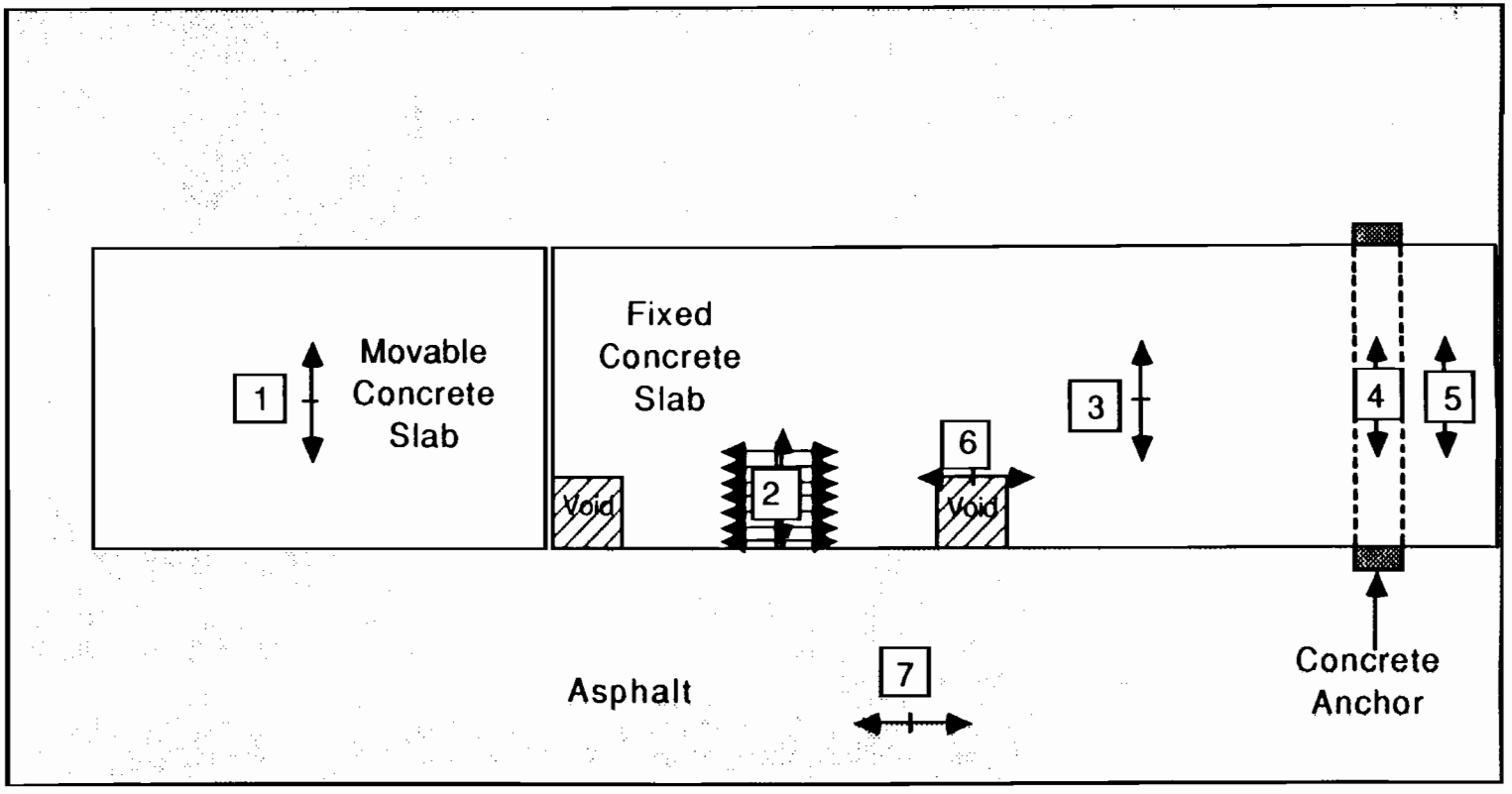

Fig. 3.2. Plan View of SASW Test Locations at the BRC Facility.

on the surface of the asphalt shoulder. These tests were performed over a period from early January, 1986, to February, 1987.

3.3. SIMPLIFIED MATHEMATICAL MODEL FOR A LAYERED SYSTEM WITH DIRECT AND REFLECTED WAVES

No theoretically complete solution yet exists for wave propagation with vertical, horizontal, and oblique boundaries in a layered system which involves all seismic waves. In an attempt to simulate wave propagation problems associated with such kinds of systems, a simplified mathematical model was developed herein. This simplified modeling technique assumes that a true dispersion curve derived solely from direct surface waves is known. The dispersion curve which includes the effects of reflected and/or other direct waves is calculated based on the true dispersion curve by simply adding the influence of any reflected and/or additional direct waves to the true dispersion curve. To evaluate the validity of this approach, modeled dispersion curves are compared to actual dispersion curves measured in the field. After confidence in this model is established with these comparisons, the model is further used to predict the behavior of dispersion curves in other systems of interest. Derivation of the simplified model is discussed next.

Imagine a vertical forcing function is applied at a point on the surface of a layered system, and a pure sine wave with a frequency, f_0, is generated. Two receivers are attached to the surface of the layered system and aligned with the point source to form a lineal array. The receivers are used to track vertical surface motion. Surface waves propagate along the surface in all directions from the source. In addition, reflected waves are created due to the existence of discontinuities in the layered system. As a result, surface (vertical) motion detected by the two receivers is a combination of direct (surface and/or body) waves and reflected (surface and/or body) waves.

Schematic representations of the time records of each receiver are shown in Fig. 3.3. Suppose time signals detected by the two receivers after the surface is excited by this point forcing function are represented by g(t) and h(t), respectively. Then g(t) and h(t) can be expressed by:

$$g(t) = \sum a_{1p} \sin 2\pi f_0 (t - t_{1p}) \tag{3.1}$$

$$h(t) = \sum a_{2q} \sin 2\pi f_0 (t - t_{2q}) \tag{3.2}$$

in which a_{1p} and a_{2q} are amplitudes of various wave arrivals measured by the first and second receivers, respectively, and t_{1p} and t_{2q} are the times of the various wave arrivals at the first and second receivers, respectively. The definitions of a's and t's are shown schematically in Fig. 3.4. In the above and following equations, the subscripts are used to denote a specific wave arrival at a particular receiver. The first subscript is used to denote the receiver number, and the second subscript is used to denote the number of the wave arrival. For example, a_{23} represents the amplitude recorded by the second receiver of the third wave arrival.

Let G(f) and H(f) be the Fourier transforms of g(t) and h(t), respectively. The transforms can then be expressed as:

$$G(f) = \sum_p a_{1p} \exp(-i\ 2\pi f_0 t_{1p}) \quad , \text{for} \quad f = f_0 \tag{3.3a}$$

$$G(f) = 0 \quad , \text{for} \quad f \neq f_0 \tag{3.3b}$$

and

$$H(f) = \sum_q a_{2q} \exp(-i\ 2\pi f_0 t_{2q}) \quad , \text{for} \quad f = f_0 \tag{3.4a}$$

$$H(f) = 0 \quad , \text{for} \quad f \neq f_0 \tag{3.4b}$$

The cross power spectrum, G_{yx}, for this pair of time signals is defined as:

$$G_{yx} = G^* \times H \tag{3.5}$$

in which G* denotes the complex conjugate of G. The phase of the cross power spectrum at frequency f_0, $\phi(f_0)$, is:

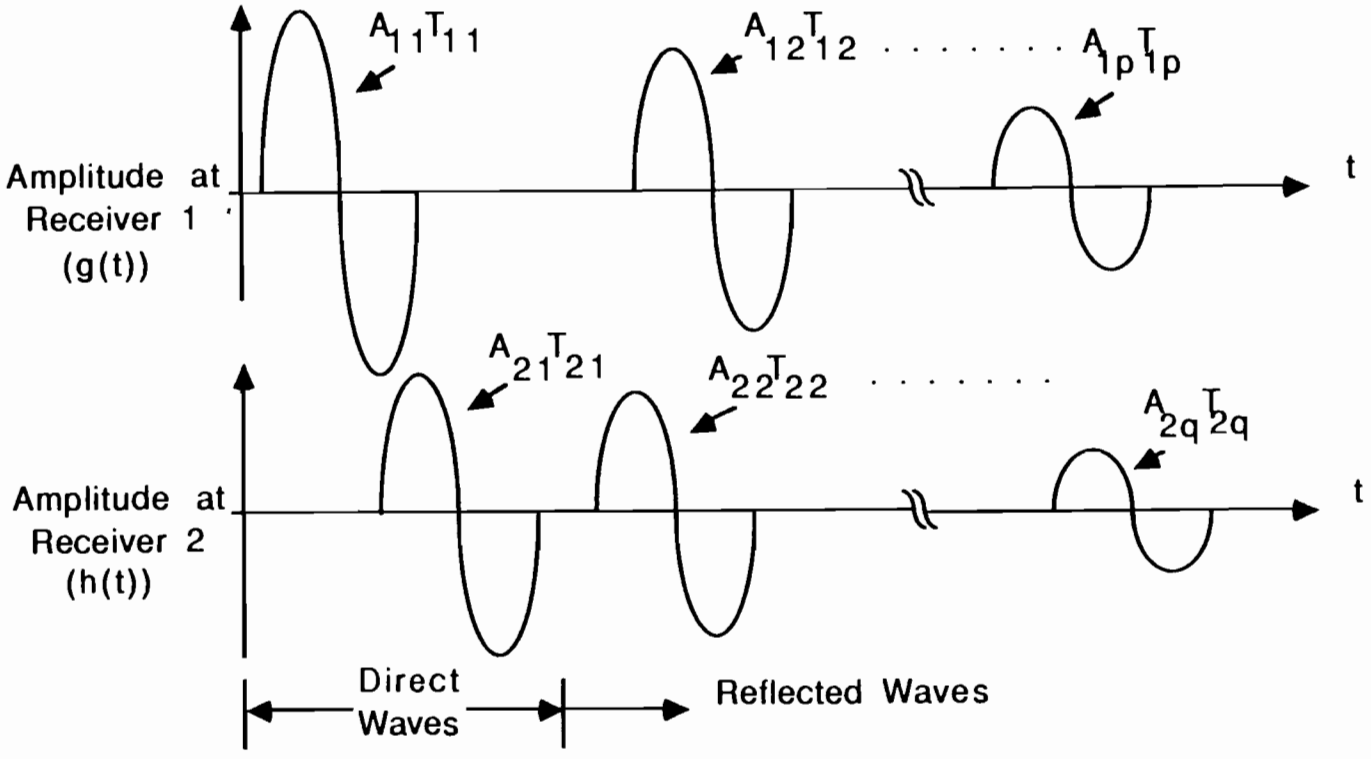

Fig. 3.3. Representation of Time Domain Records Illustrating Combined Direct and Reflected Waves Monitored by Each Receiver in SASW Testing.

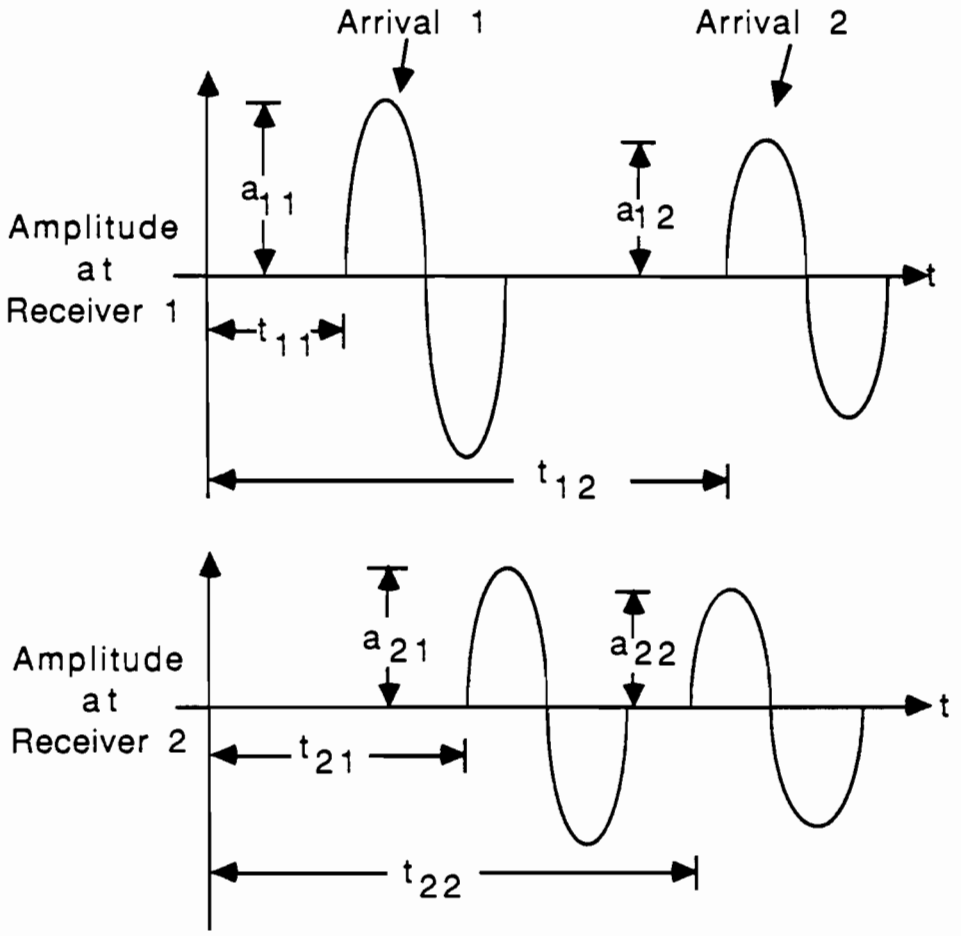

Fig. 3.4. Representations of Amplitudes (a's) and Arrival Times (t's) for Two Wave Arrivals At Each Receiver.

$$\phi(f_0) = \mathrm{Tan}^{-1}\left[\frac{\sum_p \sum_q a_{1p}\, a_{2q} \sin 2\pi f_0 (t_{1p} - t_{2q})}{\sum_p \sum_q a_{1p}\, a_{2q} \cos 2\pi f_0 (t_{1p} - t_{2q})}\right] \tag{3.6}$$

In a real SASW test, a wide range of frequencies is generated simultaneously by applying a vertical impact on the surface of the system. As a result, each arrival is no longer a single-frequency arrival but contains a certain range of frequencies. Since Eqs. 3.1 through 3.6 were derived with the consideration of only a single frequency, the following modifications are made so that they can be applied to the multiple-frequency condition. Assume while f_0 varies over a range of frequencies generated by the vertical impact, values of a_{1p}, a_{2q}, t_{1p}, t_{2q} vary accordingly. Let A_{1p}, A_{2q}, T_{1p}, and T_{2q} be the amplitude and time functions of frequency at receivers 1 and 2, respectively. Therefore, the functions can be written as:

$$A_{1p}(f) = a_{1p}(f_1) + a_{1p}(f_2) + a_{1p}(f_3) + \ldots\ldots \tag{3.7}$$

$$A_{2q}(f) = a_{2q}(f_1) + a_{2q}(f_2) + a_{2q}(f_3) + \ldots\ldots \tag{3.8}$$

$$T_{1p}(f) = t_{1p}(f_1) + t_{1p}(f_2) + t_{1p}(f_3) + \ldots\ldots \tag{3.9}$$

$$T_{2q}(f) = t_{2q}(f_1) + t_{2q}(f_2) + t_{2q}(f_3) + \ldots\ldots \tag{3.10}$$

in which the notations for each subscript of T's and A's as well as t's and a's are the same as previously defined and frequencies, f_1, f_2, f_3, etc. are the desired modeling frequencies. Hence, Eq. 3.6 can be rewritten as:

$$\phi(f) = \mathrm{Tan}^{-1}\left[\frac{\sum_p \sum_q A_{1p}(f)\, A_{2q}(f) \sin 2\pi f [T_{1p}(f) - T_{2q}(f)]}{\sum_p \sum_q A_{1p}(f)\, A_{2q}(f) \cos 2\pi f [T_{1p}(f) - T_{2q}(f)]}\right] \qquad (3.11)$$

Each A, with two subscripts, is a series of amplitudes which are a function of frequency and correspond to the particular arrival denoted by the subscripts. The absolute value of A actually represents the amplitude of the linear spectrum for this particular arrival. Each T, with two subscripts, is a series of travel times which are a function of frequency and correspond to the particular arrival denoted by the subscripts. It is necessary to note that the connotation of "arrival" used in Eq. 3.6 is somewhat different than that used in Eq. 3.11. In Eq. 3.6, each "arrival" has energy at only one frequency. On the other hand, in Eq. 3.11, each "arrival" represents a packet of energy containing a range of frequencies. Since Eq. 3.6 is a special case of Eq. 3.11 and the latter was used for all studies, the second connotation of "arrival", namely a packet of energy over a range of frequencies, is used herein.

It is important to notice that both T's and A's are functions of frequency and each arrival has its own T and A. Since T is directly related to the arrival times of different frequencies forming the arrival of a particular packet of energy, dispersive characteristics (that is, waves corresponding to different frequencies traveling at different velocities) of this particular arrival can be accurately modeled by using the proper travel time in "T" for each frequency. In addition, since the arrival of each packet of energy has its own T, waves with different dispersive characteristics can be analyzed together; that is to say, each arrival could have its own dispersion curve. A typical need of modeling waves with more than one type of dispersive characteristic is in the case when combined surface wave and body wave effects are considered. Examples of this type of modeling are illustrated in Chapter Five.

The amplitude of the linear spectrum, A, for the arrival of each impulse (packet of energy) is simply a measure of the amplitudes of the different frequencies transmitted by this packet of energy. Therefore, the value of A is directly related to the damping characteristics and reflection coefficients of the system being testing. Due to the fact that the arrival of each impulse has its own A, amplitudes of different frequencies which attenuate at different rates can be modeled by

using different ratios of amplitudes between different arrivals of the impulse at different frequencies.

It is assumed, in the present inversion process in SASW testing, that only plane surface waves exist. As a result, it is implicitly assumed that only one surface arrival is detected by the receivers. Let T_{11} and T_{21} be the arrival times of this direct surface wave at each receiver. The corresponding phase of the cross power spectrum, $\phi(f)$, can be expressed as:

$$\phi(f) = 2 \pi f [T_{11}(f) - T_{21}(f)] \tag{3.12}$$

Equation 3.12 is just a special case of Eq. 3.11 with p and q both equal to 1. (This point is discussed in detail in Section 3.4.) Also notice that in Eq. 3.11, it is not necessary to have T_{11}, T_{21}, A_{11}, and A_{21} associated with the arrival of the direct surface wave. In fact, arrivals in Eq. 3.11 can be considered in any random order. However, to avoid any possible confusion, T_{11}, T_{21}, A_{11}, and A_{21} are used to represent only direct surface wave arrivals for all discussions presented from now on.

The problem faced in typical SASW testing in terms of reflections is now clear. In the field, measured phases of cross power spectra are in the fashion of Eq. 3.11, but during the in-house inversion stage, the phases of cross power spectra are assumed to be in the fashion of Eq.3.12. The difference between these two equations is the error introduced by waves other than the direct surface wave. As such, it is possible to study the influence of reflected and direct waves on field dispersion curves by using Eqs. 3.11 and 3.12.

3.4. MATHEMATICAL MODELING PROCEDURE

A typical modeling of disturbances caused by reflected surface waves on the dispersion curve proceeds as follows. After a field test is performed, the field dispersion curve, which is a plot of wave velocity versus wavelength or wave velocity versus frequency, is calculated and plotted. This dispersion curve includes the effects of reflected waves combined with direct waves in almost all cases (as represented by Eq. 3.11). A "true" or "correct" dispersion curve, which includes only the direct surface wave (as represented by Eq. 3.12), is estimated from the field dispersion curve. This estimate is usually make by drawing a smooth curve through the field dispersion curve and neglecting most of the small ripples in the curve.

By knowing the distances between the source and the two receivers, T_{11} and T_{21} in Eqs. 3.11 and 3.12 can be found from the true dispersion curve. The times T_{11} and T_{21} simply

represent the travel times for direct surface waves corresponding to each frequency. These times equal the lengths of the travel paths for each direct surface wave divided by the corresponding wave velocity.

Next, by knowing the lateral and vertical geometrical configuration of the layered system and the locations of the source and receivers, all possible or interesting ray paths for reflected or direct waves can be found. The length of each ray path can be calculated. T's for wave travel along each ray path can be calculated for all frequencies by dividing the length of travel for each individual arrival by its corresponding wave velocity which is a function of the dispersive characteristic pertinent to each arrival. In the process of calculating these travel times (T's), surface waves and body waves are handled differently. For reflected surface waves, it is assumed that they have the same dispersive characteristics as the direct surface wave; that is, even though each surface wave arrival could have its own dispersion curve, this curve is assumed to be the same as the "true" dispersion curve. Body waves, on the other hand, are assumed to be nondispersive; that is, waves at all frequencies travel with the same velocity. Hence, T's for body waves are not a function of frequency. This also implies that the dispersion curve for body waves has a constant wave velocity through out all frequencies or all wavelengths. The assumption of constant body wave velocity is illustrated in Fig. 3.5.

The selection of the proper body wave velocities becomes an important aspect of this problem. In general, for those cases when body waves are propagating along the surface, a Poisson's ratio is selected, and body wave velocities are derived from the surface wave velocity since there is a unique relationship between surface wave velocity and body wave velocity at each Poisson's ratio. If, however, body waves travel through different material layers, an "average" velocity is selected. The selection of this "average" wave velocity is rather crude. Usually the velocity of the thickest layer (from a material properties profile derived by the inversion process) is used as the first approximation. In addition, for body waves traveling through a layered system, the ray paths will not be straight lines due to refraction, but they are modeled as straight lines in this study to reduce the complexity. The selection of body wave velocities combined with the assumption of straight ray paths through different layers probably introduces a small error in modeling the effect of body waves. However, instead of precise quantitative modeling, this approach serves more as a qualitative projection.

After all T's are calculated, the last step is to determine values for all amplitudes. A's in the field data represent the amplitude of the velocity or acceleration measured by the receivers for each arrival at every frequency. It is very difficult to determine the true values for all A's because

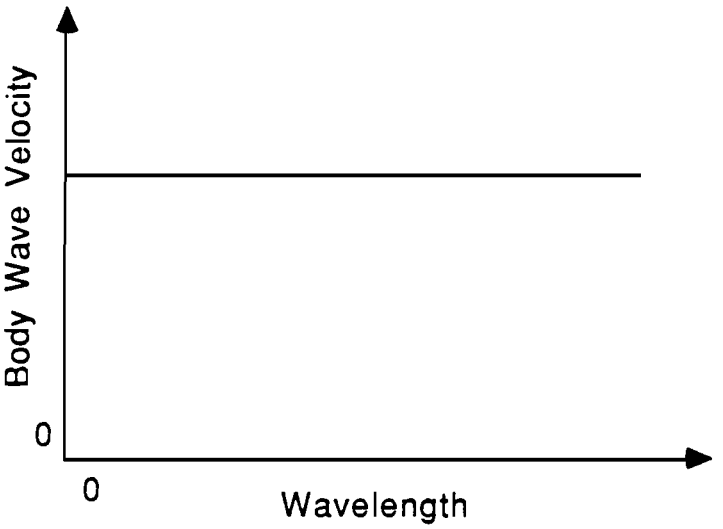

Fig. 3.5. Body Wave Dispersion Curve (Constant Body Wave Velocity) Used in the Mathematical Model.

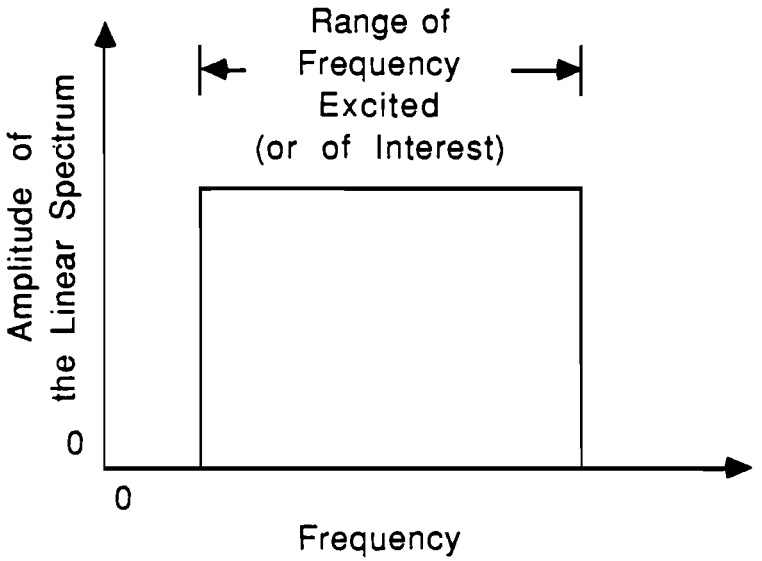

Fig. 3.6. Constant Amplitude of the Linear Spectrum (A's) Used in the Mathematical Model.

it is only possible in the field to measure the amplitude of velocity or acceleration caused by the summation of all arrivals at a particular time. There is no practical method to decompose this summation into the original components contributed by each arrival.

As a result of the difficulty outlined above, the same value of A is used for each initial arrival. This means that the A's are modeled as frequency independent. The concept of frequency independent amplitude is illustrated in Fig. 3.6. In addition, the amplitude for each arrival is more or less randomly selected except that the amplitude corresponding to a longer travel path is always smaller than the amplitude corresponding to a shorter travel path. This selection of the value of A's is inappropriate when the receivers used in the test have very different sensitivities or when time signals from different channels are amplified differently before they are recorded by the waveform analyzer.

As an example of an arrival with a longer travel path yet an arrival which exhibits a large amplitude, imagine a test arranged in such a way that receiver 1 and receiver 2 are 1 ft (0.3 m) apart and receiver 2 is 100 times more sensitive than receiver 1. Suppose a wave arrival reaches receiver 1 before it reaches receiver 2, and this arrival has a real amplitude of 10 units when it reaches receiver 1 but has a real amplitude of only 5 units when it reaches receiver 2. Also assume that the reduction of amplitude is caused by damping. Due to the different sensitivities of these two receivers, the amplitudes recorded on channel 1 and channel 2 will be 10 (10×1) units and 500 (5×100) units, respectively. As a result, the waveform analyzer "sees" that the same wave arrival has an amplitude of 10 units when it reaches receiver 1, and after it travels another 1 ft (0.3 m), its amplitude has increased to 500 units. Consequently, proper amplitudes (10 and 500 units) should be used in Eq. 3.11 to model the field dispersion curves if the model is to represent field data. In short, A's used in Eq. 3.11 should be the amplitudes of time signals that are recorded by the waveform analyzer, not the real physical amplitudes of each arrival traveling in the system (unless, of course, the real amplitudes are to be modeled). Therefore, it is necessary to know the field equipment arrangement when A's are selected. Fail to do so could result in erroneous velocity (or phase) fluctuations which are not representative of the field dispersion curve recorded by the waveform analyzer. More detailed discussion of the influence of amplitudes on the dispersion curve is presented at the end of this section.

Since all field studies presented herein use two similar receivers with the same amplification, the difference between their sensitivities should be within a few percent. Consequently, the assumption that arrivals with longer travel distances have smaller amplitudes is valid in most cases.

As an aside, the amplitudes of time signals have never been considered in the past for any SASW tests. In some cases when spacing between receivers were very large (on the order of 50 to 100 ft (15 to 30 m)), signals monitored by the receiver far from the source usually were too small to be compared to the signals monitored by the receiver near to the source. Different magnitudes of amplification were applied to each receiver so that the amplitudes of the time signals recorded by each channel of the spectral analyzer were within a similar range. It was assumed that the amplitudes of the time signals input to the spectral analyzer had no effect on phase information. A close inspection of Eq. 3.11 indicates that one has to be very cautious in making this assumption.

Assume there are only direct surface waves arriving at the receivers. In Eq. 3.11, this means that only one term inside the summation sign exists, or p = 1 and q = 1. Equation 3.11 then becomes:

$$\phi(f) = \mathrm{Tan}^{-1}\left[\frac{A_{11}(f)\,A_{21}(f)\sin 2\pi f\,[\,T_{11}(f) - T_{21}(f)\,]}{A_{11}(f)\,A_{21}(f)\cos 2\pi f\,[\,T_{11}(f) - T_{21}(f)\,]}\right] \tag{3.13}$$

The terms $A_{11}(f)A_{12}(f)$ in Eq. 3.13 appear in both the numerator and denominator and cancel out. As a result, Eq. 3.13 becomes Eq. 3.12, and amplitude has no effect on the phase of the cross power spectrum. However, suppose a reflection is detected only by receiver 1. Then p and q in Eq. 3.11 become 2 and 1, respectively, and Eq. 3.11 becomes:

$$\phi(f) = \mathrm{Tan}^{-1}\left[\frac{A_{11}(f)\,A_{21}(f)\sin 2\pi f\,[\,T_{11}(f) - T_{21}(f)\,] + A_{12}(f)\,A_{22}(f)\sin 2\pi f\,[\,T_{12}(f) - T_{22}(f)\,]}{A_{11}(f)\,A_{21}(f)\cos 2\pi f\,[\,T_{11}(f) - T_{21}(f)\,] + A_{12}(f)\,A_{22}(f)\cos 2\pi f\,[\,T_{12}(f) - T_{22}(f)\,]}\right] \tag{3.14}$$

Note that in Eq. 3.14, the numerator represents one summation over all arrivals and the denominator represents a second similar summation.

It is impossible for A's in Eq. 3.14 to cancel unless $A_{11}(f)A_{21}(f)$ equals $A_{12}(f)A_{21}(f)$ which is very unlikely. As a result, the effect of amplitude can be neglected only when direct

surface waves are measured without any influence of other reflected surface waves or body waves.

Another important factor that has to be considered in selecting A's is the corresponding characteristics of the reflecting boundaries. It is known that a reflected wave from a free boundary will have particle displacements in-phase with the incident wave. Thus, A's used for such reflected waves have to bear the same sign as incident waves. The reflected wave from a fixed boundary, on the other hand, will generate particle motions 180 degrees out-of-phase with the incident wave. Thus, A's used for such reflected waves have to bear the opposite sign of the incident waves. For example, if a positive sign is used for all A's in the incident waves, a positive sign should be used for all A's of waves reflected from free boundaries and a negative sign should be assigned to all A's of waves reflected from fixed boundaries. In pavement testing, there is no such thing as a rigid boundary in the writer's experience.

After all necessary amplitudes (A's) are selected, it is possible to calculate the modeled dispersion curves by employing Eq. 3.12.

Reflected waves, in general, create (or impose) ripples in the folded phase plots and the dispersion curves. The error introduced by improper selection of A's and T's can be characterized as follows. The locations (on the frequency axis or wavelength axis) of ripples are controlled by times (T's). Erroneous T's can shift the locations of the imposed ripples away from their proper locations. However, T's have no effect on the amplitudes of the ripples. On the other hand, wave amplitudes (A's) act quite differently in that they affect the amplitudes of the ripples. Different values of A's lead to different amplitudes in the ripples, but they never change the locations of those ripples.

In most studies conducted so far for reflected waves, T's were much better estimated than A's. As a result, it is important to keep in mind that the locations of the imposed ripples on the phase and dispersion curves are usually better modeled than the amplitudes of those ripples.

3.5. EXAMPLE OF FIELD DISPERSION CURVE AFFECTED BY ONE REFLECTED SURFACE WAVE

A simple example is given here to illustrate the use of the equations and procedures outlined above. This example models a field test performed at the BRC research facility on January 3, 1986. The test was performed on the north end of the concrete slab at location 4 shown in Fig. 3.2. A detailed layout of this test is shown in Fig. 3.7. Three near-by reflecting boundaries are denoted as A, B, and C, as shown in Fig. 3.7. Receivers were placed with a 4-ft

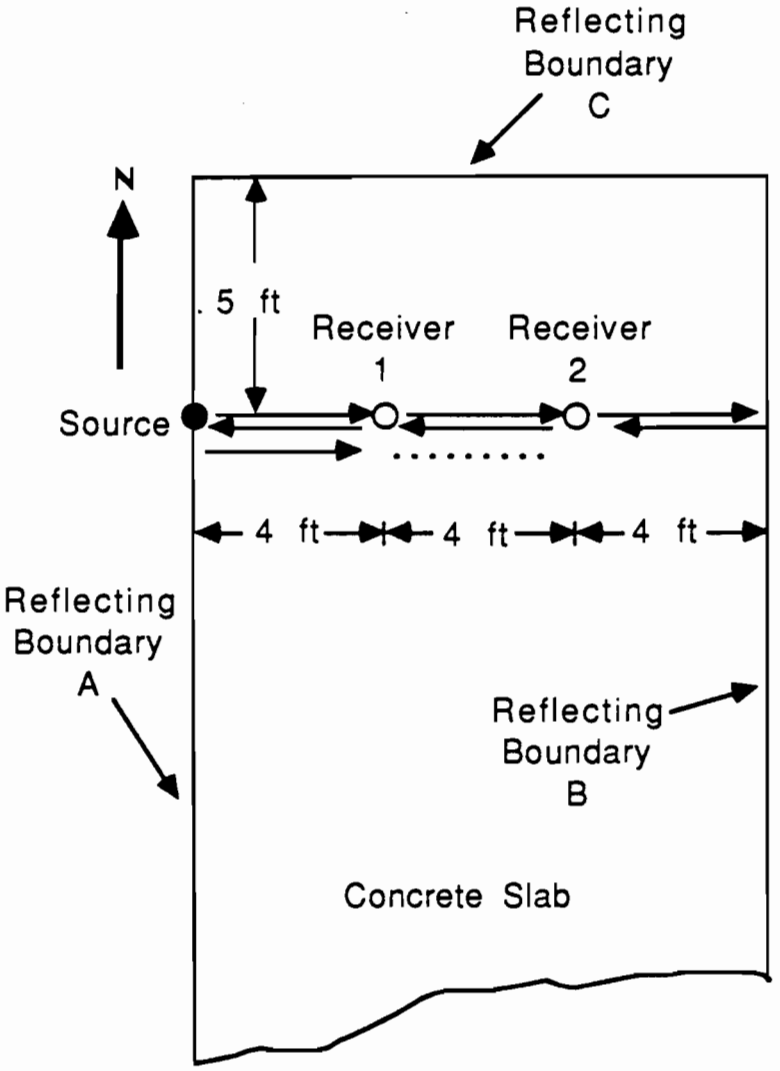

Fig. 3.7. Detailed Layout of SASW Testing at Location 4.

(122 cm) spacing between them, and each one was 4 ft (122 cm) away from the nearest reflecting boundary. The source was placed at the edge of reflecting boundary A. Assume the existence of reflecting boundary C can be neglected.

As soon as the source generates a pulse, this pulse starts to travel from the source to receiver 1 and then receiver 2 and finally reaches reflecting boundary B. Before this pulse reaches reflecting boundary B, it is considered as a direct wave. After the pulse reaches reflecting boundary B, it will reflect back and be considered a reflected wave from now on. The reflected pulse will travel past receiver 2 and then receiver 1 and finally reach reflecting boundary A. It will then be reflected by boundary A and head towards reflecting boundary B. The pulse will eventually be bounced back and forth by reflecting boundaries A and B until all energy is dissipated. Typical field time records for this site are shown in Fig. 3.8. The reflected surface waves detected by each receiver can easily be identified and are indicated by the arrows shown in the figure.

To simplify this example, the effect of reflecting boundary C is neglected and only the first reflected wave from boundary B is considered. By following the procedure outlined earlier, the field dispersion curve is plotted first. The field curve is shown by the solid line in Fig. 3.9. The "true" dispersion curve for this case should look like the smooth dashed line drawn through the dispersion curve in Fig. 3.9. From Fig. 3.7, the distances that a direct pulse travels from the source to receiver 1 and receiver 2 are 4 and 8 ft (122 and 244 cm), respectively. Since the "true" dispersion curve is known (Fig. 3.9), $T_{11}(f)$, $T_{21}(f)$ and "true" phase corresponding to each frequency can be calculated. The "true" phase derived from this "true" dispersion curve is shown in Fig. 3.10a, and the corresponding "true" dispersion curve (which has been shown in Fig. 3.9) is shown in Fig. 3.10b.

It is interesting to notice that although there is a significant wave velocity change in the dispersion curve shown in Fig. 3.10b at a wavelength of about 2 ft (61 cm), the change is barely observed in the phase of the cross power spectrum (corresponding to Fig. 3.10a when the frequency is smaller than about 4000 Hz.). This point illustrates one serious difficulty currently encountered in field SASW testing. By observing only phases of cross power spectra displayed on a waveform analyzer, it is generally difficult, if not impossible, to "see" wave velocity changes at depth at the test site. Fortunately, this problem has recently been solved by interfacing a minicomputer with the waveform analyzer to calculate and display the dispersion curve right at the test site after the data are collected. From Fig. 3.7, the first reflected pulse detected by receiver 1 is the one which travels from the source to reflecting boundary B and then back to receiver 1.

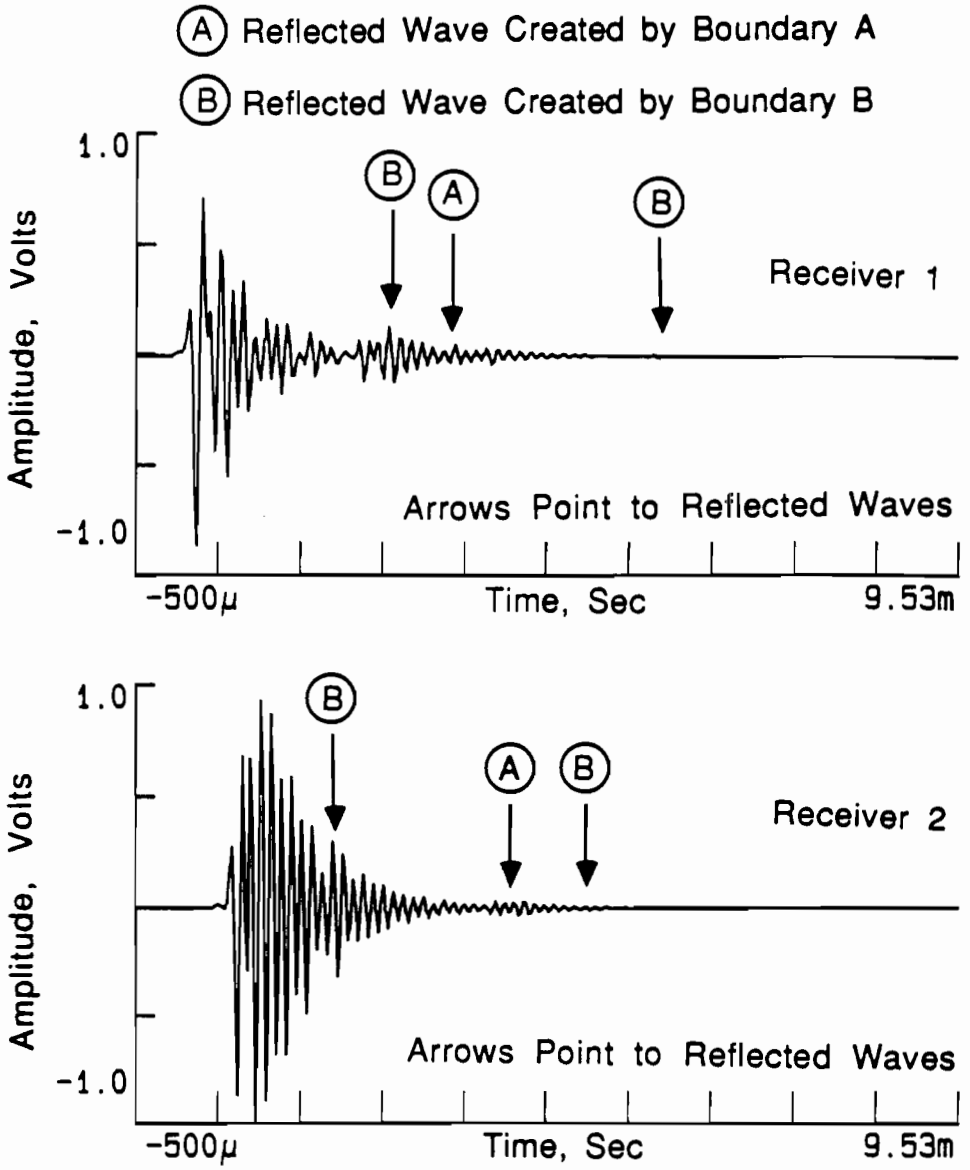

Fig. 3.8. Typical Time Records Illustrating Direct and Reflected Surface Waves for Test Arrangement Shown in Fig. 3.7.

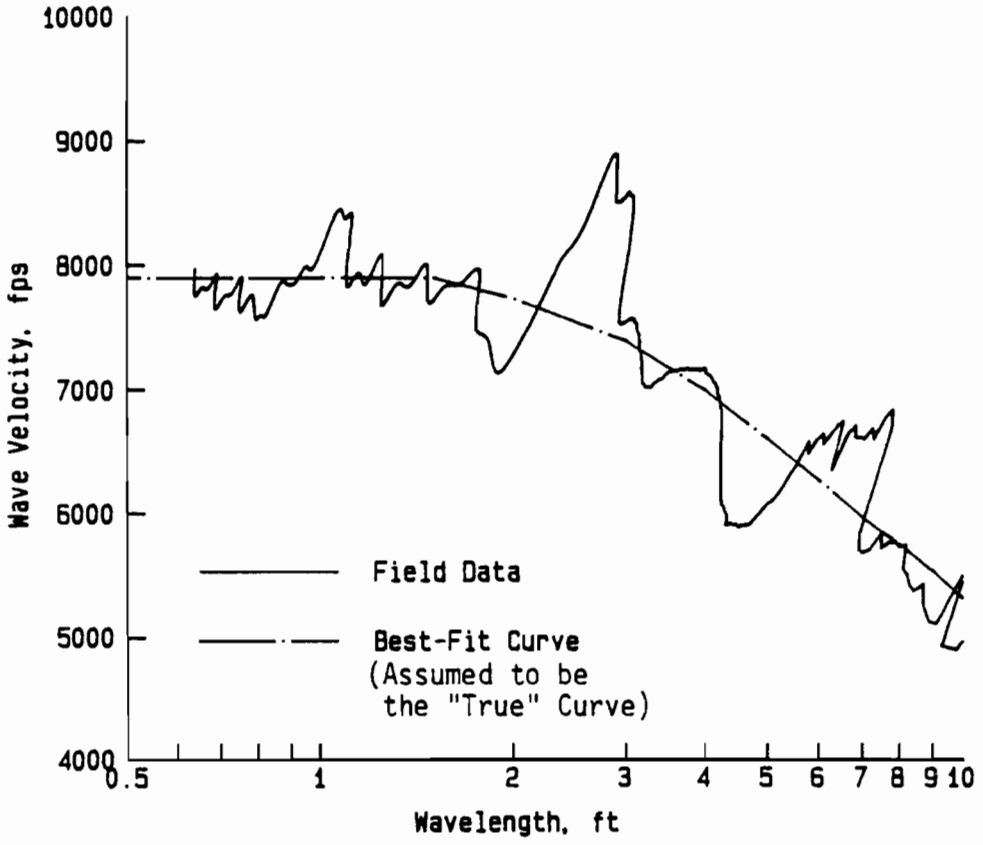

Fig. 3.9. Comparison of Field (Measured) Dispersion Curve with the Dispersion Curve ("True") for No Reflections.

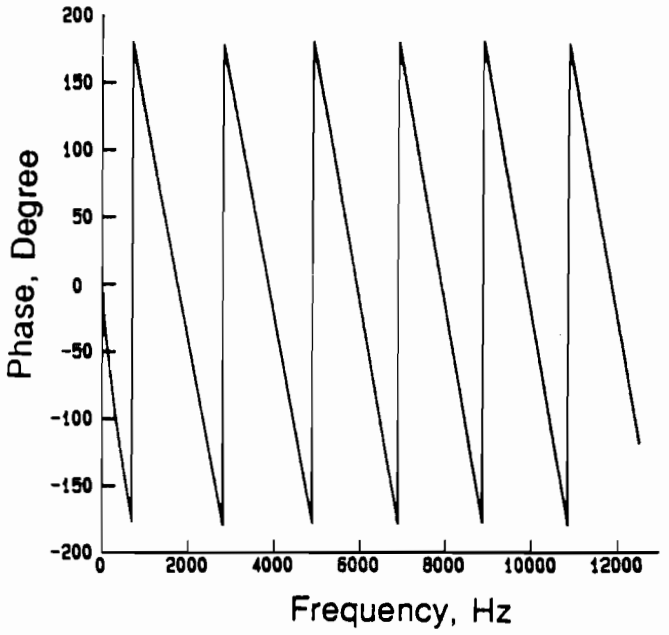

a. Phase of Cross Power Spectrum for 4-ft Receiver Spacing

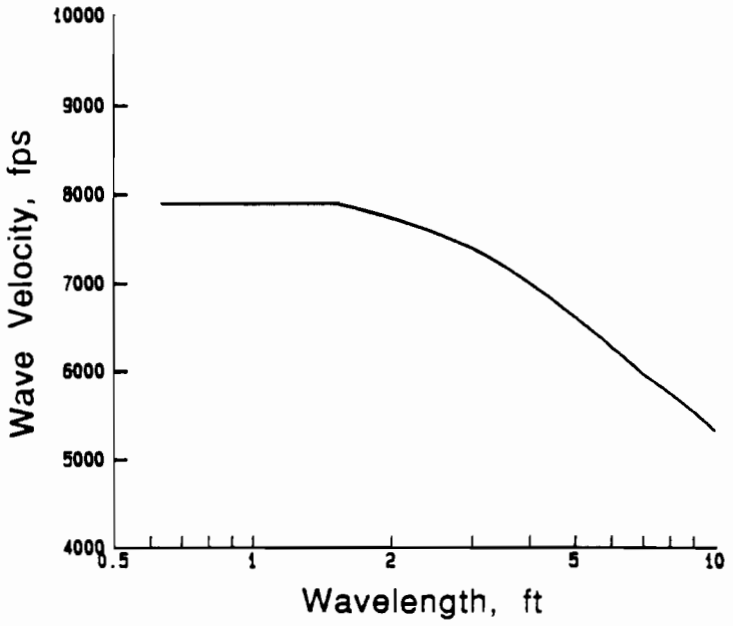

b. Dispersion Curve Associated with Phase Shown Above

Fig. 3.10. "True" Phase of the Cross Power Spectrum and Corresponding "True" Dispersion Curve for Test Arrangement Shown in Fig. 3.7.

The distance of travel for this pulse is 20 ft (6.1 m). By the same token, the first reflected pulse detected by receiver 2 is the one which travels from the source to reflecting boundary A and then back to receiver 2. The distance of travel for this pulse is 16 ft (4.9 m). Based on this information and by assuming that reflected surface waves have the same dispersive characteristics (same dispersion curve shown in Fig. 3.10b) as direct surface waves, it is possible to calculate $T_{12}(f)$ and $T_{22}(f)$ at all frequencies for both reflected waves.

Reflecting boundary B represents a free boundary at the edge of the concrete pavement. Therefore, reflected waves should have displacements in-phase with direct waves. (All A's should have the same sign.) The amplitudes for each impulse detected by receiver 1, $A_{11}(f)$ and $A_{12}(f)$, are assumed to be 1.0 and 0.36, respectively. The amplitudes detected by receiver 2, $A_{21}(f)$ and $A_{22}(f)$, are assumed to be 0.9 and 0.4, respectively. The relative magnitudes of the amplitudes used for the direct and reflected surface waves are more or less in the same order as shown in Fig. 3.8. However, it is not correct to use the exact amplitudes measured from the time records shown in Fig. 3.8 because reflected waves tend to overlap with the direct waves and with other reflected waves. As a result, their real amplitudes are distorted. All needed information is complete at this point, and the modeled dispersion can be calculated by using Eq. 3.11.

Comparison of the modeled and measured phases of the cross power spectrum is shown in Fig. 3.11. Comparison of the modeled and field dispersion curves is shown in Fig. 3.12. These two comparisons indicated that Eq. 3.11 is quite capable of modeling the fluctuations (ripples) that appear in the field data. The amplitudes and locations of the modeled ripples are some what different but close to the field data. The similarity of modeled and field data give strong support to the modeling process discussed earlier. It also seems that even though the lack of knowledge about amplitudes of all arrivals led to crude estimates of A's in Eq. 3.11, the model still generated a dispersion curve which is similar to the field data.

It is also interesting to note that all ripples in the modeled phase (Fig. 3.11) have very similar amplitudes, but the amplitudes of the ripples in the dispersion curve (Fig. 3.12) have an increasing trend as wavelength increases. This same phenomenon is found in the field data. In fact, past experience indicates that this phenomenon commonly exists in most field data. This is due to the fact that when the phase of the cross power spectrum is translated to the dispersion curve, any disturbance in the high-frequency range, which corresponds to the short-wavelength range, is deamplified. Any disturbance in the low-frequency range, on the other hand, corresponds to the long-wavelength range and is amplified. As a result, disturbances in the low-frequency range cause more problems than disturbances in the high-frequency range. In terms of

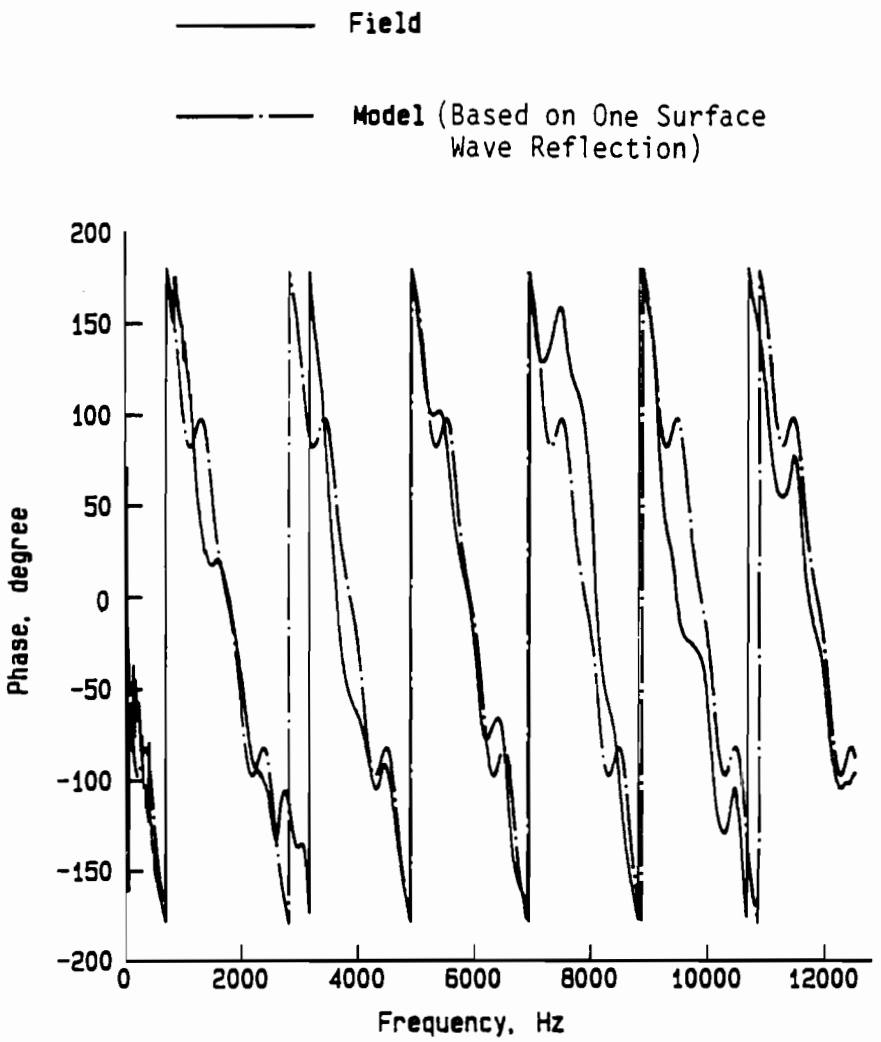

Fig. 3.11. Comparison of Field and Modeled Phases of the Cross Power Spectrum.

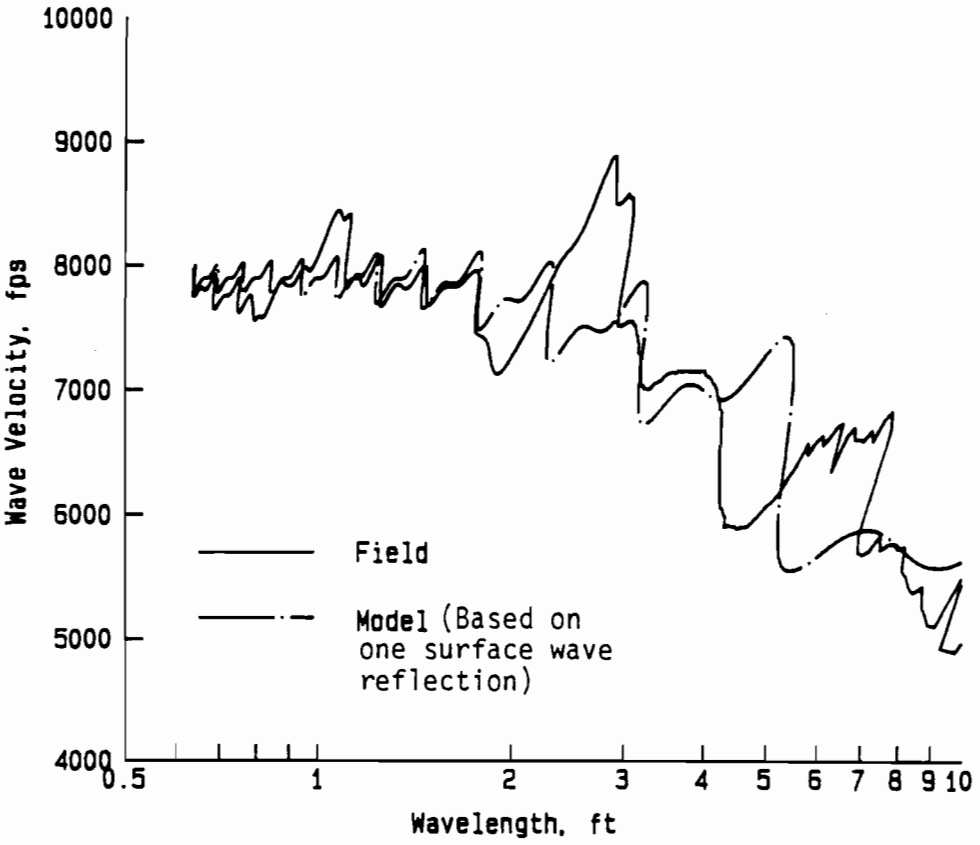

Fig. 3.12. Comparison of Field and Modeled Dispersion Curves.

sampling depth, short wavelengths sample shallow depths. Therefore, material properties sampled at shallow depths are less sensitive to disturbances caused by reflected surface or body waves. This material sampling characteristic of the SASW method is very critical and is used to determine the near-surface material properties as discussed in Chapter Eight.

3.6. SUMMARY

A mathematical model was developed for the purpose of studying the effects of reflected surface waves and/or direct and reflected body waves on dispersion curves. The derivation of this mathematical model and its usage are discussed in detail in this chapter. An example simulation is also presented to develop a better understanding about the application of this model. The modeled and field dispersion curves agree very well in this example which lends credibility to the model. The model is further used in Chapters Four and Five for more sophisticated modeling of reflected surface waves (Chapter Four) and of direct and reflected body waves (Chapter Five).

CHAPTER FOUR

EFFECT OF REFLECTED SURFACE WAVES ON DISPERSION CURVES

4.1. INTRODUCTION

The existence of reflected surface waves created by discontinuities, such as joints or edges of a pavement system, is inevitable. As a result, an understanding of the effect of reflected surface waves on field dispersion curves is necessary and important. With this knowledge, possible limitations imposed on the SASW method by reflected surface waves can be better understood, and methods for identifying and avoiding their effect can be developed.

The study presented in this chapter is divided into three major subjects: 1. the effect of reflected surface waves from a vertical reflecting boundary oriented perpendicularly to the source/receiver array, 2. the effect of reflected surface waves from a vertical reflecting boundary oriented parallel to the source/receiver array, and 3. the effect of distance between a vertical reflecting boundary and the source/receiver array. Model and experimental studies were performed on all subjects, with the exception that no model study was performed on the effect of distance between the source/receiver array and a vertical reflecting boundary oriented perpendicularly to this array. This problem is directly related to the damping (not geometry) of the system and is outside the scope of the simplified mathematical model.

All experimental work was performed on the concrete pavement at the BRC research facility (White et al, 1984). The thickness of this concrete pavement is 10 in. (25 cm). (A more complete description of the facility is given in Chapter Nine.) Surface wave reflections are created mainly by the edges (and a joint) of this concrete pavement.

4.2. VERTICAL BOUNDARY ORIENTED PERPENDICULARLY TO TEST ARRAY

The first case studied is the case of reflected waves created by a vertical boundary when the source/receiver array is oriented perpendicularly to the reflecting boundary. A good example of this situation is when SASW testing is performed in the wheel path near a joint in concrete pavement. Initially, a qualitative description of the problem is presented so that the general phenomenon is more easily understood and recognized.

4.2.1. Creation of Reflected Surface Waves

When the SASW array is oriented perpendicularly to a vertical reflecting boundary, the source can be located either on the same side or on the opposite side of the receiver relative to the boundary. In the case when the source and reflecting boundary are on the same side of the receivers as shown in Fig. 4.1, reflected waves travel in the same direction as direct waves when they reach the receivers. On the other hand, when receivers are placed between the source and reflecting boundary as shown in Fig. 4.2, reflected waves travel in the opposite direction to the direct waves when they reach the receivers.

One can imagine that the most detrimental arrangement for phase measurements is the case when the receivers are placed between the source and the reflecting boundary. Under this condition, reflected surface waves travel in exactly the opposite direction as direct surface waves. Therefore, reflected waves arrive at receiver 2 before they arrive at receiver 1 as illustrated in Fig. 4.3. On the other hand, when the source is placed between the receivers and reflecting boundary, reflected waves and direct waves propagate in the same direction. Therefore, reflections in the time record are simply a repeat of the relative times of the direct waves as shown in Fig. 4.4. Theoretically, the existence of the boundary under this condition (Fig. 4.4) has no influence because reflected waves combine with direct waves in such a manner that the combination can be treated as one incoming wave. As long as the time record has sufficient duration for both receivers to capture all waves, the combined reflected and direct surface waves can be considered as one direct wave with simply a longer duration.

4.2.2. Field and Model Studies

To verify the explanations discussed above as well as to study the effect of the distance between the reflecting boundary and the test array, field experiments were designed and performed at location 2 of the BRC facility shown in Fig. 3.2. Typical tests were carried out in the following manner.

1. Fixed spacings between the source and the first receiver and between the two receivers were selected. In all cases, these two spacings were kept equal.
2. With a given spacing, the whole array was moved along an axis perpendicular to the edge of the concrete slab. Hence, the distance from the boundary to the array was varied.
3. After the set of tests in Step 2 was completed, another spacing for the source and receivers was selected, and the whole array was again moved along the same axis.

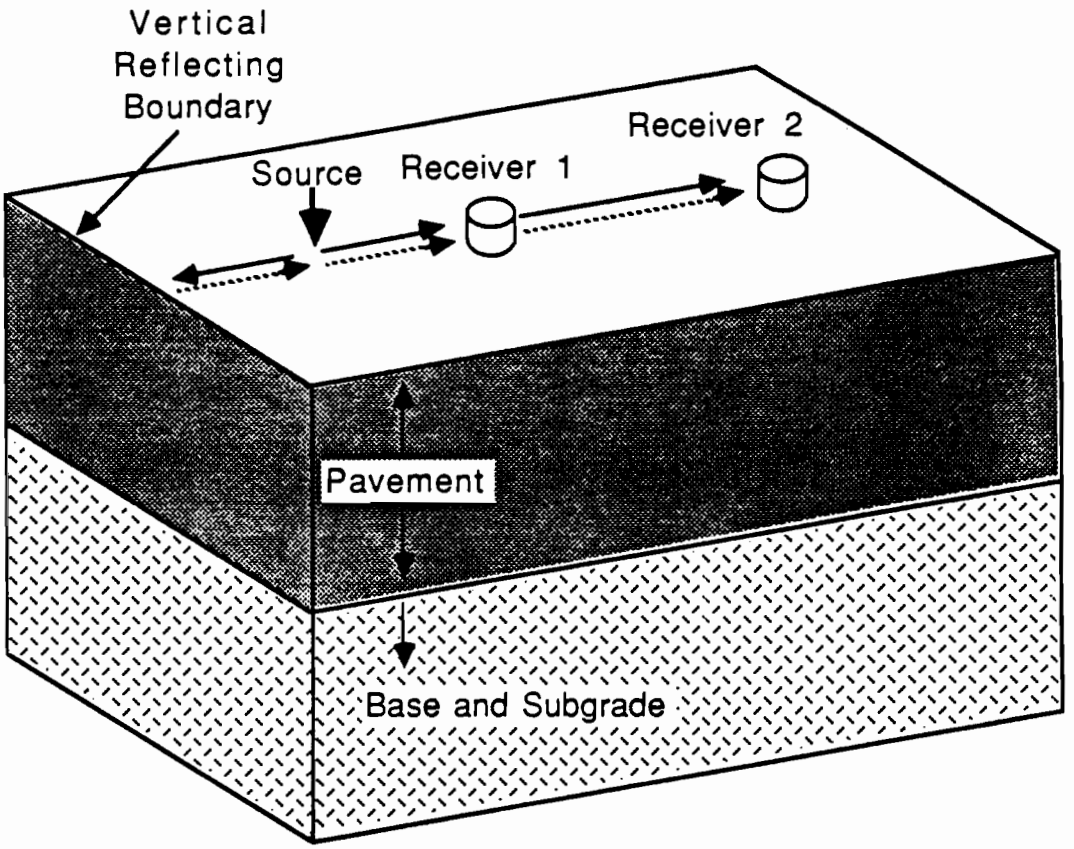

Fig. 4.1. Direct and Reflected Surface Waves Created During SASW Testing with Source Placed Between Receivers and Vertical Reflecting Boundary.

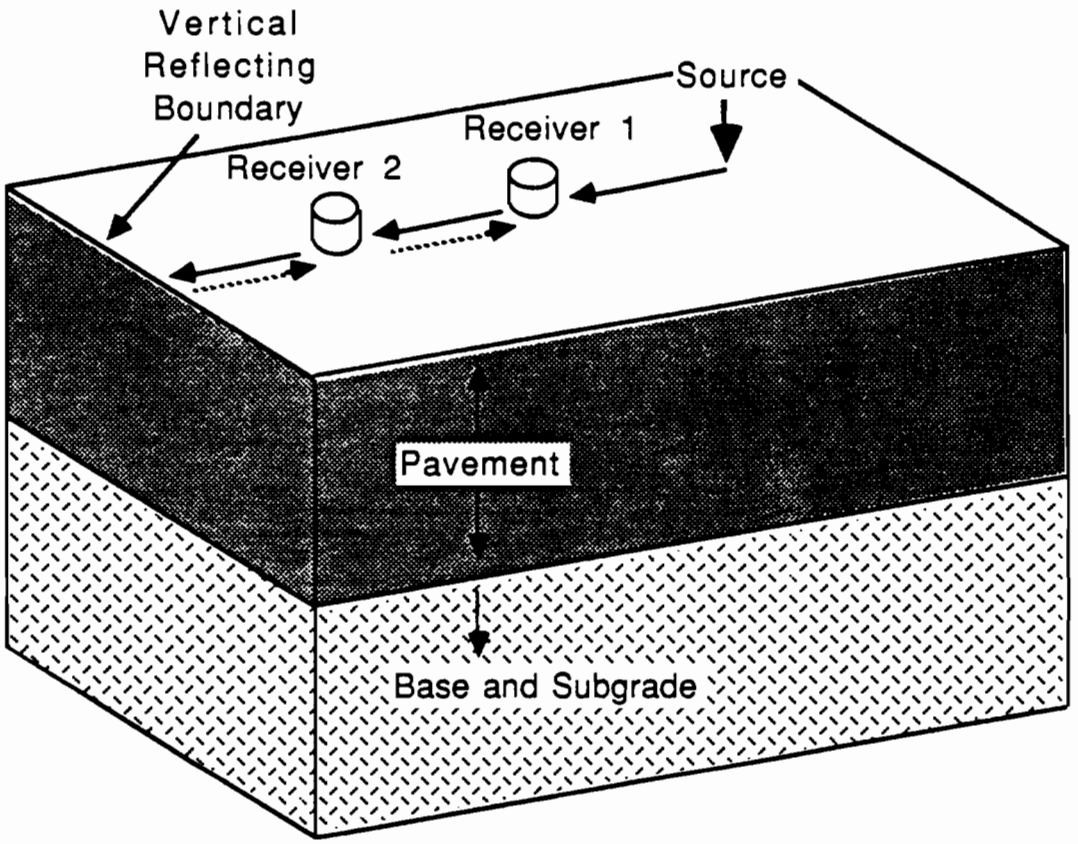

Fig. 4.2. Direct and Reflected Surface Waves Created During SASW Testing with Receivers Placed Between Vertical Reflecting Boundary and Source.

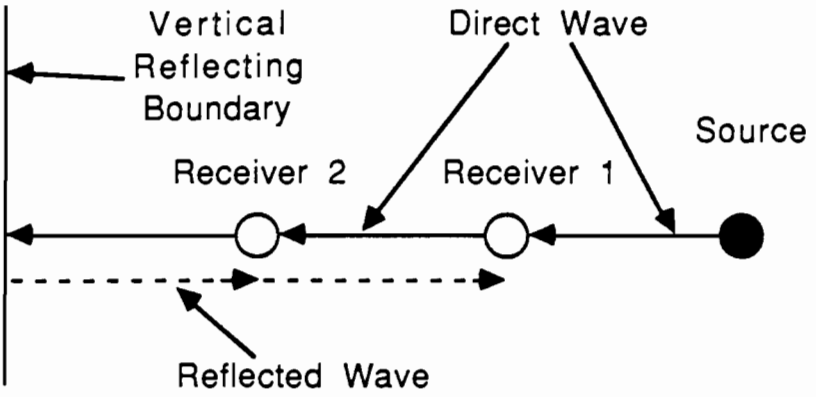

a. Plan View of Test Array and Reflecting Boundary

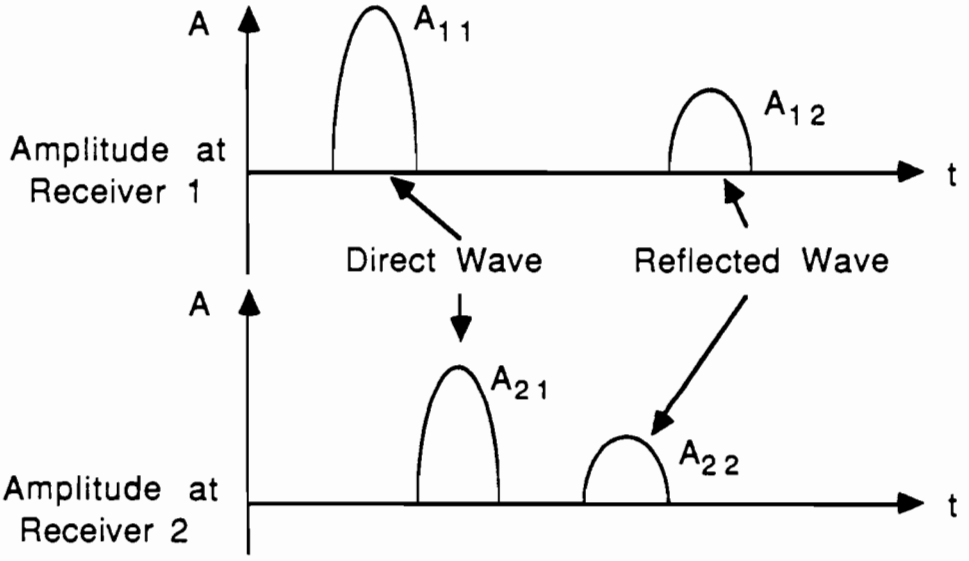

b. Representation of Time Domain Records

Fig. 4.3. Plan View and Idealized Time Records for Direct and Reflected Surface Waves: Receivers Placed Between Source and Vertical Reflecting Boundary.

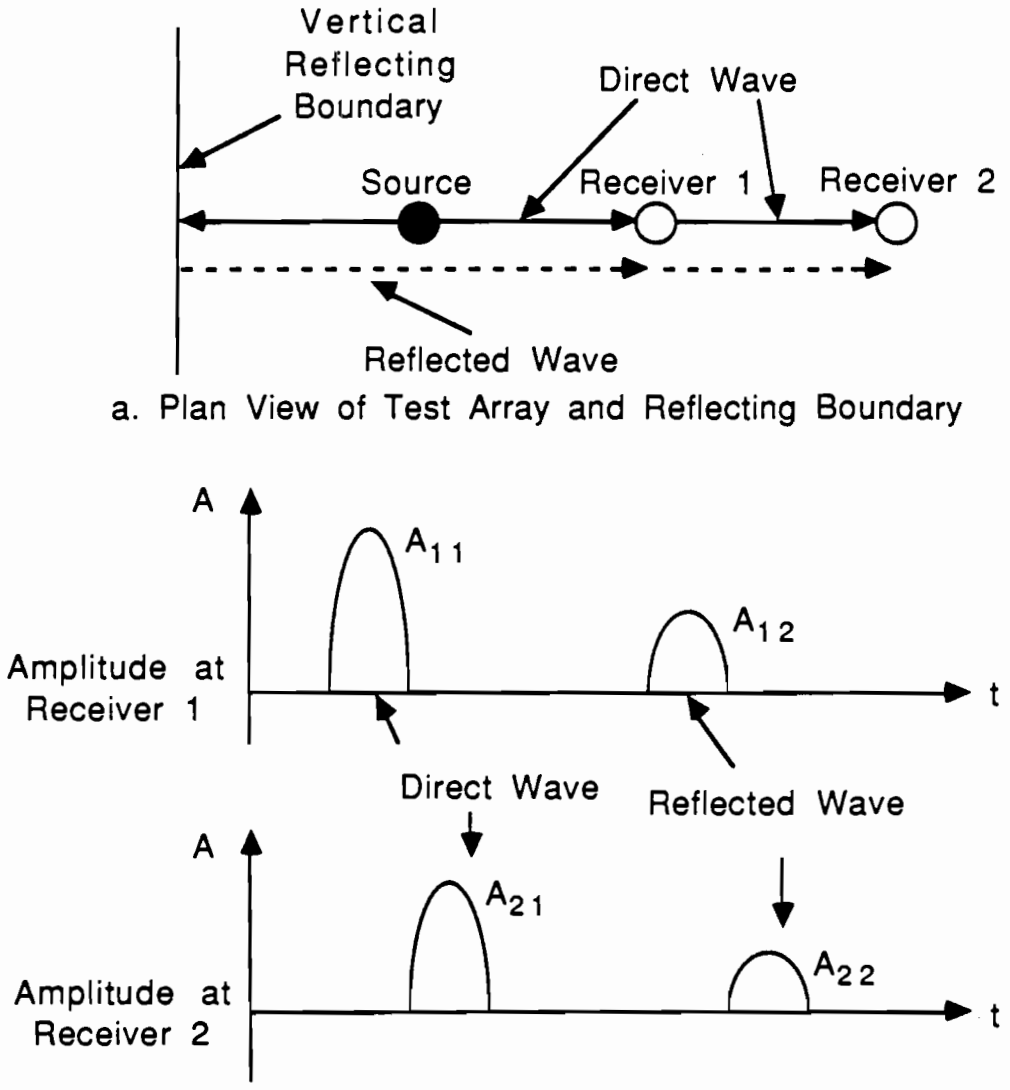

Fig. 4.4. Plan View and Idealized Time Records for Direct and Reflected Surface Waves: Source Placed Between Receivers and Vertical Reflecting Boundary.

A complete list of the test conditions is presented in Tables 4.1 and 4.2. Test layouts are illustrated in Fig. 4.5. Modeled dispersion curves were generated by the modeling process as presented in Chapter Three. To simplify the problem, only one reflecting boundary and one reflected wave were considered in most of these tests. Since amplitudes of the second and third reflections are small compared to the amplitude of the first reflection in the field (as illustrated in Fig. 3.8), this approximation introduced a minor to negligible error in the results.

Receivers Located Between Source and Reflecting Boundary

Typical field and modeled dispersion curves with 1-ft (30 cm) source/receiver spacings are presented in Figs. 4.6 through 4.9. The distances from the vertical reflecting boundary to the near receiver varied from 3 to 5 ft (91 to 152 cm) in these figures. Keep in mind that, in this case, reflected waves are propagating in the opposite direction to that of the direct waves.

Consider the field dispersion curves shown in Figs. 4.6 through 4.9. These curves consist of a basic smooth curve upon which ripples or fluctuations are imposed. In the range of wavelengths shorter than about 0.5 ft (15 cm), this basic curve can be approximated by a horizontal line with an average wave velocity of about 7800 fps (2377 m/s) in all cases except for Fig. 4.9. The imposed ripples or fluctuations are caused by reflections as discussed next. In Fig. 4.9, the wave velocity is about 7500 fps (2286 m/s). The cause of this slightly lower velocity is not known. Very localized material nonuniformity is one possible explanation.

The reason for the basically horizontal curve for wavelengths less than 0.5 ft (15 cm) is that only surface waves in the concrete slab are being measured. In other words, at high frequencies (or at short wavelengths such as shorter than 0.5 ft (15 cm) for this particular material property profile), surface waves only sample the material properties in the top layer. Material properties below the top layer do not affect these measurements of surface wave velocity.

The "true" dispersion curve used for modeling wave propagation at the BRC facility is shown in Fig. 4.10. This curve was derived simply by fitting several field dispersion curves. Based on the above discussion, a horizontal line was used in the range where wavelengths are less than 1 ft (30 cm). This straight-line approximation in the wavelength range from 0.5 to 1 ft (15 to 30 cm) is just for the purpose of simplyfing the problem. For longer wavelengths, curved lines were used. Most field dispersion curves exhibit large fluctuations in the wavelength range from about 1 to 2 ft (30 to 61 cm) caused by unknown factors (such as reflections and additional modes of vibration). However, past experience shows that these fluctuations are a real

TABLE 4.1. TEST LOCATIONS WITH SOURCE PLACED BETWEEN RECEIVERS AND VERTICAL BOUNDARY

Receiver Location*, 1st, 2nd	Distances			Figure Number
	Source to 1st Receiver (ft)	1st Receiver to 2nd Receiver (ft)	Boundary to Source (ft)	
B, C	0.4	0.5	0.1	A-1b
C, D	0.5	0.5	0.5	
D, E	0.5	0.5	1.0	
E, F	0.5	0.5	1.5	
F, G	0.5	0.5	2.0	
G, H	0.5	0.5	2.5	
C, E	0.9	1.0	0.1	4.12b
D, F	1.0	1.0	0.5	
E, G	1.0	1.0	1.0	
F, H	1.0	1.0	1.5	
G, I	1.0	1.0	2.0	
H, J	1.0	1.0	2.5	
I, K	1.0	1.0	3.0	
K, M	1.0	1.0	4.0	
D, G	1.4	1.5	0.1	A-2b
F, I	1.5	1.5	1.0	
H, K	1.5	1.5	2.0	A-3b
J, M	1.5	1.5	3.0	
E, I	1.9	2.0	0.1	A-4b
G, K	2.0	2.0	1.0	

* Refer to Fig. 4.5.

TABLE 4.2. TEST LOCATIONS WITH RECEIVERS PLACED BETWEEN SOURCE AND VERTICAL BOUNDARY

Receiver Location*, 1st, 2nd	Distances			Figure Number
	Source to 1st Receiver (ft)	1st Receiver to 2nd Receiver (ft)	Boundary to Source (ft)	
B, A	0.5	0.4	0.1	
C, B	0.5	0.5	0.5	A-1a
D, C	0.5	0.5	1.0	
E, D	0.5	0.5	1.5	
F, E	0.5	0.5	2.0	
G, F	0.5	0.5	2.5	
H, G	0.5	0.5	3.0	
C, A	1.0	0.9	0.1	
D, B	1.0	1.0	0.5	
E, C	1.0	1.0	1.0	4.12a
F, D	1.0	1.0	1.5	
G, E	1.0	1.0	2.0	
H, F	1.0	1.0	2.5	
I, G	1.0	1.0	3.0	4.6
J, H	1.0	1.0	3.5	4.7
K, I	1.0	1,0	4.0	4.8
M, K	1.0	1.0	5.0	4.9
D, A	1.5	1.4	0.1	
F, C	1.5	1.5	1.0	
G, D	1.5	1.5	1.5	A-2a
I, F	1.5	1.5	2.5	
K, H	1.5	1.5	3.5	A-3a
M, J	1.5	1.5	4.5	
E, A	2.0	1.9	0.1	
I, E	2.0	2.0	2.0	A-4a
K, G	2.0	2.0	3.0	

* Refer to Fig. 4.5.

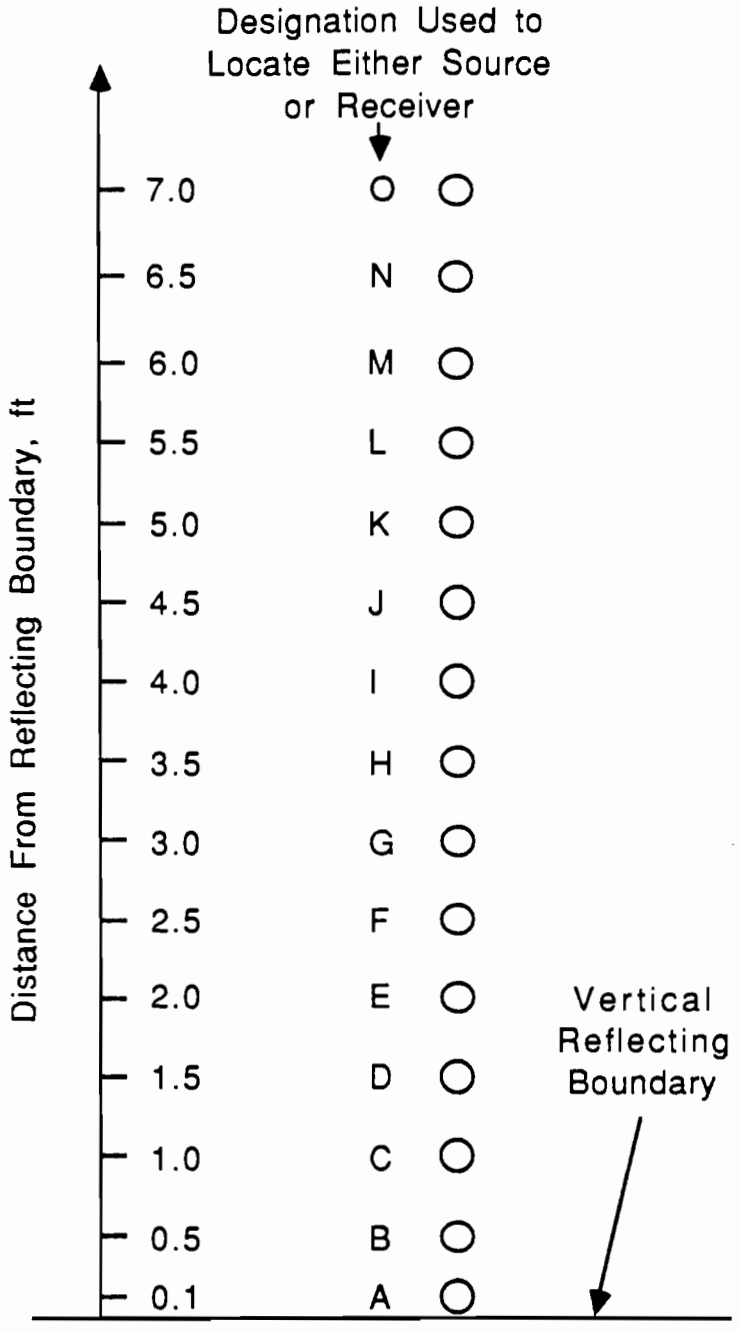

Fig. 4.5. Plan View of Vertical Reflecting Boundary and Various Source/Receiver Locations.

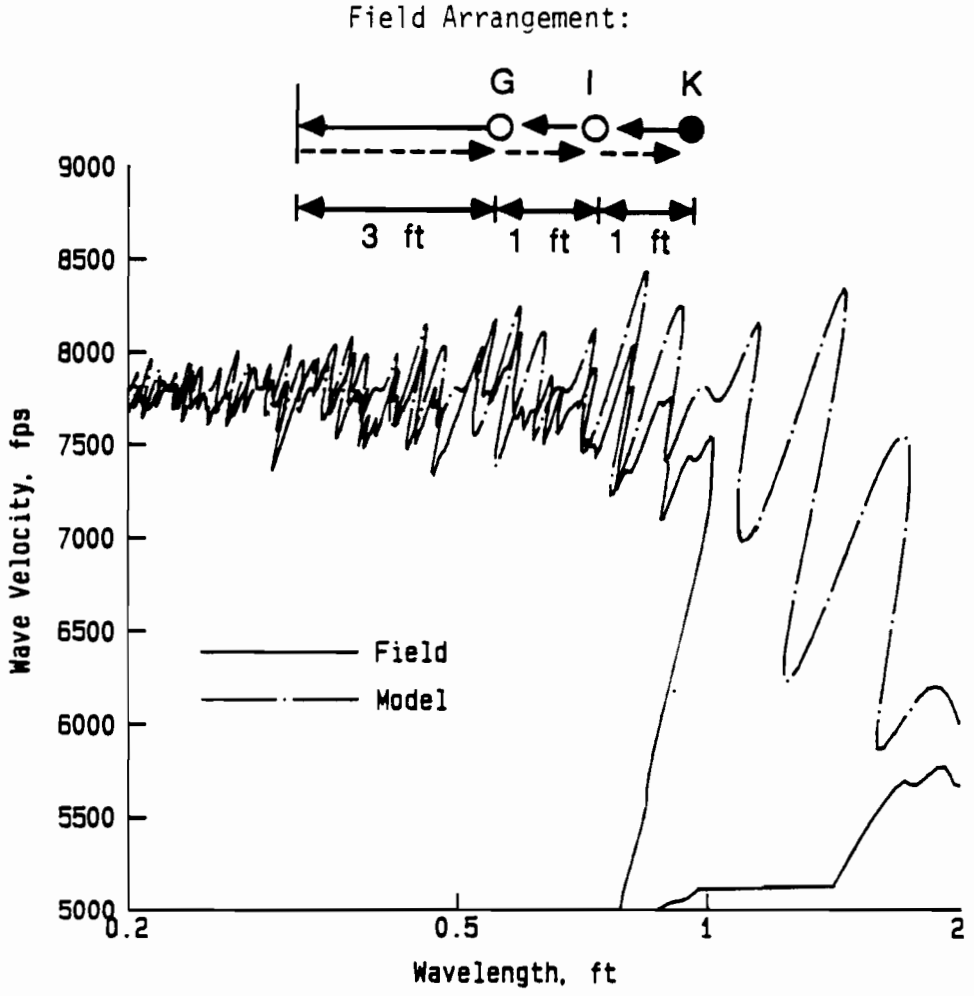

Fig. 4.6. Comparison of Field and Modeled Dispersion Curves for Surface Waves Reflected from a Vertical Boundary: Receivers (Located at G and I) Placed Between Source and Reflecting Boundary.

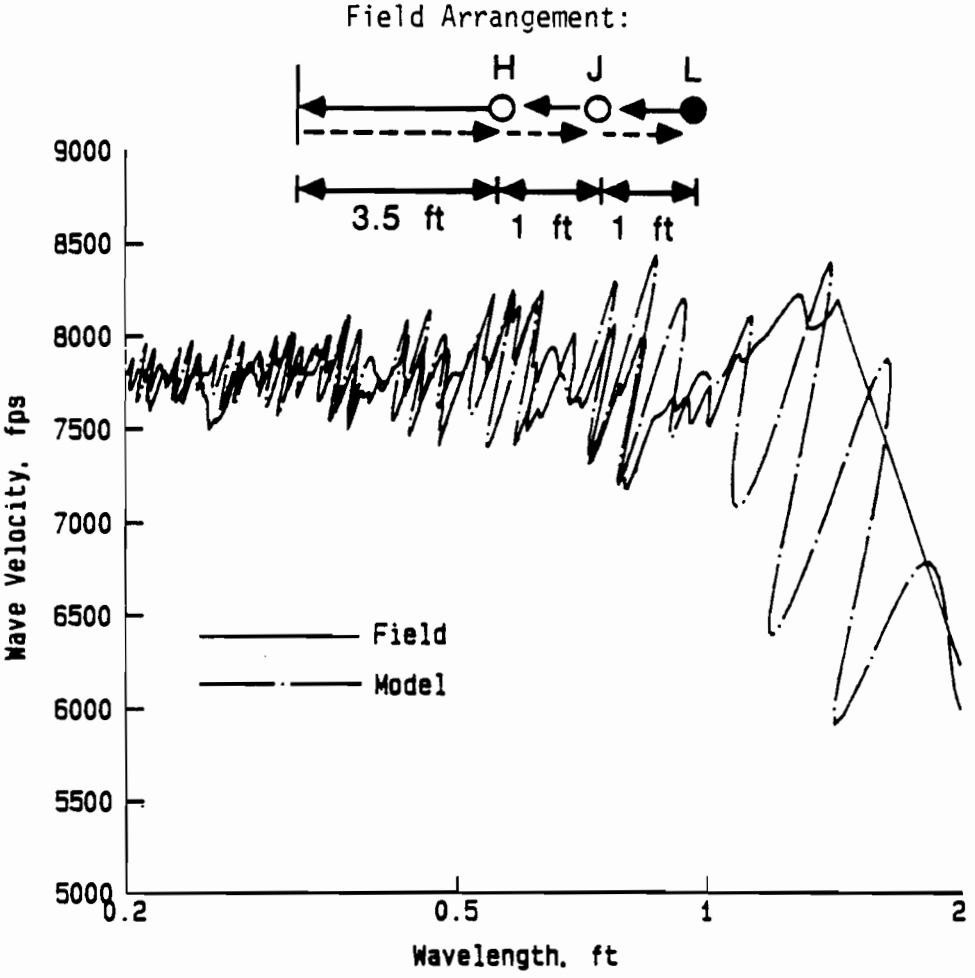

Fig. 4.7. Comparison of Field and Modeled Dispersion Curves for Surface Waves Reflected from a Vertical Boundary: Receivers (Located at H and J) Placed Between Source and Reflecting Boundary.

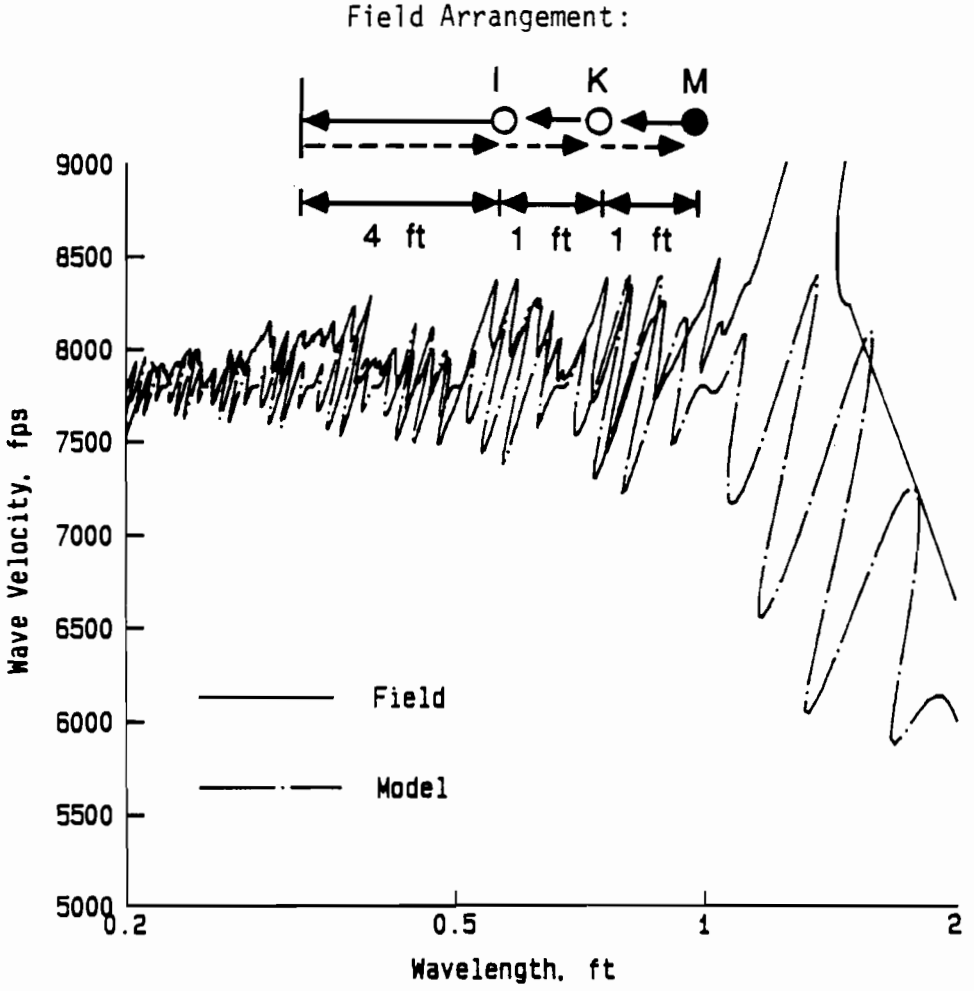

Fig. 4.8. Comparison of Field and Modeled Dispersion Curves for Surface Waves Reflected from a Vertical Boundary: Receivers (Located at I and K) Placed Between Source and Reflecting Boundary.

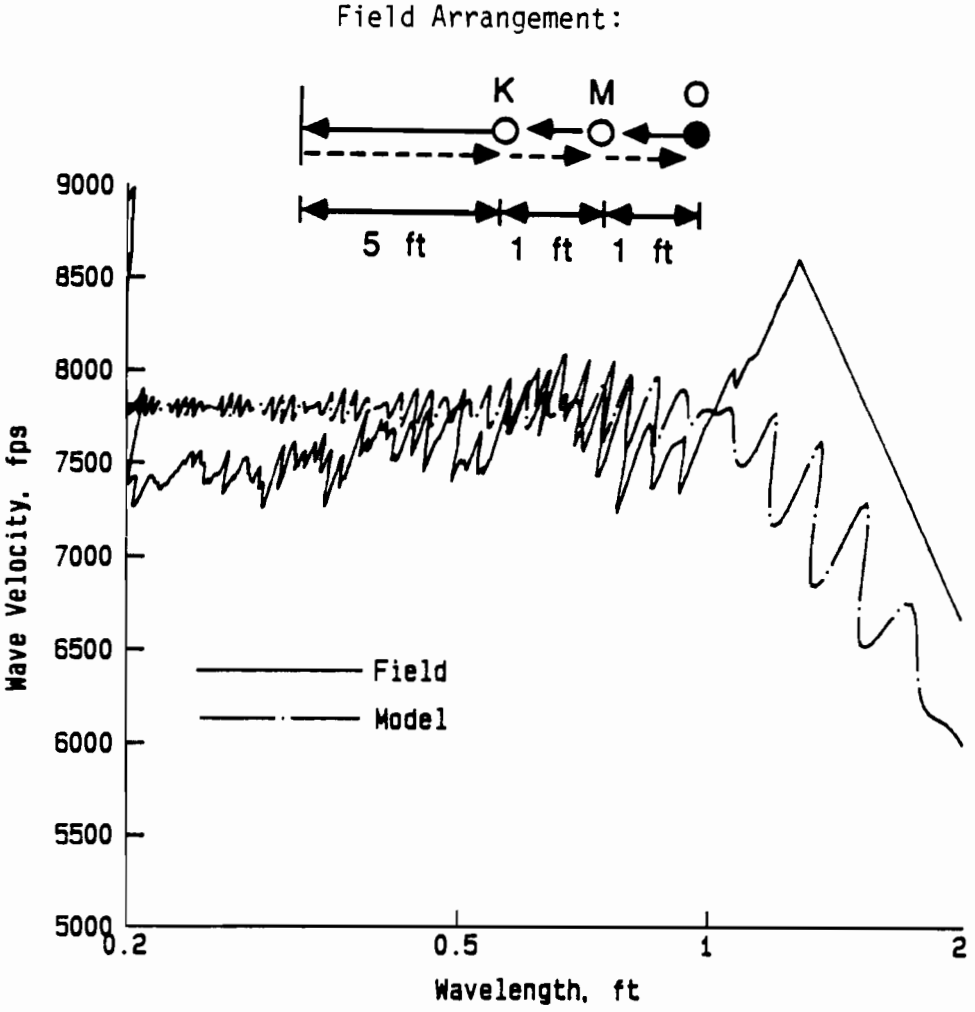

Fig. 4.9. Comparison of Field and Modeled Dispersion Curves for Surface Waves Reflected from a Vertical Boundary: Receivers (Located at K and M) Placed Between Source and Reflecting Boundary.

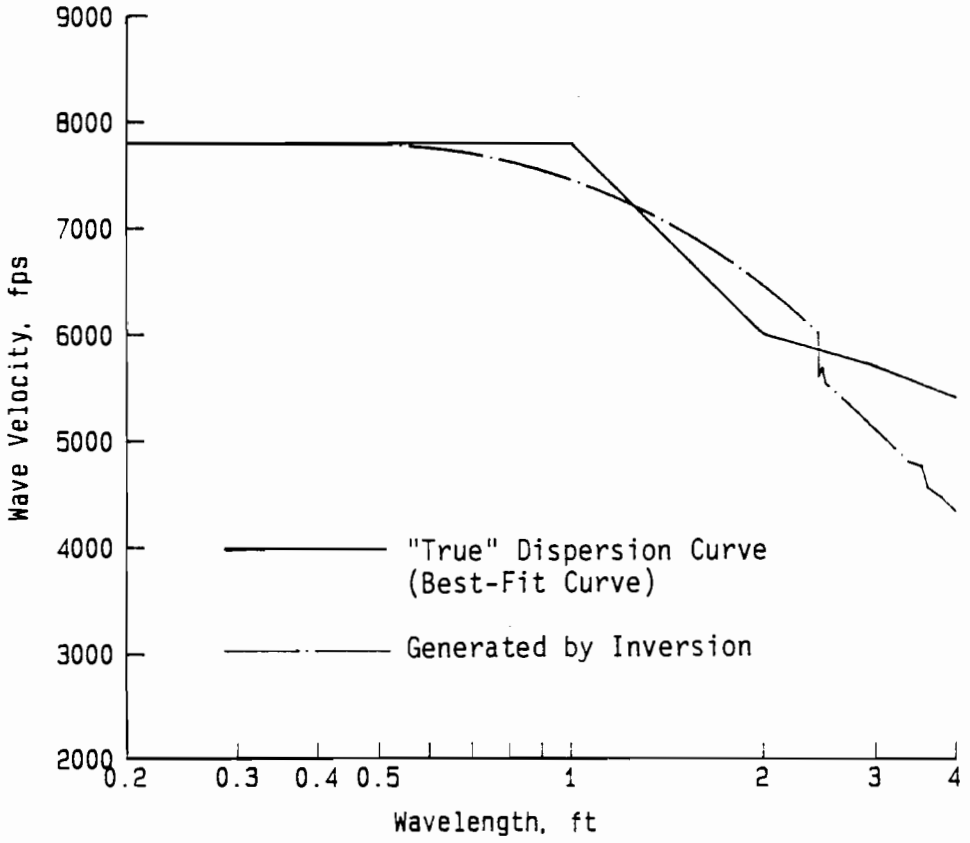

Fig. 4.10. Comparison of "True" Dispersion Curve and Dispersion Curve Generated by the Inversion Program.

characteristic of the site. The "true" dispersion curve was, therefore, fit "by eye" with an average value in this wavelength range.

To verify the correctness of this "fit-by-eye" approach, a dispersion curve generated from the inversion program with the known profile of the test facility is presented in Fig. 4.10 for comparison. (Detailed material property profiles at this facility are discussed in Chapter Nine.) It appears that the "true" dispersion curve derived from the "fit-by-eye" approach reasonably represents the theoretical dispersion curve in the short wavelength range. It is no surprise to see that these two curve start to diverge in the range where the wavelength is greater than about 2.5 ft (76 cm). Since the spacing between the two receivers was 1 ft (30 cm) and the source was 1 ft (30 cm) away from the first receiver for all field dispersion curves shown in this section, dispersion curves corresponding to wavelengths longer than about 2.5 ft (76 cm) bear no significance. (This point is discussed in Chapter Two.) While the dispersion curve generated from the inversion program is based on the known profile, this curve should be representative throughout the whole wavelength. Because these two dispersion curves represent two different ideas, they are not expected to agree with each other in the long wavelength range.

Modeled dispersion curves shown in Figs. 4.6 through 4.9 closely describe the main ripples (fluctuations) present in the field data. To examine this point in more detail, an enlargement of the dispersion curve shown in Fig. 4.6 is presented in Fig. 4.11 for measurements in the short-wavelength range. It is clear that reflections impose ripples or fluctuations onto the dispersion curves. Although not all peaks and troughs overlap for both curves, the modeled dispersion curve shows the significant characteristic of the fluctuations. Since only one kind of reflected wave with only one reflection is considered in this model, minor discrepancies between the modeled and field data are possibly due to other reflected waves which are not considered in this first-approximation model. In addition, uncertainties in estimating amplitudes and times (A's and T's) also introduce some errors into the modeled dispersion curves.

It is also interesting and valuable to note that among all cases studied herein, the average amplitudes of the ripples imposed on the field dispersion curves vary from one case to the other. The field dispersion curve shown in Fig. 4.6 exhibits the largest fluctuations among all of the cases over almost the full range of wavelengths, especially for wavelengths less than 1 ft (30 cm). On the other hand, the field dispersion curve shown in Fig. 4.9 exhibits the least fluctuations. By examining the test locations of the arrays corresponding to each figure, it is found that the amplitudes of the imposed fluctuations at one particular wavelength decrease as the test array is

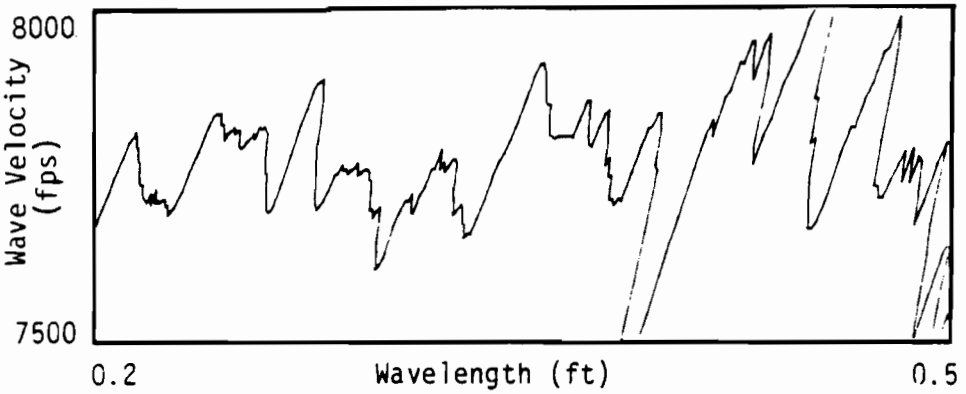

a. Field Dispersion Curve

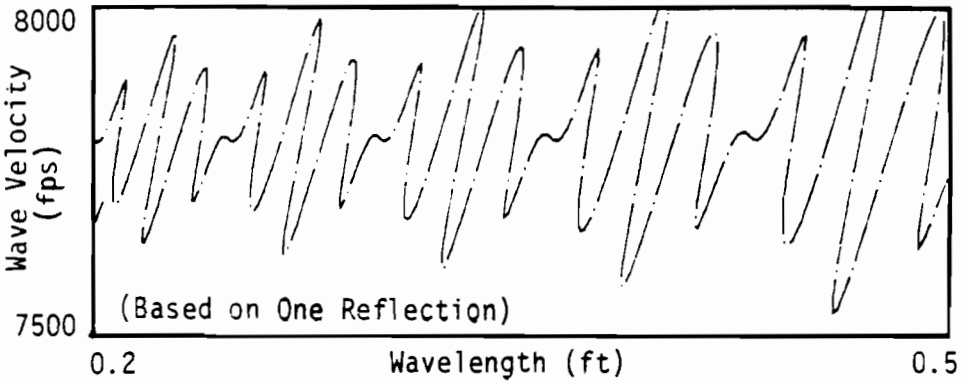

b. Modeled Dispersion Curve

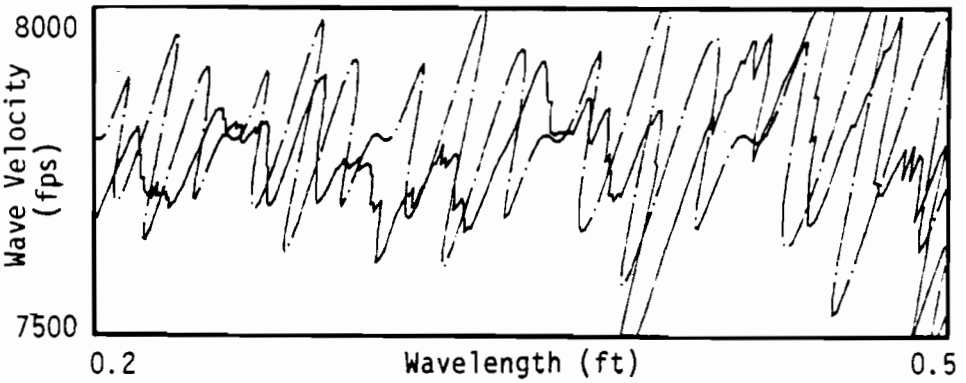

c. Comparison of Field and Modeled Dispersion Curves

Fig. 4.11. A Close-Up Comparison in the Short-Wavelength Range of Field and Modeled Dispersion Curves Shown in Fig. 4.6.

moved further away from the reflecting boundary. The reason is that, when the test array is moved further away from the reflecting boundary, the reflected waves need to travel longer and longer distances to reach the receivers. Therefore, their amplitudes become smaller and smaller. As a result, the effect of reflected waves on the dispersion curve is reduced. This is an important consideration when selecting the location of the test array; that is, the array should be placed as far away from the reflecting boundary as possible.

4.2.3. Reducing Effect from Boundary Reflections

As discussed in Section 4.2.1, it is better to have reflected waves travel in the same direction as the direct waves because the effect of reflected waves is minimized under such a condition. The field data support this concept. One example of this situation is shown in Fig. 4.12. Other examples are presented in Appendix A as noted in Tables 4.1 and 4.2.

The dispersion curve shown in Fig. 4.12a was obtained by placing receivers at locations C and E (shown in Fig. 4.5) while the source was first placed at location G. This type of arrangement is shown in Figs. 4.2 and 4.3 for the case when reflected waves travel in the opposite direction to the direct wave. After completing this test, the source was moved to location A while the two receivers remained in place. The test array then became the type of arrangement shown in Figs. 4.1 and 4.4 where reflected waves travel in the same direction as the direct wave. The dispersion curve from this test is shown in Fig. 4.12b. Modeled dispersion curves are also presented in Fig. 4.13 in which one surface wave reflection was considered. The ripples appearing on the field dispersion curve in Fig. 4.12a have the same pattern as the ripples on the modeled dispersion curve shown in Fig. 4.13 (case (a)). As a result, it can be concluded that these ripples are, in large part, from reflected surface waves created by the near boundary.

Upon comparison of the two dispersion curves shown in Fig. 4.12, in the range of wavelengths shorter than about 0.35 ft (11 cm), the amplitudes of the ripples are similar for both dispersion curves. It is clear that the ripples appearing in Fig. 4.12a are caused by surface reflections, but it is not clear about the cause of the ripples appearing on the dispersion curve shown in Fig. 4.12b. In the range of wavelengths from about 0.35 to 0.75 ft (11 to 23 cm), the amplitudes of the ripples in Fig. 4.12a are much larger than those in Fig. 4.12b as predicted by the model shown in Fig. 4.13. This is because that, for the case shown in Fig. 4.12a, the reflected surface wave is propagating in the opposite direction to the direct surface wave. Hence, there is an adverse effect on the dispersion curve in Fig. 4.12a. In the case shown in Fig. 4.12b, the reflected surface wave is propagating in the same direction as the direct surface wave.

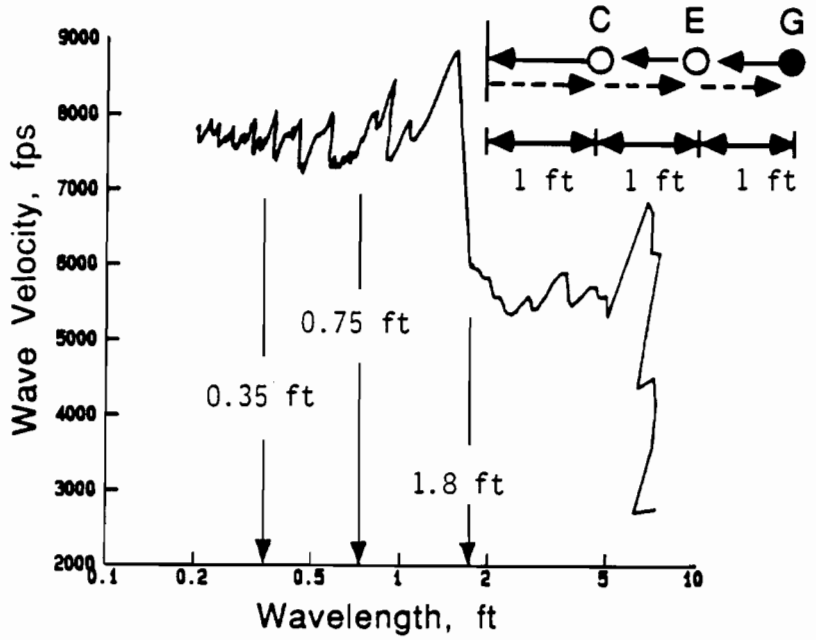

a. Receivers Placed Between Source and Reflecting Boundary

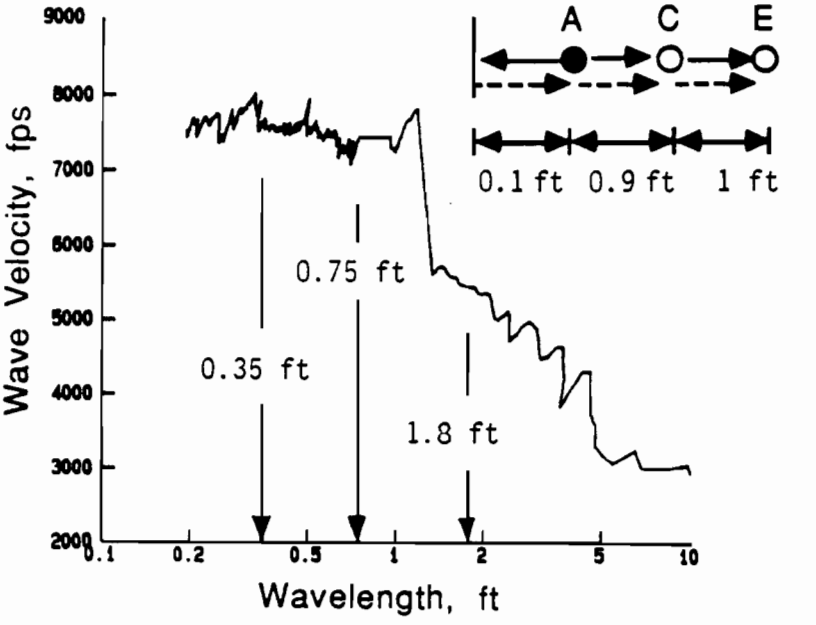

b. Source Placed Between Receivers and Reflecting Boundary

Fig. 4.12. Comparison of the Effect on Dispersion Curves of Source Location with Respect to Locations of Receivers and Reflecting Boundary.

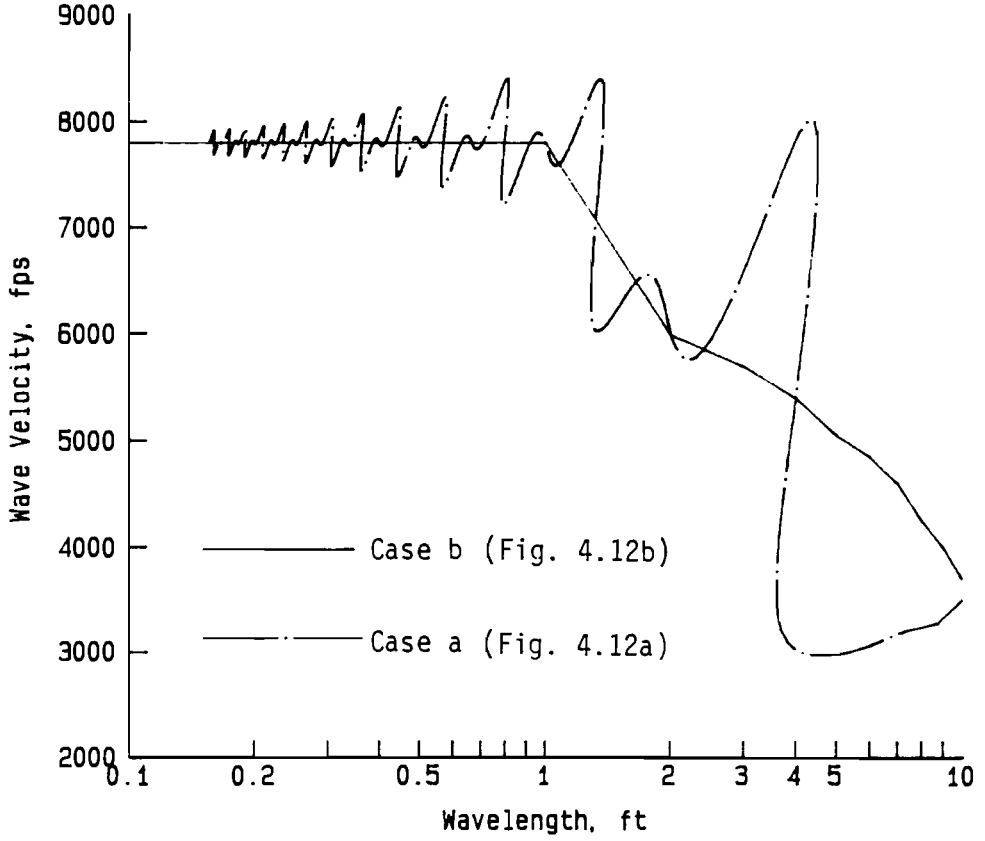

Fig. 4.13. Modeled Dispersion Curves for Test Conditions Shown in Fig. 4.12.

Therefore, it should have no effect on the dispersion curve as shown in the model (Fig. 4.13, case (b)). There is a range of wavelengths [about 0.75 to 1.8 ft (23 to 55 cm)] where data can not be recovered and no conclusion can be drawn. In the range of wavelengths of 1.8 ft (55 cm) and above, the dispersion curve shown in Fig. 4.12a indicates a big lobe (variation) in the dispersion curve. This big change is known to be representative of the site and is predicted by the model shown in Fig. 4.13. The dispersion curve shown in Fig. 4.12b, on the other hand, exhibits relatively smaller-amplitude ripples. It can be concluded that the quality of data shown in Fig. 4.12b is superior to data shown in Fig. 4.12a because of the smaller fluctuations.

It should be mentioned that when the source is placed at location G, reflected surface waves have to travel 5 ft (152 cm) from the source to reach receiver 1 and 4 ft (30 cm) to reach receiver 2. When the source is placed at A, reflected surface waves need to travel only 1.2 ft (37 cm) to reach receiver 1 and 2.1 ft (64 cm) to reach receiver 2. The lengths of the travel paths to both receivers for reflected waves are longer when the source is placed at location G rather than at location A. Therefore, the amplitudes of reflected waves are larger when the source is placed at G than when it is placed at A. Suppose the amplitudes of the reflected waves are the only controlling factor governing the amplitudes of the ripples imposed on the dispersion curve. In this case, the dispersion curve shown in Fig. 4.12a should exhibit smaller ripples than the dispersion curve shown in Fig. 4.12b. However, the field dispersion curves show just the opposite result. The field data actually verify the concept discussed earlier; that is, when reflected waves travel in the same direction as direct waves, both direct and reflected waves can be combined and treated as one direct wave with a longer duration. Consequently, the amplitudes of same-propagation-direction reflected waves are relatively unimportant. This is the only condition when the amplitudes of reflected waves are unimportant.

From the above discussion, it can be concluded that the effect of reflected surface waves can be important to the fluctuations measured in dispersion curves. Reflected waves can impose ripples or fluctuations on the "true" dispersion curves and make the dispersion curves misleading. Before this study was performed, it was a puzzle whether the material properties really fluctuated as indicated by the dispersion curves or not. Now, it is obvious that most of the fluctuations (with the pattern discussed in this section) on the dispersion curves are from reflected surface waves. It is fair to assume that the material property is relatively uniform in the top concrete layer. In addition, one can conclude that test arrays should be placed in such a way that amplitudes of reflected waves are minimized or, best of all, that reflected waves propagate in the same direction as the direct waves.

4.2.4. Additional Considerations in the Modeling Process

There are several other points which need to be mentioned about modeling these test conditions. Firstly, the aforementioned modeling only takes one reflected wave into consideration; namely, the one which is from the nearest reflecting boundary. In actuality, there are more reflected surface waves in these tests because the concrete slab is 12 ft (366 cm) wide and about 40 ft (1219 cm) long, and test location 2 is 13 ft (396 cm) away from the joint as shown in Fig. 3.2. Reflected waves from the far end of the slab and the joint also influence the field dispersion curves. However, amplitudes of these reflections were assumed to be small and were not considered. Reflections of body waves from the bottom of the concrete slab is another factor that was not considered here. The impact of body waves on these tests is discussed in Chapter Five.

Secondly, in all modeled cases, it was assumed that wave attenuation with distance (damping) is the same for direct and reflected waves. This can be illustrated as follows. Suppose a direct wave reaches the first receiver with an amplitude of 1 unit and reaches the second receiver with an amplitude of 0.9 units. Then, when the reflected wave reaches the first receiver with an amplitude of, say 0.2 units, the amplitude at the second receiver would be assumed to be 0.18 units. That is, the amplitude ratio measured by the two receivers for the same arrival is assumed to be a constant (0.9 units this particular example). This is a reasonable assumption if damping is independent of wave amplitude. If damping indeed depends upon wave amplitude, then the amplitude ratios at the two receivers would not be the same for the direct and reflected waves. Under this circumstance, the reflected waves can no longer be considered as part of the direct waves even though they travel in the same direction as the direct waves.

A modeling of this amplitude-dependent damping is shown in Fig. 4.14. This simulation assumes that the source is located at point C, and receivers are placed at locations E and G (shown in Fig. 4.5). The amplitudes of the direct surface waves measured by receivers 1 and 2 are assumed to be 1 and 0.9 units, respectively. In one case, amplitudes of reflected waves measured by receivers 1 and 2 are assumed to be 0.3 and 0.27, respectively, which assumes that the damping effect for different amplitudes is the same (because for one particular arrival, the amplitude of the time signal received by receiver 2 is always 0.9 times the amplitude received by receiver 1). The dispersion curve with this assumption exhibits no reflected waves, that is the dispersion curves are the same with or without reflected waves. This curve will overlap the "true" dispersion curve and is shown in Fig. 4.14. In another case, the amplitudes of the direct

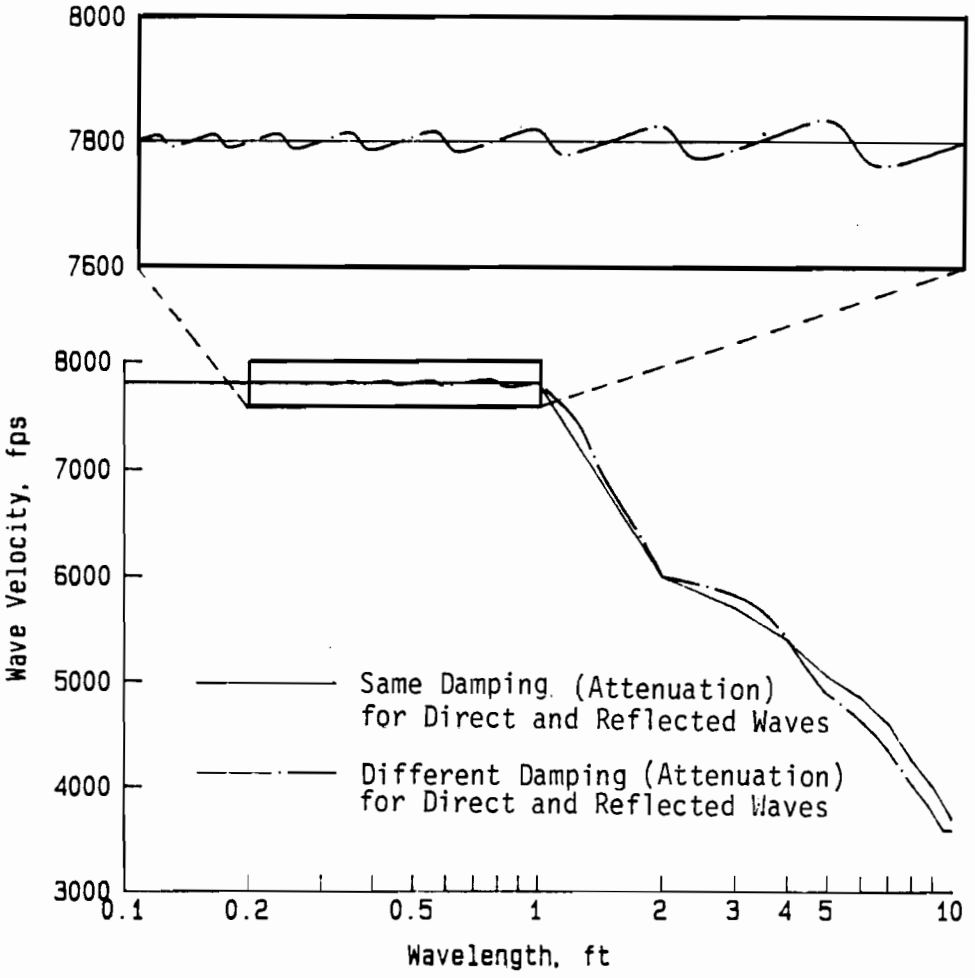

Fig. 4.14. A Close-Up Examination of the Effect on the Dispersion Curves of Different Attenuation Relationships for Direct and Reflected Surface Waves.

wave measured by receivers 1 and 2 are assumed to be the same as before, but amplitudes of reflected wave measured by receivers 1 and 2 are both selected to be 0.3. Thus, the amplitude ratio between two receivers is 0.9 for the direct waves and 1.0 for the reflected waves. This variation in ratios was selected with the thought that damping ratio could be smaller at lower strain levels. As can be seen in Fig. 4.13, the different amplitude ratios induced some noise (small fluctuations) onto the dispersion curve even if reflected waves are traveling in the same direction as direct waves, but the effect is relatively small. It seems that, in reality, possibly some of the data fluctuations do come from the fact that different amplitudes of waves have different damping associated with them, but the importance is minor and can be neglected.

4.3. VERTICAL BOUNDARY ORIENTED PARALLEL TO TEST ARRAY

The reflection of surface waves from a vertical reflecting boundary oriented parallel to the test array is shown schematically in Figs. 4.15 and 4.16a. The idealized time domain signals recorded by the two receivers in these tests are shown in Fig. 4.16b. As seen in these figures, the reflected waves are generally propagating in the same direction as the direct wave. To better understand this type of source/receiver configuration, field tests and model studies were performed as discussed below.

4.3.1. Creation of Reflected Waves

In the past, most SASW tests on pavement sites have been performed with the source/receiver array oriented parallel to the edge of the pavement. One practical reason for this array layout is that large spacings could be used between the source and receivers while the array still remained on the pavement surface. Therefore, the material profile remained constant laterally no matter what source/receiver spacings were selected. Another obvious advantage is that one lane of traffic control provided enough room for performing the test.

It is easy to imagine that the boundary which is oriented parallel to an SASW array could create reflections, both surface wave and body wave, which might adversely affect the test results. Therefore, this condition was investigated. In this section, the effect of only surface waves is considered.

4.3.2. Influence of Distance Between Array and Reflecting Boundary

Field tests were carried out in the area of location 2 at the BRC slab facility shown in Fig. 3.2. Standard SASW tests were performed with seven different arrays. A detailed layout of the

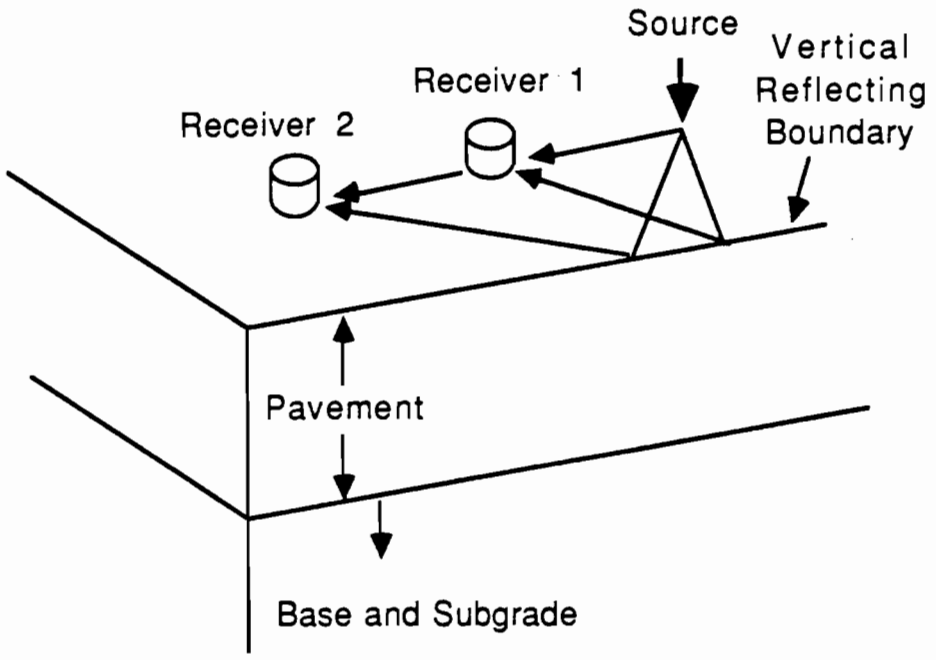

Fig. 4.15. Direct and Reflected Surface Waves Created by a Vertical Reflecting Boundary Oriented Parallel to the Test Array.

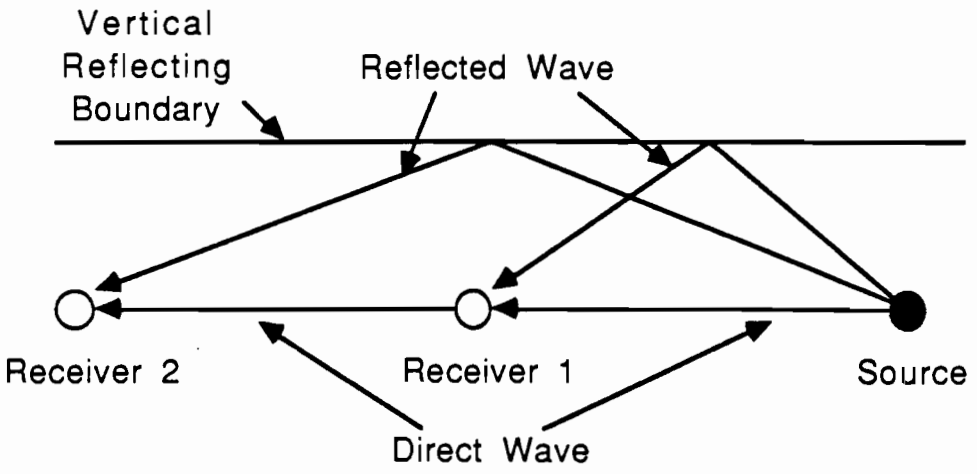

a. Plan View of Test Array and Reflecting Boundary

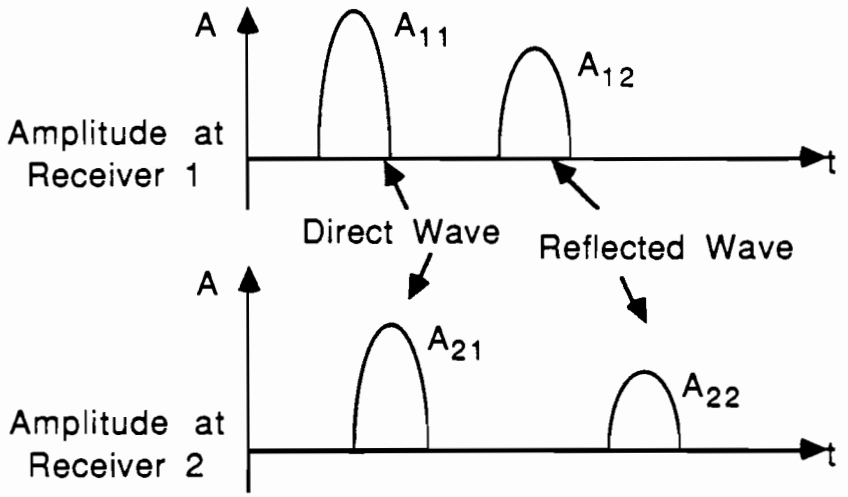

b. Representation of Time Domain Records

Fig. 4.16. Plan View and Idealized Time Records for Direct and Reflected Surface Waves: Reflecting Boundary Oriented Parallel to Test Array.

tests is shown in Fig. 4.17 and the test conditions are listed in Table 4.3. All arrays were oriented with their axes parallel to the concrete pavement boundary. The distance between the test array and the pavement boundary was varied from 1 in. to 4 ft (2.5 to 1.22 cm). For each array, receiver spacings were varied from 6 in. to 5 ft (15 to 152 cm).

Model analyses were performed to identify possible problems. Only one reflection from the nearest boundary was considered. Rough estimates of values for the amplitudes (A's in Eq. 3.11) were used for the reflected waves due to the difficulty in estimating the amplitudes as discussed in Section 4.2.

The model simulation was first performed for the 1-ft (30 cm) source/receiver spacing for all seven arrays. The ray paths of the reflected surface waves for each array are presented schematically in Fig. 4.18. Comparisons of the modeled and field dispersion curves are presented in Figs. 4.19 through 4.25. It is clear that the model identifies this type of reflection irrefutably. There are small fluctuations not identified in the modeled dispersion curves, but these are minor and are not unexpected because only one type of reflection is being taken into account in the model. (A similar set of tests except that a 2-ft source/receiver spacing was used is presented in Appendix B.)

By closely examining the field data and modeled dispersion curves, it is found that, for a fixed source/receiver spacing, the array closest to the slab edge showed the least influence of the boundary (Fig. 4.19). As the distance between the reflecting boundary and test array was increased, the influence of the boundary increases drastically and reaches a maximum at a distance of about 0.5 to 1 times the source/receiver spacing (Figs. 4.20 and 4.21). The influence of the boundary then decreases to a steady level at greater distances (Figs. 4.23 through 4.25). The reason for this pattern is that when the array is very close to the boundary, reflected waves travel about the same distance as direct waves to reach the receivers (Fig. 4.19),. Therefore, they are generally in-phase with the direct waves. As a result, the reflected waves do not have much influence on the dispersion curve as indicated by test array 1. As the center line of the array is moved away from the pavement edge, reflected surface waves have to travel longer and longer distances compared to the direct wave to reach the receivers. Consequently, these reflected waves are more and more out-of-phase with respect to the direct wave and, thus, have more adverse effect on the dispersion curves. Ray paths shown in Fig. 4.18 clearly demonstrate this point.

Another factor which also needs to be considered is the amplitudes of the reflected waves. As the distance of travel of the reflected waves increases, the amplitudes decrease because of damping (material and geometrical). Hence the effect of reflected waves decreases as distance of

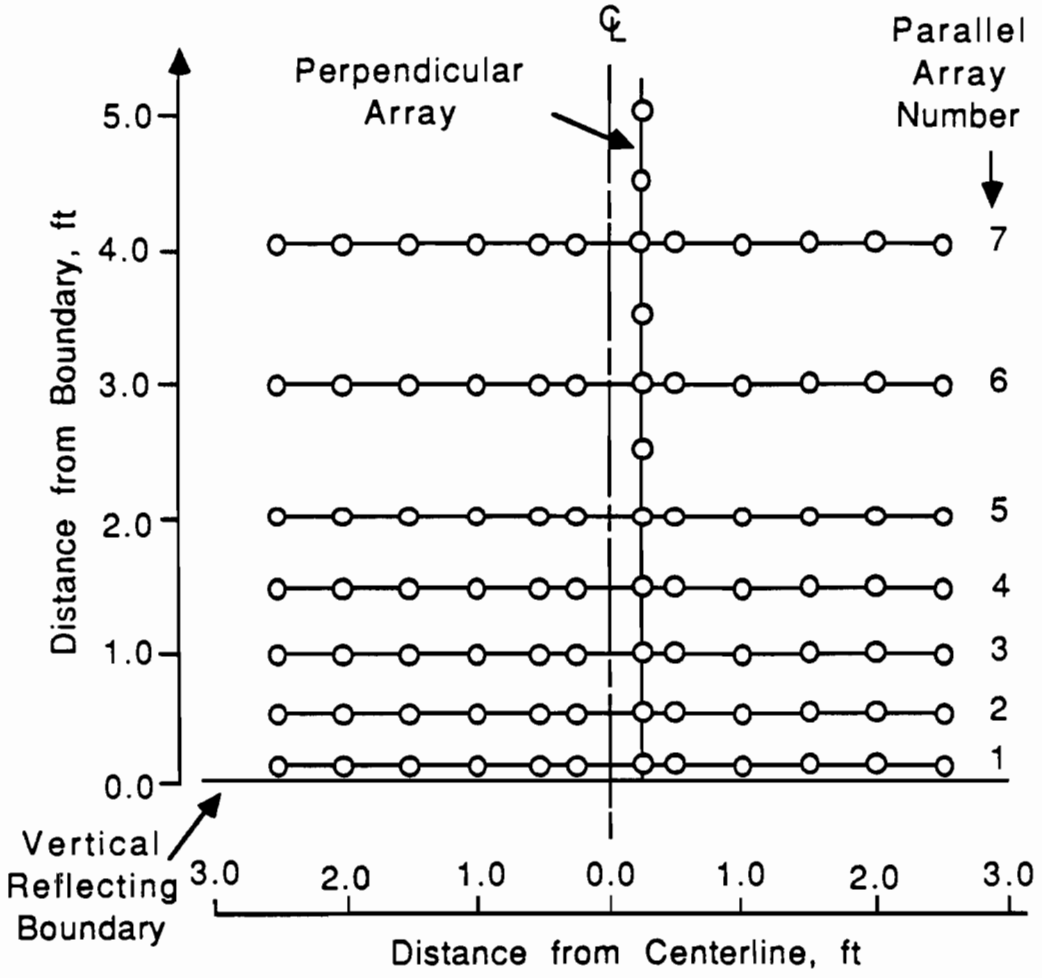

Fig. 4.17. Arrangement of SASW Arrays Used to Study the Influence of Surface Wave Reflections from Boundaries Oriented Parallel to the Test Array.

TABLE 4.3. TEST LOCATIONS FOR ARRAY PLACED PARALLEL TO REFLECTING BOUNDARY

Array No.*	Distance to Reflecting Boundary (ft)	Distances:** Source to 1st Receiver (ft)					
1	0.1	0.5	1.0	2.0	3.0	4.0	5.0
2	0.5	0.5	1.0	2.0	3.0	4.0	5.0
3	1.0	0.5	1.0	2.0	3.0	4.0	5.0
4	1.5	0.5	1.0	2.0	3.0	4.0	5.0
5	2.0	0.5	1.0	2.0	3.0	4.0	5.0
6	3.0	0.5	1.0	2.0	3.0	4.0	5.0
7	4.0	0.5	1.0	2.0	3.0	4.0	5.0

* Locations Given in Fig. 4.17

** Distance between 1st and 2nd receivers equalled distance from source to 1st receiver in all tests

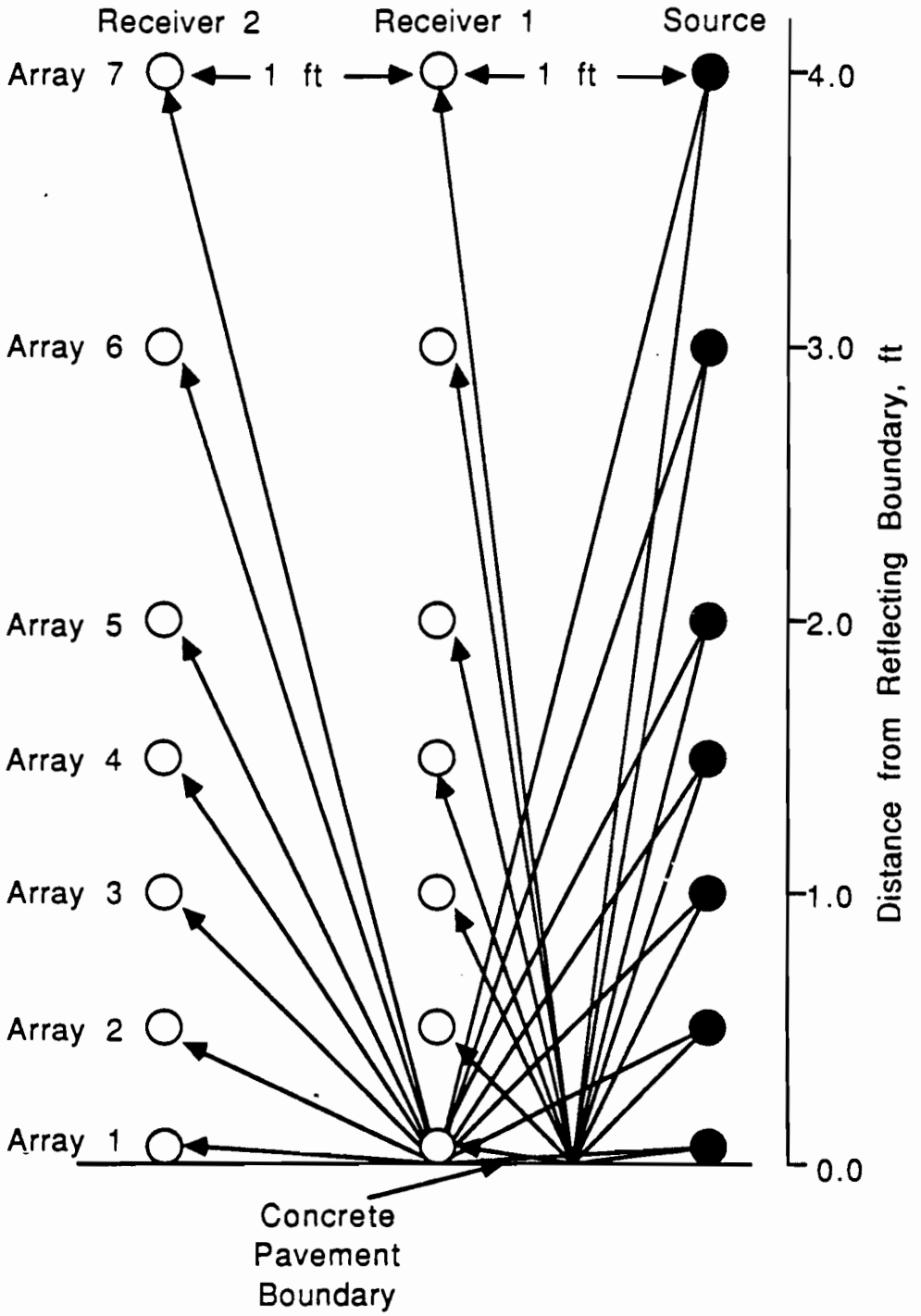

Fig. 4.18. Ray Paths Assumed for Reflected Surface Waves When Test Array was Oriented Parallel to Reflecting Boundary.

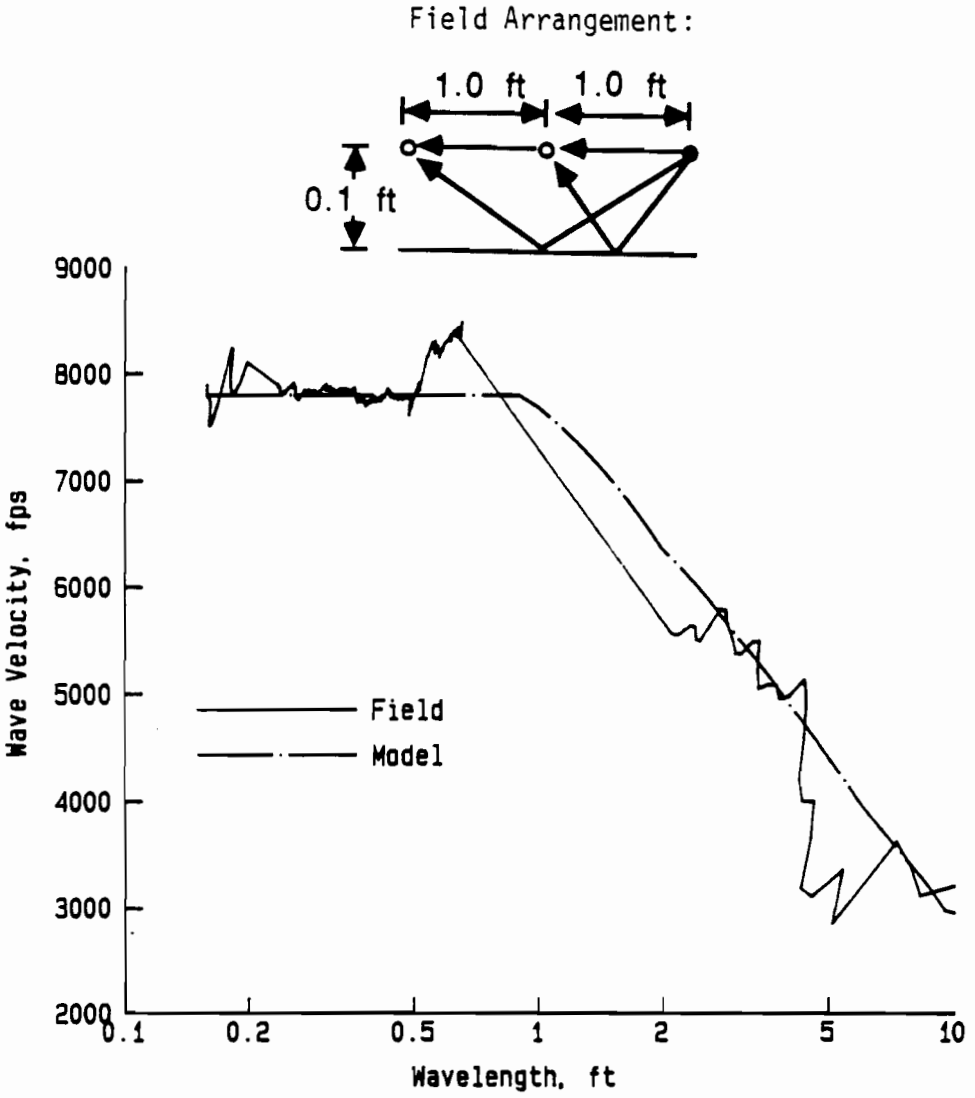

Fig. 4.19. Comparison of Field and Modeled Dispersion Curves for Surface Waves Reflected from a Vertical Boundary: Test Array 1 Oriented Parallel to Reflecting Boundary.

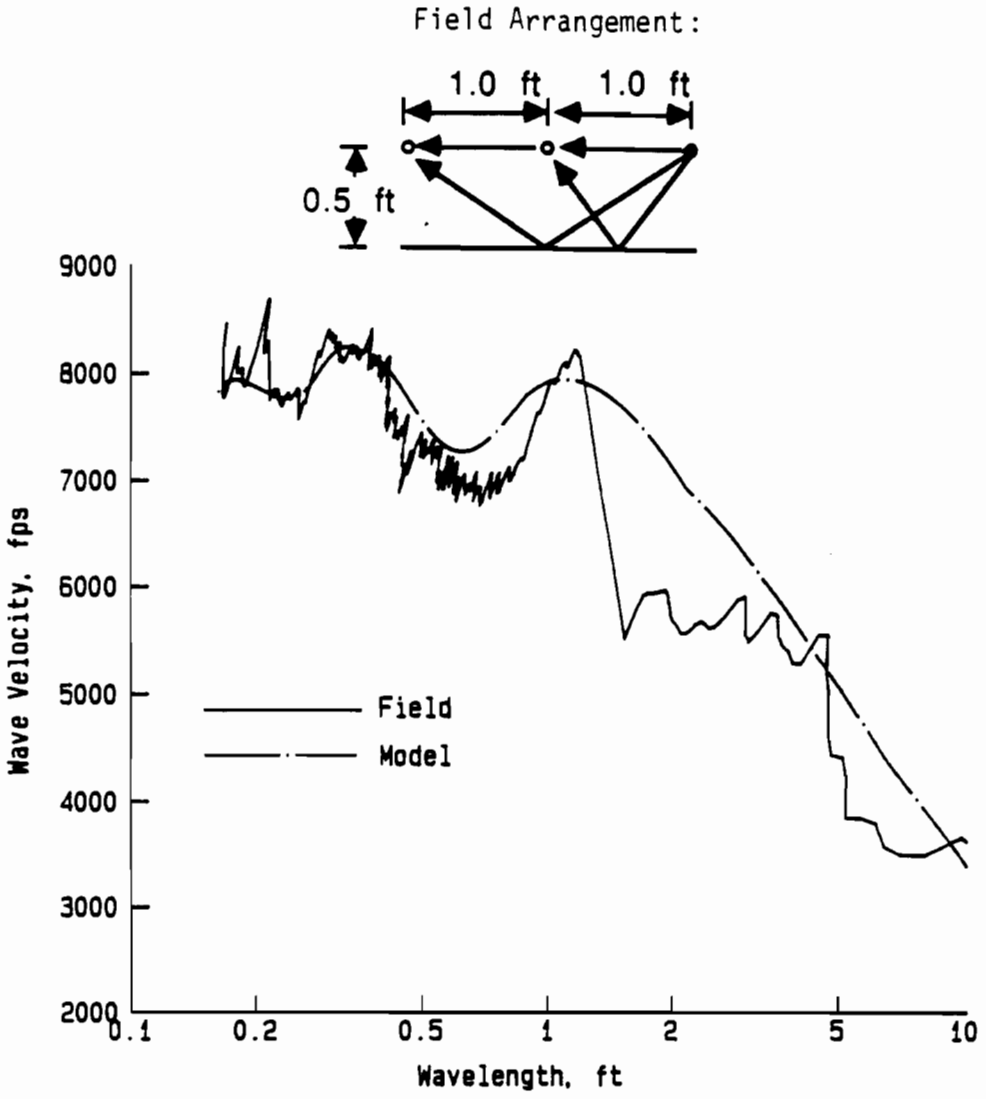

Fig. 4.20. Comparison of Field and Modeled Dispersion Curves for Surface Waves Reflected from a Vertical Boundary: Test Array 2 Oriented Parallel to Reflecting Boundary.

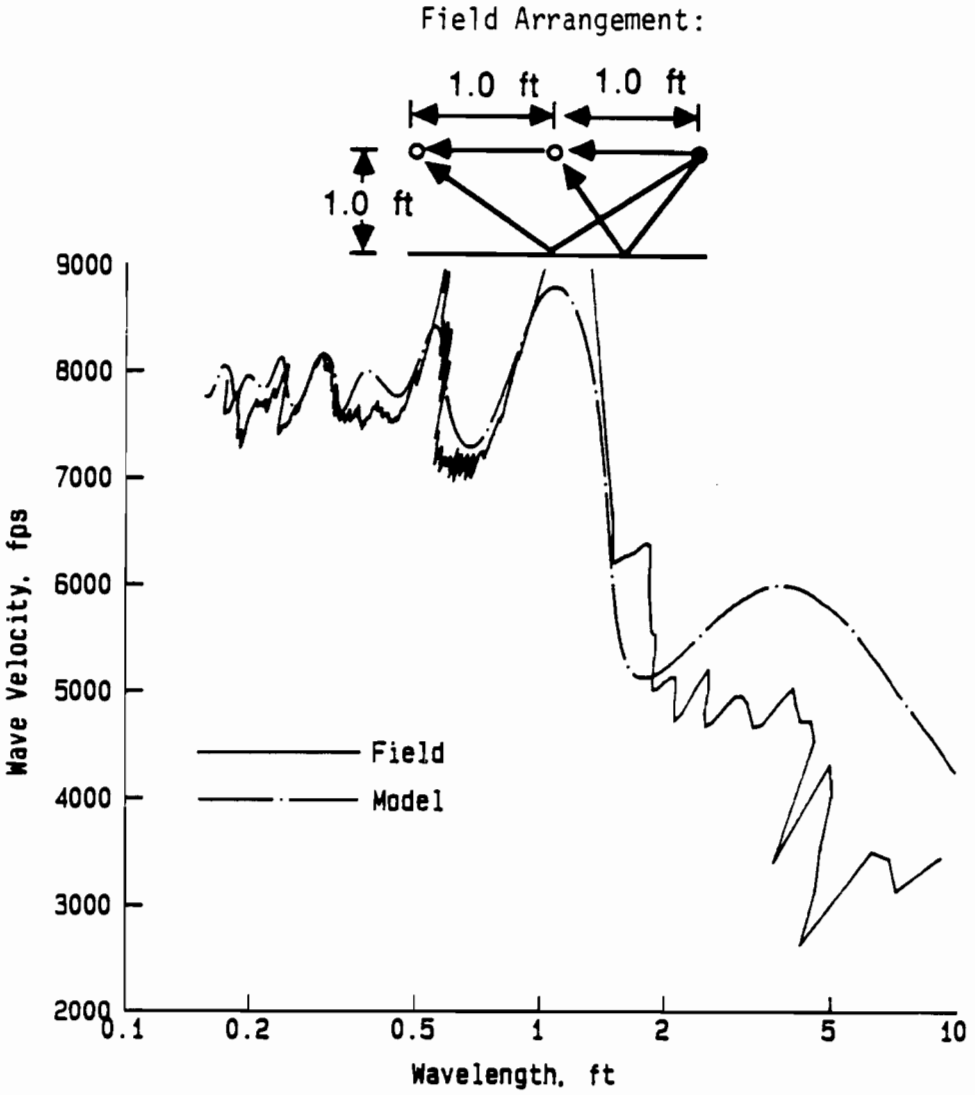

Fig. 4.21. Comparison of Field and Modeled Dispersion Curves for Surface Waves Reflected from a Vertical Boundary: Test Array 3 Oriented Parallel to Reflecting Boundary.

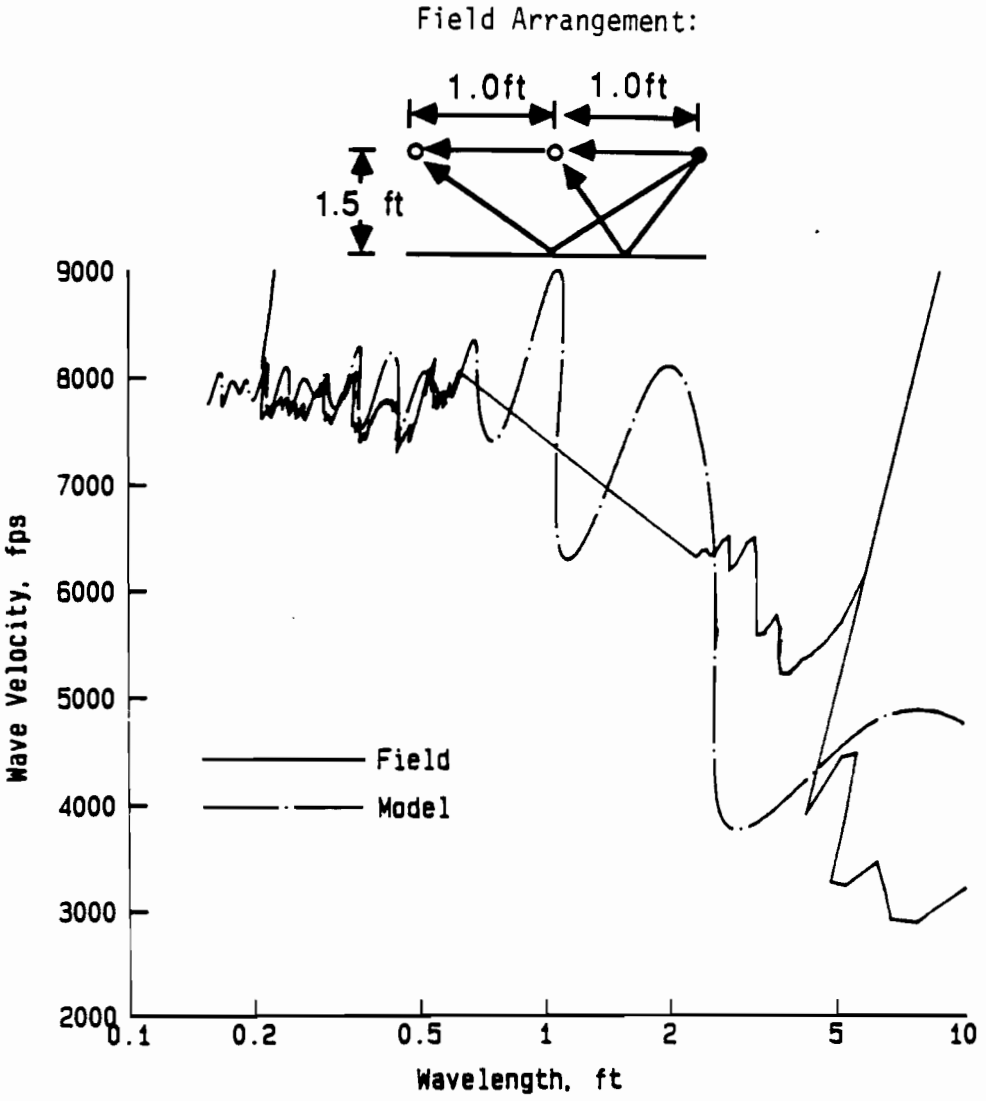

Fig. 4.22. Comparison of Field and Modeled Dispersion Curves for Surface Waves Reflected from a Vertical Boundary: Test Array 4 Oriented Parallel to Reflecting Boundary.

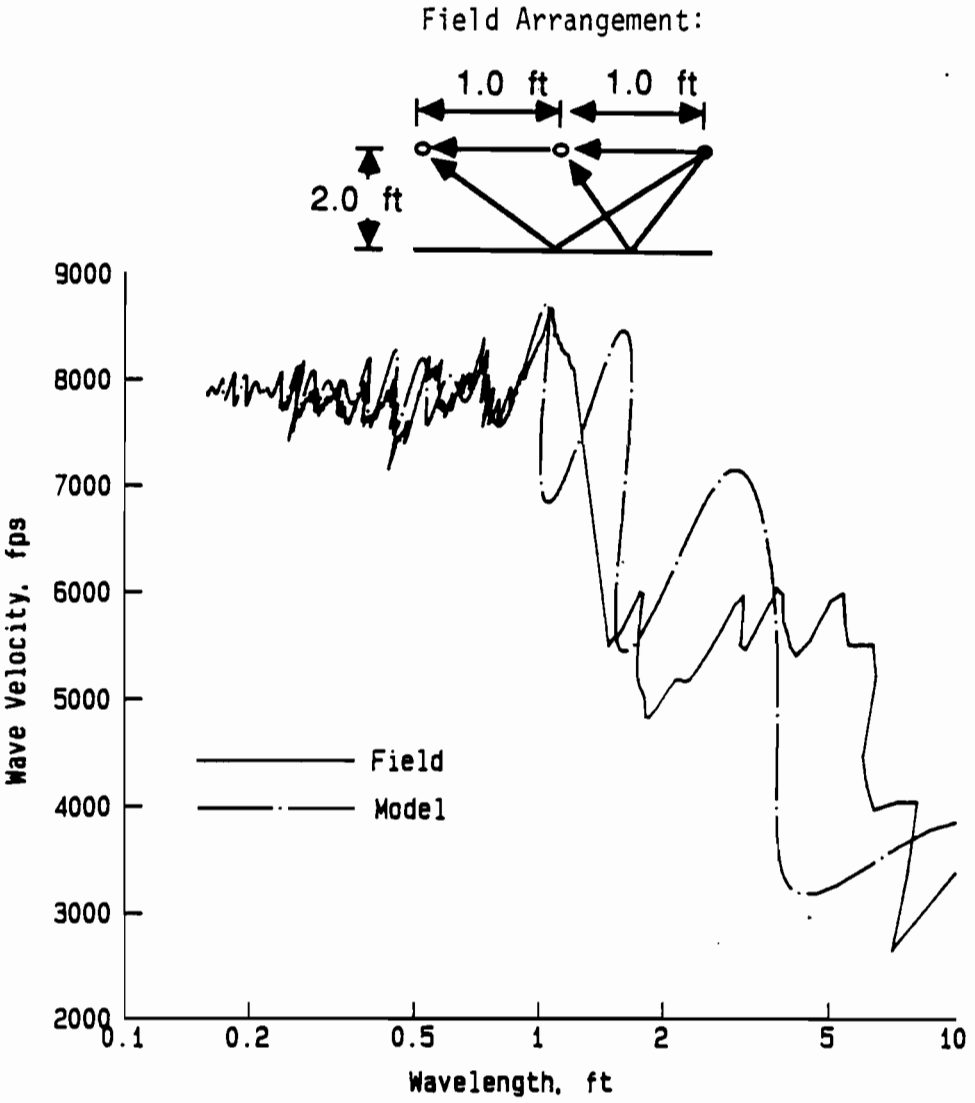

Fig. 4.23. Comparison of Field and Modeled Dispersion Curves for Surface Waves Reflected from a Vertical Boundary: Test Array 5 Oriented Parallel to Reflecting Boundary.

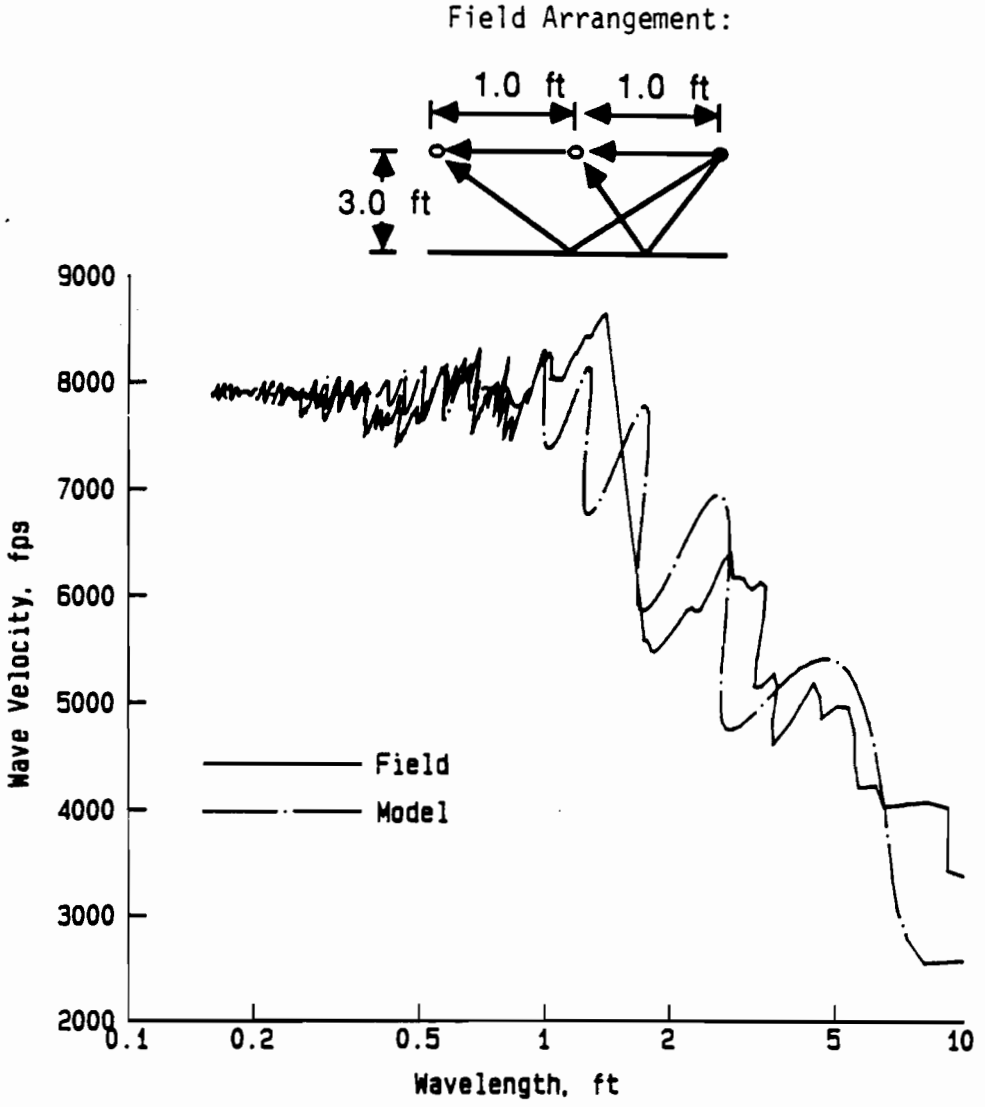

Fig. 4.24. Comparison of Field and Modeled Dispersion Curves for Surface Waves Reflected from a Vertical Boundary: Test Array 6 Oriented Parallel to Reflecting Boundary.

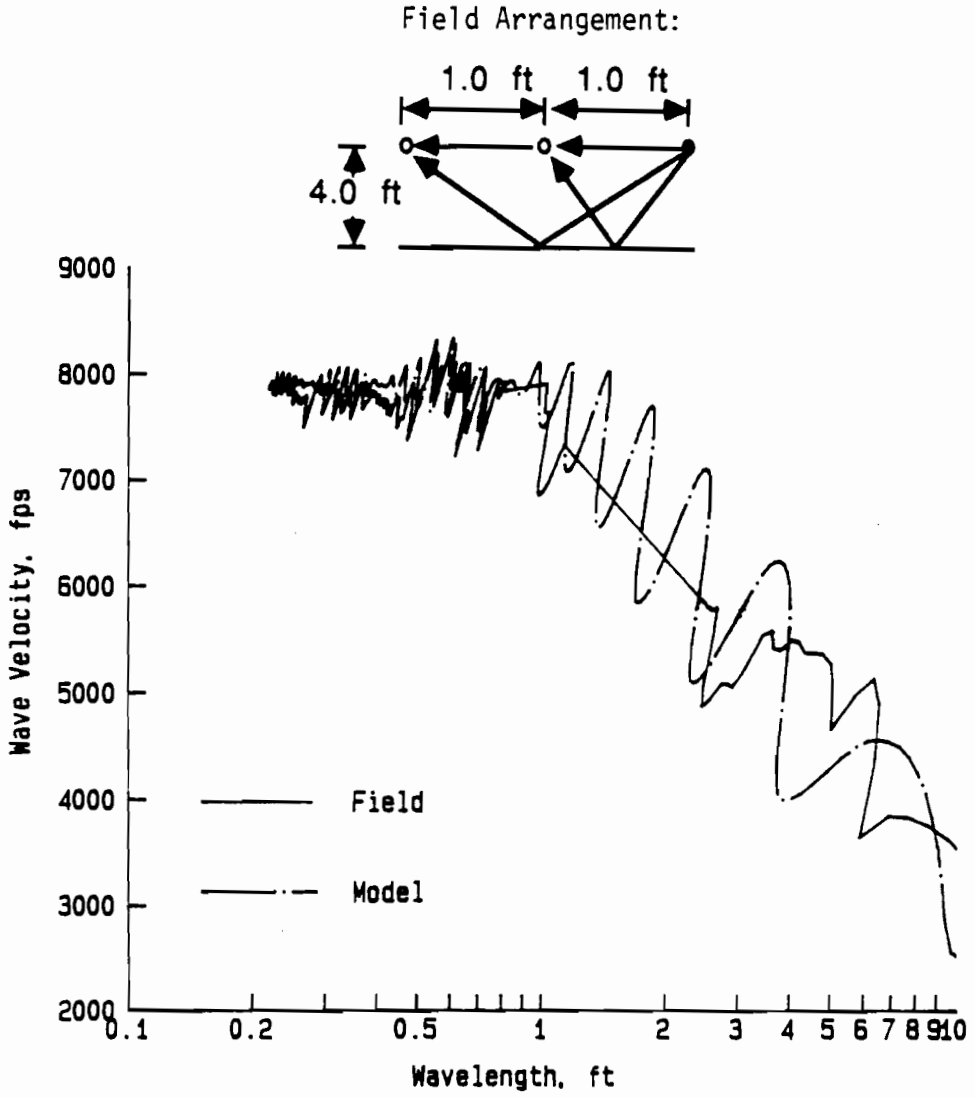

Fig. 4.25. Comparison of Field and Modeled Dispersion Curves for Surface Waves Reflected from a Vertical Boundary: Test Array 7 Oriented Parallel to Reflecting Boundary.

the array from the boundary increases. The field data of arrays 6 and 7 (Figs. 4.24 and 4.25) demonstrate this as the fluctuations in the dispersion curves are relatively small compared to the other arrays (except array 1).

From the above discussion, it can be concluded that as the center line of the array is moved away from the pavement edge, reflected surface waves are more and more out-of-phase with respect to the direct wave and have a more adverse effect on the dispersion curves. However, at the same time, the amplitudes of reflected waves decrease with increasing distance from the boundary which reduces the adverse effect on the dispersion curves. The combination of these two effects makes the choice of the best center-line location of the array relative to the pavement edge not completely straightforward. The following study was done to further explore this problem.

4.3.3. Influence of Distance Between Source and Receivers

A second general study of the influence of parallel reflecting boundaries was conducted to investigate the situation of fixing the distance between the array and the reflecting boundary while varying the source/receiver distances. Test array 2 was selected for this study. Ray paths for direct and reflected waves for array 2 are shown in Fig 4.26.

Comparison of field and modeled dispersion curves are shown in Figs. 4.27 through 4.32. In the case when source and receivers were 0.5 and 2 ft (1.3 and 61 cm) apart (Figs. 4.27 and 4.29), modeled dispersion curves predict the correct trend in the fluctuations in the field dispersion curves, but the locations of the fluctuations are slightly off. In the case when the source and receivers were 1 ft (30 cm) apart, the agreement between field and modeled dispersion curves is very good. In those cases when source and receivers were 3, 4, and 5 ft (91, 122 and 152 cm) apart, it became more difficult to collect data in the high frequency range (frequencies above about 20 kHz). Therefore, there are not enough data to support the modeled dispersion curves. However, all available data, which are in the range of about 0.5 ft (15 cm) or greater, agree well with the modeled dispersion curves.

When the spacings between source and receivers were 5 ft (152 cm), it was virtually impossible to collect data in the high frequency range. As a result, it is not possible to compare field and modeled dispersion curves in the wavelength range shorter than about 1 ft (30 cm).

For all comparisons of field and modeled dispersion curves with source and receivers spacings in the range of 0.5 to 4 ft (15 to 122 cm), it is fair to conclude that the model is capable

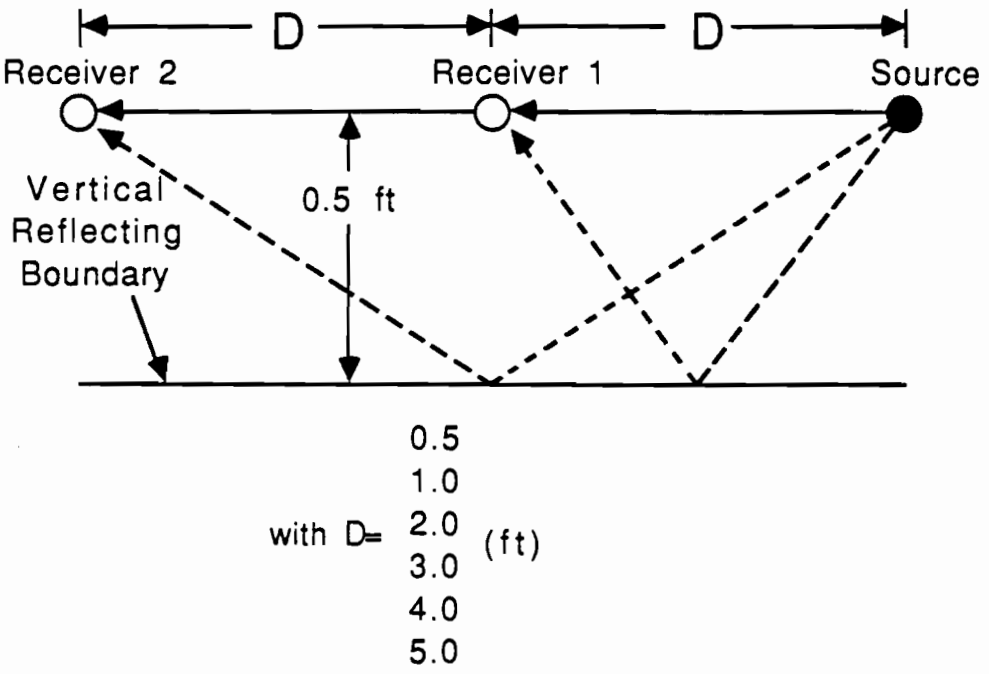

Fig. 4.26. Plan View of Field Arrangement Used to Study the Influence of Source/Receiver Spacing at a Fixed Distance from a Parallel Reflecting Boundary.

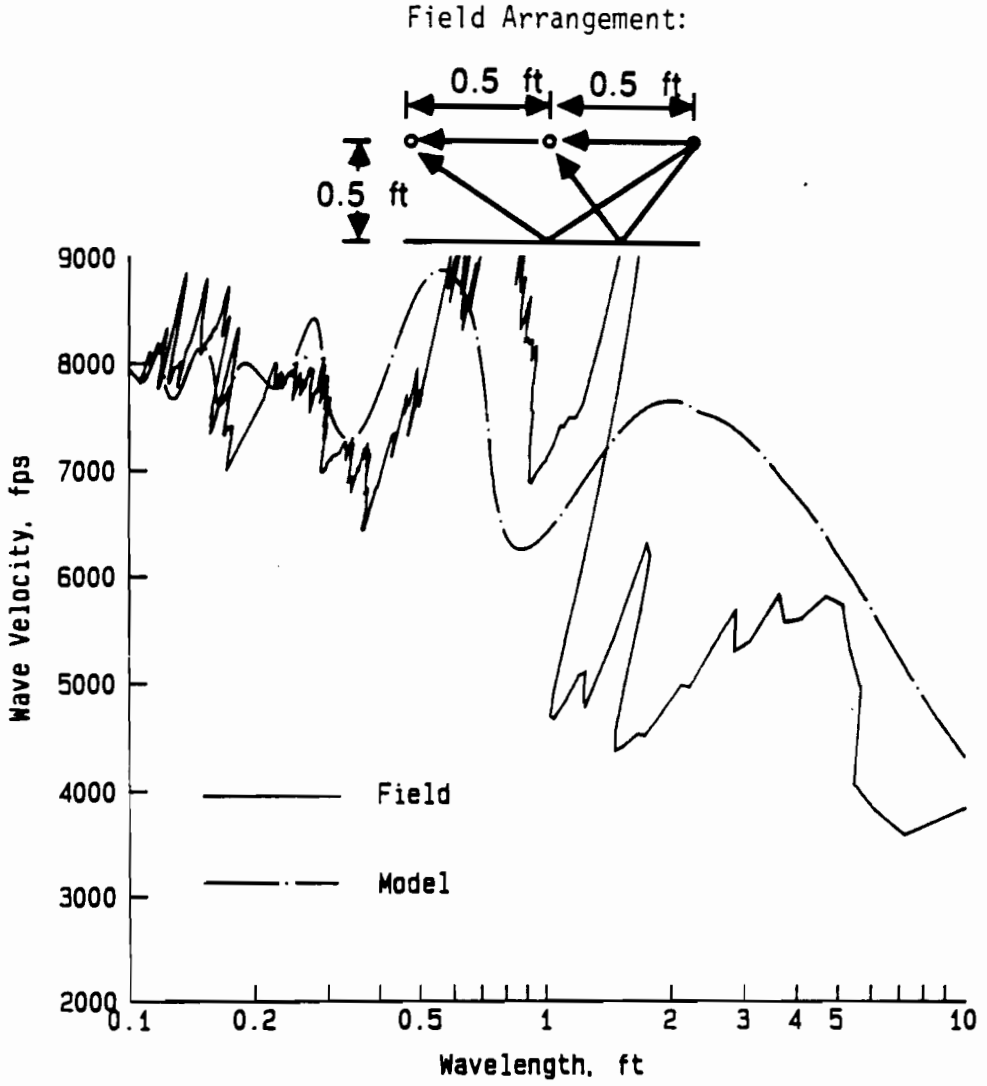

Fig. 4.27. Comparison of Field and Modeled Dispersion Curves for Surface Waves Reflected from a Vertical Boundary: Test Array 2 with 0.5-ft Source/Receiver Spacings.

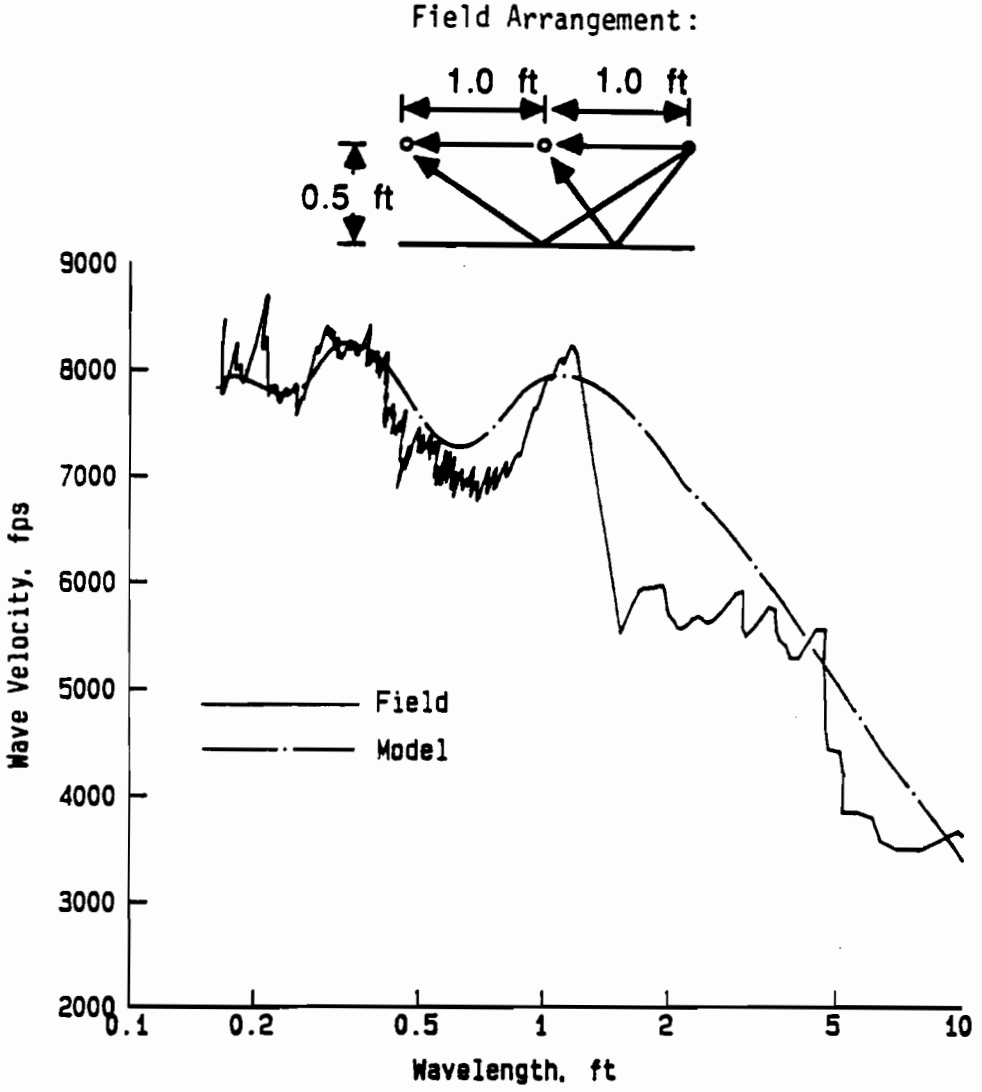

Fig. 4.28. Comparison of Field and Modeled Dispersion Curves for Surface Waves Reflected from a Vertical Boundary: Test Array 2 with 1-ft Source/Receiver Spacings.

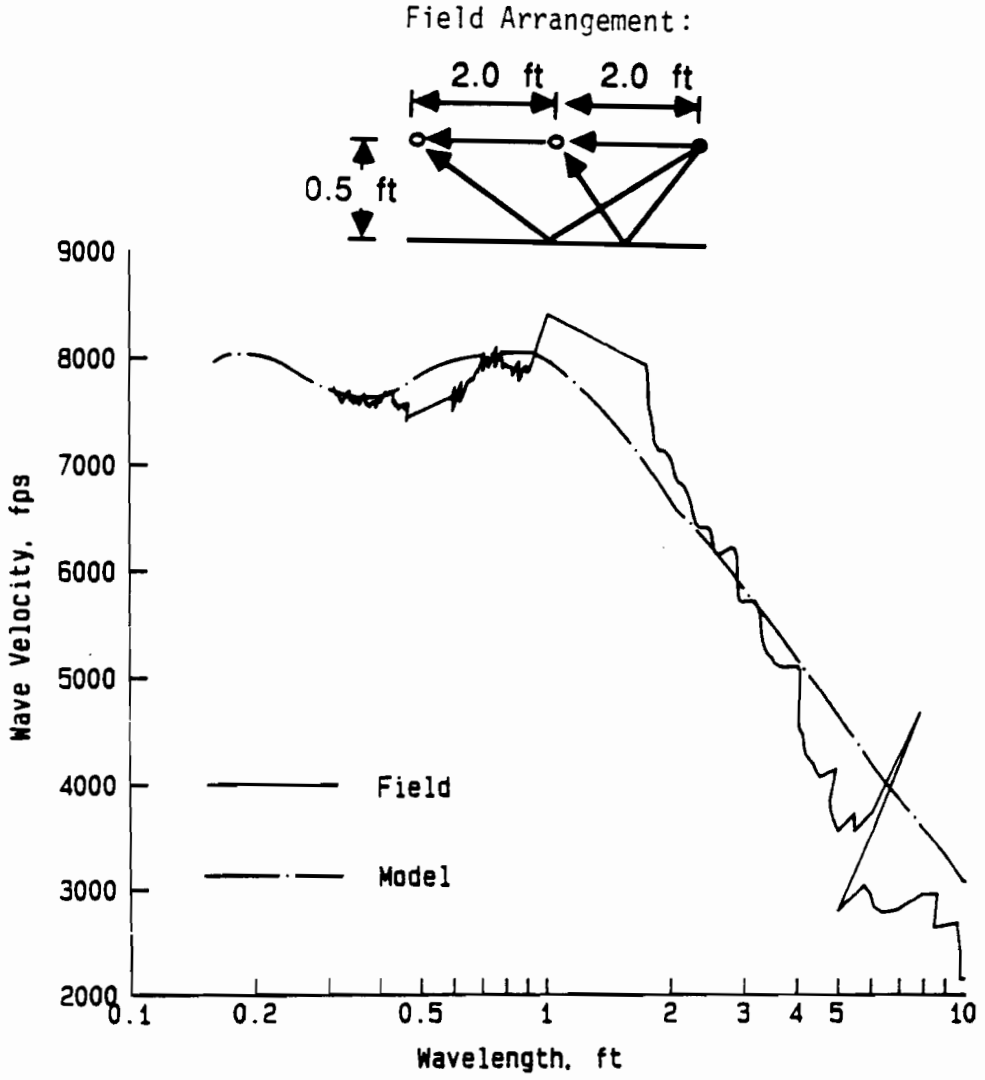

Fig. 4.29. Comparison of Field and Modeled Dispersion Curves for Surface Waves Reflected from a Vertical Boundary: Test Array 2 with 2-ft Source/Receiver Spacings.

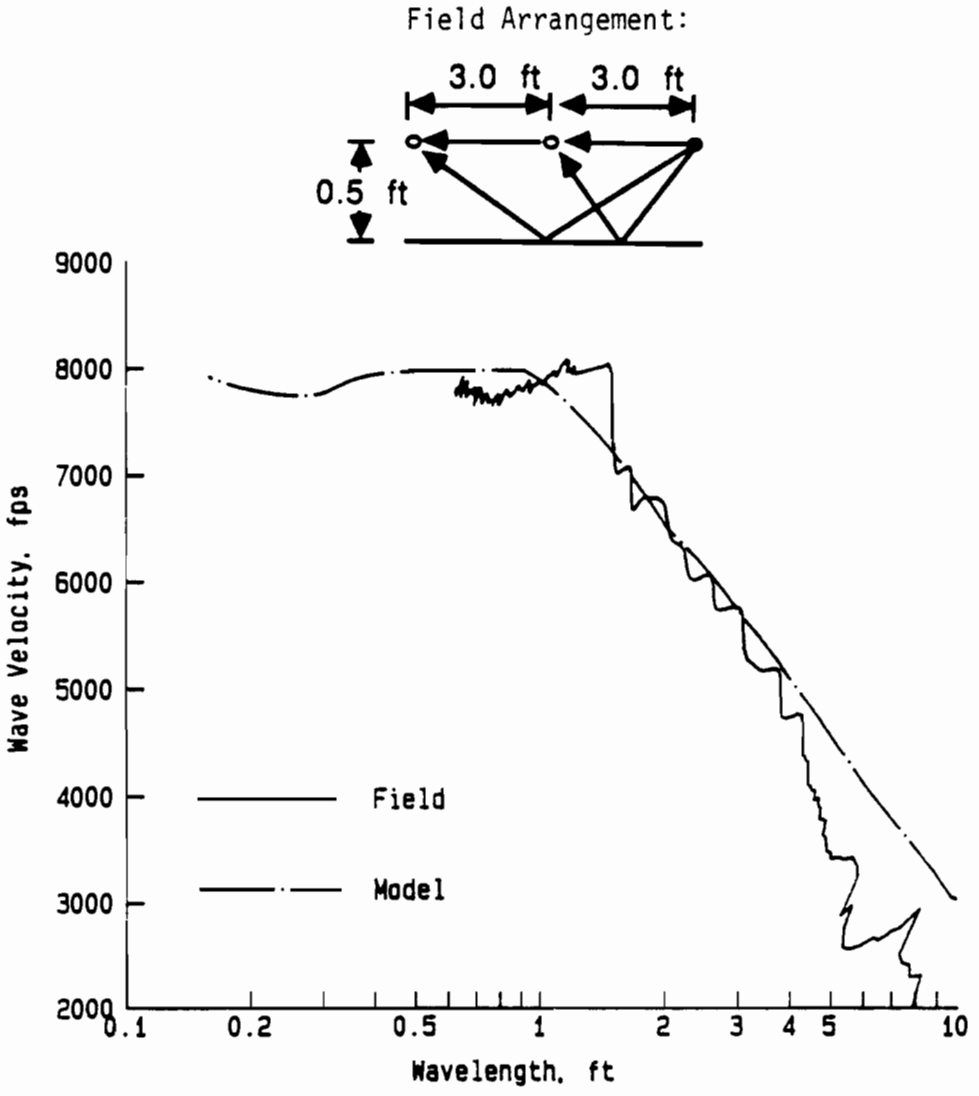

Fig. 4.30. Comparison of Field and Modeled Dispersion Curves for Surface Waves Reflected from a Vertical Boundary: Test Array 2 with 3-ft Source/Receiver Spacings.

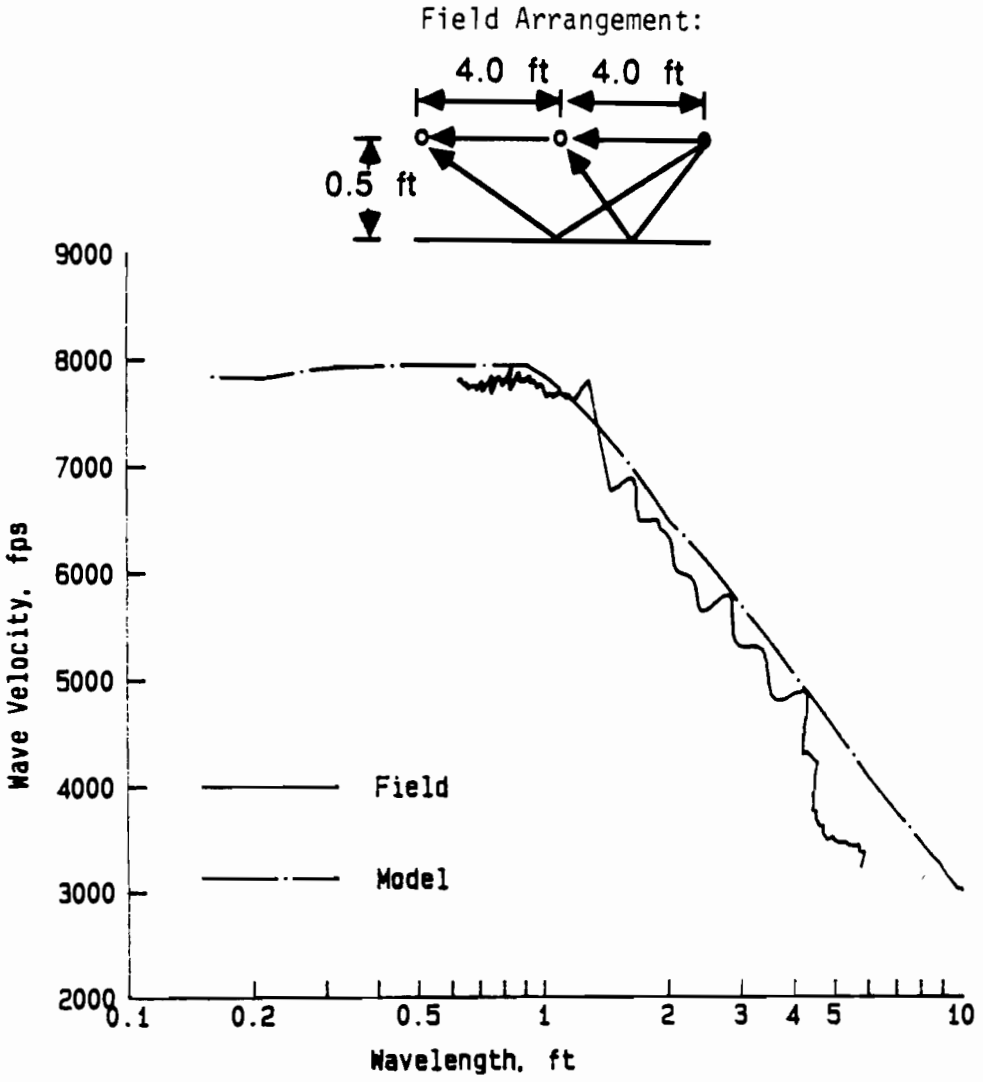

Fig. 4.31. Comparison of Field and Modeled Dispersion Curves for Surface Waves Reflected from a Vertical Boundary: Test Array 2 with 4-ft Source/Receiver Spacings.

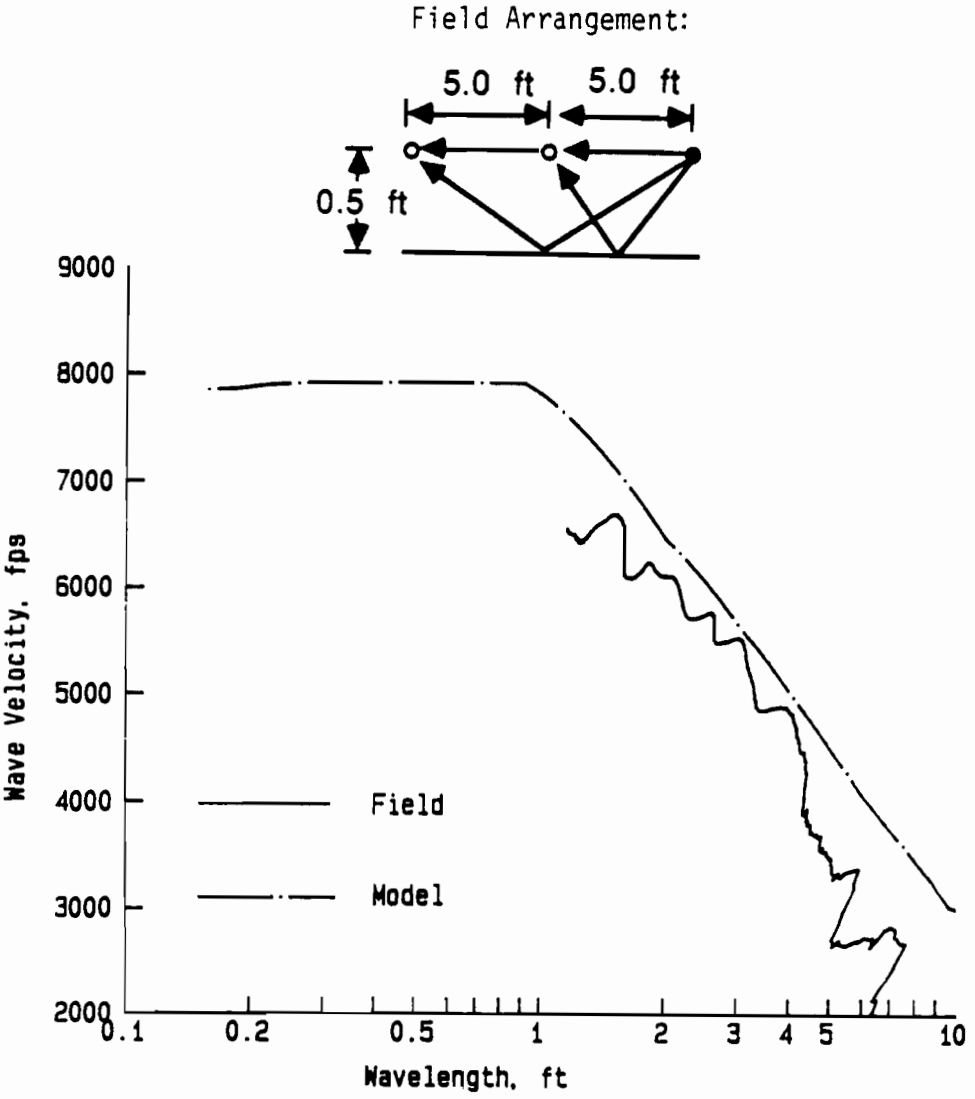

Fig. 4.32. Comparison of Field and Modeled Dispersion Curves for Surface Waves Reflected from a Vertical Boundary: Test Array 2 with 5-ft Source/Receiver Spacings.

of correctly modeling the field dispersion curves. In Fig. 4.33, all modeled dispersion curves for array 2 are presented together. It is easy to see that the dispersion curves corresponding to source/receiver spacings of 2, 3, and 4 ft (61, 91, and 122 cm) are practically identical and are almost unaffected by the existence of reflected surface waves.

4.3.4. A Generalized Approach for Determining the Best Source/Receiver Arrangement

To combine results from the above two studies and draw a conclusion, the following approach was used. Suppose that the source/receiver spacing is defined as D as shown in Fig. 4.34 and the distance between the array and the boundary is k times D. In the first model simulation when the source/receiver spacing was 1.0 ft (30 cm), values of k ranged from 0.1 to 4.0 for arrays 1 through 7, respectively In the model simulation for array 2, values of k ranged from 1.0 to 0.1 for receiver spacings of 0.5 ft to 5.0 ft (15 to 152 cm), respectively. The values of k for these two situations are listed in Table 4.4.

The field data as well as the modeled data lead to the conclusion that there are two possible ranges for k which result in minimizing the effect of reflected surface waves. These ranges for k can be expressed as:

$$k \geq 3.0 \tag{4.1}$$

or

$$k \leq 0.2 \tag{4.2}$$

Either one of these criteria will result in making the influence of reflected surface waves relatively small. These values can then be used as a guide for locating the test array.

4.3.5. Additional Considerations

One should notice that, to keep the value of k low,spacings between the source and receivers have to be rather large. However, as the distance between the source and receivers is increased, it becomes more difficult to collect high-frequency signals because the high-frequency signals tend to attenuate very rapidly with distance. As a result, it becomes impossible to sample material stiffness at shallow depths with large source-to-receiver spacings. This phenomenon is clearly shown in Fig. 4.32. When source-to-receiver spacing was 5 ft (152 cm), it was not possible to acquire any data with wavelengths shorter than about 1 ft (30 cm).

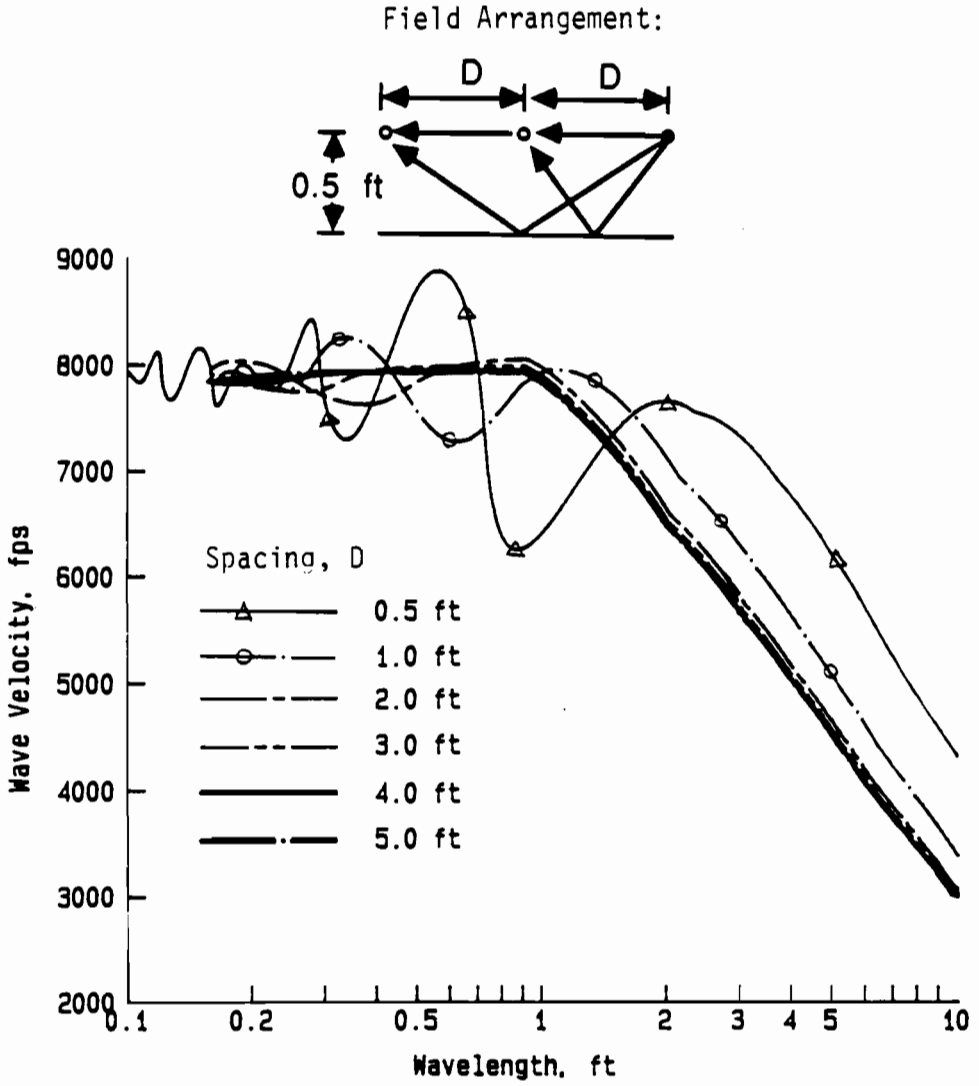

Fig. 4.33. Comparison of Field and Modeled Dispersion Curves for Surface Waves Reflected from a Vertical, Parallel Boundary: Test Array 2 with Various Source/Receiver Spacings.

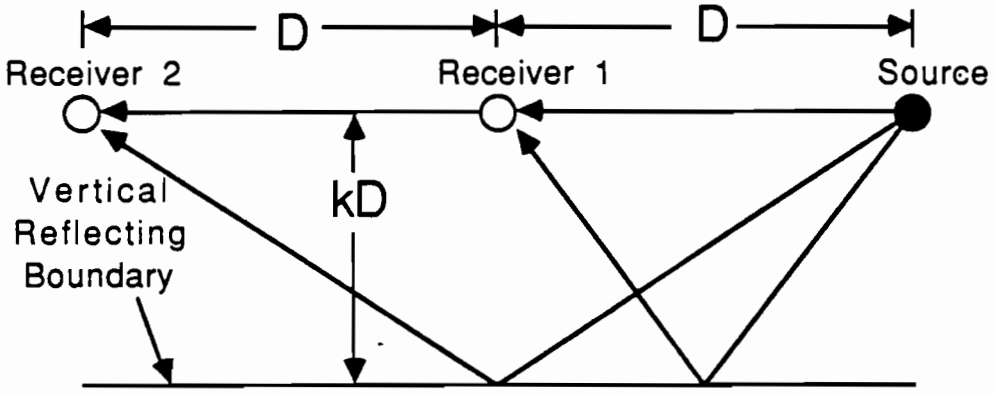

Fig. 4.34. Normalized Scale Illustrating Array/Boundary Configuration for the Test Array Oriented Parallel to the Reflecting Boundary.

TABLE 4.4. RATIOS OF DISTANCE FROM PARALLEL REFLECTING BOUNDARY TO RECEIVER SPACING USED IN FIELD TESTS

I. With 1-ft Spacing Between Receivers for Each Array (Figs. 4.19 through 4.25)

Array No.	k
1	0.1
2	0.5
3	1.0
4	1.5
5	2.0
6	3.0
7	4.0

II. Array 2 with Different Spacings Between Source and Receivers (Figs. 4.27 through 4.32)

Distance, Source to Receiver 1* (ft)	k
0.5	1.00
1.0	0.50
2.0	0.25
3.0	0.17
4.0	0.13
5.0	0.10

* Same as the distance between two receivers

In addition, even if high-frequency signals can be collected, interpretation of data in the high-frequency range becomes more and more difficult as the spacing increases. This point is further explained below.

Imagine that an SASW test is performed in a system with uniform material properties and the spacing between receivers is 0.5 ft (15 cm). Assume that the phase of the cross power spectrum is as shown in Fig. 4.35a. Since the highest frequency corresponds to the shortest wavelength which results in sampling the shallowest material, point A in Fig. 4.35a corresponds to the shortest wavelength that is used to sample. In Fig. 4.35a, the number of cycles at A is 4, and the corresponding wavelength at this point is:

$$\text{Wavelength} = \frac{\text{Receiver Spacing}}{\text{Number of Cycle}} = \frac{0.5 \text{ ft}}{4} = 0.125 \text{ ft} \tag{4.3}$$

The wave velocity corresponding to point A is:

$$\begin{aligned} \text{wave velocity} &= \text{wavelength} \times \text{frequency} \\ V_R &= 0.125 \times 100{,}000 = 12{,}500 \text{ fps} \end{aligned} \tag{4.4}$$

(The value of V_R of 12,500 fps (3813 m/s) is too high for concrete and is simply used in this example for illustrative purposes.)

Suppose the same system is tested with a 3-ft (91-cm) spacing between receivers. Assume that data can be collect in the same frequency range. Then the phase of the cross power spectrum is as shown in Fig. 4.35b. At point B, where the highest frequency is found, the corresponding wavelength is:

$$\text{Wavelength} = \frac{3.0 \text{ ft}}{24} = 0.125 \text{ ft} \tag{4.5}$$

and

$$\text{wave velocity} = 0.125 \times 100{,}000 = 12500 \text{ fps} \tag{4.6}$$

This example shows that, to sample with a 0.125-ft wavelength in this system, the sampling frequency has to be 100 KHz. The corresponding phase goes from 4 cycles for a

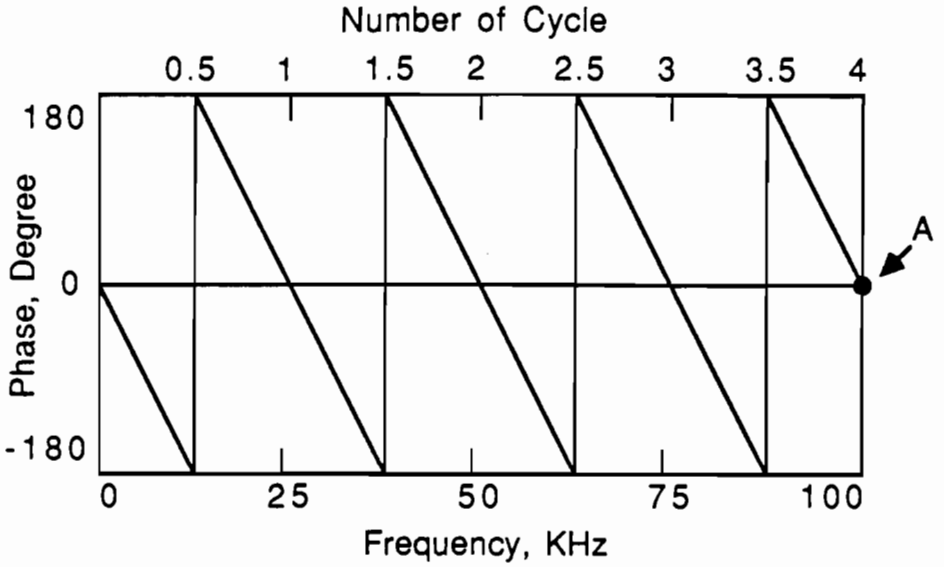

a. Phase of Cross Power Spectrum, Receiver Spacing = 0.5 ft

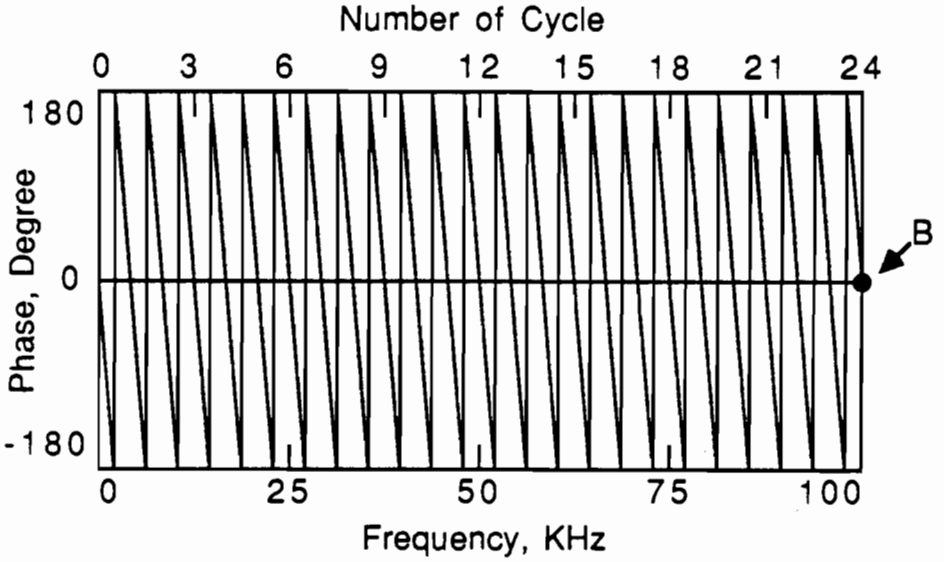

b. Phase of Cross Power Spectrum, Receiver Spacing = 3 ft

Fig. 4.35. Comparison of Phases of Cross Power Spectra for the Same Material Profile but Different Receiver Spacings.

receiver spacing of 0.5 ft (15 cm) to 24 cycles for a receiver spacing of 3 ft (91 cm). Thus, to sample the same shallow depth in this system with different spacings between receivers, the highest sampling frequency has to be the same for each receiver spacing. However, the number of cycles in phase is directly proportional to the spacing between receivers and, thus, increases as receiver spacing increases.

In this example, phase information for both receiver spacings shown in Fig. 4.35 are well defined. Therefore, they are equally easy to interpret. However, in reality, data in some ranges of frequency may not be available. Suppose data in the same range of frequency are lost in both cases. It will still be easy to count the number of cycles in Fig. 4.35a since each cycle is well separated from the adjacent one. However, it will be very difficult to count the number of cycles in Fig. 4.35b because each cycle is so close to the adjacent one. In fact, as receiver spacing increases, there could be a point when those cycles are so closely spaced that they can not be separated. As a result, it is not practical to increase receiver spacing too much. One possible way to resolve this problem is to keep the distance between the two receivers small and only increase the distance between the source and first receiver since the number of cycles in phase is a function of spacing between receivers only. But this type of source/receiver configuration will still induce loss of high-frequency signals mentioned earlier.

4.4. SUMMARY

In this chapter, creations of reflected surface waves and their influence on dispersion curves are discussed in detail. Basically, there are two kinds of reflecting boundaries commonly encountered in field SASW tests. The first case is when the reflecting boundary is oriented perpendicularly to the test array. The second case is when the reflecting boundary is oriented parallel to the test array. All test condtions can be mathematically modelled by the method discussed in Chapter Three. Field and model studies show that the model closely describes the effect of reflected surface waves on dispersion curves under both kinds of test conditions.

In the past, it was a puzzle to know if the fluctuations in the dispersion curves measured during SASW testing were really caused by the fluctuations in material properties or whether there was some other explanation for these fluctuations. In this study, it is found that reflected surface waves impose ripples (fluctuations) on the "true" dispersion curve. If the effect of reflected waves on the dispersion curve is removed, the dispersion curve is basically a smooth curve. At most pavement sites, the dispersion curve corresponding to short wavelengths (equal to the thickness of the top pavement layer and less) is very flat and close to a straight line which

indicates that the stiffness in the top pavement layer is uniform. This finding about the effect of reflections not only solved the puzzle, but also provided an easy method to access the stiffness of the top pavement layer as discussed in Chapter Eight.

Based on both model and field studies, it is conclude that the adverse effects of reflected surface waves on dispersion curves can be reduced by proper arrangement of the location of the source and receivers relative to the reflecting boundary. In the case when the vertical reflecting boundary is oriented perpendicularly to the test array, the adverse effect of reflected waves can be reduced to a minimum by placing the source in between the reflecting boundary and the receivers. In the case when the reflecting boundary is oriented parallel to the test array, it is better to have the test array located very close to the reflecting boundary (so that reflected surface waves are nearly in phase with direct surface waves), or place the array as far away as possible from the reflecting boundary (so that the amplitudes of reflected surface waves are relatively low compared to direct surface waves). A guideline for locating the array is presented in Section 4.3.4 for this type of field arrangement.

CHAPTER FIVE

EFFECT OF DIRECT AND REFLECTED BODY WAVES ON DISPERSION CURVES

5.1. INTRODUCTION

Surface impacts from hammers or drop weights have been used in the past to generate surface waves in all SASW tests. This type of mechanical source has been employed because hammer sources are simple, inexpensive, easy to use and capable of generating energy over the desired frequency ranges for most instances. However, in addition to generating surface waves, surface impacts also generate unwanted body waves. These body waves reach the receivers either directly or through reflections. Problems arise from the fact that body waves propagate with different velocities and dispersive characteristics than surface waves. As a result, body waves can alter the dispersion curve adversely.

The adverse impact of body waves on the dispersion curve is expected to be less than the effect of reflected surface waves shown in Chapter Four. This expectation is based on the fact that the energy generated by a vertically oscillating source on the surface of a homogeneous half-space is distributed as follows (Richart et al, 1970) : 67 percent in Rayleigh (surface) waves, 26 percent in shear waves (S-waves), and 7 percent in compression waves (P-waves). It is clear, therefore, that body waves carry only a small portion of the total energy generated by a surface impact. Furthermore, geometrical damping for body waves is much higher than for surface waves which means that the negative impact from body waves is further diminished.

There are instances when the boundary which reflects body waves is much closer to the test array than the boundary which reflects surface waves. Under these conditions, reflected body waves may become important, and their influence on dispersion curves needs investigation. The effect of body waves on dispersion curves has never been justified in the past. Therefore, studies are presented in this chapter in an attempt to identify their influence, to evaluate the severeness of their influence, and to provide guidelines for reducing their adverse effect on dispersion curves. The simplified mathematical model presented in Chapter Three is used. In addition, field tests using the concrete pavement at the BRC facility are employed for comparison.

Reflected body waves created by boundaries at material discontinuities are well known, and their existence has formed the basis for much seismic exploration in the past (Richart et al, 1970; and Robinson and Treitel, 1980). The generation of reflected body waves is shown

schematically in Fig. 5.1. Three kinds of body waves commonly exist in a pavement system. They are: P-waves, SH-waves, and SV-waves. Since both the direction of the impacts and the direction of the receivers are oriented vertically in SASW testing, particle motions in the vertical direction are dominant and are the most appropriate motions to measure. As a result, the influence of direct SV-waves, reflected SV-waves, and reflected P-waves are of most concern.

5.2. REFLECTED SHEAR WAVES FROM BOTTOM OF PAVEMENT SURFACE LAYER

Field tests on the concrete pavement at the BRC facility were performed at general location 2 shown in Fig. 3.2. A fixed receiver-to-receiver spacing of 1.0 ft (30 cm) was used. Source/receiver distances were varied from 0.25 to 5.0 ft (7.6 to 152 cm). A list of distances from the source to first receiver and between the two receivers is presented in Table 5.1. Field data are shown in Fig. 5.2 for all test spacings. Since the highest sampling frequency used was 10 KHz, it was not possible to have any data for wavelengths shorter than about 0.8 ft (24 cm). There is a relatively constant band of fluctuations in wave velocity (about 1000 fps (305 m/s)) throughout the complete range of wavelengths with one exception. In the range of wavelengths from about 1 to 2 ft (30 to 61 cm), an even bigger fluctuation in wave velocity occurs for which the cause is unknown.

Ray paths of body waves used in the model simulation are shown in Fig. 5.3. Only one reflecting boundary is considered in this study which is the bottom of the concrete pavement layer. Because this interface represents a location of significant stiffness change, a fair amount of energy will be reflected by this interface. (An interface with a large stiffness change tends to reflect more energy than an interface with a small stiffness change.) In addition, this interface usually is much closer to the source and receivers than any other reflecting boundaries. Therefore, this reflecting boundary is selected for study.

The modeled dispersion curves are shown in Fig. 5.4. The amplitudes, A's, used for direct surface waves at receivers 1 and 2 are 1 and 0.9, respectively,and for reflected shear waves are 0.15 and 0.12, respectively. These amplitudes are used without any change for all cases so that the effect of source/receiver distance can be more easily identified. Since shear (body) waves attenuate at a much faster rate than surface waves, their effect on the dispersion curves will decrease as the source/receiver distances increase. Therefore, the effect of reflected waves are somewhat overestimated for larger source/receiver spacings in the model.

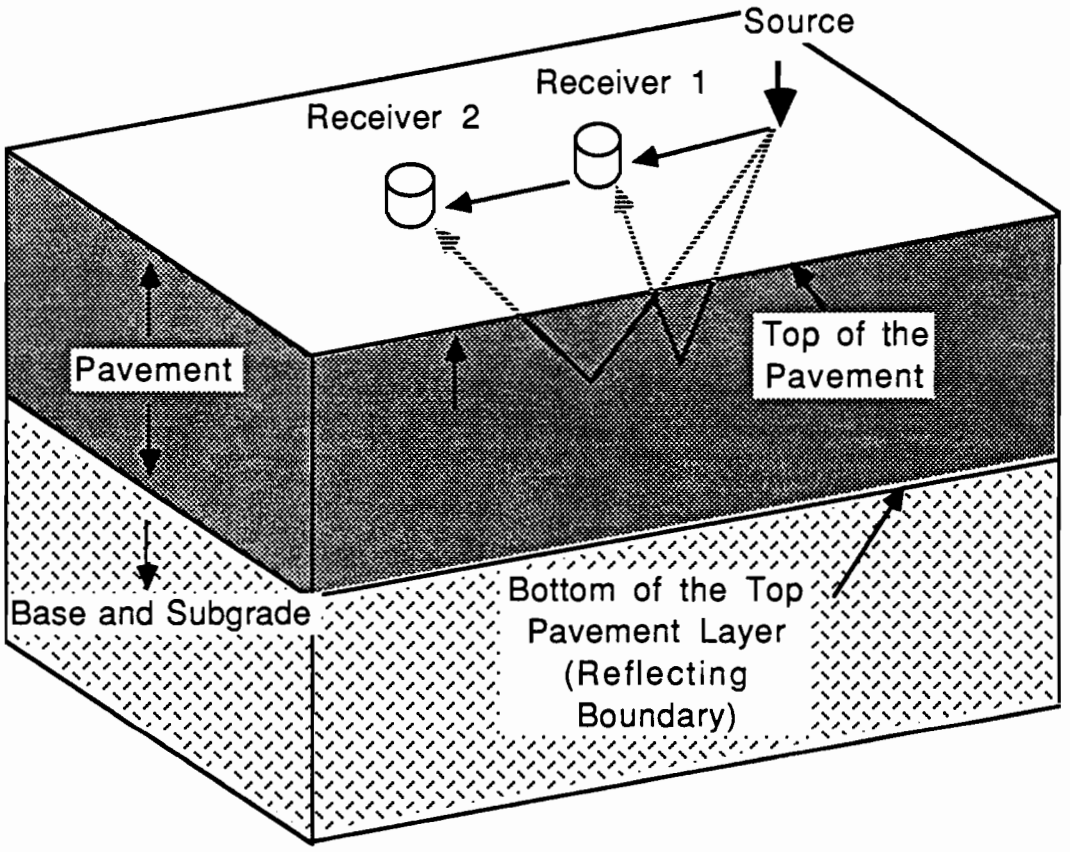

Fig. 5.1. Generation of Reflected Body Waves from Bottom of Pavement Surface Layer.

TABLE 5.1. DISTANCES FROM SOURCE TO RECEIVER AND BETWEEN RECEIVERS IN REFLECTED BODY WAVE TESTS

Distance from Source to Receiver 1 (d_1)* (ft)	Distance Between Two Receivers (D) (ft)
0.25	1.00
0.50	1.00
1.00	1.00
1.50	1.00
2.00	1.00
3.00	1.00
4.00	1.00
5.00	1.00

* Field Arrangement:

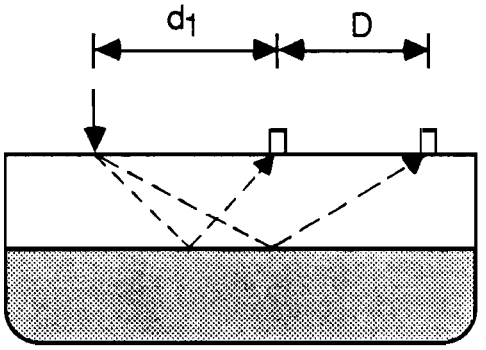

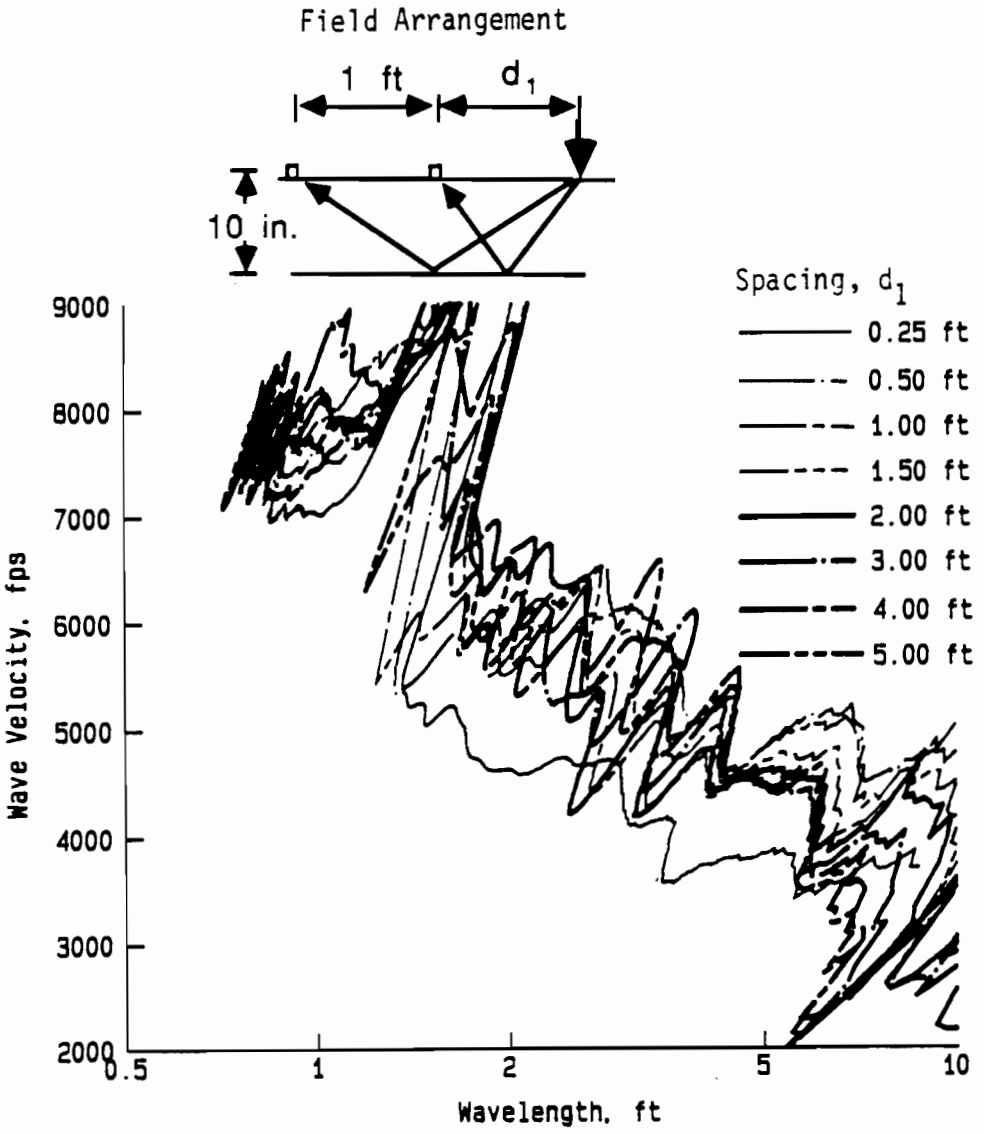

Fig. 5.2. Field Dispersion Curves for Concrete Pavement Site with 1-ft Receiver-to-Receiver Spacing and Various Source-to-Receiver 1 Distances.

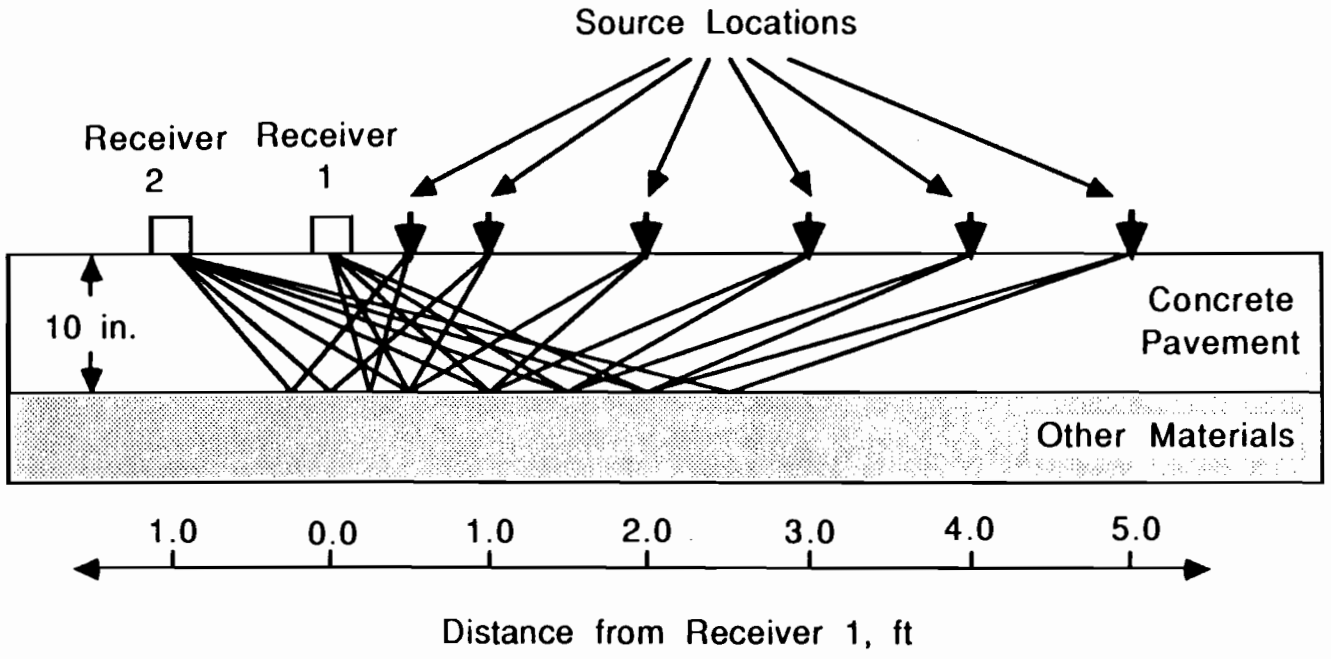

Fig. 5.3. Ray Paths Assumed for Body Waves Reflected from Bottom of Concrete Pavement.

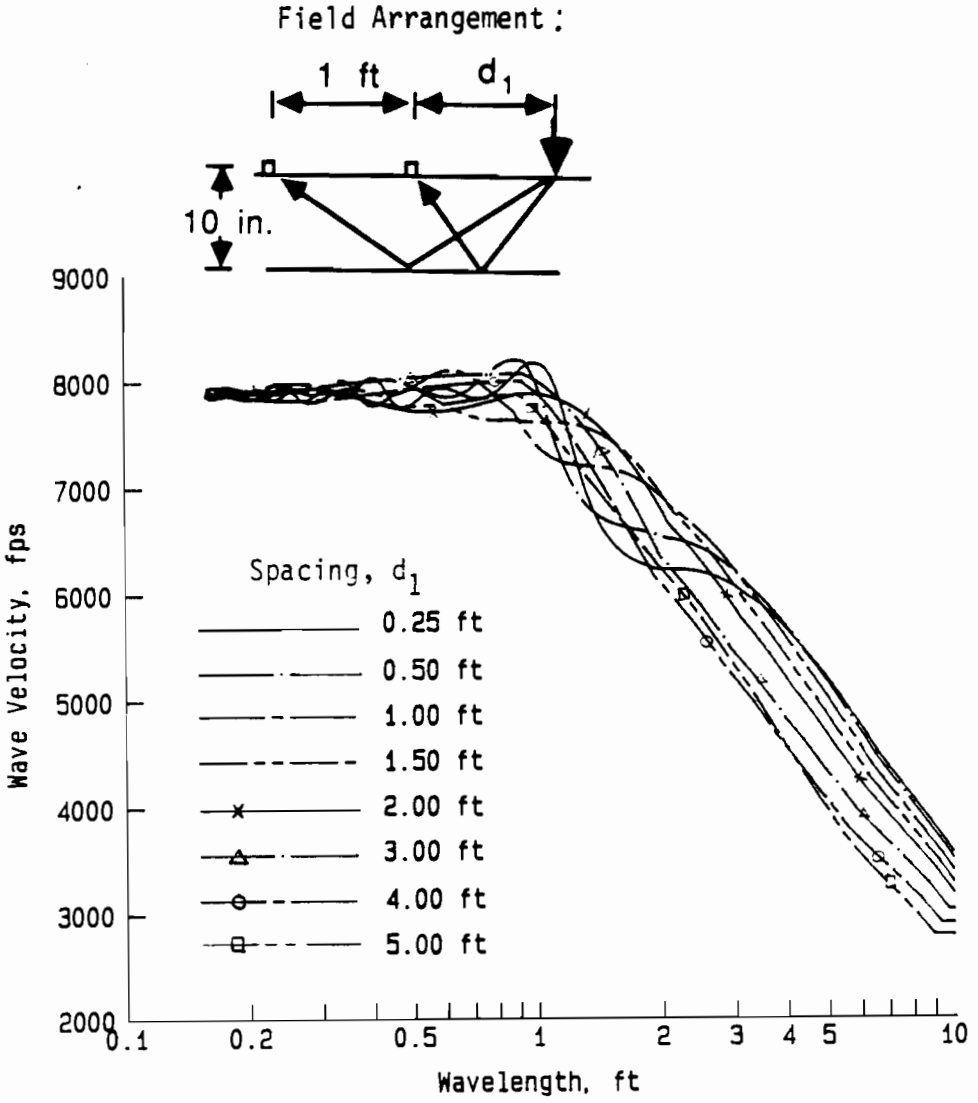

Fig. 5.4. Modeled Dispersion Curves for Reflected Shear Waves: Concrete Pavement with a Fixed Receiver Spacing of 1 ft and Various Source-to-Receiver 1 Distances.

The modeled dispersion curves are shown in Fig. 5.4. These curves demonstrate that, as the source/receiver spacing increases, fluctuations in the dispersion curve decrease. In addition, the shear wave has more influence in the long-wavelength range (greater than 0.7 ft (21 cm)) than in the short -wavelength range. For wavelengths less than about 0.5 ft (15 cm), the effect is negligible. Since surface waves with wavelengths less than 0.5 ft (15 cm) sample basically the top concrete layer, it appears that reflected shear waves barely affect the measurement of material stiffness in the concrete layer.

Because the measured dispersion curves shown in Fig. 5.2 exhibit a lot of high-frequency fluctuations, possibly caused by the surface wave reflections, it is rather difficult to judge the success of the shear wave modeling. However, the field dispersion curves seem to be more or less parallel to each other in the long wavelength range (wavelengths longer than about 1.5 ft (46 cm)), and the modeled dispersion curves exhibit this characteristic in the same fashion. In addition, because both field and modeled dispersion curves are more or less parallel to each other, the field data also exhibit slightly higher velocities at shorter spacings as predicted by the model, with the exception of data from the source/receiver spacing of 0.25 ft (7.6 cm). The reason why this set of data shows a relatively low velocity is unknown. However, with these similar trends between field and modeled dispersion curves, it seems that the model is working quite well.

5.3. REFLECTED COMPRESSION WAVES FROM BOTTOM OF PAVEMENT SURFACE LAYER

The same study as the one presented in Section 5.2 was performed for P-wave reflections in this section. The amplitudes,A's, used at receivers 1 and 2 are 1 and 0.9, respectively, for direct surface waves and 0.1 and 0.08, respectively, for reflected P-waves. Modeled dispersion curves are shown in Fig. 5.5. As opposed to reflected shear waves, there are many cross-overs in this set of dispersion curves (curves are not parallel), and the increase of source/receiver spacing does not seem to either decrease or increase the amplitudes of the fluctuations. Also, it is necessary to keep in mind that P-waves attenuate much faster than surface waves, and the dispersion curves corresponding to larger source/receiver spacings are somewhat overestimated.

The modeled dispersion curves also demonstrate that reflected P-waves have more effect in the long-wavelength range than in the short-wavelength range just as was found for shear waves. For wavelengths shorter than about 0.7 ft (21 cm), the effect of reflected P-waves on the dispersion curve is negligible which implies that the measurement of material stiffness in the top

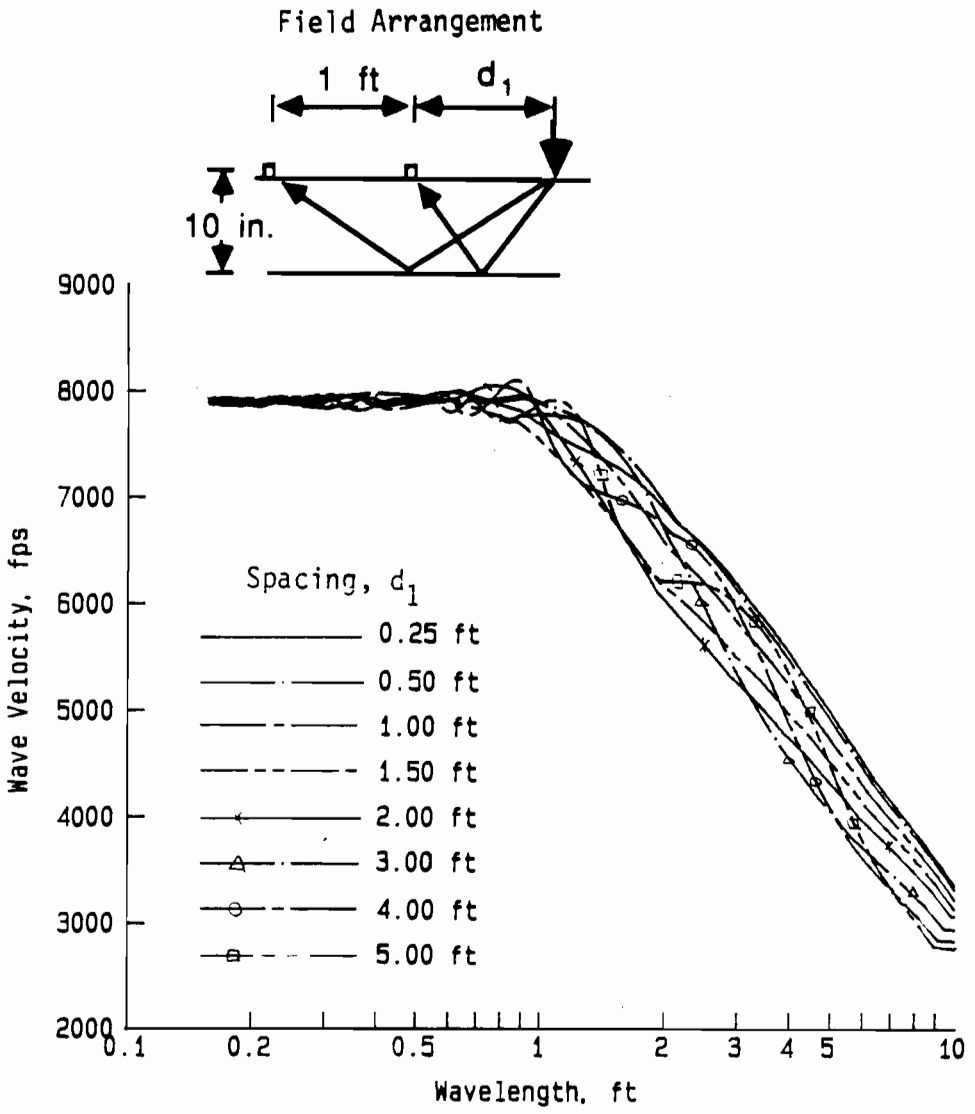

Fig. 5.5. Modeled Dispersion Curves from Reflected Compression Waves: Concrete Pavement with a Fixed Receiver Spacing of 1 ft and Various Source-to-Receiver 1 Distances.

concrete layer will not be affected by reflected P-waves based on the same reasoning stated in the last section on reflected S-waves.

5.4. DIRECT COMPRESSION AND DIRECT SHEAR WAVES

As mentioned in Section 3.6, shear and compression waves not only transmit a very small portion of the impact energy from the source but also exhibit larger geometric damping (attenuation) than surface waves. Consequently, the influence of body waves on dispersion curves is expected to be minor in most instances.

Direct (rather than reflected) compression waves are further reduced in influence due to their relatively small amplitude. Because the direction of impact from the source is perpendicular to the pavement surface, one can imagine that very little impact energy is distributed to horizontally propagating compression waves. As such, direct compression waves propagating at the surface take an even smaller portion of the total impact energy.

A modeling of the influence of direct compression waves on dispersion curves is shown in Fig. 5.6. The "true" dispersion curve is shown in the same figure for comparison. This example assumes that the distances from source to receiver 1 and between the two receivers are both equal to 1 ft (30 cm). Amplitudes selected in this model for each arrival are proportional to the impact energy distribution (67 percent for surface waves and 7 percent for P-waves) and includes geometric damping to demonstrate a more realistic modeling. The amplitude of surface waves decreases with the square root of propagation distance while body wave amplitude decreases with the square of the propagation distance. Hence, the amplitudes used for direct surface waves are 1.0 and 0.707 at receivers 1 and 2, respectively, and for direct P-waves the amplitudes are 0.01 and 0.025 at receivers 1 and 2, respectively. As shown in Fig. 5.6, the "true" and modeled curves are nearly the same. Therefore, direct compression waves have a negligible effect on the direct surface wave ("true") dispersion curve.

Direct shear waves, on the other hand, take a significant portion of the total impact energy because the direction of impact is perpendicular to the pavement surface. However, due to the fact that direct shear waves and surface waves have similar velocities, direct shear waves tend to be more or less in-phase with surface waves because they arrive at similar times at the receivers. Therefore, the influence of direct shear wave on dispersion curves is not expected to be very significant.

A modeling of dispersion curves with and without the influence of direct shear waves is shown in Fig. 5.7. Amplitudes used for each arrival are assumed to be proportional to their

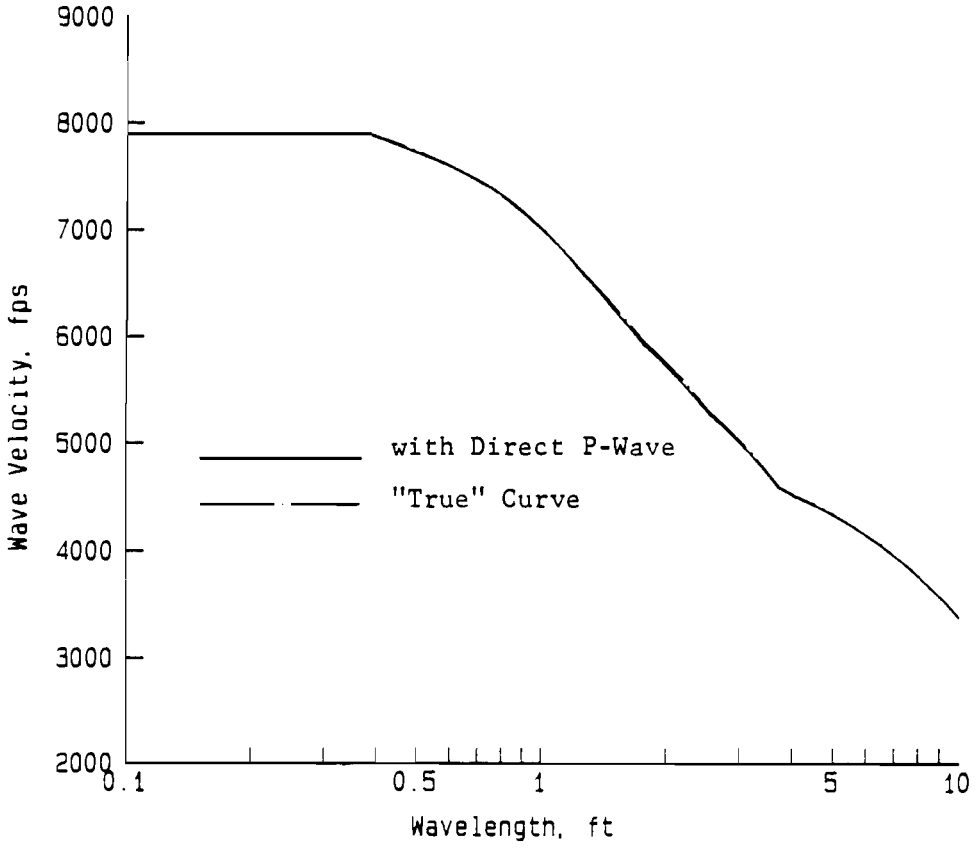

Fig. 5.6. Effect of Direct Compression Wave on the Dispersion Curve.

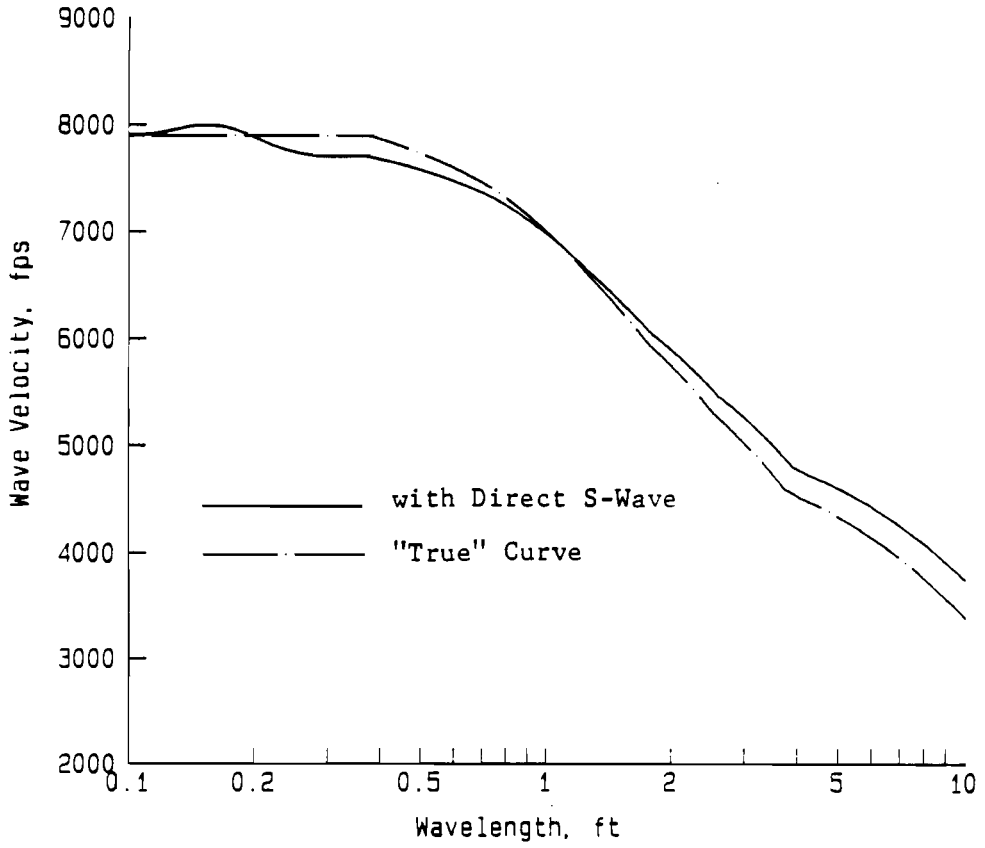

Fig. 5.7. Effect of Direct Shear Wave on the Dispersion Curve.

energy distribution (67 percent for surface waves and 26 percent for S-waves). Geometric damping is also considered. The amplitudes, A's, used for direct surface waves are 1 and 0.707 at receivers 1 and 2, respectively. For direct S-waves, they are 0.388 and 0.097 at receivers 1 and 2, respectively. Both curves shown in Fig. 5.7 follow each other closely, with the difference between them being relatively small.

In summary, direct shear waves and direct compression waves are relatively unimportant in SASW testing compared to other reflected waves and need not be considered in most instances.

5.5 MULTIPLE REFLECTIONS OF SHEAR AND COMPRESSION WAVES IN THE PAVEMENT SURFACE LAYER

All reflections considered in Sections 5.2 and 5.3 are those which have only been reflected once by the bottom boundary of the top layer before they reach the receivers. However, reflected waves can be reflected more than once before they reach the receivers. Reflected waves composed of one and two reflections are presented schematically in Fig. 5.8. Modeled dispersion curves for one reflection and for the combined first and second reflections in the top layer are shown in Fig. 5.9 for shear waves and Fig. 5.10 for compression waves. The distances from source to receiver 1 and between the two receivers are assumed to be 1 ft (30 cm). In the case of reflected S-waves, amplitudes, A's, used at receivers 1 and 2 are 1 and 0.9 for direct surface waves, 0.15 and 0.12 for one-time reflections, and 0.1 and 0.08 for two-time reflections. In the case of reflected P-waves, amplitudes, A's, used at receivers 1 and 2 are 1 and 0.9 for direct surface waves, 0.1 and 0.08 for one-time reflections, and 0.06 and 0.05 for two-time reflections.

For both cases of reflected P-waves and reflected S-waves shown in Figs. 5.9 and 5.10, the one-time reflected wave imposes low-frequency fluctuations on the "true" dispersion curve. However, the two-time reflections impose higher frequency fluctuations than those seen on the one-time reflection dispersion curves. Although the rule of superposition does not apply here (that is, the dispersion curve corresponding to the combined one-time and two-time reflected waves is not simply the superposition of the dispersion curve corresponding to a one-time reflected wave and the dispersion curve corresponding to a two-time reflected wave), it still seems that more reflected waves just add more to the fluctuations on the "true" dispersion curve.

A modeled dispersion curve with combined first and second reflected S-waves and first and second reflected P-waves (the combination of all reflected waves shown in Figs 5.9 and 5.10) is shown in Fig. 5.11. This modeled dispersion curve shows that the combined effect (reflected S- and P-waves) still does not increase the amplitudes of the fluctuations significantly in

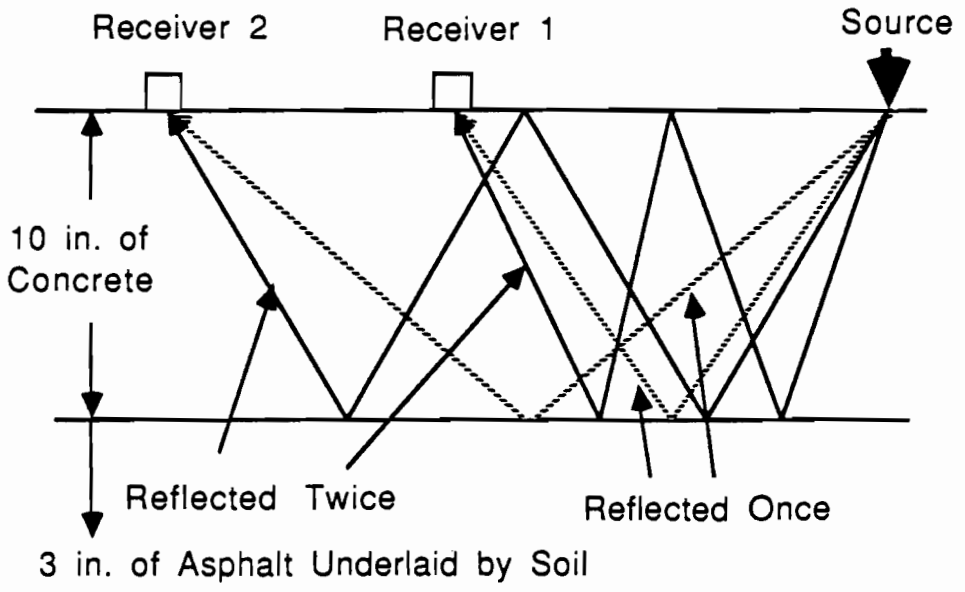

Fig. 5.8. Ray Paths for Multiple Reflections of Body Waves.

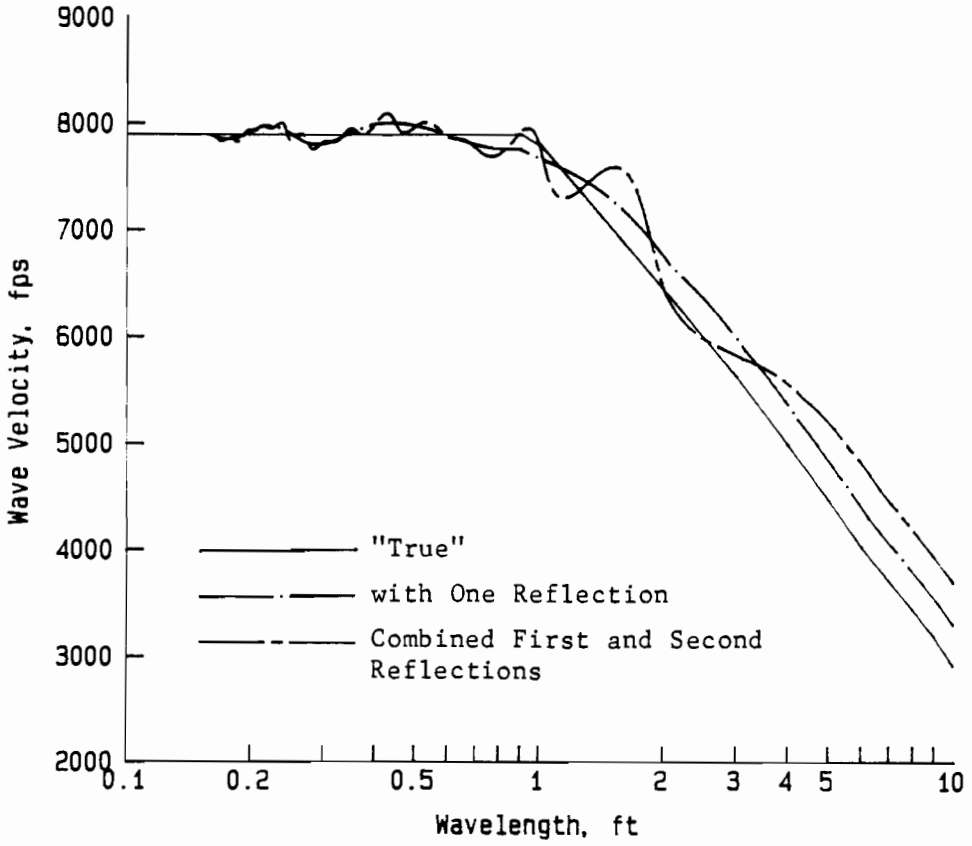

Fig. 5.9. Effect on Dispersion Curve of Reflected Shear Waves: One Reflection versus Combined First and Second Reflections.

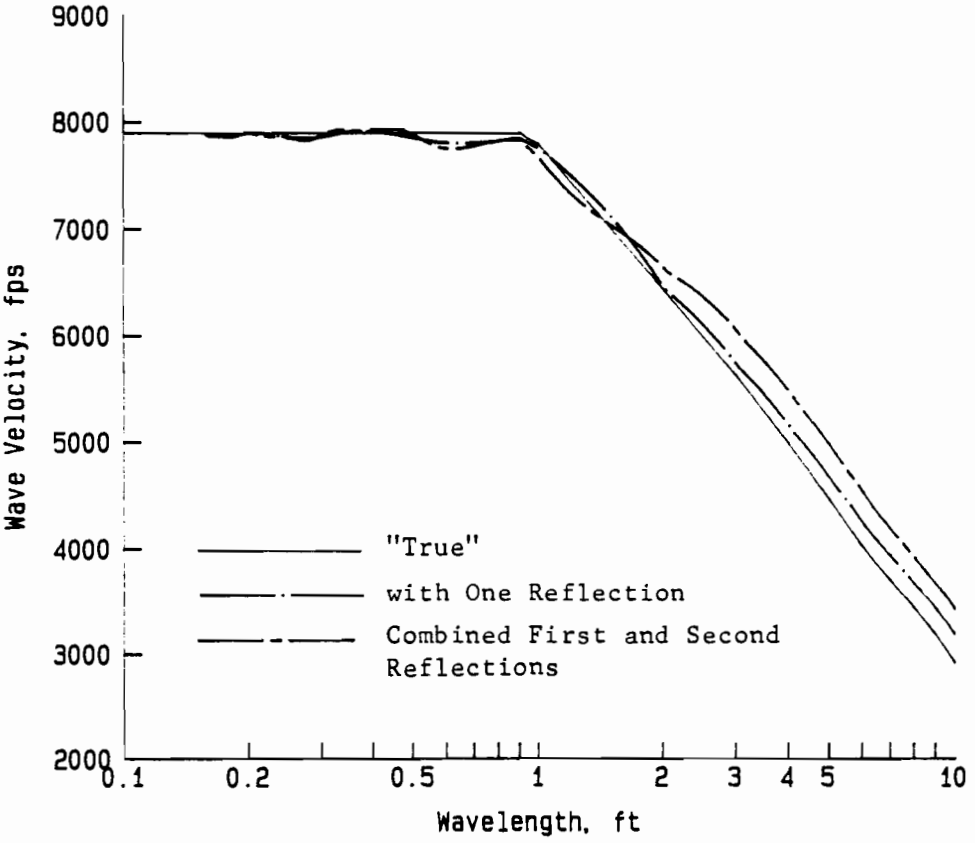

Fig. 5.10. Effect on Dispersion Curve of Reflected Compression Waves: One Reflection versus Combined First and Second Reflections.

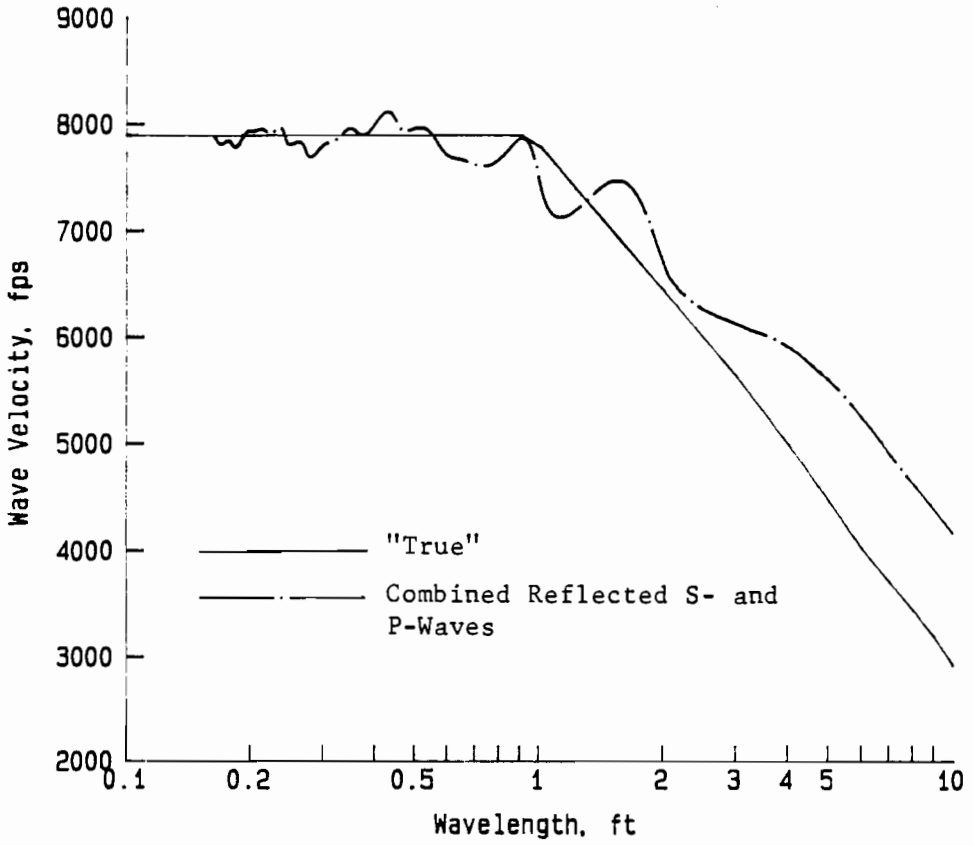

Fig. 5.11. Effect on Dispersion Curve of Combined First and Second Reflected S-waves and First and Second Reflected P-waves.

the short-wavelength range (about 0.7 ft (21 cm) and less in this example). There is, however, some noticeable wave velocity change in the longer wavelength range (say 1 ft (30 cm) and longer in this example). It is necessary to stress here that the amplitudes, A's, for all reflected body waves are all relatively over-conservative. Therefore, the adverse effect from these reflected body waves is slightly overestimated.

A modeled dispersion curve which combines all reflected waves discussed above (S- and P-waves with one and two reflections) and a reflected surface wave is shown in Fig. 5.12. It is assumed that distances from source to receiver 1 and between the two receivers are 1 ft (30 cm) and the reflecting boundary is 1 ft (30 cm) away from the near receiver. Receivers are placed in between the source and the reflecting boundary so that reflected surface waves are propagating in the opposite direction relative to the direct surface waves (which will cause the larger adverse effect). It appears that the effect of the reflected surface wave is easier to identify than the effect from the combined body waves. This phenomenon, of course, is partly caused by the relative large amplitude, A's, used for the surface wave reflections (0.3 and 0.27). However, earlier discussion has noted that the body wave effect is overestimated in most cases. As such, it is fair to conclude that the effect of reflected surface waves is more important than the combined effect of direct and reflected body waves.

The modeled dispersion curve shown in Fig. 5.12 is compared to an actual field dispersion curve in Fig. 5.13. A modeled dispersion curve in which only one surface wave reflection is included for the same test condition is compared in Fig. 5.14 with the same field dispersion curve. Upon comparing Figs. 5.13 and 5.14, the agreement between the field data and modeled dispersion curves is not improved much by including the effect of reflected body waves. It is possible that the simplified model is not capable of properly simulating the effect of body waves. But it seems logical at this time to simply neglect the effect of body waves because their energy is relative low compared to surface waves and inclusion of their effect does not significantly improve the agreement between modeled and field dispersion curves.

5.6. SUMMARY

Both model and field studies are performed to investigate the effect of body waves on surface wave dispersion curves. The agreement between modeled and field dispersion curves is reasonable but not perfect. The difference between modeled and field curves may be caused by insufficient information for determining the arrival times and amplitudes of the body waves (T's and A's) used in modeling. It is also possible that the model is not sophisticated enough to

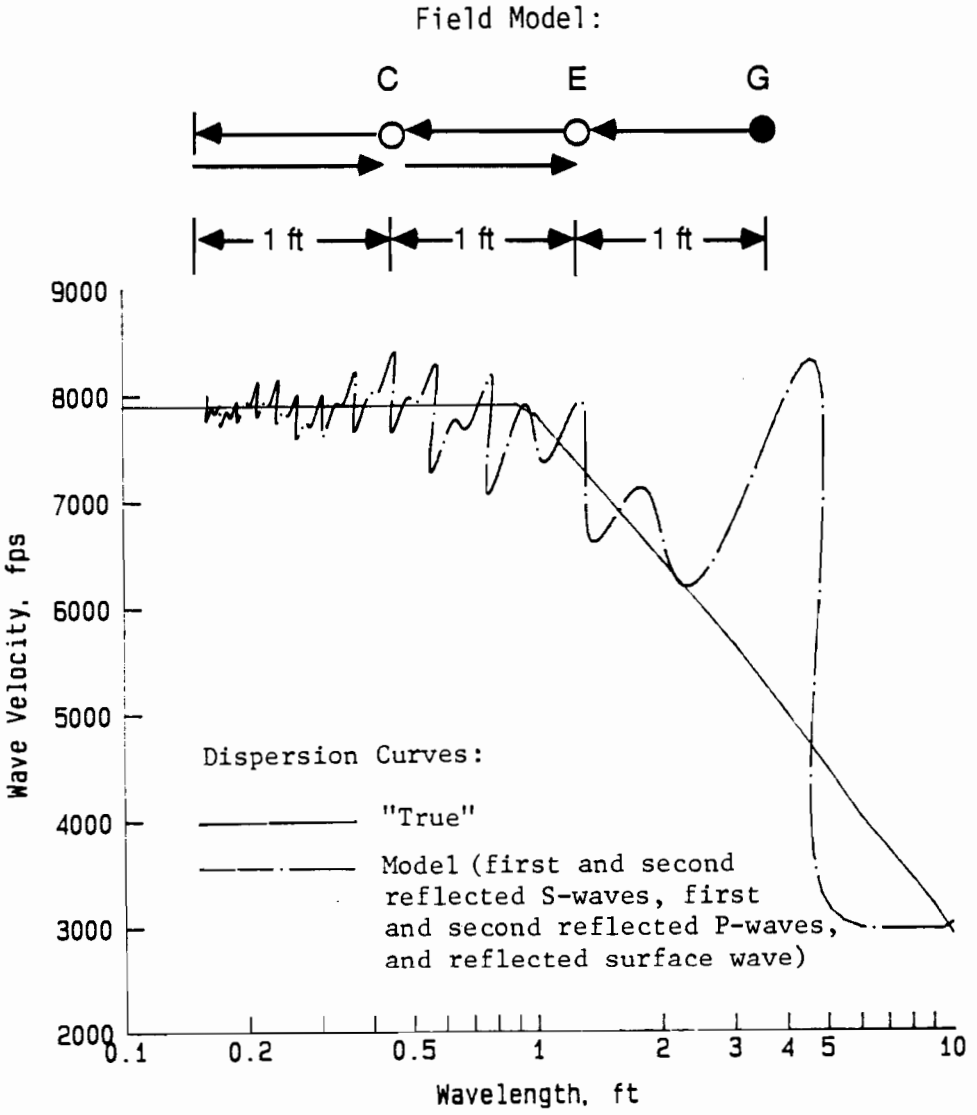

Fig. 5.12. Modeled Dispersion Curve with Combined Effect from Multiple Body Wave Reflections and Reflected Surface Wave.

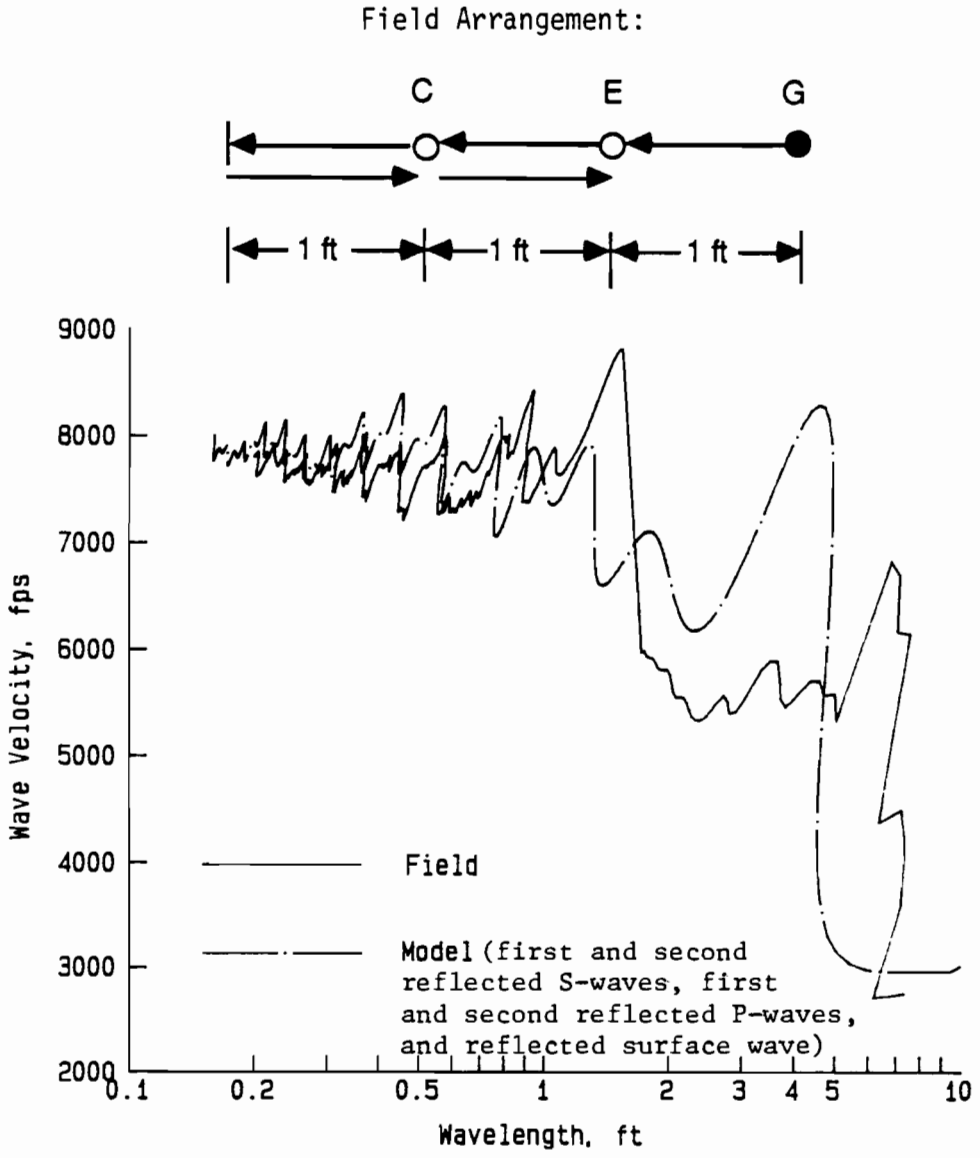

Fig. 5.13. Comparison of Field and Modeled Dispersion Curves: Modeled Curve Includes Reflected Surface Wave and Multiple Body Wave Reflections.

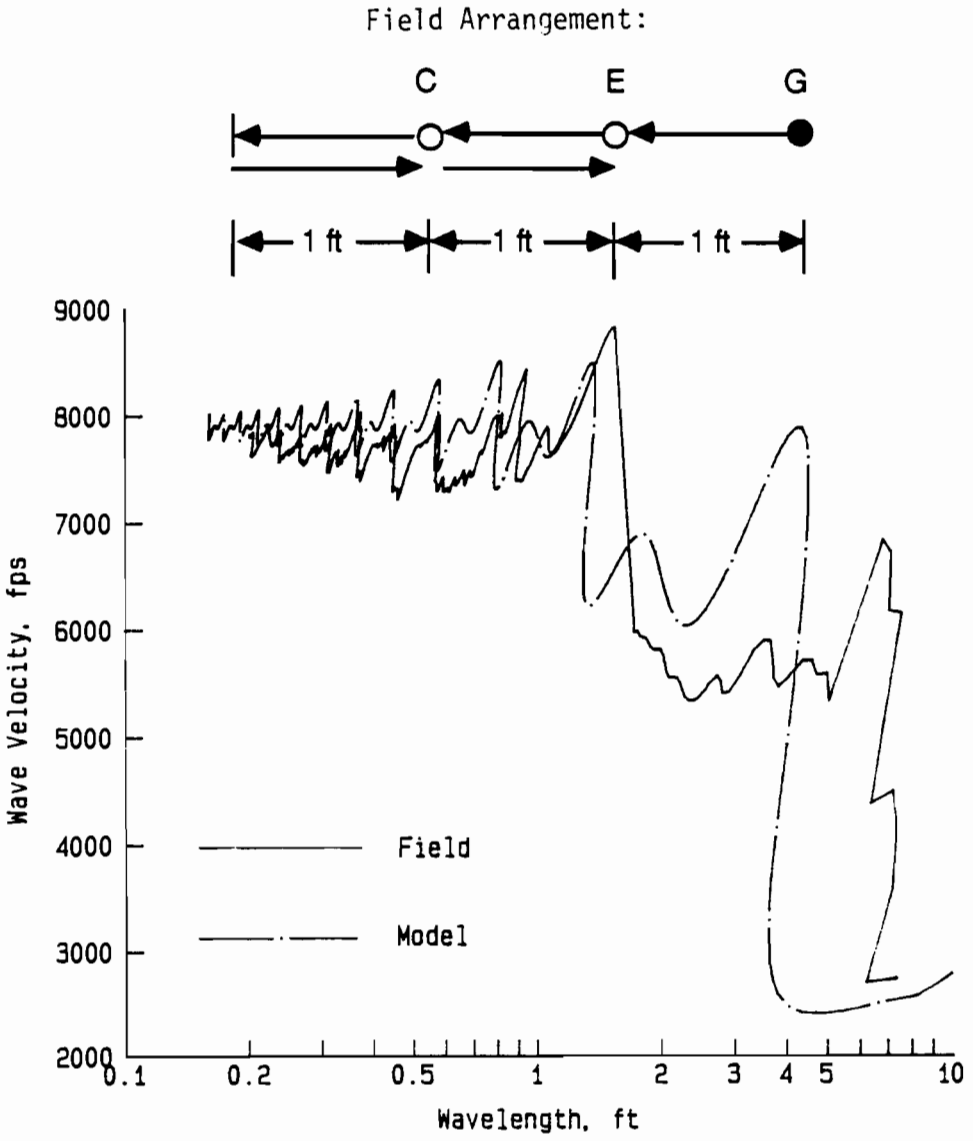

Fig. 5.14. Comparison of Field and Modeled Dispersion Curves: Modeled Curve Includes Only Reflected Surface Wave.

describe the behavior of the dispersion curves affected by these undesired body waves. Despite these uncertainties, the study suggests that the effect of body waves are secondary to the effect of reflected surface waves, and it is not necessary to consider body waves in most situations.

CHAPTER SIX

DATA PROCESSING TECHNIQUES

6.1. INTRODUCTION

The influence of reflected surface waves, direct body waves, and reflected body waves on surface wave dispersion curves is discussed in Chapters Four and Five. Obviously, any factors which might contaminate field data should be avoided or reduced to a minimum during the period when time signals are being captured because to decompose contaminated data into pure signals and noise after data collection is extremely difficult and often impossible. The location of SASW testing should always be selected to minimize reflections. For example, testing should be performed at the center of the layered pavement system, as far as possible from any material irregularity such as voids, pipes, joints, and edges. (Unless, of course, one is trying to investigate the material irregularity.) In many instances, the existence of reflected waves is not avoidable. Therefore, precautions have to be made during interpretation of the field data.

In this chapter, several methods that can be used during the data processing stage to reduce or understand the effects from undesired waves on the dispersion curves are presented. The data processing procedure currently used in SASW testing is discussed. Examples from SASW testing on the concrete pavement at the Balcones Research Center facility are used to illustrate the discussion.

6.2. EXPONENTIAL TIME WINDOW

Since all reflected waves need to travel longer distances than direct waves to reach the receivers, it is fair to assume that reflected waves always appear after direct arrivals in the time records. (This assumption is not always correct, but it does represent a starting point.) Consequently, one method to reduce the influence of reflected waves is to apply a window to the time records in such a manner that the amplitudes of reflected waves are reduced or totally eliminated. An exponential window is used in this initial study. Other more complex windows can certainly be employed.

To apply an exponential window, time domain signals are multiplied by a exponential function, e^{-at}, where "a" is the parameter that determines how fast this exponential function decays with respect to time "t". The effect of multiplying the time signals by an exponential function is that damping or attenuation in the system is increased artificially. The amount of

damping introduced to this system is controlled by the parameter "a", with larger values of "a" introducing more attenuation in the system than smaller values of "a". The value selected for parameter "a" is critical. A large value of "a" could reduce the reflection problem to a minimum because it could also damp out all signals received in the later part of the time record. As a result this window would also eliminate useful signals which correspond to direct surface waves with lower wave velocities since these signals may arrive later relative to the faster direct arrivals. Therefore, care must be exercised when applying an exponential window.

Theoretically, total elimination of reflections by applying a window is possible only if all reflected waves arrive later than the direct waves. In reality, faster reflected waves usually mix with slower direct waves which makes the problem more complex. One can imagine that if reflected waves are the only factor that cause measurement problems, application of exponential windows is more likely to introduce error into the data in the low-velocity range than in the high-velocity range. For example, in a system where stiffer material is underlaid by softer materials (such as a pavement system), application of exponential windows may cause some inaccuracy in measurements of the subsoil wave velocity. On the other hand, in a system where softer material is underlain by stiffer materials (such as a typical soil site), slower wave velocities which appear near the surface may be influenced the most by application of exponential windows. The reason behind this general relationship is that signals corresponding to those slow traveling waves are always recorded in the later part of the time records. Once exponential windows are applied, the amplitudes of these slow arrivals are reduced or totally eliminated. As a result, velocities corresponding to these slow arrivals cannot be calculated correctly from the windowed time records.

As an example, a pair of time records is processed with exponential windows with different values of "a". Typical time records before and after windowing are presented in Fig. 6.1 (a = 3200 in this example). The window effectively damped out reflected waves. Dispersion curves processed by applying different exponential windows to the time record are presented in Fig. 6.2. Each window effectively improved the dispersion curve at short wavelengths (less than about 3 ft (91 cm)) which corresponds to high-frequency signals and high wave velocities for this concrete pavement. However, the process leaves questionable results (seems to be too high an estimation) in the long wavelength range (greater than about 3 ft (91 cm)) which corresponds to low-frequency signals and low wave velocities.

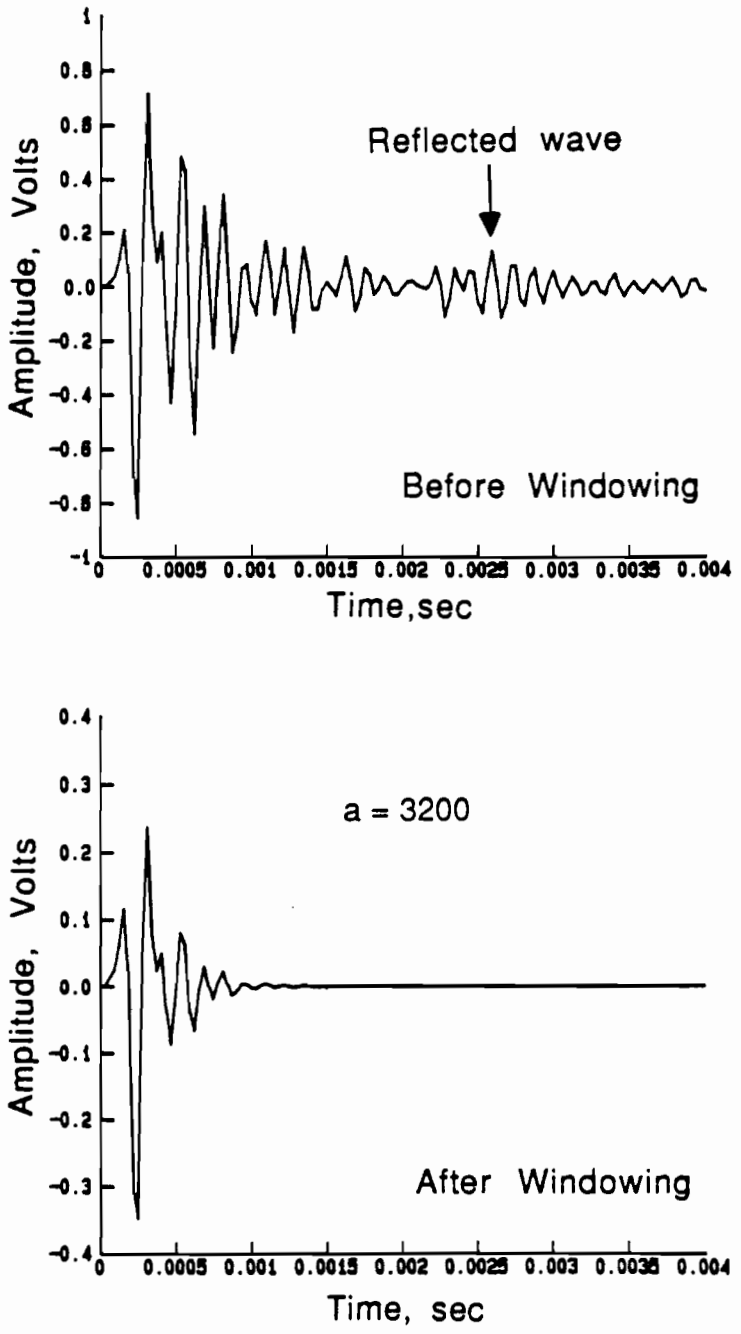

Fig. 6.1. Comparison of Time Signals Before and After Exponential Windowing.

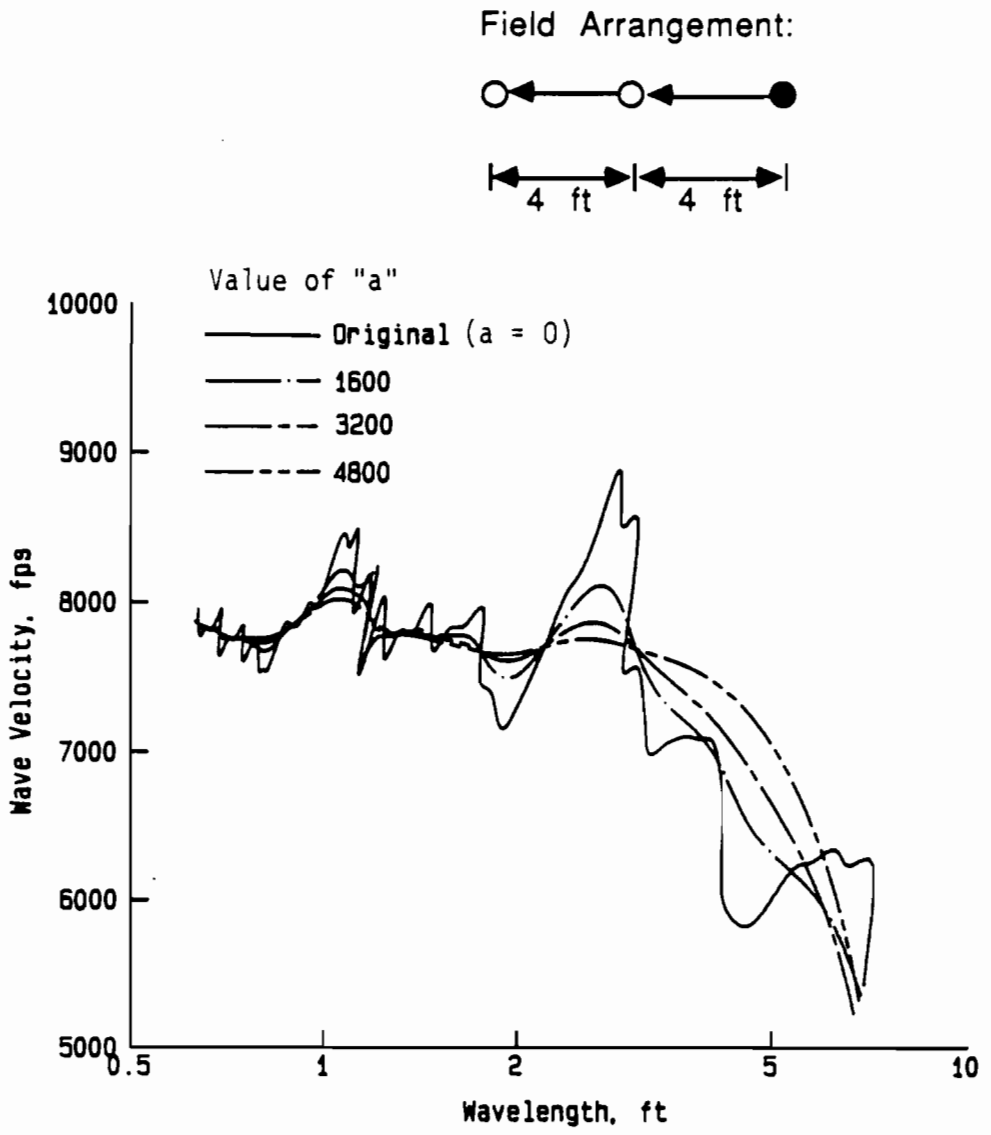

Fig. 6.2. Comparison of Dispersion Curves Generated from Time Records to Which Different Exponential Windows were Applied.

6.3. SMOOTHING DISPERSION CURVES

The exponential window discussed above has to be applied to the time domain data before any frequency analysis is performed. Therefore, it is more a time domain approach. In the case when frequency analysis has been performed on the field data and the dispersion curve has been reconstructed, there are other methods to remove the effect of reflected waves on dispersion curves. Since these methods operate on the frequency domain data, they can be considered as frequency domain approaches.

6.3.1. Moving Window Averaging

Ripples and fluctuations are observed in most field dispersion curves. Many of these ripples and fluctuations are caused by reflected waves, ambient noise or other unidentified factors. This kind of fluctuation, therefore, is not representative of the site and is considered as noise in the dispersion curve.

One method of filtering out noise is by using a moving window averaging technique (Thornhill, 1980). By taking the average of data points in a window with a fixed or varying size, some irregularities in the test data can be filtered out. An example of data before and after moving window averaging is presented in Fig. 6.3. The window used in this example has a variable size through the full wavelength range, the size at two locations shown in the figure. The size of the window was chosen in such a way that the averaged wave velocities were about equally spaced along the wavelength axis. This moving window basically gives the general trend in the dispersion curve and eliminates some fluctuations in the short wavelength range (say less than 2 ft (61 cm).

Generally speaking, a window eliminates all fluctuations with periods less than the size of the window (Thornhill, 1980). Therefore, the bigger the window, the smoother will be the dispersion curve. On the other hand, details in the dispersion curve are lost as the size of the moving window increases. So far there is no rule in terms of determining the best size of the window. Too big a window is certainly not desirable for preserving details in dispersion curves under processing.

6.3.2. Curve Fitting Method

A cubic spline curve fitting technique can also be employed to filter out some of the reflected waves as well as some of the inherent scattering in the dispersion curve. The required computer programs can readily be found in the IMSL library (IMSL manual) implemented in the

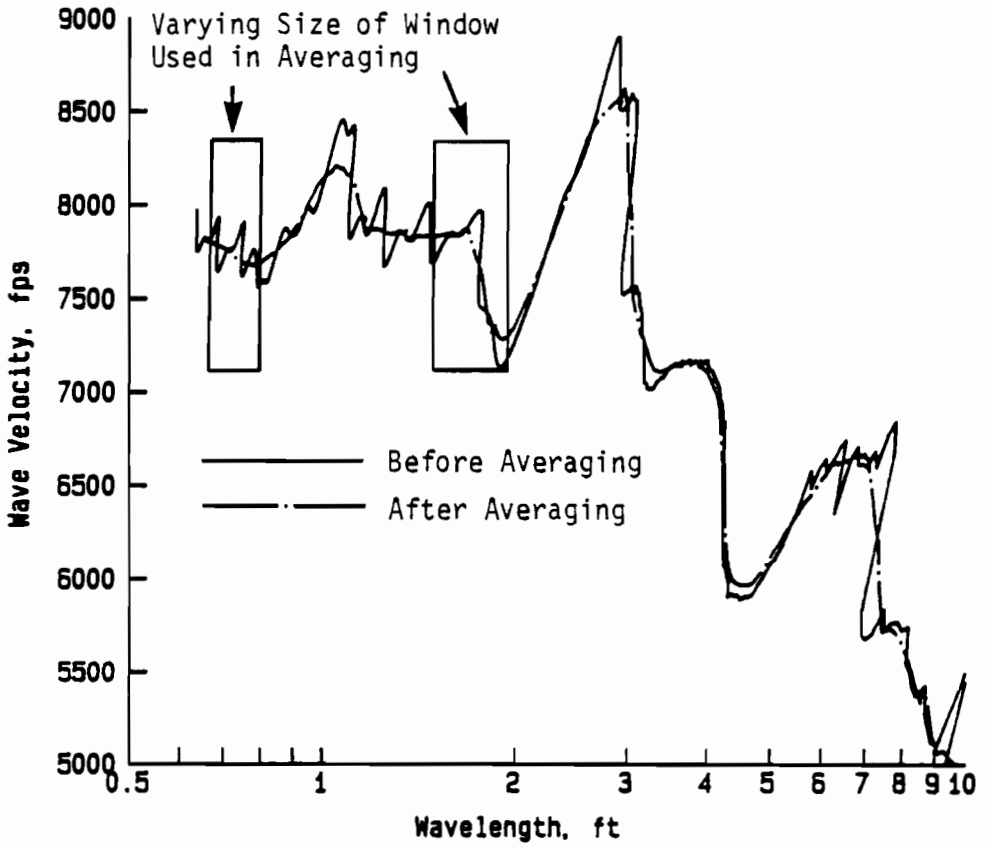

Fig. 6.3. Comparison of Dispersion Curves Before and After Variable-Sized Moving Window Averaging.

MASSCOMP computer. The degree of smoothness of the fitting curve is controlled easily by the input parameters. Different degrees of smoothness fitting are presented in Fig. 6.4.

It is obvious that fitting a smoother curve through the dispersion curve removes more details. Therefore, the proper degree of smoothness is hard to decide and can vary with the purpose. It might depend not only on a case by case basis but also on the operator's preference.

The inherent problem associated with both smoothing techniques outlined above is that neither of the fitting techniques bear any physical significance to the layered system tested. Each technique can only be considered as a black box (filter) which contains certain mathematical processors which, with certain input, produce certain output. The correctness of the output is not guaranteed. Human judgement has to be involved to steer the filtering process in the proper direction, otherwise erroneous results are bound to be reached.

6.4. PRESENT LEVEL OF DATA PROCESSING

The quality of SASW data can be affected by many factors such as undesired reflected and direct waves, ambient and electronic noise, and other unidentified effects. As a result, there were cases when low quality data were acquired and proper interpretation was difficult to perform. In this section, the basic data interpreting process currently used by the writer is summarized. This summary also represents an example of one approach to eliminating questionable data.

Based on past experience, there is a strong need to examine the field dispersion curve at the moment when field data are collected. By examining the field dispersion curves, inconsistencies or unacceptable dispersion curves can be readily identified, and the operator can promptly adjust the testing process with this feed-back so that field dispersion curves with the best quality are collected. For example, if the sampling wavelength is not as short or as long as desired. This will immediately appear in the dispersion curve. One can change the test set-up immediately so that needed data are collected. If data inconsistency is suspected to be caused by localized nonuniformity, one can move the test location to a nearby place and performed the test again. Some effort has been devoted to implementing the capability of examining the dispersion in the field, and the implementation is close to being complete. However, a traditional guideline used in the past is presented here.

A flow chart of the field data reduction procedure currently used is present in Fig. 6.5. At a given SASW site, phases of cross power spectra are first filtered manually for each receiver spacing to eliminate any obviously erroneous phases such as phases corresponding to low values of the coherence function, phases with obvious wrong numbers of cycles, etc., After all records

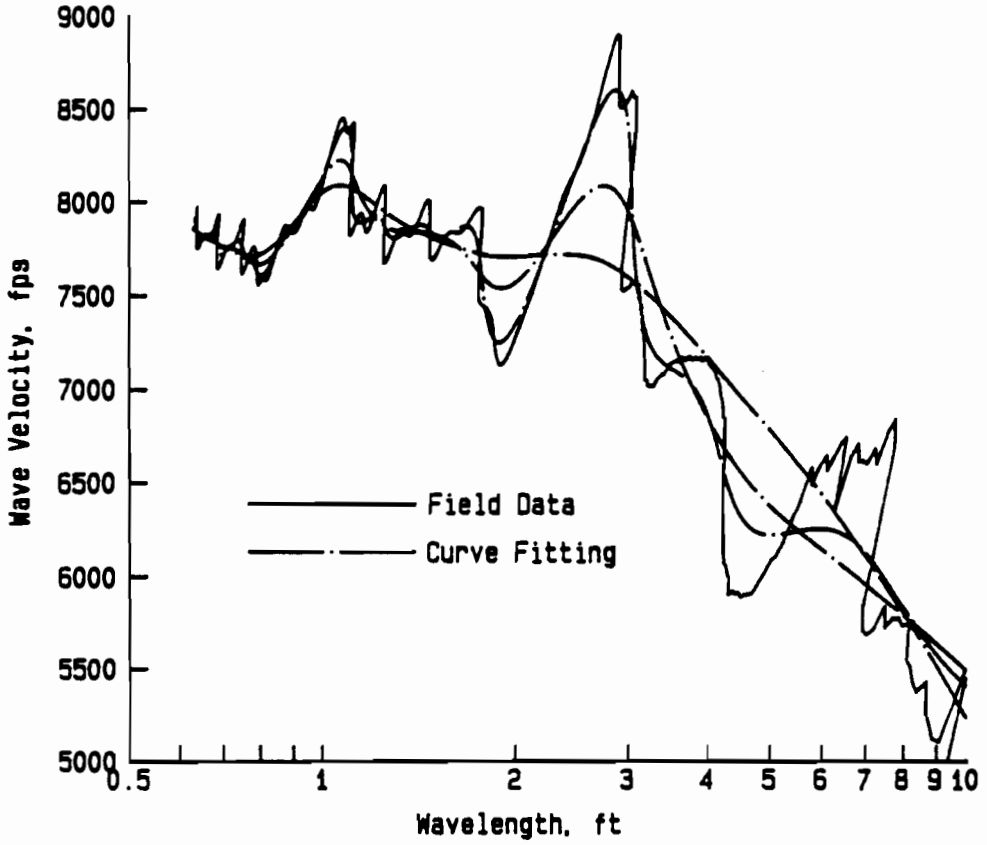

Fig. 6.4. Dispersion Curves Smoothed by Fitting Various Cubic Spline Curves.

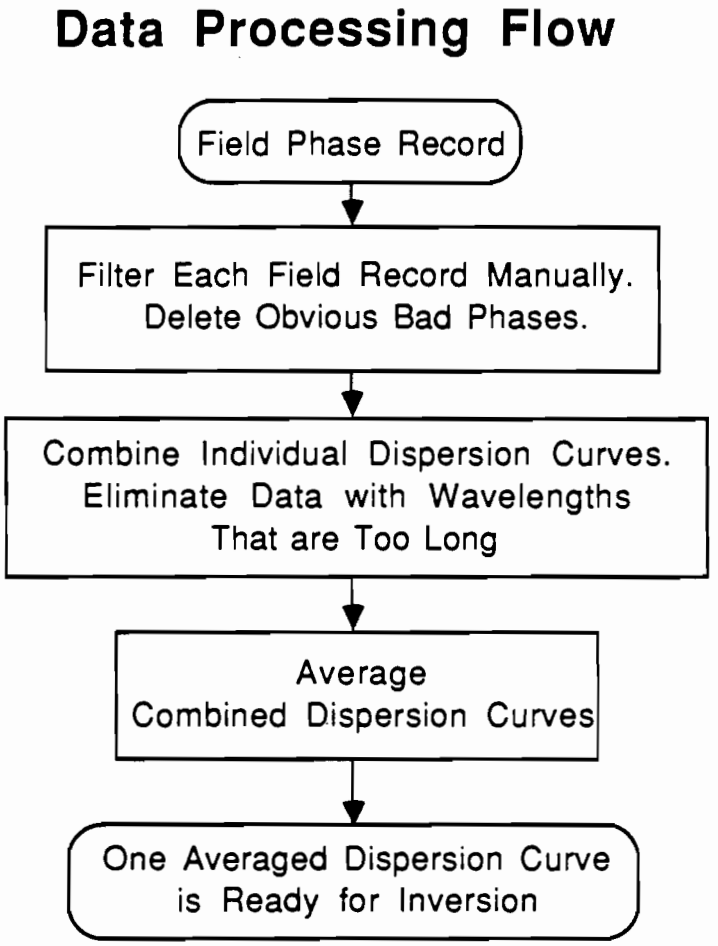

Fig. 6.5. Flow Chart of Data Processing Currently Used to Develop Dispersion Curve Used for Inversion.

with different receiver spacings have been filtered manually, they are then transformed into individual dispersion curves, and data corresponding to wavelengths that are too long for the receiver spacing (details are discussed in Chapter Two) are eliminated. The remaining individual dispersion curves are then plotted together. Theoretically, all curves should more or less fall on top of each other, if the near-field effect is disregarded and higher modes are not existent, because they represent dispersion curves at the same location. However, the individual dispersion curves usually formed a general trend, with most curves scattering in a relatively narrow band and a few sections of curves offset from this main trend. Sections of curves falling inside the main trend are considered to be "representative data". Those sections of curves which are offset from this main trend are reexamined to eliminate any possible errors which might have entered in the interpreting process. If no errors are found, data which are far away from the main trend are simply disregarded. The last step is to combine all curves from different receiver spacings into one curve. An averaging process is used, and some degree of smoothing is done due to this averaging process. After the averaging process, the data is ready to be used for inversion.

Throughout the whole process, suppose at one stage some doubts arise about the validity and correctness of data being processed. One should always loop back to the previous the step or even go back to the original field data to look for answers. Fortunately, our experience shows that this is only necessary in a very few instances. In most cases, this complex looking process is quite straightforward and easy to perform.

6.5. SUMMARY

In this chapter, several in-house methods for reducing the noise and fluctuations in dispersion curves are discussed. Application of an exponential time window for eliminating the influence of unwanted wave arrivals in the time signals seems to be a good approach. However, its effectiveness decreases as unwanted waves become mixed with direct surface waves. Curve smoothing methods, the moving window averaging method and the cubic spline curve fitting method, are capable of eliminating some fluctuations in the dispersion curves, but they bear no physical significance to the pavement system and errors can occur if used without proper precautions. The best approach to collecting representative data in the field is to develop dispersion curves at the time of testing. With this approach, one can repeat any part of the test based upon the quality of the collected data.

CHAPTER SEVEN

SOME PRACTICAL CONSIDERATIONS IN PERFORMING SASW TESTS

7.1. INTRODUCTION

Since the SASW method is an in situ seismic method, good field equipment and proper test arrangements are required to ensure high quality test results. In this chapter, some practical considerations about conducting SASW tests in the field are studied. Factors that could affect the accuracy of field data are discussed in detail. Some factors, such as the variety of time domain signals, impact stress level, and near-field effect, that were considered intuitively to be important in the past, turn out to be unimportant. It is also found that some factors, such as receiver-ground coupling and resonant frequencies, are more important than they were first believed to be.

Most of the tests presented in this chapter were performed on the concrete pavement at the BRC facility. (A few tests were also performed in the Soil Dynamics Laboratory located on the main campus of The University of Texas at Austin.) Because the distances used between the two receivers and from the source to the first receiver were usually small (less than about 2 ft (61 cm)), these tests basically sampled the properties of the concrete layer only. Therefore, the wave velocity used for reference is the wave velocity of the concrete layer, and the "true" dispersion curve is simply a horizontal line for wavelengths less than about 0.5 ft (15 cm).

7.2. INFLUENCE OF VARIABILITY IN TIME DOMAIN SIGNALS

One of the concerns when performing SASW tests in the field is the influence of variability in the time domain signals from one impact to the next for a fixed source/receiver arrangement. It was initially assumed that different types of time domain signals would give different frequency domain data and, hence, different stiffness profiles upon inverting the dispersion curves. Consequently, to accept or reject a set of time domain signals during SASW testing is often a concern for the operator. In general, the operator looks for a collection of five frequency domain records whose corresponding time domain signals "look alike". The operator then takes the average of these five frequency domain records and assumes that this set of data is representative data because of their repeatable nature. However, it is not always easy to judge which kind of signals are most representative just by looking at the time records from the first few impacts with the given a source/receiver arrangement. As a result, time and effort can be wasted

in collecting data just to give the operator a vague feeling about what type of data should be accepted or rejected. In addition, this understanding is necessary in future automation of the SASW method. Suppose time records with different appearances would lead to similar dispersion curves (as discovered in this study). Then a significant savings of time and effort would occur in the field because one would simply take every record unless a drastic change appeared.

To determine how much a dispersion curve might vary because of differences in time domain signals, SASW tests were performed on the concrete slab at the BRC facility at location 6 (see in Fig. 3.1). Two, PCB model 308B02 accelerometers were used to track the pavement surface motion. The distance between the two receivers was 0.5 ft (15 cm), and the source was 0.5 ft (15 cm) away from the first receiver. These accelerometers have a sensitivity of about 1000 mV/g and a weight of about 67 gm. A hammer (weight of 4 oz (114 g)) was used to generate different types of time signals by different impact techniques.

The different types of time signals and corresponding frequency spectra are present in Figs. 7.1 through 7.3. In each of these figures, the top two records are outputs from receivers 1 and 2, respectively, for a single hammer impact. With a collection of five similar time signals, frequency analysis was performed, and the averaged auto power spectra for receivers 1 and 2 are presented as the third record in Figs. 7.1 through 7.3. The averaged phase of the cross power spectrum and coherence function are presented as the fourth and fifth records, respectively.

The basic difference between the time domain records in Figs. 7.1 through 7.3 is the high-frequency content. By examining the time domain records, one can see that the time signals in Fig. 7.1 appear to contain the most high-frequency energy while the time signals in Fig. 7.3 appear to contain the least high-frequency energy. The auto power spectra corresponding to each time signal indicate that the time signal shown in Fig. 7.1 has a relatively uniform energy distribution over the whole frequency span of 0 to 100 KHz, with a significant amount of energy in the range of 50 to 80 KHz. The auto power spectra in Figs. 7.2 and 7.3 are quite similar to each other. The auto power spectra in Figs. 7.2 and 7.3 indicate an opposite conclusion compared with that from the time domain data. (The time domain data seemed to imply that signals shown in Fig. 7.2 contain more high-frequency energy than the signals shown in Fig. 7.3.) The coherence functions seem to be more related to the energy level of the auto power spectra than the time signals since the coherence function in Fig. 7.1 (in the range of 10 to 40 KHz) is the best. The coherence function in Fig. 7.3 is, in general, better than the one shown in Fig. 7.2, especially in the range higher than about 50 KHz (except in the range of 70 to 80 KHz).

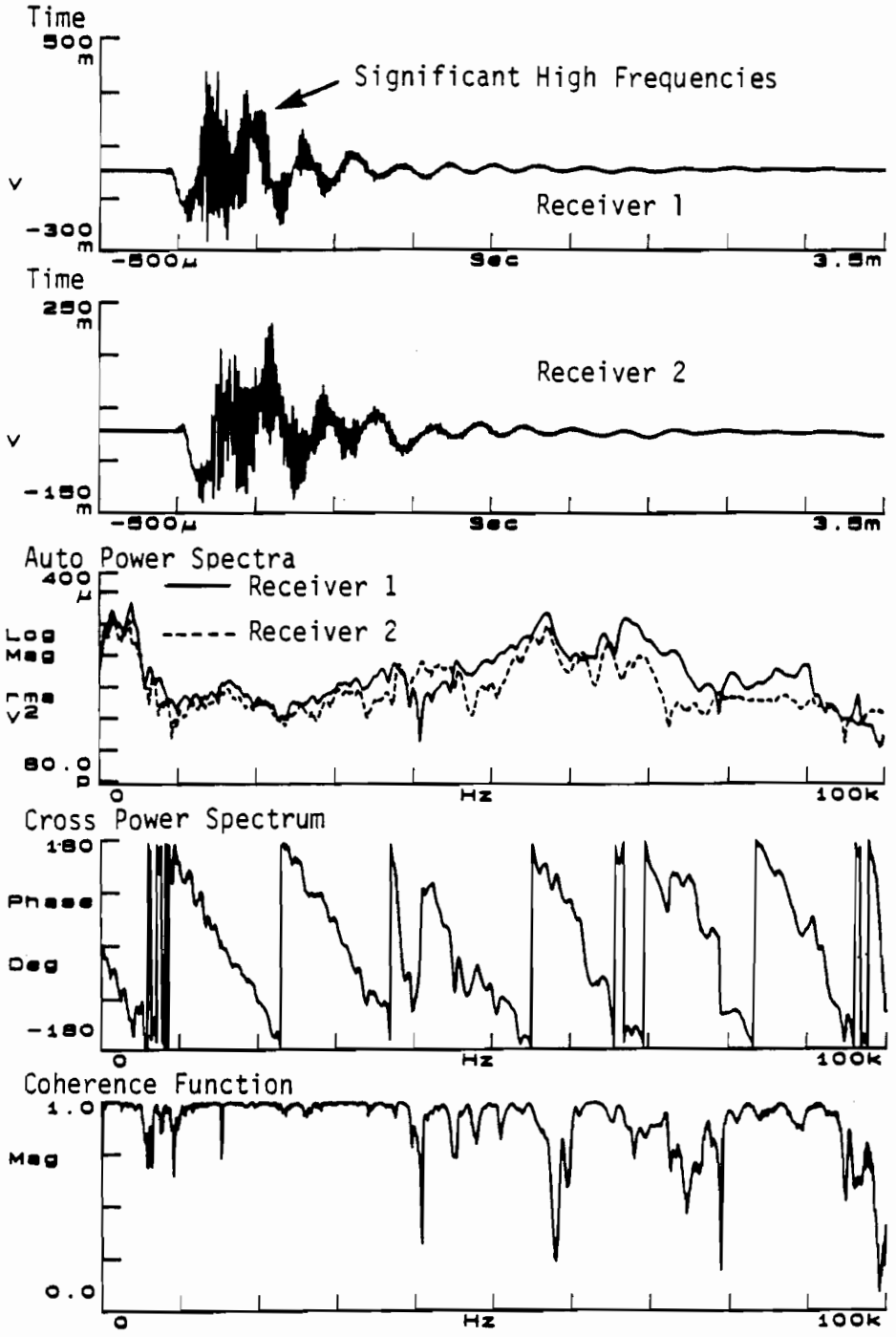

Fig. 7.1. Time Domain Signals with Significant High Frequency Content and Corresponding Frequency Spectra.

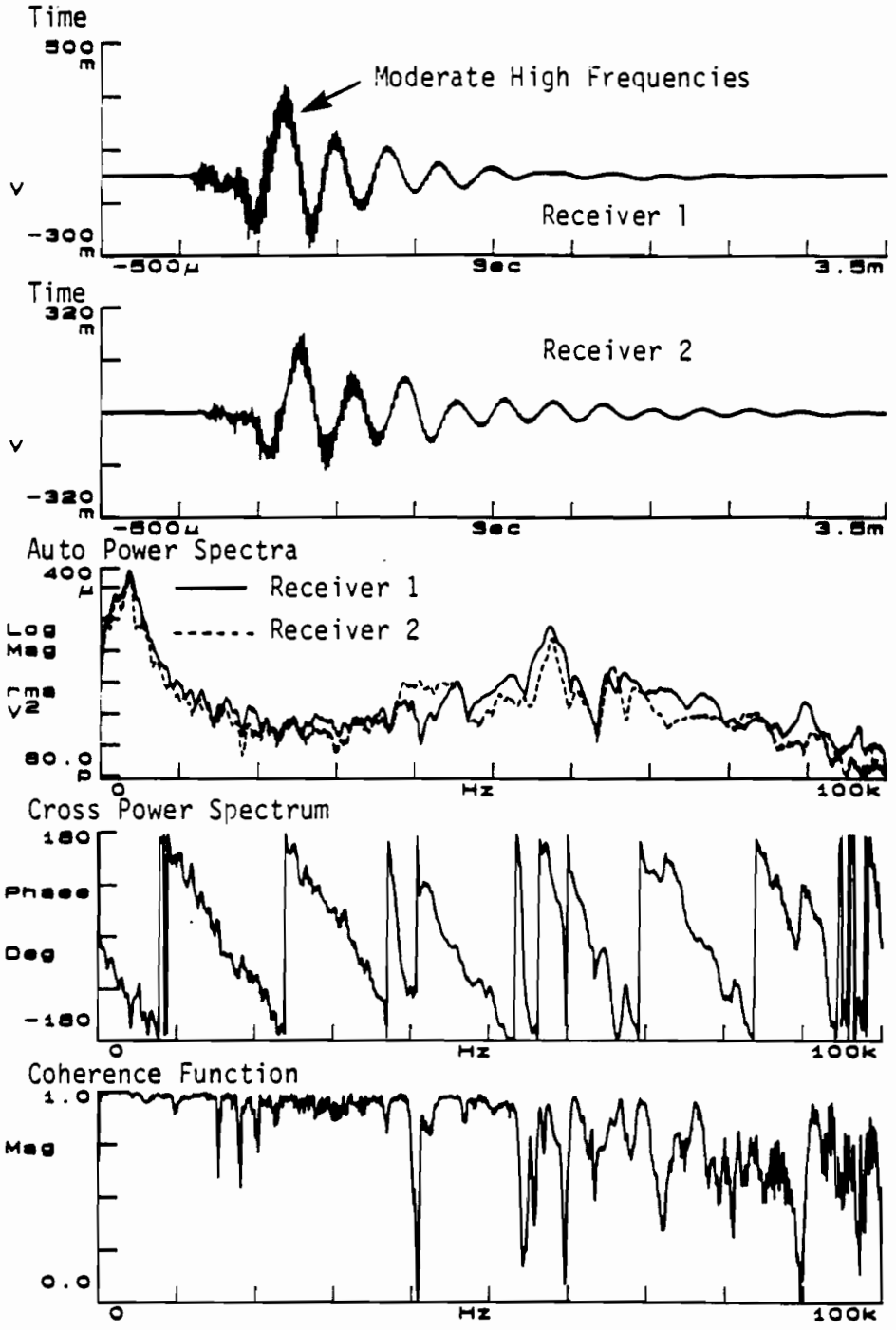

Fig. 7.2. Time Domain Signals with Moderate High Frequency Content and Corresponding Frequency Spectra.

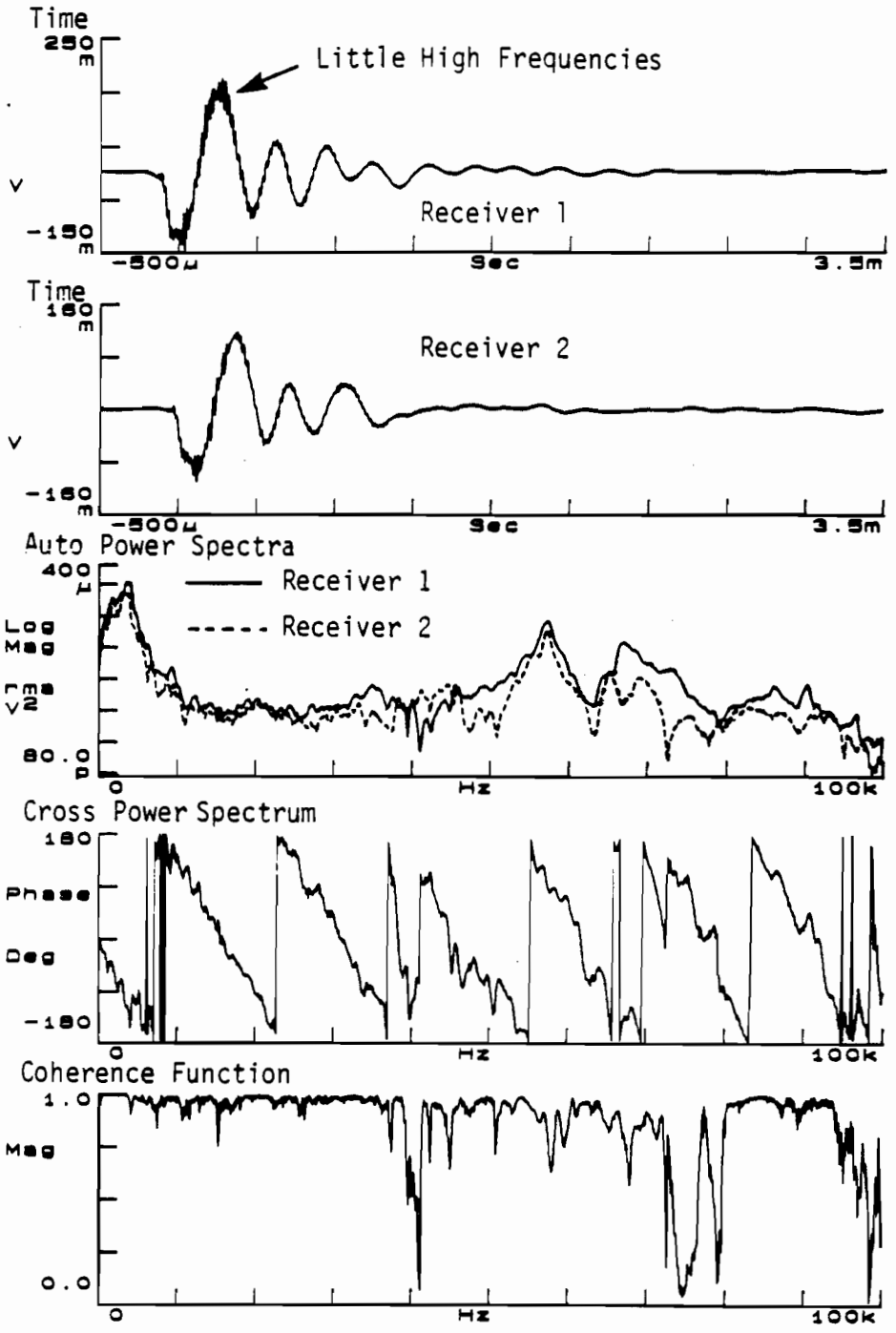

Fig. 7.3. Time Domain Signals with Little High Frequency Content and Corresponding Frequency Spectra.

The auto power spectra, in the range of 50 KHz and higher, indicate a higher energy level in the records in Fig. 7.3 than in Fig. 7.2. However, none of the coherence functions are very good above about 40 KHz even though the energy level of the auto power spectra in this range is not lower than in some of the low-frequency ranges (say 15 to 30 KHz). It seems that, upon comparing different records, a higher energy level is associated with a better coherence function. But this is not true upon comparing the energy level within a given record. The cause of this phenomenon is not clear.

Dispersion curves determined from each of the three phase records shown in Figs. 7.1 through 7.3 are presented in Fig. 7.4. One can see that differences between these dispersion curves are very minor. This comparison shows that the phases of the cross power spectra are not very sensitive to this particular kind of high frequency content in the time domain signal as long as the frequency span under investigation is excited and the energy level is large enough to override ambient noise. In addition, it is easy to be fooled by the time signals because time signals shown in Fig. 7.3 seem to have less energy in the high-frequency range than the time signal shown in Fig. 7.2. However, the energy level of the auto power spectra corresponding to each time signal indicated just the opposite trend. Also, the quality of the coherence function seems to be closely related to the auto power spectra. In Section 8.2, a "V" meter is introduced as a source which is capable of generating a lot more energy in the high-frequency range. Tests with this source show a significant improvement in the frequency domain data at high frequencies and support the finding discussed above that values of the coherence function are closely related to the amplitudes of energy levels of auto power spectra.

7.3. INFLUENCE OF IMPACT STRESS LEVEL

To determine how different impact stress levels might affect dispersion curves, several SASW tests were performed on the concrete pavement at the BRC facility (location 6 shown in Fig. 3.1). Very strong impacts were used to generate surface waves. The impacts were delivered by hitting the pavement surface as hard as possible with a hammer (weights 4 oz (114 g)) but not too hard to damage the surface. A pair of PCB model 308B accelerometers with a sensitivity of about 100 mV/g were used as receivers, with the distance between receivers of 0.5 ft (15 cm) and the source was 0.5 ft (15 cm) away from the first receiver. Model 308B accelerometers are ten times less sensitive than the model 308B02 accelerometers used in previous tests.The purpose of using a pair of less sensitive accelerometers in this test was to reduce the excessive output voltage

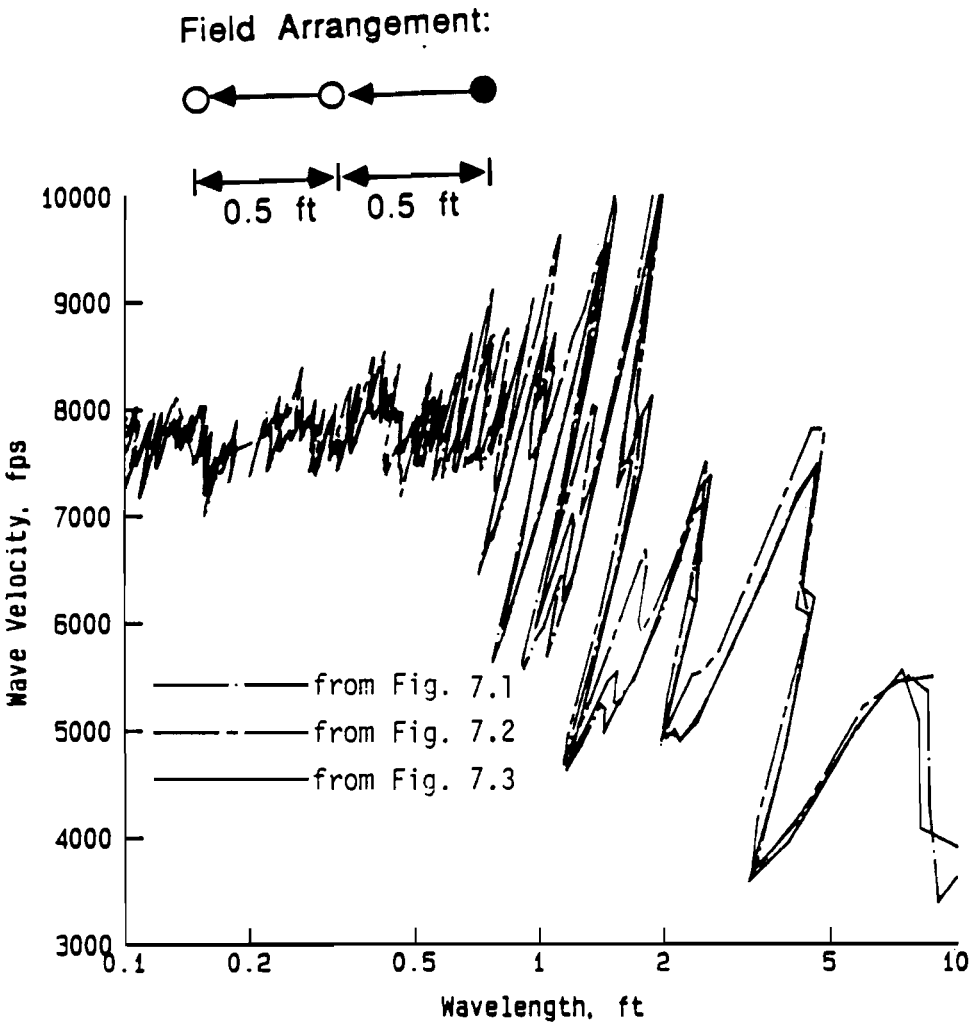

Fig. 7.4. Influence on Dispersion Curves of Varying Amounts of High-Frequency Energy in Time Domain Signals.

caused from the high acceleration levels applied to the pavement surface and to prevent input signals from overloading the analog-to-digital (A/D) convertors in the spectral analyzer.

Typical time domain signals and corresponding frequency response data are shown in Figs. 7.5 and 7.6. One can notice that the amplitudes of the time signals in these two figures are approximately five times higher than those shown in Figs. 7.1 through 7.3. However, the accelerometers used in these tests are ten times less sensitive than those used in the tests presented in Section 7.2. This means that the peak ground surface accelerations in these two tests were about fifty times larger than those shown in Figs. 7.1 through 7.3. However, the phases of the cross power spectra from these hard impacts are essentially the same as in the tests discussed in Section 7.2.

Furthermore, the comparison of dispersion curves shown in Fig. 7.7 demonstrates insignificant differences among the soft-impact and hard-impact tests, especially in the range where wavelengths are less than about 0.6 ft (18 cm). In the range where wavelengths are longer than about 0.6 ft (18 cm), larger fluctuations are found. A very interesting finding discovered from this figure is that even though the dispersion curves fluctuate over a very wide range when wavelengths are longer than about 0.6 ft (18 cm), all dispersion curves follow each other very well which indicates that the fluctuations are not random but are representative of the pavement system. Unfortunately, the cause of the fluctuations is not completely understood. Influence from reflected surface or body waves discussed in Chapters Four and Five is certainly one possible reason.

Fluctuations in the dispersion curves at short wavelengths (less than about 0.5 ft (15 cm)) result mainly from reflected surface waves as discussed in Chapter Four. If the fluctuations in the dispersion curves caused by reflected waves were removed, these dispersion curves would be essentially the same.

This study suggests that, even though a wide range of impact forces can be generated by a hammer which results in very different levels of surface motion, field dispersion curves constructed from phases of the cross power spectra measured at these different levels are nearly the same. The possible development of a nonlinear zone in the area of the impact by an excessively hard impact must be very localized as shown in Fig. 7.8. Hence, material between the receivers is still in the linear elastic range. Therefore, signals monitored by the receivers still correspond to waves traveling in the elastic strain range of the material being tested.

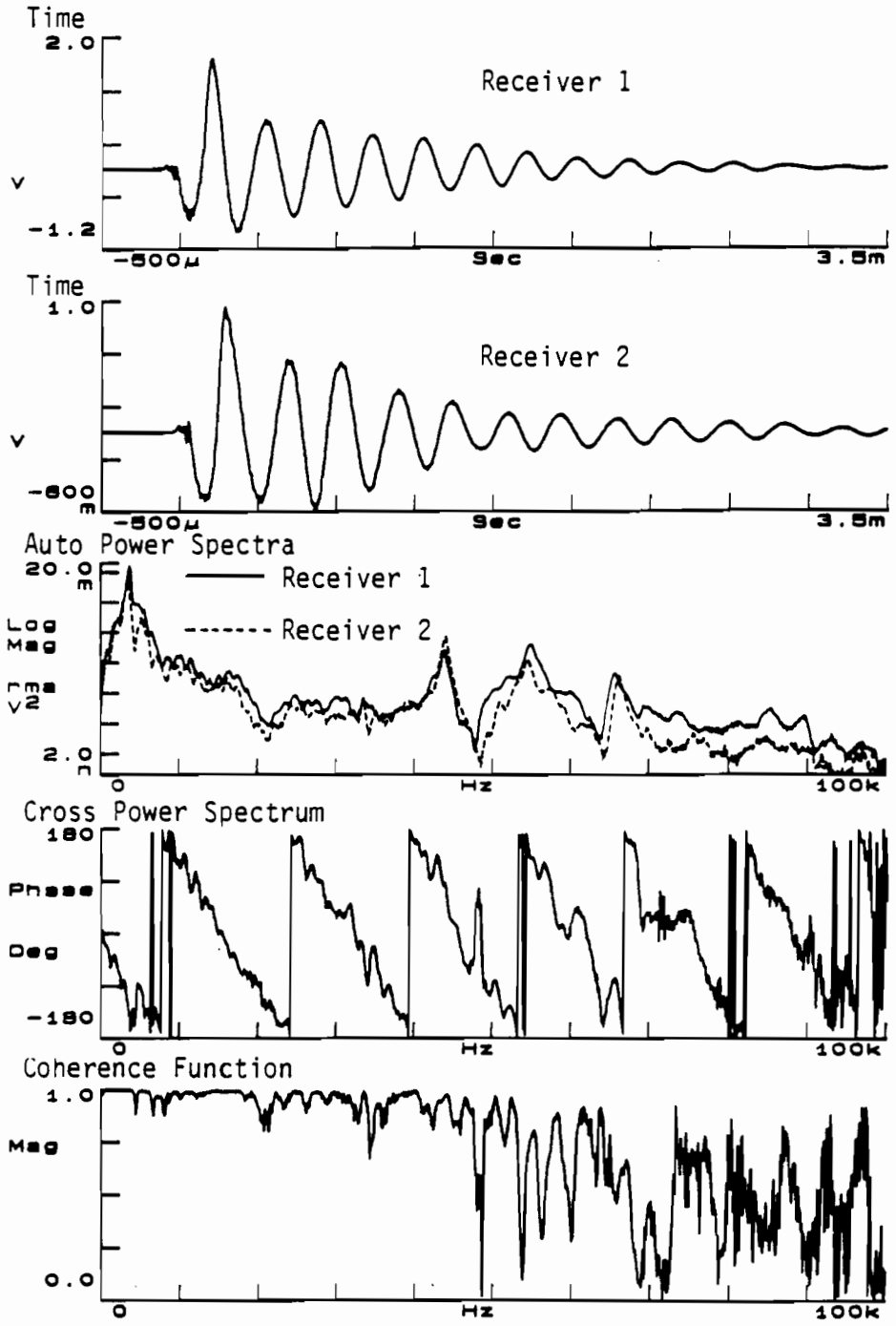

Fig. 7.5. Time Domain Signals and Corresponding Frequency Spectra for High Energy Impacts.

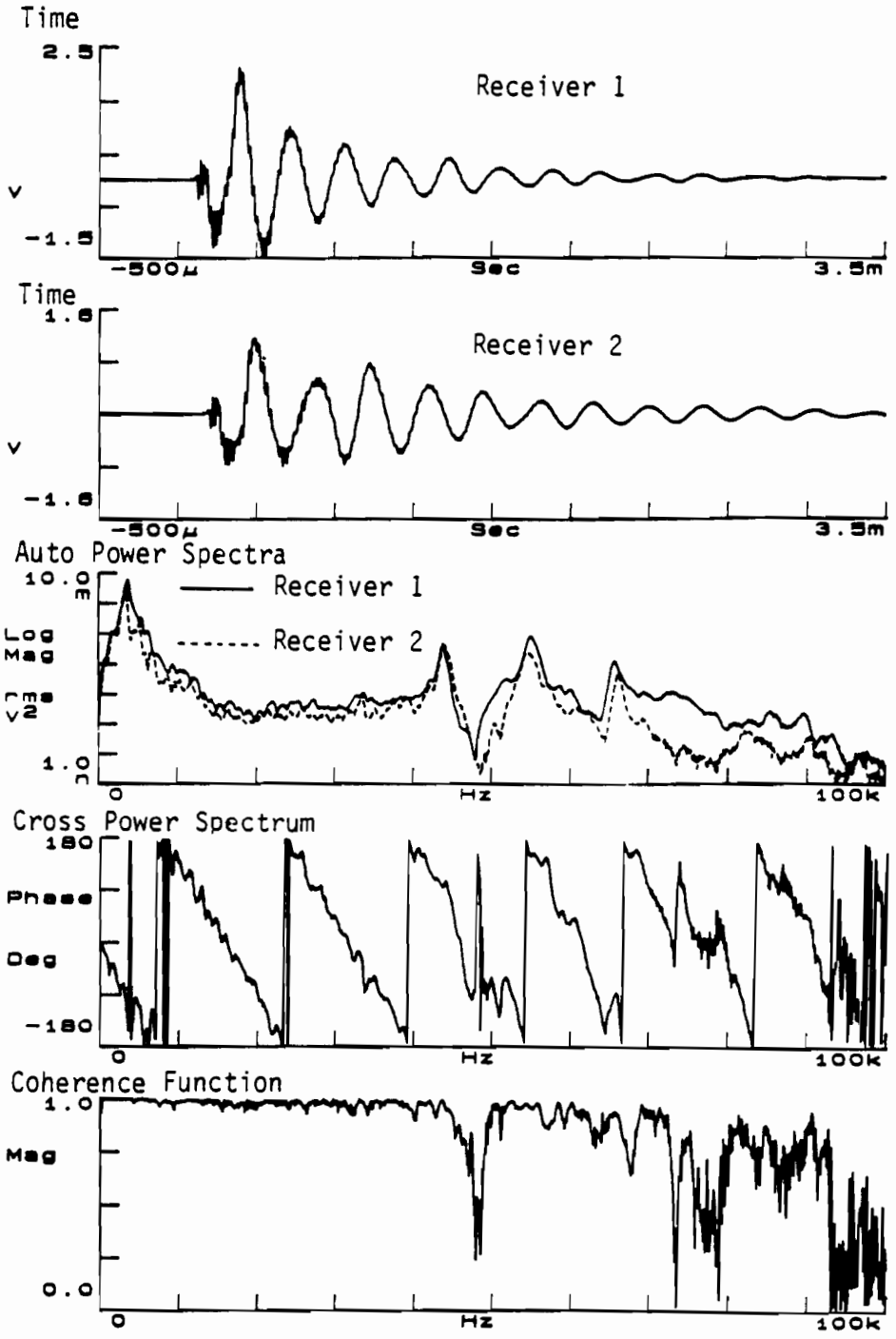

Fig. 7.6. Time Domain Signals and Corresponding Frequency Spectra for Very High Energy Impacts.

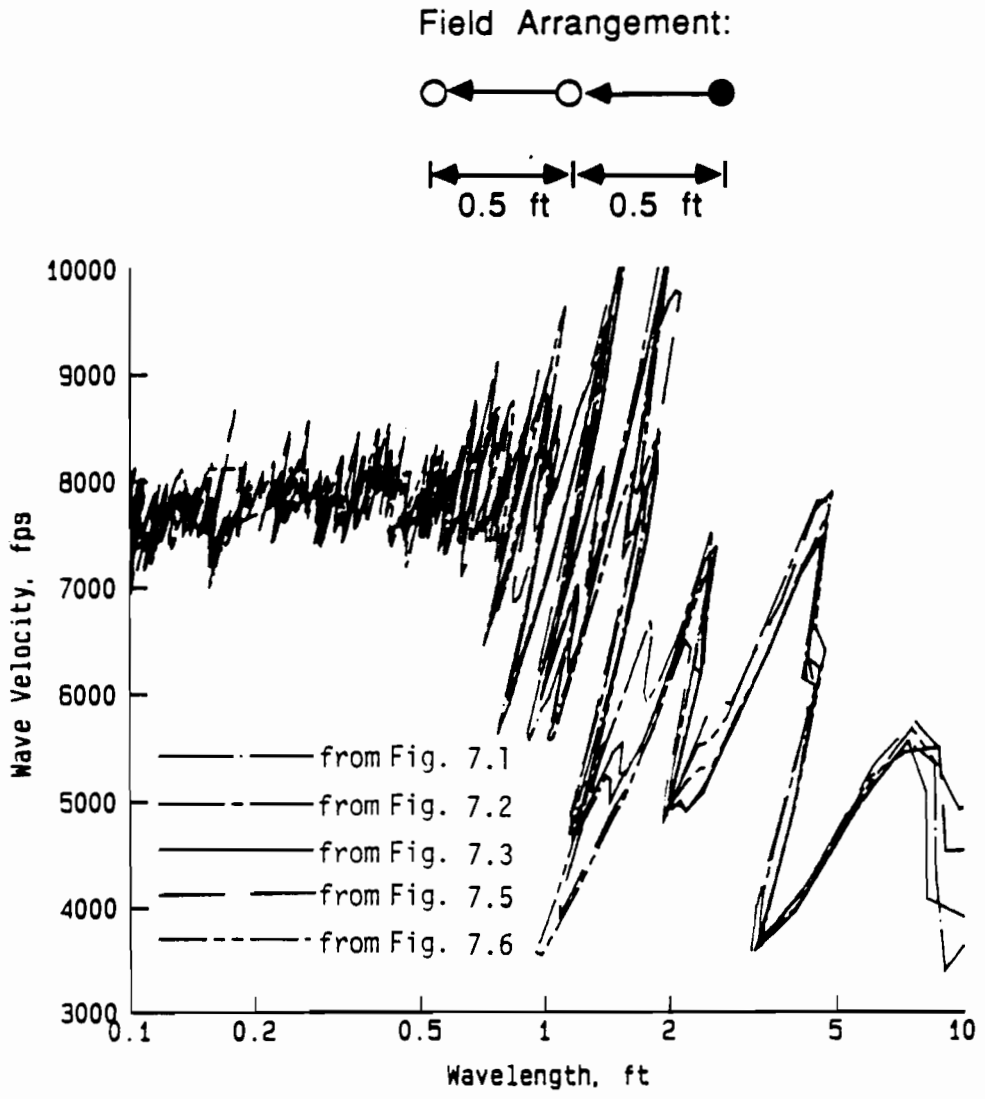

Fig. 7.7. Influence on Dispersion Curves of Impact Stress Levels Used to Generate Time Domain Signals.

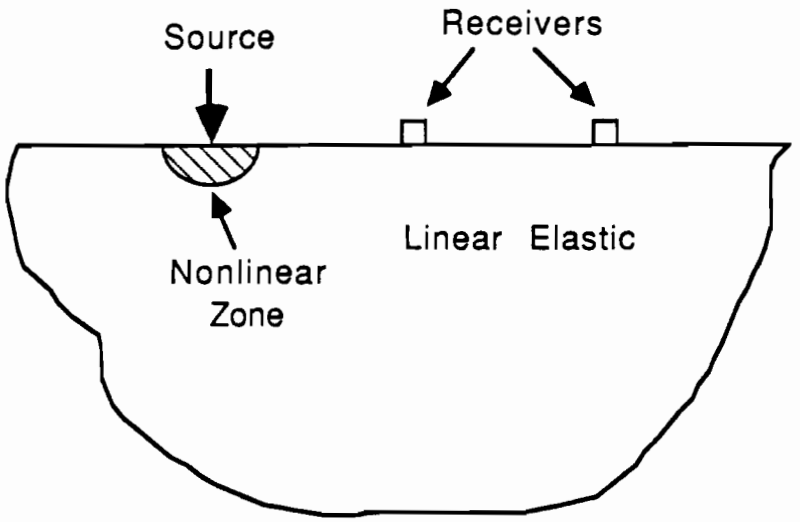

Fig. 7.8. Possible Zone of Material Stressed into Nonlinear Behavior by Hammer Impact.

7.4. EFFECTIVENESS OF VARIOUS METHODS FOR ATTACHING ACCELEROMETERS ON PAVEMENT SURFACE

To measure high-frequency surface motion (say above 10 KHz), accelerometers are used.These accelerometers have to be attached firmly to the pavement surface so that they can track surface motion as closely as possible. A few methods have been used in the past to attach accelerometers, but the effectiveness of these methods has never been justified. Therefore, three methods of attaching accelerometers to the pavement surface were used herein to observe their effectiveness in monitoring ground surface motion.

The first method was to use "super glue" to attach threaded holders (nuts) onto the pavement surface to which the accelerometers were subsequently attached. The second method was to apply a thin layer of modeling clay on the pavement surface and then press the accelerometers firmly onto this thin clay layer. The third method was just to place the accelerometers on the pavement surface freely with no special coupling mechanism.

Testing was performed at the BRC facility. The concrete pavement was used at location 2, parallel array 6, as shown in Fig. 3.1. The spacing between the receivers was 0.5 ft (15 cm), and the source was located 0.5 ft (15 cm) away from receiver 1. The "V" meter was used to generate impulses for this set of tests. (The "V" meter is discussed in Chapter Eight.) Two, PCB model 308B02 accelerometers were used as receivers. Time and frequency domain records for each method are shown in Figs. 7.9 through 7.11.

The time records indicate that coupling the accelerometers to the pavement surface by holders glued on the surface (Fig. 7.9) provides very good contact between the accelerometers and pavement. As a result, the receivers seemed to be able to record more high-frequency signals than the other two methods. However, the auto power spectra and coherence function do not support this point of view completely. The auto power spectra for accelerometers coupled with both glued holders and with modeling clay (Figs. 7.9 and 7.10) show a very uniform energy distribution throughout most of the frequency span. The modeling clay (Fig. 7.10) shows some low energy transmission in the frequency range of about 3 to 5 KHz which makes the corresponding coherence function low but very good energy transmission over the high-frequency range. Glued holders (Fig. 7.9), on the other hand, show insufficient energy transmission in the range of 75 to 100 KHz at receiver 2. The auto power spectra and coherence functions show that the performance of the modeling clay fixture in the high-frequency range is better than glued holders. This is another strange example (in addition to Section 7.2) that implications given by observing time domain signals may be misleading. The amplitudes of the

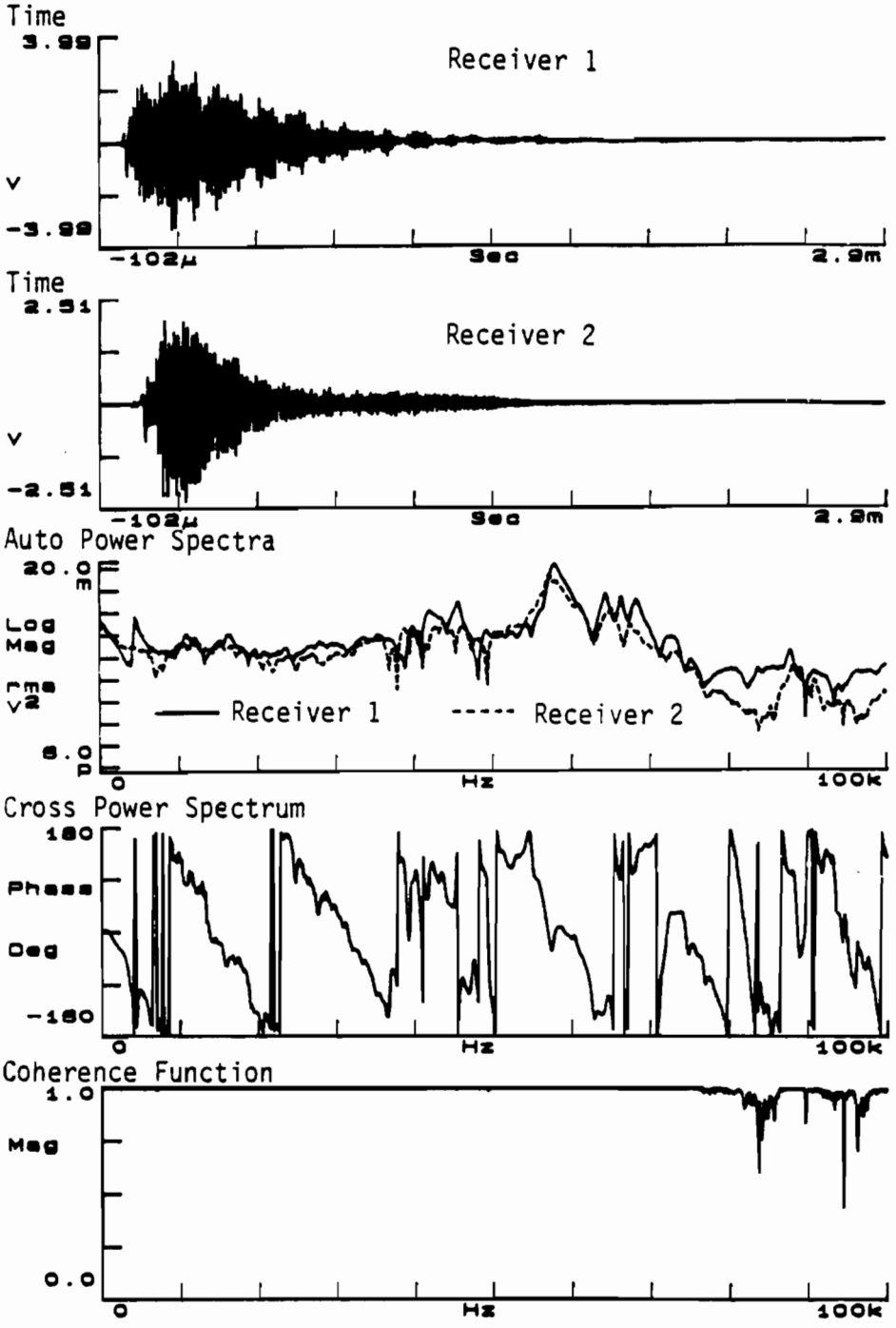

Fig. 7.9. Time Domain Signals and Corresponding Frequency Spectra for a Concrete Pavement with Good Accelerometer-Pavement Coupling (Glued Holders).

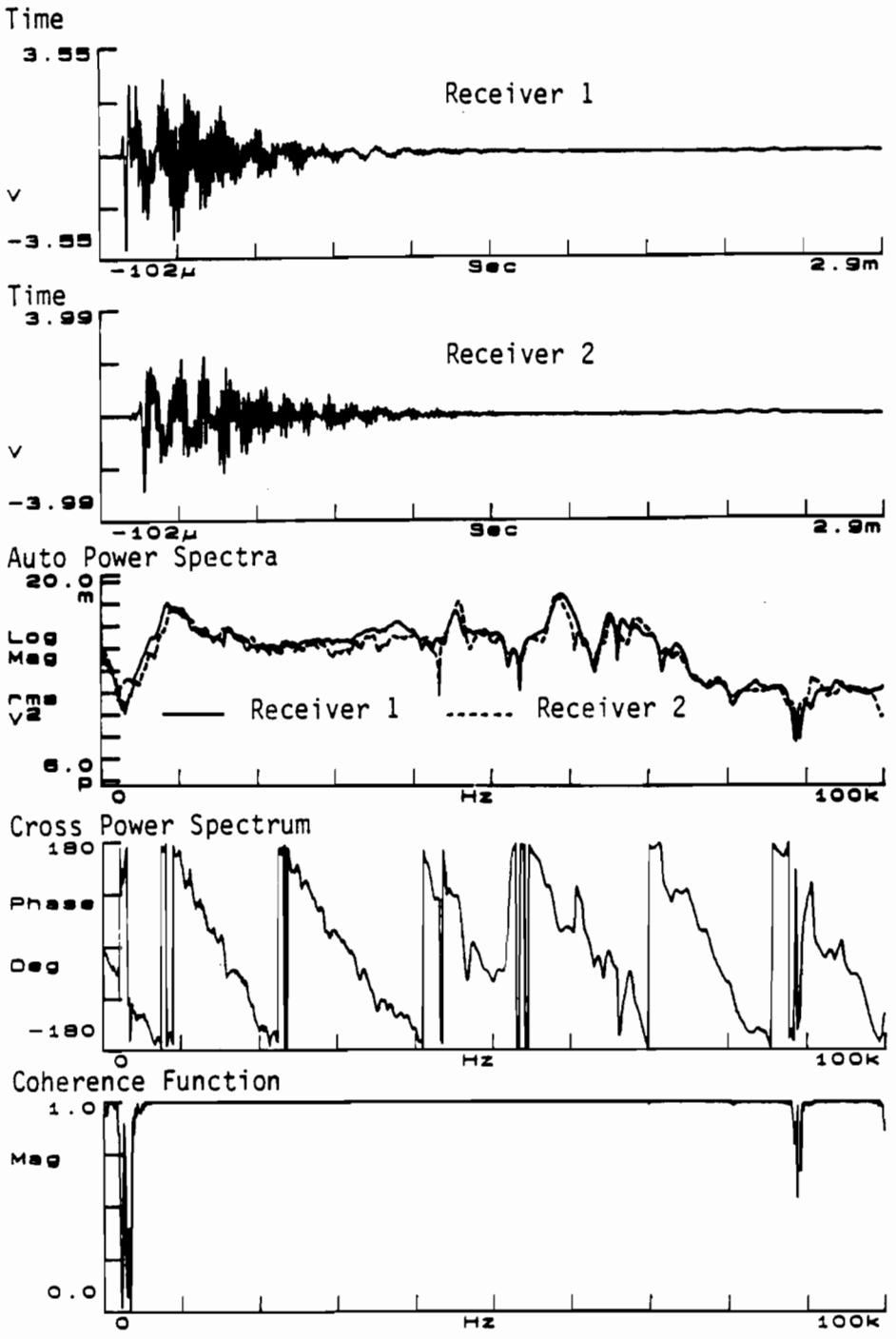

Fig. 7.10. Time Domain Signals and Corresponding Frequency Spectra for a Concrete Pavement with Relatively Good Accelerometer-Pavement Coupling (Modeling Clay).

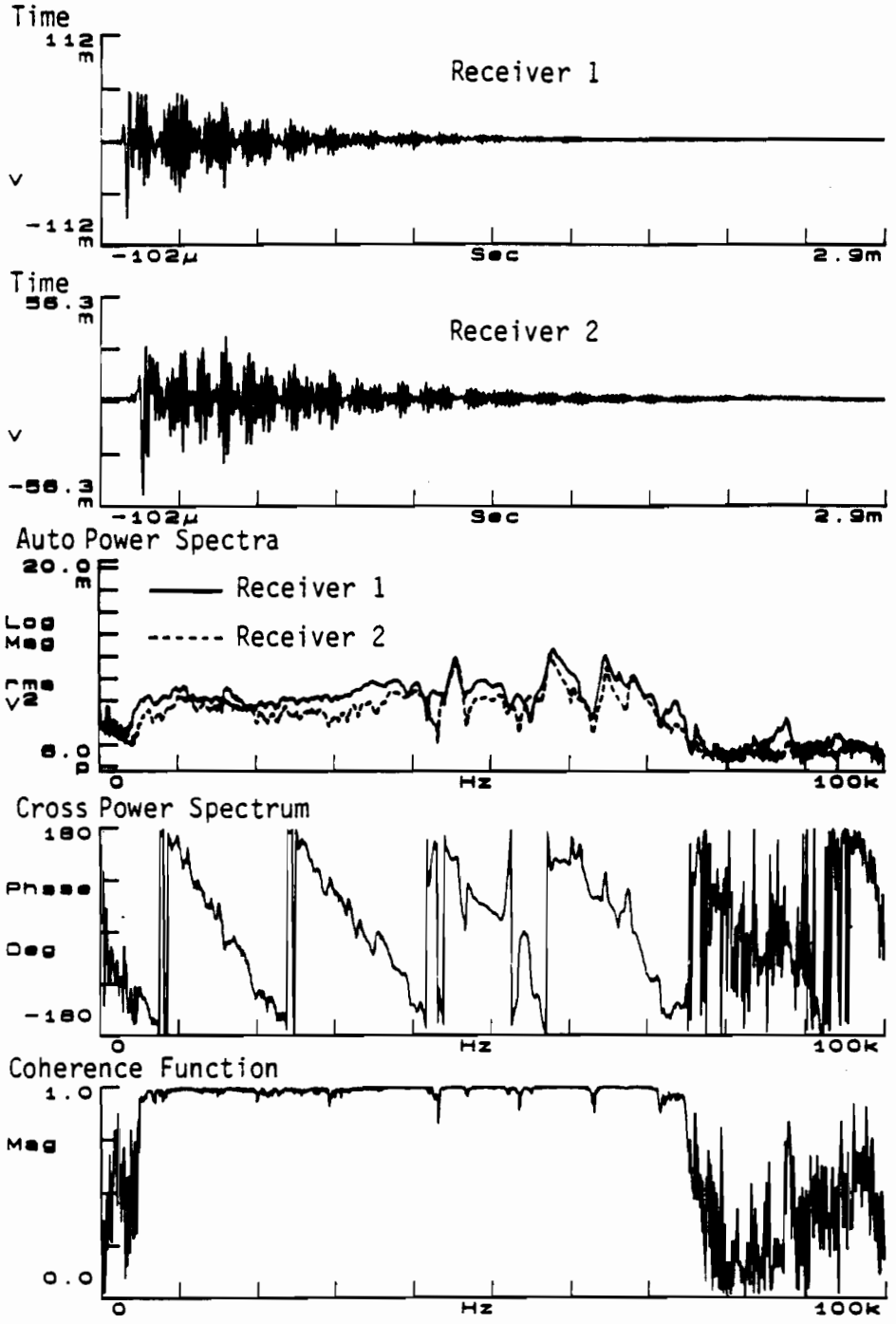

Fig. 7.11. Time Domain Signals and Corresponding Frequency Spectra for a Concrete Pavement with Poor Accelerometer-Pavement Coupling (No Coupling Mechanism).

time signals and auto power spectra for receivers set freely on the ground surface (Fig. 7.11) are very low compared to the other two attachment methods Energy transmission above 75 KHz and below 5 KHz is insufficient, and low-quality data were collected in these two frequency ranges with accelerometers simply placed on the pavement surface.

Comparison of dispersion curves from these three attachment methods is shown in Fig. 7.12. Receivers without any coupling mechanism tend to overestimate wave velocities (about 6 percent in this example). Receivers coupled with glued holders or the modeling clay seem to measure similar wave velocities, except that coupling with modeling clay renders a slightly higher estimation of wave velocities in the very short wavelength range (for wavelength less than about 0.2 ft (6 cm) in this example).

Glued holders have been used for coupling accelerometers to pavement surfaces throughout almost all tests at the BRC facility, it is the most stable (not affected by time and temperature) and preferred method. The modeling clay seems to be equally good as glued holders and has been used in many other field tests. However, the problem with modeling clay is that the ambient temperature has to be moderate (say 60 to 75 degrees Fahrenheit (15 to 24 degrees Centigrade)) because too high or too low a temperature can make the modeling clay too soft or too hard to use. Receivers placed freely on the ground surface without any coupling mechanism tend to collect relatively low-quality data, and this method of attachment is not recommended.

7.5. INFLUENCE OF RESONANCES OF ACCELEROMETERS AND COUPLED ACCELEROMETER-PAVEMENT SYSTEM

7.5.1 Nature of the Problem

There are many devices which can be used to measure the motion of a pavement surface. The devices can be categorized into two major groups depending on the type of contact with the pavement surface. The first group has direct physical contact with the measured system. Strain gauges, geophones, and accelerometers are typical of this group. The other group has no physical contact with the measured system. Proximitors and laser beams are typical devices in this group.

At present, due to the high cost and performance limitations, it is not feasible to use noncontacting devices to monitor pavement surface motions in SASW testing. At most pavement sites, accelerometers are used because they are relatively inexpensive, have high sensitivities and have a wide frequency response. Unfortunately, once there is any physical contact between the

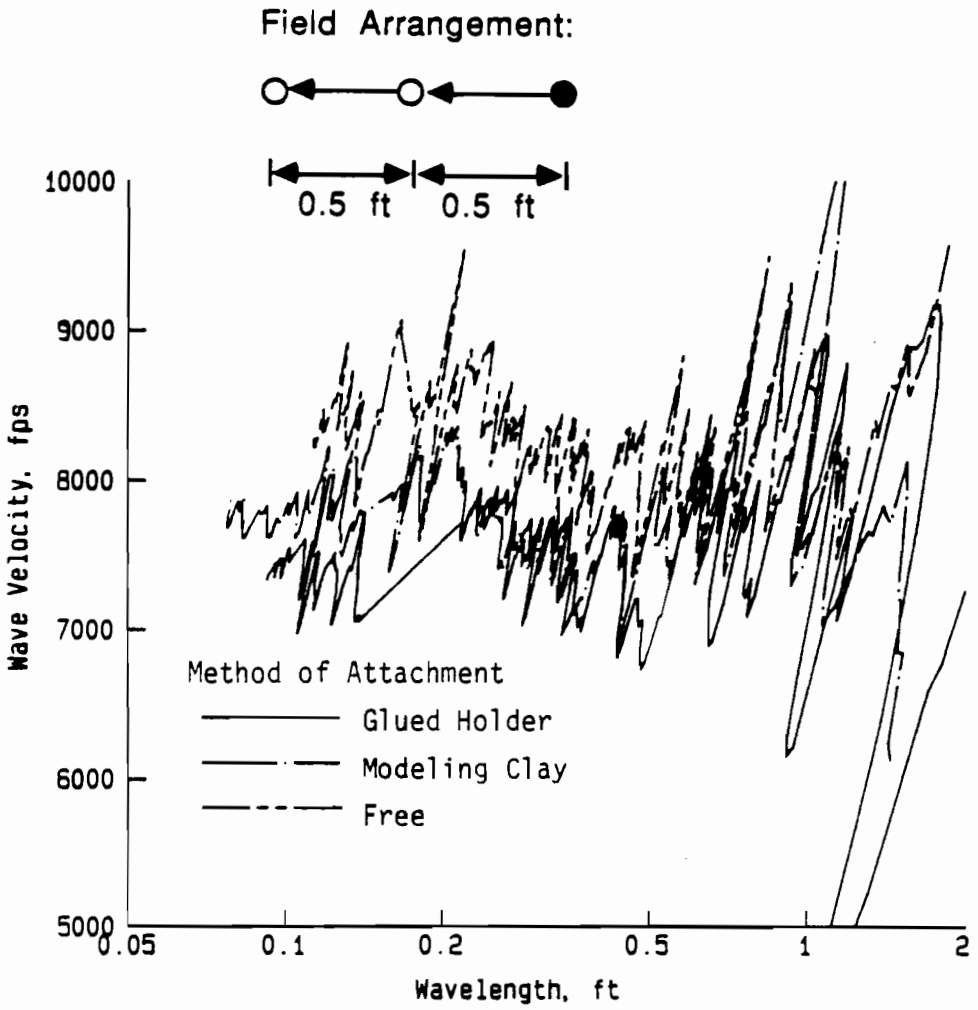

Fig. 7.12. Influence on Dispersion Curves of Different Methods of Accelerometer-Pavement Coupling.

measuring device and the measured pavement, these two systems interact with each other and form a coupled system which can exhibit different behavior from either of the original two systems in some frequency ranges. For example, suppose an accelerometer is properly attached to the pavement surface. When the surface moves, the accelerometer will move accordingly. However, the surface has to exert a force on the accelerometer to move it, and this force in turn changes the original surface motion. As a result, the boundary condition for the pavement is no longer a "free surface" under the accelerometers. The surface motion for a system with no accelerometer attached will be different in some frequency ranges from the same system with an accelerometer attached. In general, this kind of influence can only be reduced but not totally eliminated. For example, use of accelerometers with small mass can reduce their effect on the pavement surface motion because the inertial forces induced by light-weight accelerometers are small.

In addition, each measuring device is itself a system and has its own characteristics. These characteristics, in many instances, limit the effectiveness of the measuring device. The resonant frequency of an accelerometer is one of these characteristics. Each accelerometer has a natural frequency at which the output signal from the accelerometer is no longer meaningful because of resonances set up in the accelerometer. Usually, accelerometers are used to monitor frequencies well below their resonant frequencies. The difficulty of SASW tests on pavement sites arises from the need to measure motions at very high frequencies, say 20 to 100 KHz, if one wants to know accurately the stiffness of the top layer. At this time, it is not feasible to acquire calibrated devices with resonant frequencies above 100 KHz. One solution, therefore, is to use accelerometers in the frequency range above their resonant frequencies. However, this solution requires some experimental justification.

For the purpose of understanding the questions cited above, field tests were performed. Six different accelerometers were used in those tests. Characteristics of each accelerometer are given in Table 7.1.

7.5.2. Natural Frequencies of Coupled System

The vibration of the coupled accelerometer-pavement system can be observed by examining most SASW time records of tests performed at the BRC facility. A majority of these records can be seen to contain one or more predominant frequencies. Time records shown in Figs. 7.1 through 7.6 are good examples. The predominant frequency or frequencies are

TABLE 7.1. CHARACTERISTICS OF ACCELEROMETERS USED IN STUDY OF RESONANT FREQUENCIES

Model Number	Weight (gm)	Resonant Frequency (KHz)	Sensitivity (mV/g)
301A04	130	60	10
303A11	2.5	76	100
303A12	2.5	76	100
30813	76	27	100
308B02	76	30	1000
393C	1000	6	1000

believed to be the resonant frequencies of the coupled accelerometer-pavement system (Krohn 1984, 1985).

To investigate resonances in the accelerometer-pavement system, the following tests were performed. A model PCB 308B02 accelerometer (weight of 76 gm) was attached to the pavement surface at location 2 (see Fig. 3.1). Glued holders were used for the coupling of accelerometer-pavement system. The coupled accelerometer-pavement system was first excited by vertically tapping on top of the accelerometer with a paper clip, and the output of the accelerometer was recorded. By tapping the accelerometer with a paper clip, an impulsive force was applied to the coupled system, and resonant frequencies were found from the system response spectra (peaks in the auto power spectra or linear spectra). The same coupled system was then excited by a hammer blow on the pavement surface about 1 ft (30 cm) away from the accelerometer, just like a regular SASW test. The output of the accelerometer was again captured. Both time records were Fourier transformed to the frequency domain for analysis.

Time domain signals and power spectra for both tests with the model 308B02 accelerometer are presented in Fig. 7.13. Resonant frequencies can be identified from the peaks in the auto power spectra. In each case, resonant frequencies appear at about 7 and 16 KHz as indicated by arrows in these figures. The resonant frequencies appear at the same location whether the coupled accelerometer-pavement system is excited by a hammer tap on the pavement surface or by a paper clip tapping on the accelerometer. Notice that there are two resonant frequencies in each case. The first peak of the auto power spectra appears at a lower frequency (about 7 KHz) and is believed to be the resonant frequency in vertical vibration for this coupled system. The second peak appears at a higher frequency (about 13 KHz) and is expected to be another mode of vibration of this coupled system.

The same test was repeated with model PCB 303A12 accelerometers. Since the 303A12 accelerometer weighs only 2.5 gm, a higher resonant frequency than for the 308B02 accelerometer was expected. The test data presented in Fig. 7.14 shows that the resonant frequency appears at about 13 KHz which is higher and agrees with the expectation.

Another test was performed in the laboratory to identify more precisely the resonant frequencies of the coupled system. A concrete block was used in place of the pavement system. A PCB model 301A04 accelerometer which weighs 130 gm was first attached on top of the concrete block and tapped with a paper clip. The resulting response is shown in Fig. 7.15a. A PCB model 308B accelerometer, which weighs 76 gm, was then attached on top of the PCB 301A04 accelerometer as a dead weight. The combined system was again tapped, and this

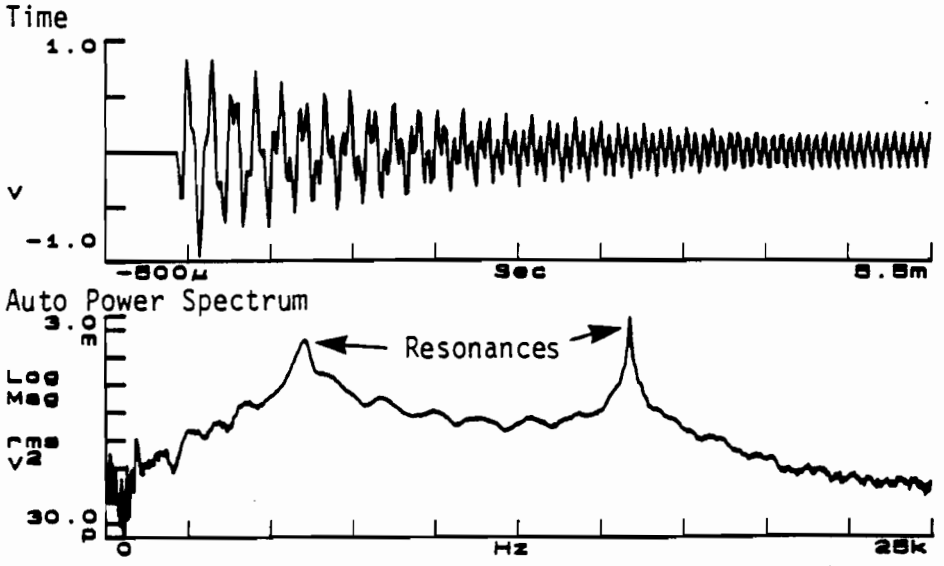

a. Vertical Tap on Accelerometer with a Paper Clip

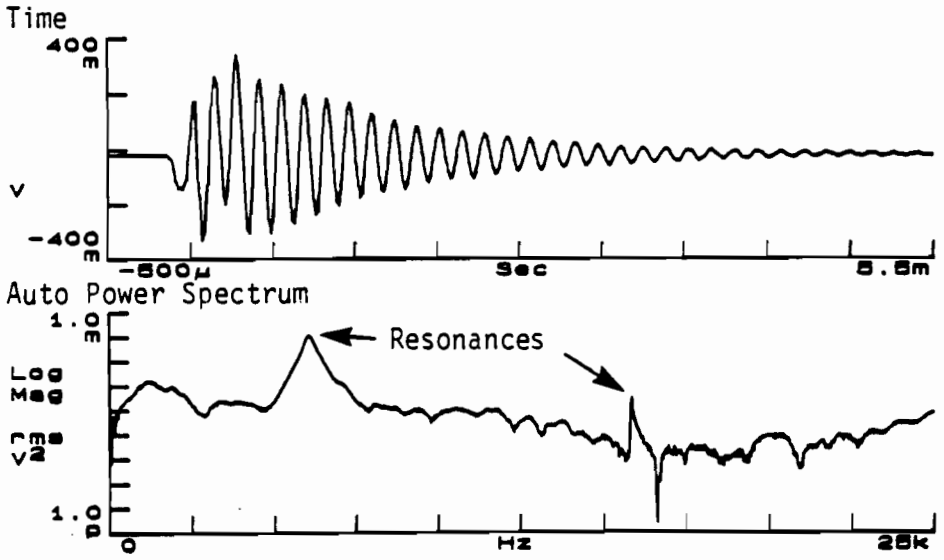

b. Vertical Tap on the Pavement Surface with a Hammer

Fig. 7.13. Time Domain Signals and Auto Power Spectra of Coupled Accelerometer (Model 308B02)-Pavement System with Two Different Methods of Excitation.

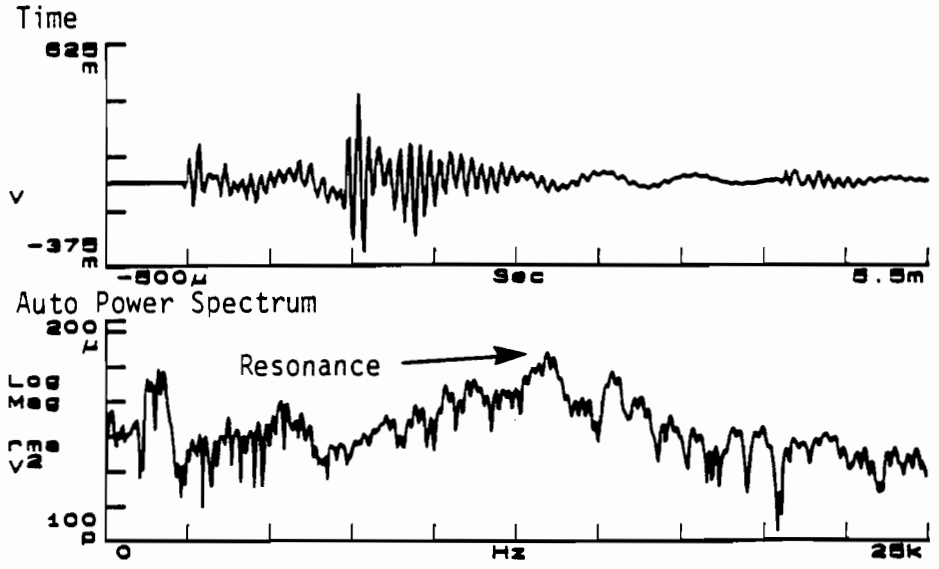

a. Vertical Tap on Accelerometer with a Paper Clip

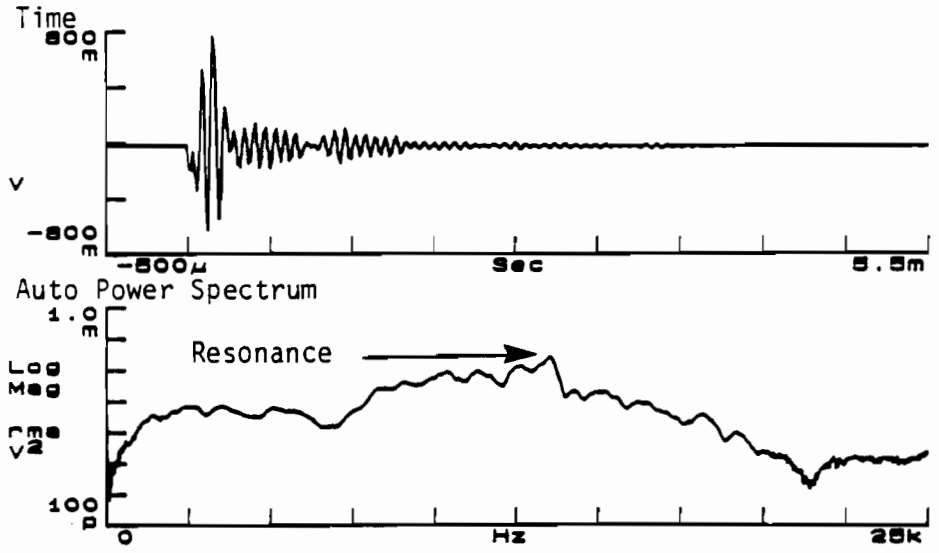

b. Vertical Tap on the Pavement Surface with a Hammer

Fig. 7.14. Time Domain Signals and Auto Power Spectra of Coupled Accelerometer (Model 303A11)-Pavement System with Two Different Methods of Excitation.

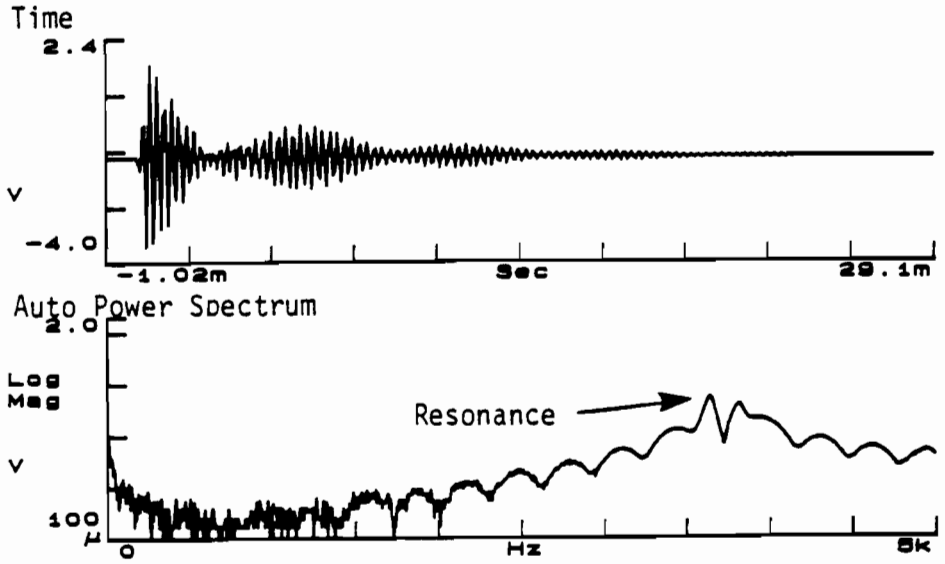

a. With No Additional Deadweight

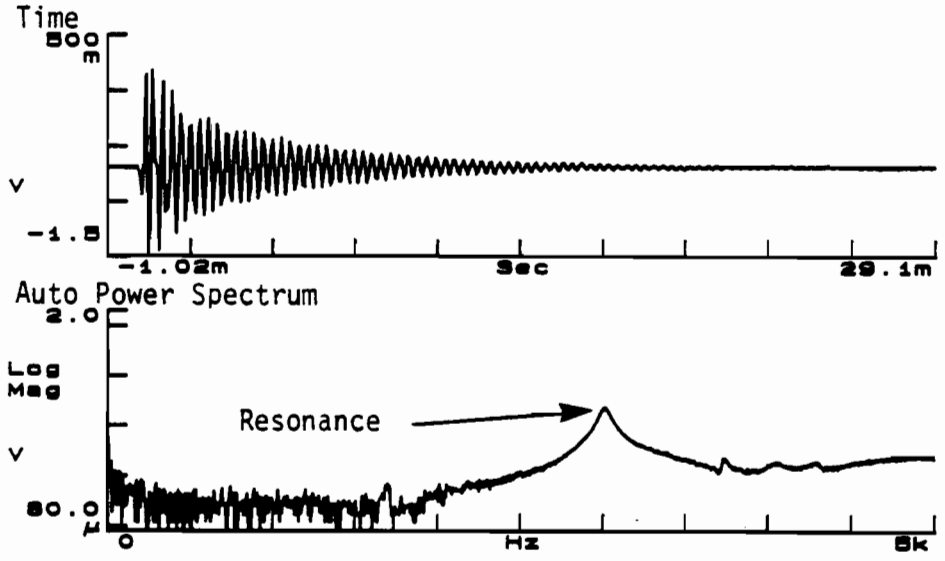

b. With Model 308B02 Accelerometer Added as Deadweight

Fig. 7.15. Change in Time Domain Signals and Resonant Frequencies for Coupled Accelerometer (Model 301A04)-Pavement System Caused by Adding Deadweight to the Accelerometer.

response is shown in Fig. 7.15b. Both records were then Fourier transformed to the frequency domain to find the resonant frequencies.

To investigate the change in resonant frequency, the following calculation was made. The natural frequency of a rigid body vibrating vertically on the surface of a elastic half space can be expressed as:

$$f_n = \frac{1}{2\pi} \sqrt{\frac{k}{m}} \tag{7.1}$$

where:

f_n = resonant frequency, Hz,

k = equivalent vertical spring constant, and

m = mass.

The equivalent vertical spring constant, k, is controlled by the stiffness of the concrete pavement and the shape of the glued holder. The mass, m, is the mass of the accelerometer (and other attachments such as part of the cable, connector etc.).

With the 308B02 accelerometer on top of the 301A04, the natural frequency, f_n, is 3020 Hz (from Fig. 7.15a). If one assume that k remains constant, with the help of Eq. 7.1, the resonant frequency for the 303A04 alone is:

$$f_n = 3020 \text{ Hz} \times \sqrt{\frac{67.36 + 130.50}{130.50}} = 3720 \text{ Hz} \tag{7.2}$$

The linear spectra shown in Fig. 7.15b reveals two peaks at 3.65 and 3.82 KHz, respectively. It is not clear which one (or the combined peak) is the resonant frequency of this coupled system. However, either of them is very close to the value estimated by Eq. 7.2 indicating the reasonableness of the assumption..

7.5.3. Impact on Test Results of Coupled Resonant Frequencies

The previous experiments have identified the existence of resonant frequencies for the coupled accelerometer-pavement system in the accelerometer records. These resonant frequencies combined with the natural frequency of the accelerometer itself make the validity of measurements

in the neighborhood of these frequencies questionable. It is important to know how these resonant frequencies affect the test results.

Further experiments were performed in an attempt to answer these questions. Experiments were performed at the BRC facility at location 6 (see Fig. 3.1). Three types of accelerometers were used at the same location to monitor pavement surface motions; PCB models 303A11, 308B02, and 393C. The distance between the two receivers was 1 ft (30 cm), and the source was 1 ft (30 cm) away from the first receiver. Accelerometers were coupled with the pavement surface by glued holders. In the initial tests, the first and second receivers were of the same type (same model number). In the second series of tests, different types of accelerometers were used for receiver 1 and receiver 2. (That is, an accelerometer of one model number was used as receiver 1 and an accelerometer of another model number was used as receiver 2.)

Same Type of Accelerometers in One Pair

A composite plot for phases of the cross power spectra and coherence functions from each individual pair of the same type of accelerometers is shown in Fig. 7.16. The three sets of accelerometer gave almost the same information. Notice that the resonant frequency of model 393C is around 6 KHz, but the phase of the cross power spectrum from model 393C in the neighborhood of 6 KHz is similar to the phase from the other types of accelerometers which have a lot higher resonant frequencies (30 KHz for model 308B02 and 76 KHz for model 303A11). No noticeable alternation on the phase of the cross power spectrum is found. This result shows that the resonant frequency of accelerometer itself does not affect the phase of cross power spectrum if a pair of similar accelerometers is used.

To locate coupled resonant frequencies, time domain signals were collected for each type of accelerometer at the same location and Fourier transformed. Linear spectra, phases of the cross power spectra, and coherence functions of these time signals are presented in Figs. 7.17 through 7.19 for each type of accelerometer. By examining these figures, it is clear that the linear spectra for the model 303A11 accelerometers (Fig. 7.17) are relatively flat with no peaks (resonant frequencies). Notice that the natural frequency for this system (coupled 303A11) was found to be 13 KHz (Fig. 7.14) which is not observed in Fig. 7.17 because the bandwidth shown in this figure is only from 0 to 10 KHz. Also, there are no evident distortions in the phase of the cross power spectrum shown in Fig. 7.17, except in the region where coherence function is low.

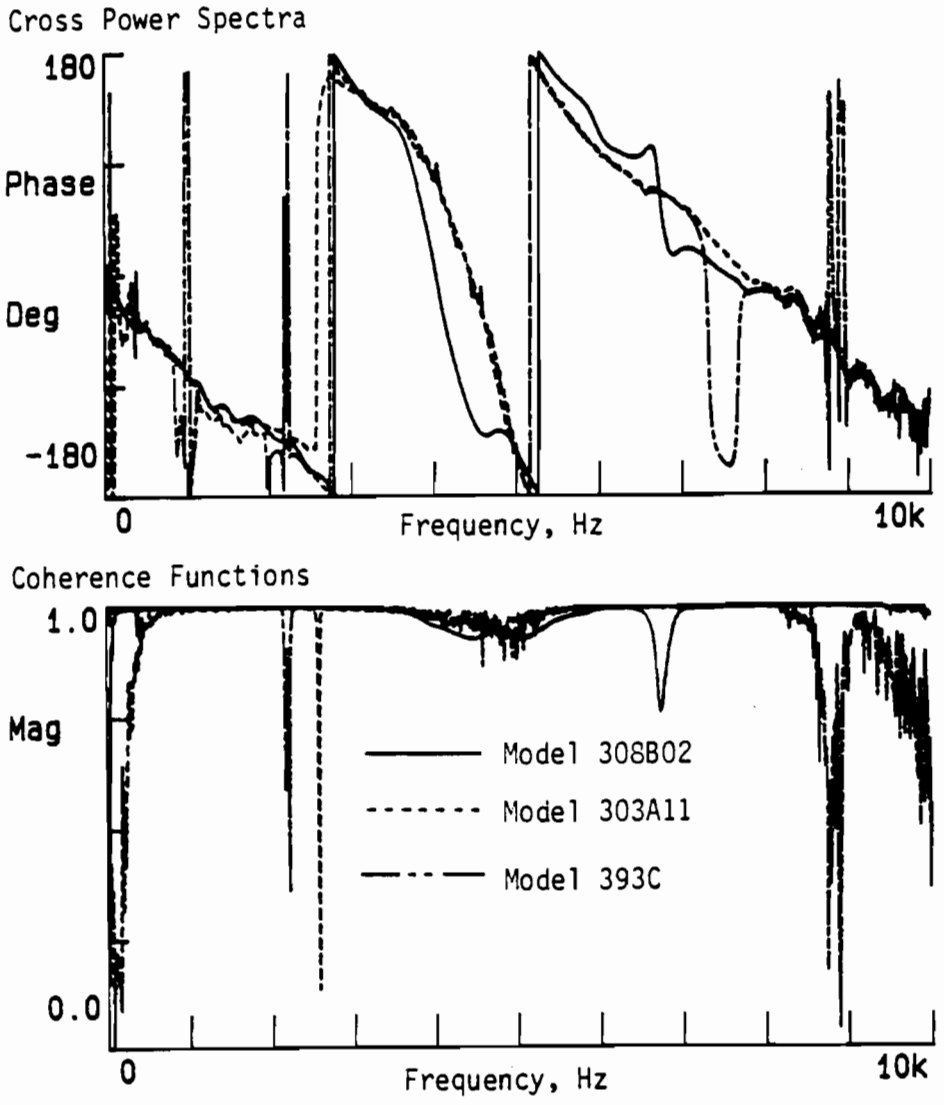

Fig. 7.16. Comparison for Phases of Cross Power Spectra and Coherence Functions Measured with Different Pairs of Accelerometers.

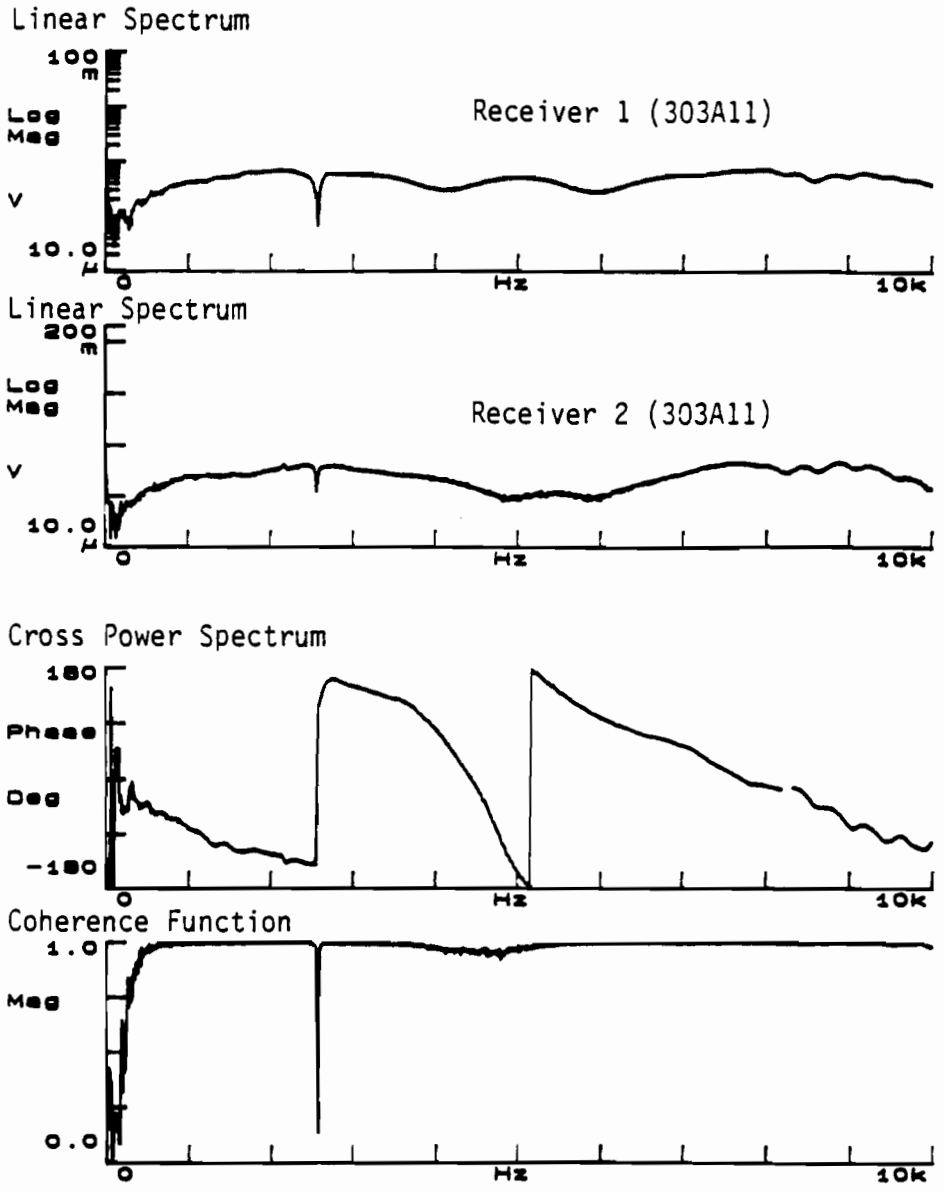

Fig. 7.17. Frequency Response of Accelerometer Pair (Model 303A11) in a Typical SASW Test: No Significant Distortion in Phase of the Cross Power Spectrum.

Distortion in the phase of the cross power spectrum because of slightly different resonant frequencies for the model 308B02 accelerometer is shown in Fig. 7.18. This distortion was minor but noticeable. The difference is especially evident in Fig. 7.16 in the frequency range from about 3.5 through 5 KHz when plotted along with other records. For the model 393C (Fig. 7.19), the phases of the cross power spectrum were distorted at all major and minor resonant frequencies of the coupled system as indicated by the arrows and hatched zones in the figure. The distortion in between two slightly different resonant frequencies is caused by the phase shift of the system output since the output of a system changes drastically in the neighborhood of the resonant frequency.

Different Types of Accelerometers in One Pair

In addition to the previous source/receiver arrangement, different types of accelerometers were mixed as receiver pairs to investigate the effect of pairing different accelerometer response characteristics. Two tests were performed by pairing models 308B02 and 393C accelerometers. In the first test, the model 393C was used as the first receiver, and the model 308B02 was used as the second receiver. In the other test, the same pair of accelerometers was used but the order was reversed. The spacings between source and first receiver as well as between the two receivers was 1 ft (30 cm). Linear spectra for both receivers, phases of cross power spectra, and coherence functions are presented in Figs. 7.20 and 7.21.

Very interesting phenomena were found by comparing the phases of these tests to the phases measured in previous tests when the same type of accelerometers were paired. As a reference, the phase from the model 303A11 pair (Fig. 7.17), which is supposed to be the correct phase, is shown with dashed lines in Figs. 7.20 and 7.21 In the case where the model 393C was used as the first receiver and the model 308B02 was used as the second receiver (Fig. 7.20), there is a phase lag of about 180 degrees right after the first resonant frequency noted in the model 393C (at about 1 KHz). This phase lag continues until the resonant frequency of the model 308B02 is reached (at about 4.8 KHz). At that point, the phase merges back to the original trace until the second resonant frequency in the auto power spectrum of the model 393C is reached (at about 7.3 KHz). Upon reaching this resonant frequency, a 180-degree phase lag starts again and lasts through the rest of the spectrum.

On the other hand, when the model 308B02 accelerometer was used as the first receiver and the model 393C was used as the second receiver (Fig. 7.21), a phase advance of about 180 degrees appears after the first resonant frequency of the model 393C (at about 1 KHz). This

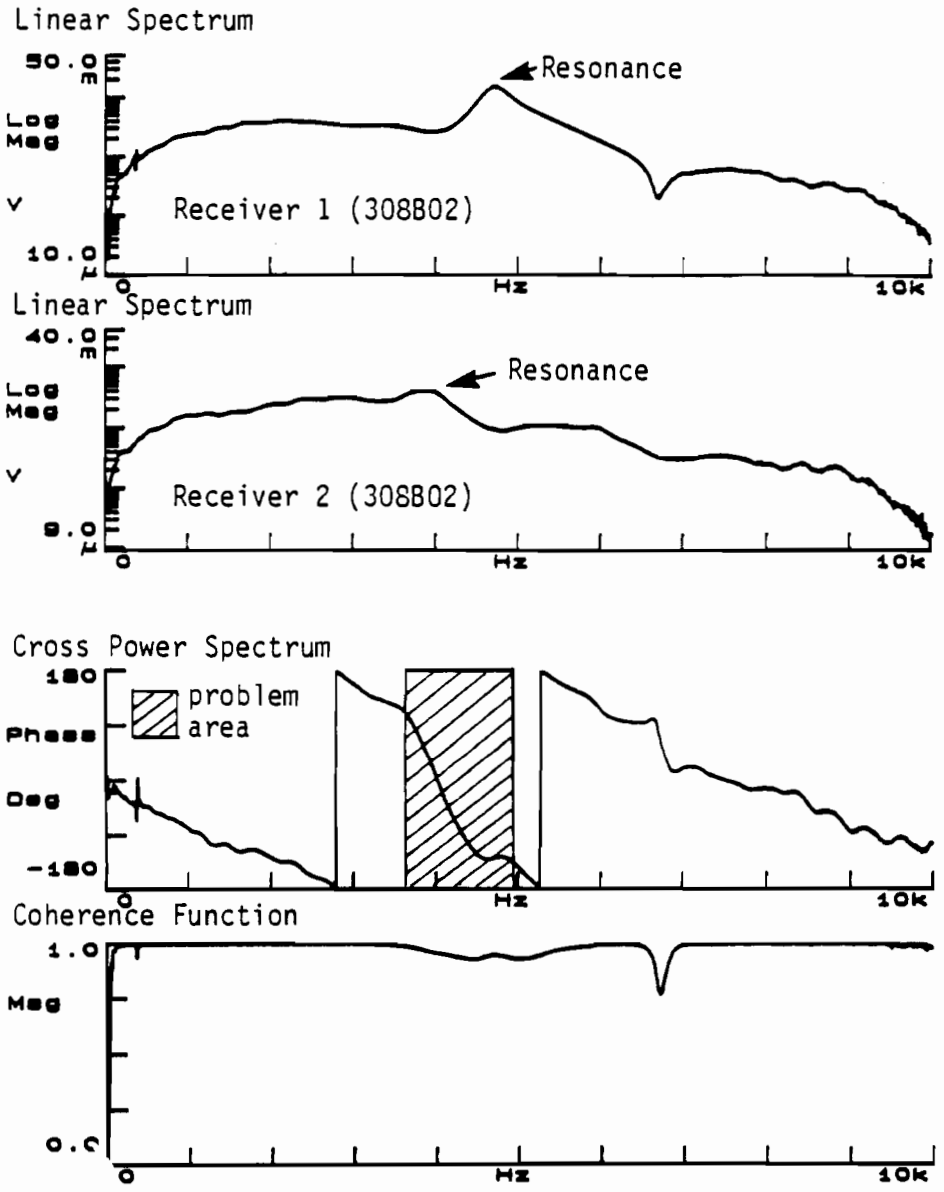

Fig. 7.18. Frequency Response of Accelerometer Pair (Model 308B02) in a Typical SASW Test: Slight Distortion in Phase of the Cross Power Spectrum.

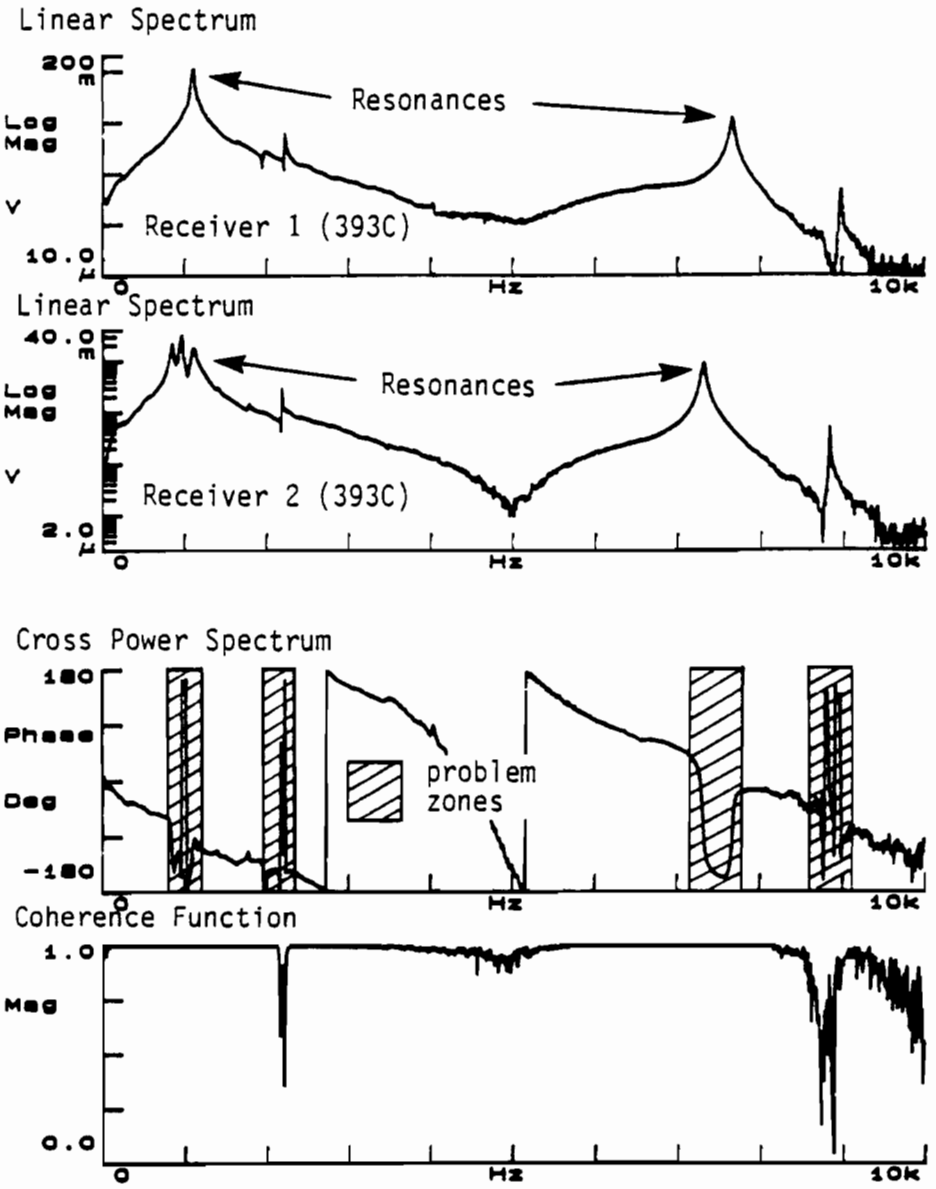

Fig. 7.19. Frequency Response of Accelerometer Pair (Model 393C) in a Typical SASW Test: Significant Distortion in Phase of the Cross Power Spectrum.

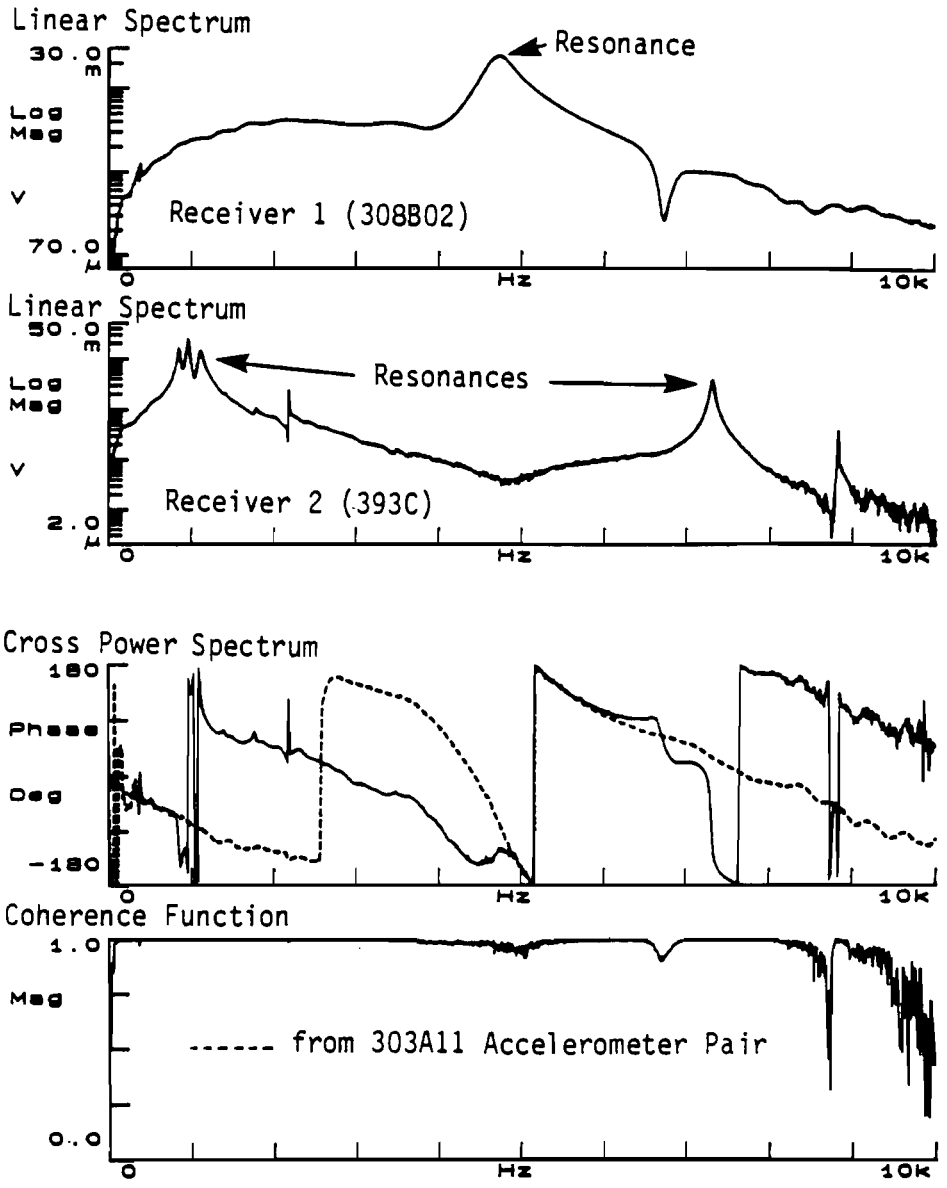

Fig. 7.20. Distortion in Phase of the Cross Power Spectrum Caused by Using Different Accelerometers: Model 308B02 Accelerometer is Receiver 1 and Model 393C Accelerometer is Receiver 2.

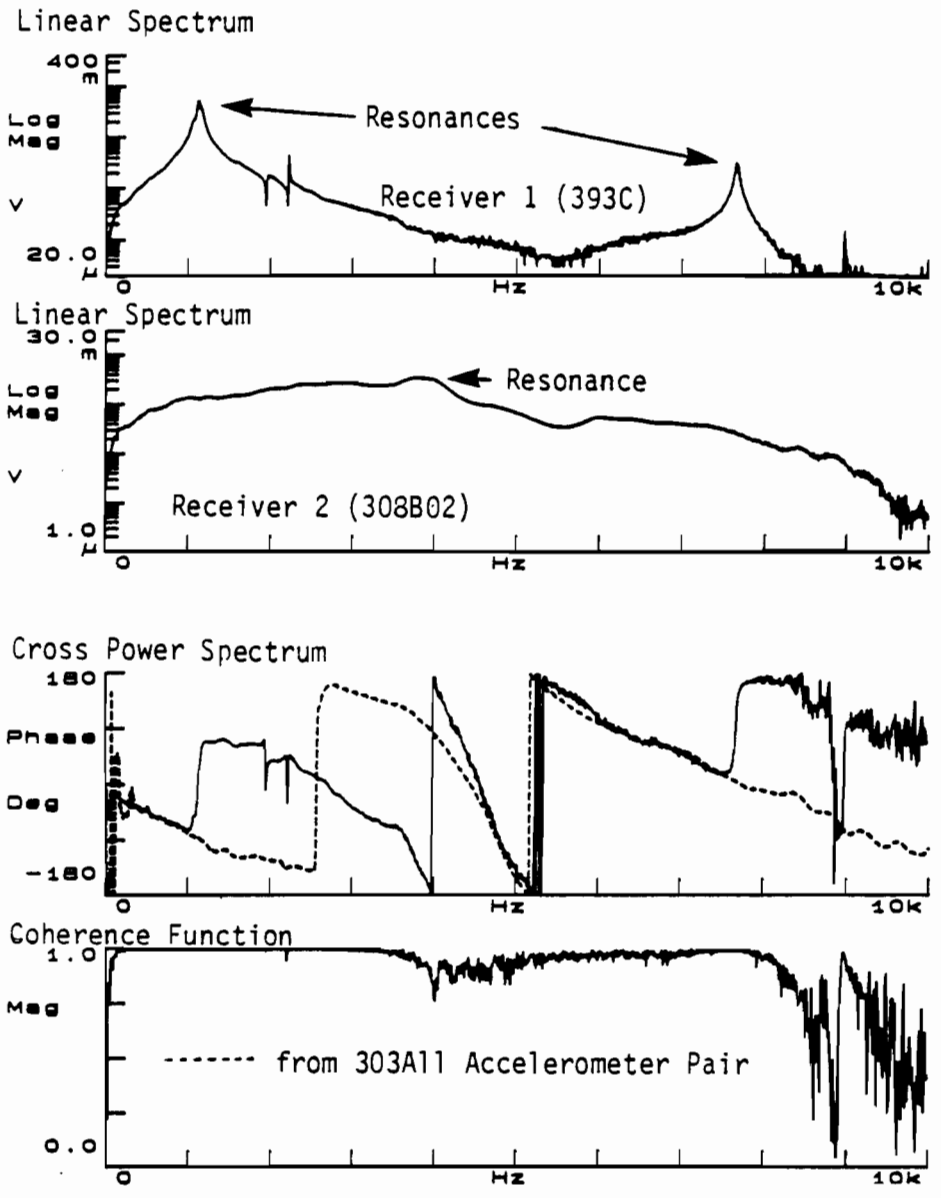

Fig. 7.21. Distortion in Phase of the Cross Power Spectrum Caused by Using Different Accelerometers: Model 393C Accelerometer is Receiver 1 and Model 308B02 Accelerometer is Receiver 2.

phase advance continues until the resonant frequency of the model 308B02 is reached (at about 4.8 KHz). Again, the phase merges back to the original trace until the second resonant frequency of the model 393C (at about 7.6 KHz) is reached. Upon reaching this second resonant frequency, a 180-degree phase advance appears and lasts to the end of spectrum.

The resonant frequency of the model 308B02 accelerometer itself is about 30 KHz. Since the frequency span in both cases are in the range of 0 Hz to 10 KHz, the model 308B02 accelerometer should be able to work properly without concern for its own resonant frequency (Figs. 7.20 and 7.21). The resonant frequency for the model 393C itself is about 6 KHz. As a result, one could expect some erroneous data appearing in the neighborhood of 6 KHz. But in Figs. 7.20 and 7.21, data around 6 KHz range are very similar to data acquired by the model 303A11 accelerometer pair and do not indicate any distortion. This outcome implies that the resonant frequency of accelerometer itself does not affect the phase of the cross power spectrum.

The same type of test was performed by pairing models 308B02 and 303A11 accelerometers. This test was performed at the same location with the same source/receiver arrangement as the previous tests. The results of using the model 308B02 as receiver 1 and the model 303A11 as receiver 2 are shown in Fig. 7.22. The results of reversing the order of the accelerometers are shown in Fig. 7.23. Again, the phase of the cross power spectrum from a pair of model 303A11 accelerometers is plotted as a dashed line for reference. The dash lines should represent the correctly measured phase (at least below about 80 KHz).

The results from this set of test seem to be very complex and difficult to interpret. There are frequencies where the phases of the cross power spectra shown by dashed lines (correct phases) coincide with the phases shown by solid lines which means the measured phase is correct. There are also frequencies where the phases of the cross power spectra shown by dashed lines (correct phases) are parallel to the phases shown by solid lines, and the differences are always about 180 degrees. The trend is more clearly defined in the range from 0 to 40 KHz where both figures show a phase lag (or advance) of about 180 degrees in the range of 0 Hz to about 20 KHz The two phases (measured and reference phases) merge at about 20 KHz which is the first significant resonant frequency of the coupled model 303A11-pavement system, and this merged phase extends from 20 KHz to about 38 KHz.

The test results by pairing models 303A11 and 308B02 accelerometers are not as conclusive as the previous one (Figs. 7.20 and 7.21), but they still suggest that pairing different types of accelerometers can cause very erroneous results.

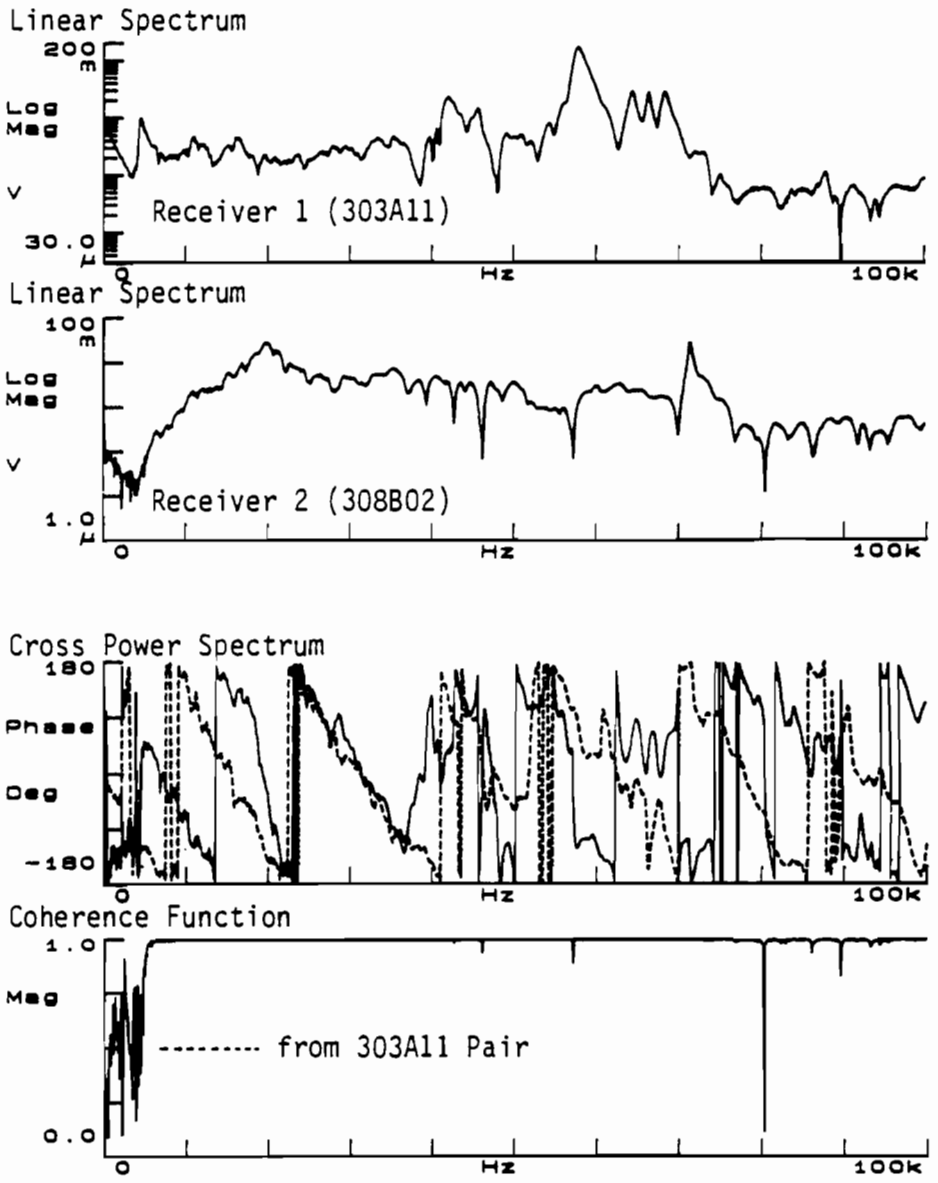

Fig. 7.22. Distortion in Phase of the Cross Power Spectrum Caused by Using Different Accelerometers: Model 303A11 Accelerometer is Receiver 1 and Model 308B02 Accelerometer is Receiver 2.

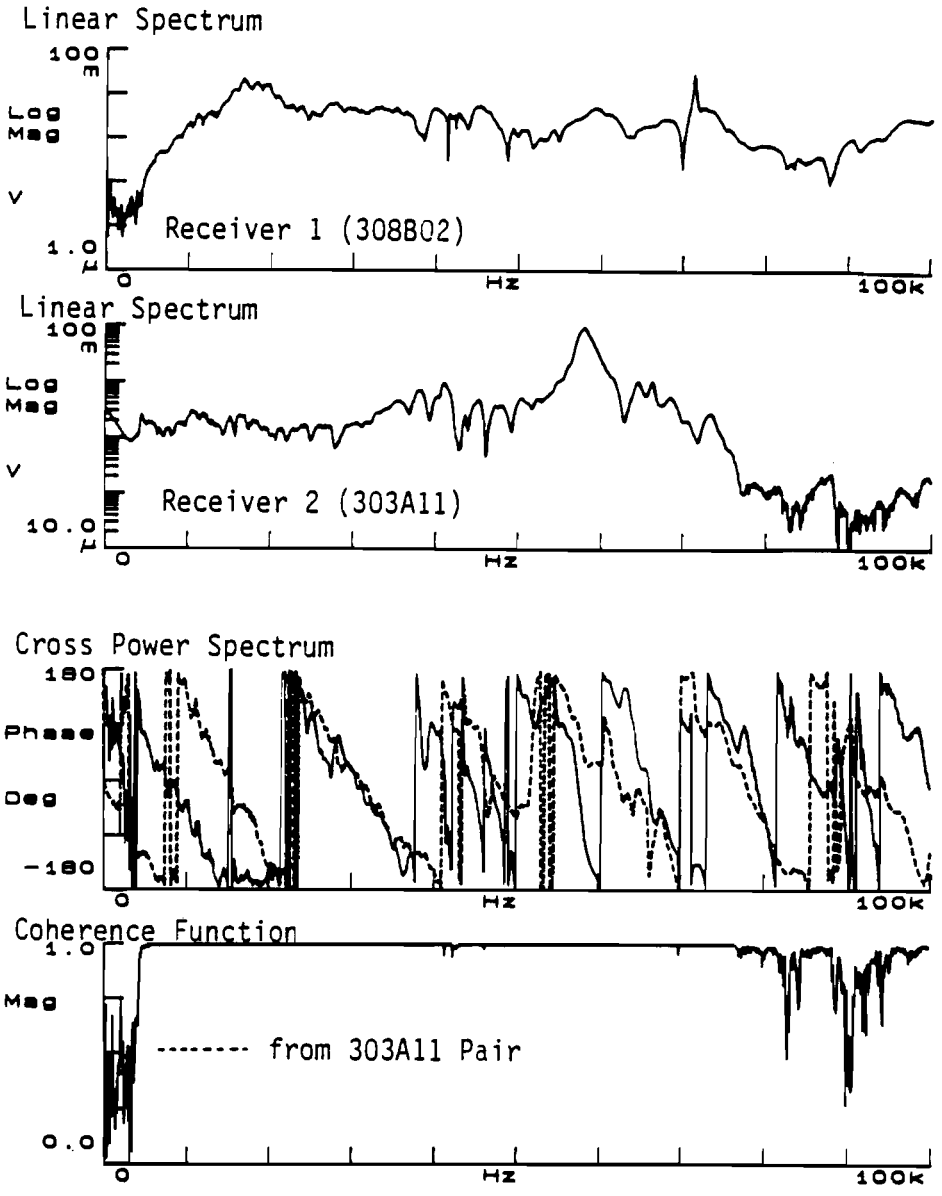

Fig. 7.23. Distortion in Phase of the Cross Power Spectrum Caused by Using Different Accelerometers: Model 308B02 Accelerometer is Receiver 1 and Model 303A11 Accelerometer is Receiver 2.

The resonant frequency of the model 308B02 accelerometers itself is about 30 KHz, and for model 303A11 itself is about 76 KHz. In Fig. 7.22 and 7.23, it is not clear if there is any error in phase caused by the resonant frequency of the model 303A11 in the neighborhood of 76 KHz due to the complex nature of the phases But at about 30 KHz where the resonant frequency for the model 308B02 itself is located, the phase of the cross power spectrum shows no sign of error in both figures.

As an aside, the second cycle between 2.5 and 5.2 KHz appearing in the phase of the cross power spectrum shown in Figs. 7.17 through 7.21 is a false cycle. The cause of this extra cycle is not fully understood but is thought to result from reflections. Also, there is an extra cycle in Figs. 7.21 through 7.23. It is known (by comparing to other tests) that the "theoretical" phase should have no second dip in the phase plot at around 40 to 52 KHz.

7.5.4. Reducing Adverse Impact of Unwanted Resonances

As shown in this study, the natural frequency of accelerometer itself has no effect on the phase of the cross power spectra and, hence, the dispersion curves. However, resonant frequencies of the coupled accelerometer-pavement surface system have a significant adverse impact on test results. It is strongly recommended to use a pair of the same model accelerometers as receivers in the SASW array. Also, the accelerometers should be attached to the ground surface by the same method so that their coupled response characteristics are the same. Even under these conditions, the phases of cross power spectra in the frequency range between the corresponding resonant frequencies are probably going to be in error and should be discarded. Coupled systems which exhibit uniform linear spectra provide the best phase information. Usually this implies that the system has significant damping which can be achieved by using accelerometers with small masses.

7.6. INFLUENCE OF INTERFACE BOND BETWEEN LAYERS ON DISPERSION CURVES

A strong bond at the interface between two layers is a critical factor for stress waves to be transmitted from one medium to the other. This bond is especially important for a low-amplitude (small strain) waves. Unless the interface is very tightly in contact, it will act as a barrier and very little energy will be transmitted. Assume a two-layer system with layer 1 on top of layer 2. The SASW test is performed on the surface of layer 1. As a result, there will be no energy transmission problem for layer 1, and the stiffness of this layer will be sampled properly.

However, to sample layer 2, it is necessary to transmit energy across the bond between layer 1 and layer 2. Under this circumstance, the interface bond becomes very important for energy transmission. The sampling of material properties in layer 2 hinges heavily upon the interface bond. In general, the interface works like a band filter. It will allow only energy in a certain frequency range to pass. As a result, the material properties in layer 2 can only be sampled by a few frequencies which represent certain depths. The sampling depth is controlled by the frequency of the energy transmitted. Experience indicates that the interface usually works like a low pass filter which allows only low frequency energy to be transmitted. In other words, only long wavelengths pass. As a result, it will only be possible to sample deeper materials in layer 2.

This phenomenon was observed in one set of SASW tests performed at the BRC facility on the movable slab (at location 1 shown in Fig. 3.2.) During construction of the movable slab, several thin plastic sheets were placed on top of the asphalt layer before the concrete was poured. These sheets were placed to ensure that no bond developed between these two layers. In addition, the slab has been moved back and forth by hydraulic rams several times after construction and before SASW testing. Hence, the bottom surface of this movable concrete slab is not bonded to the top surface of the underlying asphalt. As a result, the interface acts like an energy barrier and reduces the downward transmission of energy. At all other test locations,the concrete slab was cast-in-place. Therefore, the concrete is assumed to be bonded to the asphalt.

Dispersion curves obtained from tests on the movable slab are presented in Fig. 7.24. Comparison of these curves with those which were obtained from other test locations (say Fig. 7.25 for location 2) shows that the general trend in both dispersion curves is the same. However, dispersion curves for the movable slab contains no information in the wavelength range of 1 to 4 ft (30 to 122 cm) because of the filtering effect of the debonding between layers.

It is known that the effective sampling depth is proportional to wavelength. Short wavelengths sample material properties at shallow depths while longer wavelengths sample material properties at deeper depths. In the past before the inversion program was available, the practical method of translating the dispersion curve to the wave velocity profile was by dividing the wavelength by three. For example, a 3-ft (91-cm) wavelength wave was assumed to sample material at a depth of 1 ft (30 cm). In other words, the effective sampling depth of a 3-ft (91-cm) wavelength was 1 ft (30 cm). Although this method is very crude, the concept is on the right track.

In this manner, surface waves with wavelength less than 1 ft (30 cm) effectively sample only the concrete slab which is 10 in (25 cm) thick. Any surface waves with wavelengths in this

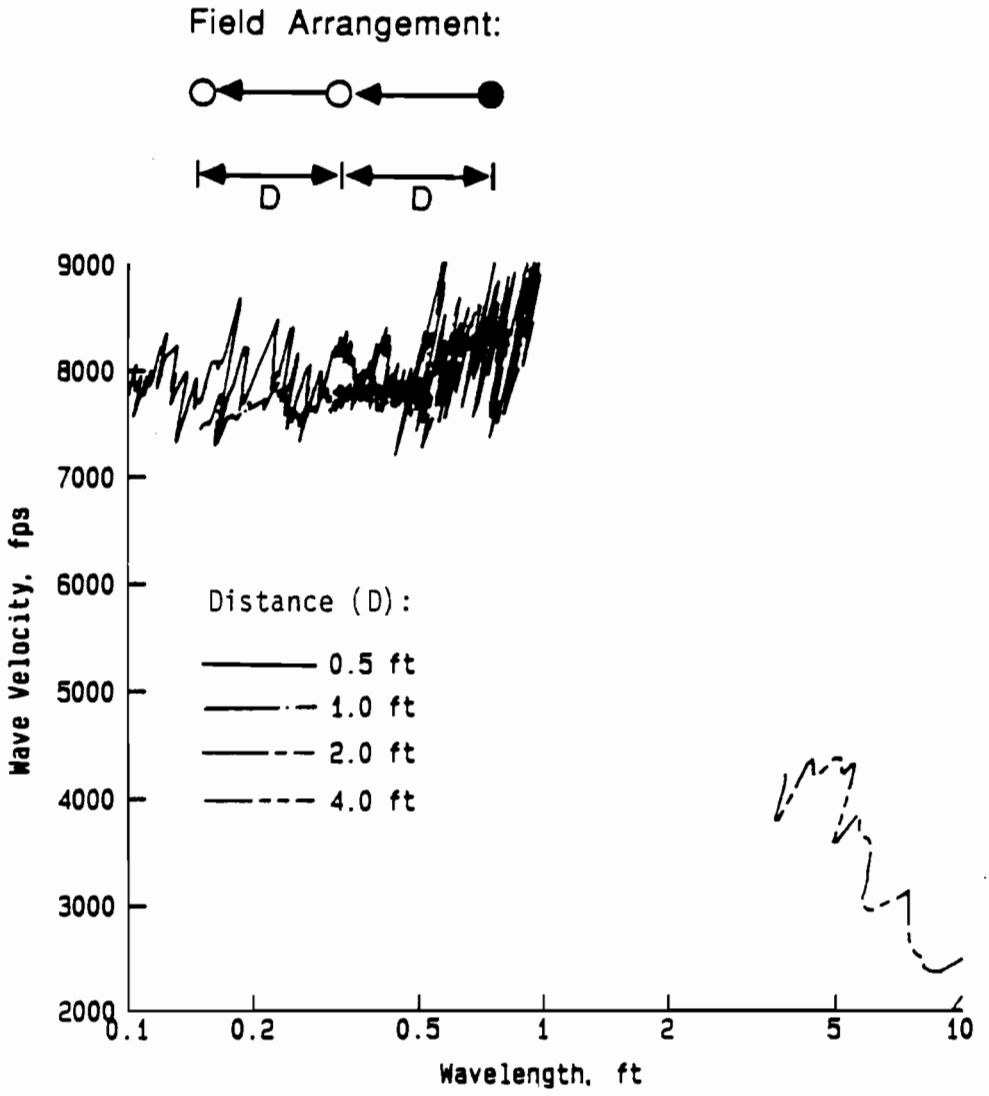

Fig. 7.24. Dispersion Curves for Typical SASW Tests Performed on the Movable Slab at Location 1.

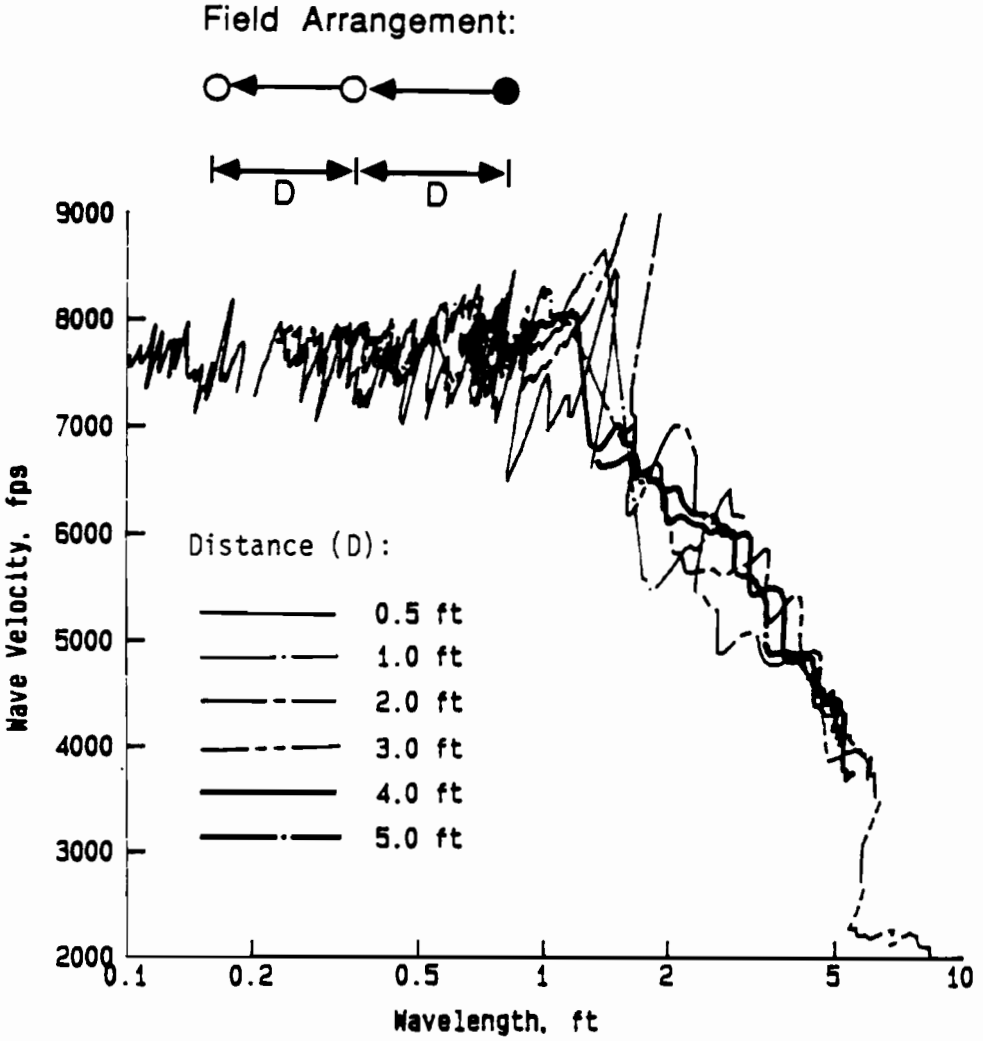

Fig. 7.25. Dispersion Curves for Typical SASW Tests Performed on Fixed Slab at Location 2.

range do not "feel" the existence of lower layers. Therefore, material properties of the upper concrete pavement are properly sampled on the movable slab. (see Fig. 7.24). As the wavelength gets longer, the effective sampling depth gets deeper, and the interface bond between the concrete and asphalt starts to play a role as a barrier and work like a low-pass frequency filter. Thus, only low-frequency waves penetrate the materials beneath the movable concrete slab. Material properties at deeper depths can still be sampled properly by low frequency waves. However, material properties at intermediate depths that correspond to 1-ft to 4-ft (30-cm to 122-cm) long wavelengths can not be sampled because too little energy is transmitted into the lower layer.

7.7. NEAR-FIELD EFFECT AND USEABLE RANGE OF WAVELENGTHS

The theoretical solution of the wave equation for a point source acting on the surface of a uniform medium contains both near-field and far-field terms. The far-field terms include P-waves, S-waves, and Rayleigh waves. The near-field terms include a complex coupling of P- and S-waves. Near-field terms die out much faster than far-field terms as the waves propagate away from the source, and their contribution is negligible once receivers are far enough from the source. However, a recent theoretical study by Sanchez-Salinero et al (1987) has shown that these near-field terms do have an appreciable adverse contribution when the receivers are very close to the source and can not be neglected. To make the complex wave equation reasonably simple to handle, near-field terms have been neglected in the inversion analysis of SASW test (Nazarian, 1984). Obviously, there is a region around the source where these near-field terms have a large enough contribution to cause a measurable error in the SASW results. This region is studied experimentally herein.

The theoretical study done on the near-field problem by Sanchez-Salinero et al, 1987 suggests that, as a rule of thumb, the contribution of near-field terms is negligibly small once the receivers are about one wavelength away from the source. In the past, each SASW test record was filtered in such a way that only data with wavelengths greater than one half of the receivers spacing and smaller than two, sometimes three, times the source-to-first-receiver distance were kept (see Chapter Two). For example, assume the source-to-first-receiver spacing is 2 ft (61 cm) and the receivers spacing is 1 ft (30 cm). Then wavelengths in the range of 0.5 ft (15 cm) (1.0/2.0) to 4 or 6 ft (122 or 183 cm) (2×2 or 3) are kept.

To study the validity of these rules experimentally, several field tests were designed and performed. Two sites were selected for this investigation, an asphalt site at location 7 and a concrete site at location 2 as shown in Fig. 3.1. Testing was conducted in the following manner.

1. A spacing between the two receivers was selected and was held constant.
2. While the spacing between receivers was held constant, the distance between the source and first receiver was varied.
3. After the set of tests in Step 2 was completed, another spacing between the two receivers was selected and the whole test procedure in Step 2 was repeated.

All spacings between the two receivers and all distances from the source to the first receiver are listed in Table 7.2. Field dispersion curves for these tests are shown in Figs. 7.26 through 7.28, with the receiver spacing a constant in each figure.

If the same rule of thumb from the study by Sanchez-Salinero et al is adopted, it should be expected that wave velocities corresponding to wavelengths longer than the source to receiver distance should bear some noticeable error due to contributions from near-field terms. For example, if the source to receiver distance is 1 ft (30 cm), any data corresponding to wavelengths greater than 1 ft (30 cm) are somewhat invalid. It is interesting to see that, at the asphalt site as shown in Fig. 7.26, there is no clear trend in the near-field effect. All dispersion curves are very close to each other in the short-wavelength range (shorter than about 1 ft (30 cm)) and longer-wavelength (longer than about 2 ft (61 cm)) range. In the medium-wavelength range (about 1 to 2 ft (30 to 61 cm), the curves scatter seriously, and the pattern can not be correlated with the source-to-first-receiver distance.

Test at the concrete site shown in Fig. 7.28 demonstrate similar results to those determined for the asphalt site. The one exception is the dispersion curve from the source-to-first-receiver spacing of 0.25 ft (7.6 cm) in which velocities are relatively low compared to other velocities. The scattering in the dispersion curves at the concrete site seems to be bigger than that observed for asphalt site, but still in a random pattern with no clear relationship with source-to-first-receiver distance. The fluctuations found in both Figs. 7.26 and 7.27 seem to be mainly caused by reflected waves as discussed in Chapters Four and Five.

The influence of the near-field effect is inconclusive in this study. It seems that there are other more important factors such as reflections that mask out the near-field effect. Unless a more accurate test method for determining the dispersion curves is employed, it does not seem necessary to consider the near-field problem. However, it is obvious that, physically, there is a limit for sampling depth, and this depth is a function of the distance between the source and receivers. To sample material stiffness at a certain depth, corresponding wavelengths have to be fully developed at that depth. Since the source used for most surface wave tests is an impact on the surface of the material being tested, it is impossible for the sampling wave to penetrate to any

TABLE 7.2. DISTANCES FROM SOURCE TO FIRST RECEIVER AND BETWEEN RECEIVERS FOR TESTS STUDYING THE NEAR-FIELD EFFECT

I. Asphalt Site (Location 7 in Fig. 3.2)

Distance from Source to Receiver 1 (ft)	Distance Between Two Receivers (ft)
0.25	0.25
0.50	0.25
1.00	0.25
2.00	0.25
0.25	1.00
0.73	1.00
0.50	1.00
1.00	1.00
1.50	1.00
2.00	1.00
3.00	1.00
4.00	1.00

II. Concrete Site (Location 2 in Fig. 3.2)

Distance from Source to Receiver 1 (ft)	Distance Between Two Receivers (ft)
0.25	1.00
0.50	1.00
1.00	1.00
1.50	1.00
2.00	1.00
3.00	1.00
4.00	1.00
5.00	1.00

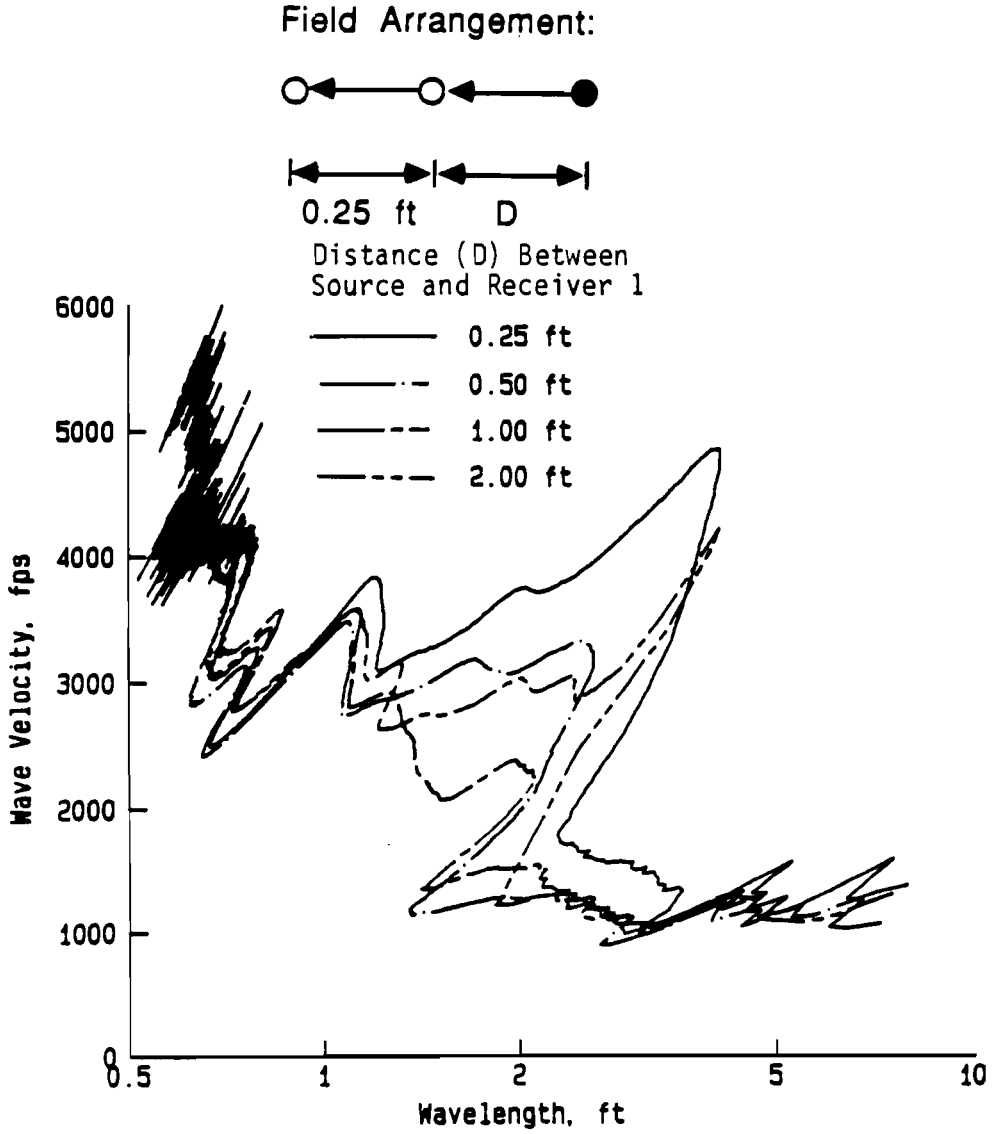

Fig. 7.26. Dispersion Curves for Asphalt Site: 0.25-ft Spacing Between Receivers and Varying Distances Between Source and Receiver 1.

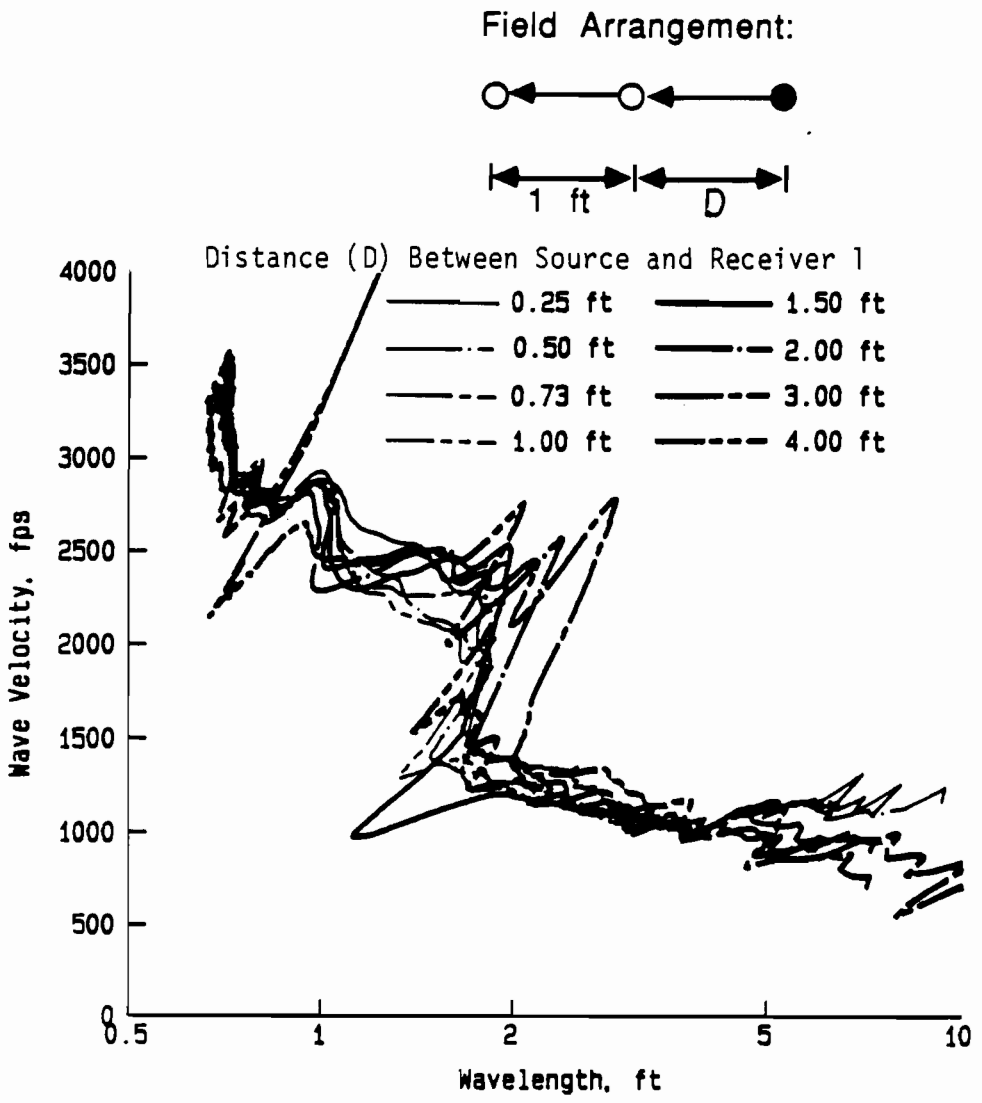

Fig. 7.27. Dispersion Curves for Asphalt Site: 1-ft Spacing Between Receivers and Varying Distances Between Source and Receiver 1.

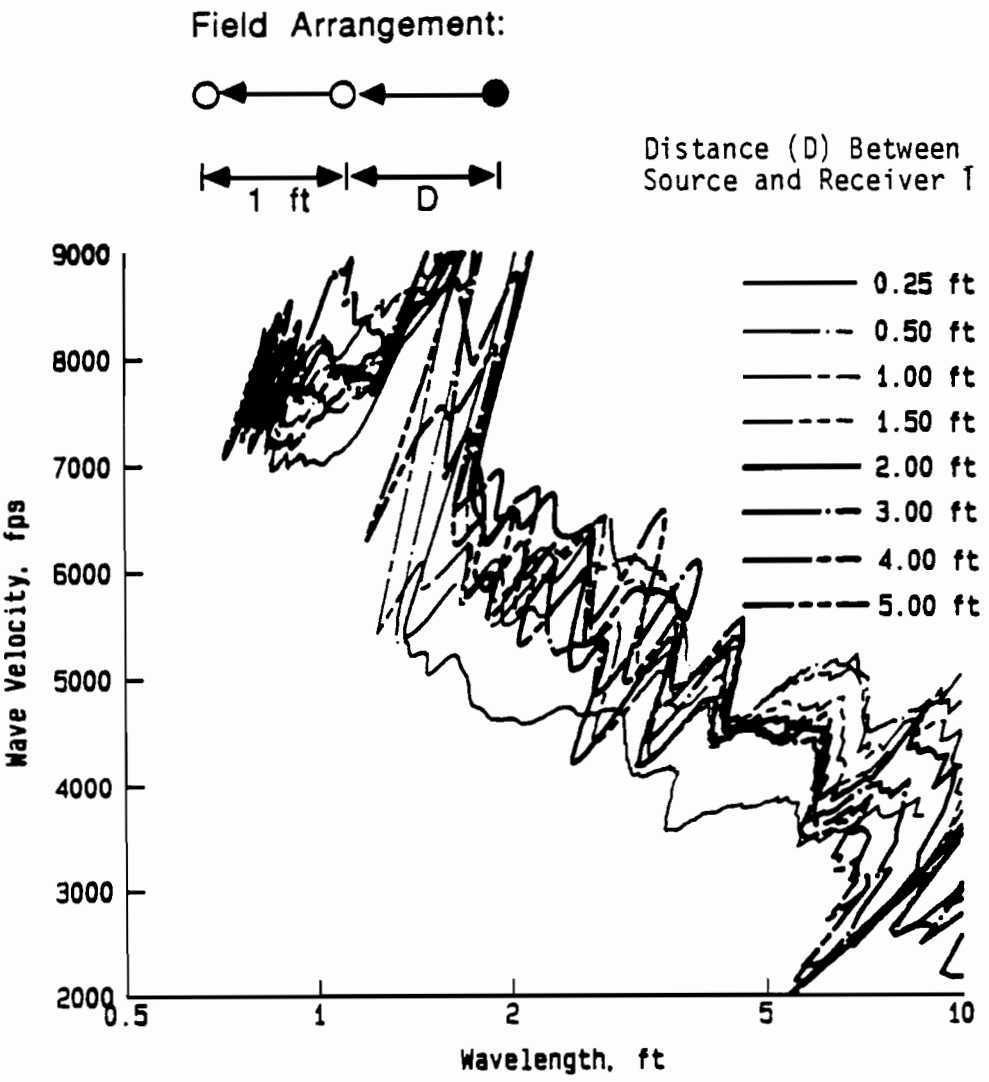

Fig. 7.28. Dispersion Curves for Concrete Site: 1-ft Spacing Between Receivers and Varying Distances Between Source and Receiver 1.

depth instantaneously. It takes time for the wave to propagate vertically as well as horizontally. Therefore, to sample deeper materials, the source has to not only be able to provide enough energy at the sampling wavelength but also has to be located far enough away from the receivers so that the sampling waves have enough time to fully develop. The question remains as to how far is far enough.

Some SASW tests were performed at the BRC facility before placement of the concrete or asphalt materials. These early tests were performed for the purpose of determining directly the properties of the supporting materials. An earth embankment was built on top of a dipping limestone. The embankment has an average height of about 8.5 ft (259 cm) before the pavements were placed. Field dispersion curves collected during this construction stage are presented in Figs. 7.29 and 7.30. Because the surface soil was desiccated, soil in the top few feet show relatively high velocities. The wave velocity then drops as wave length increases because of the softer soil underneath the desiccated soil. Wave velocity increases for wavelengths greater than about 10 ft (305 cm) because of the existence of the bedrock. By examining these dispersion curves, it is interesting to see that some dispersion curves exhibit a trend of increasing velocity as the sampling wavelength increases above about 10 ft (305 cm). There are others which do not "feel" the existence of the bedrock. More precisely, source-to-first-receiver spacings of 4 ft (122 cm) and greater "see" the bedrock in this particular case. This observation shows that the sampling depth (8.5 ft (259 cm) is about twice the distance (4 ft (122 cm)) between the source and the first receiver at this site. The wavelength corresponding to this depth (8.5 ft (259 cm)) is about 25 ft (762 cm)) (the depth of the bedrock, 8.5 ft (259 cm) multiplied by about 3, see Chapter Two), which is about six times the source-to-first-receiver spacing. The rule that has been followed in the past is two to three times of the source to receiver spacing and seems to be relatively conservative in this particular case but safe to be used.

This study also shows that there seems to be no lower limit on the usable wavelengths because dispersion curves developed for large spacings all show increasing wave velocities in the short-wavelength range indicating that they can "see" well at shallow depth too. Thus, as long as the field data can clearly be interpreted and the coherence function is good, data should be accepted.

7.8. SUMMARY

Factors such as the variability in time domain signals, impact stress level, methods for attaching accelerometers on the pavement surface, resonant frequencies of the coupled

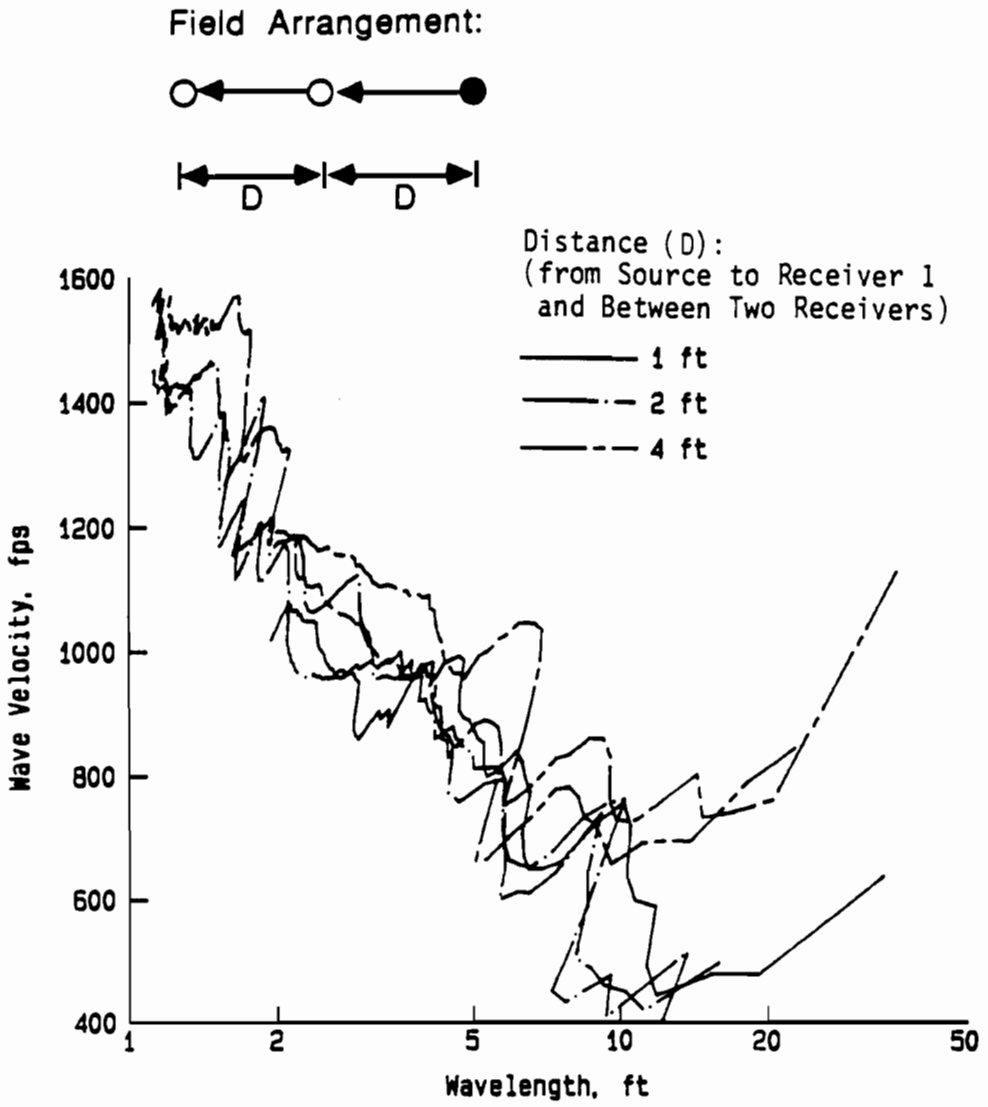

Fig. 7.29. Dispersion Curves from SASW Testing at the BRC Facility Before Placement of the Pavement Surface: 1-, 2-, and 4-ft Receiver Spacings.

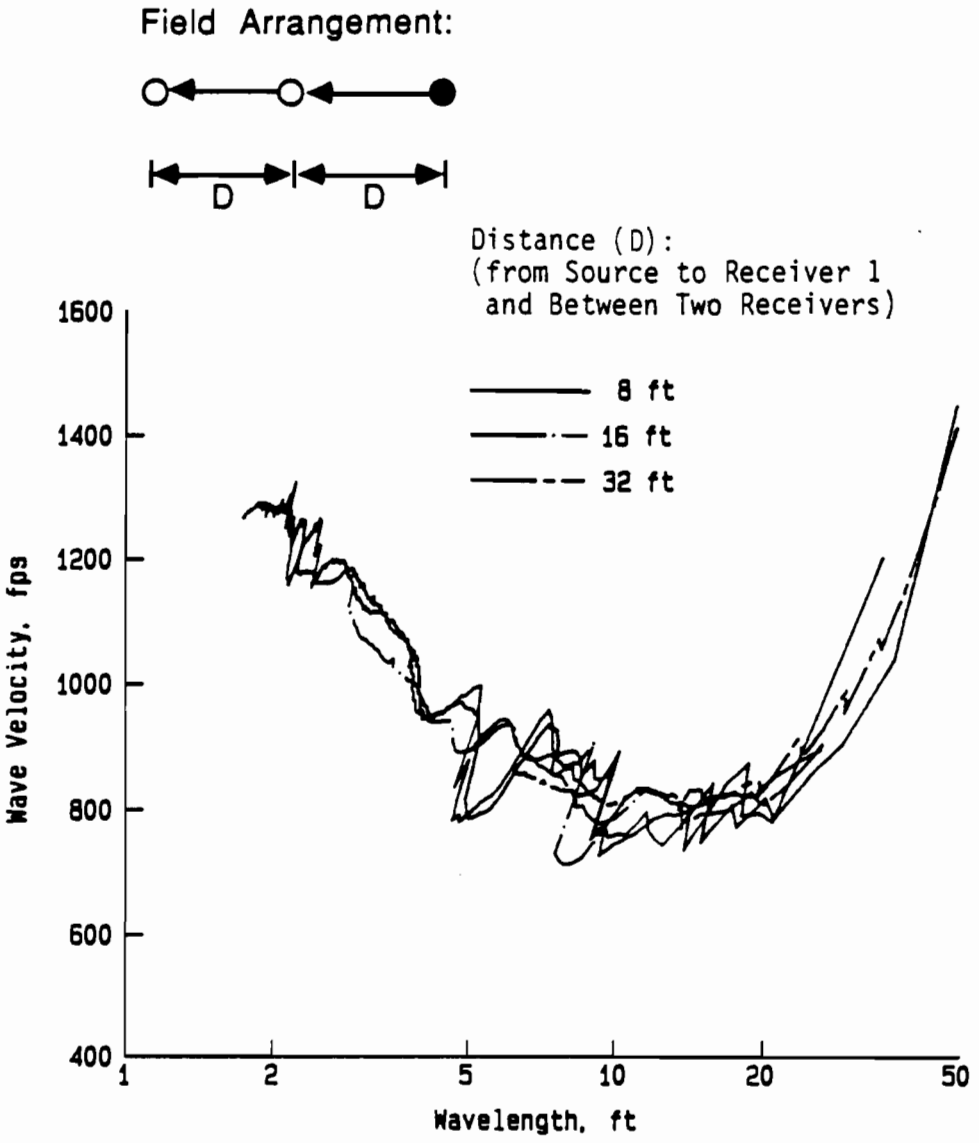

Fig. 7.30. Dispersion Curves from SASW Testing at the BRC Facility Before Placement of the Pavement Surface: 8-, 16-, and 32-ft Receiver Spacings.

accelerometer-pavement system, interface bond between pavement layers, and near-field effects which have been implicitly assumed to influence field dispersion curves are investigated experimentally. The studies show that phases of cross power spectra are essentially unaffected by factors such as the appearance of time domain signals and impact stress level. On the other hand, resonant frequencies of the coupled accelerometer-pavement system are very important and should not be overlooked. It is necessary to use a pair of the same type of receivers with the same method of attaching the receivers to the measuring surface to guarantee the correct measurement. The resonant frequency of the accelerometer itself, on the other hand, does not affect measurement of the field dispersion curves.

The near-field effect is found to be secondary to the effect of reflected waves discussed in Chapters Four and Five and is considered to be unimportant in most instances. However, a reasonable distance between the source and the first receiver should still be maintained. The studies show that in the case when the distance from source to receiver 1 is the same as the distance between the two receivers, wave velocities corresponding to three times this distance or less can be used.

CHAPTER EIGHT

HIGH-FREQUENCY MEASUREMENTS

8.1. INTRODUCTION

Two major goals have been pursued in the past with the SASW method. One is improving this method both theoretically and experimentally. The other is to explore new applications of the method. In this chapter, a new source, the "V" meter is presented. This source is capable of generating high-frequency energy (up to 100 KHz) which is very useful for near-surface profiling. In addition, these high frequencies present some new applications of the SASW method such as estimating maximum aggregate size as discussed in the chapter.

8.2. "V" METER AS A HIGH-FREQUENCY SOURCE

8.2.1. Need for a High-Frequency Source

In the past, one obstacle associated with application of the SASW method at pavement sites has been the lack of high-frequency energy generated from the hammer impact on the pavement surface. As a result, ambient and electronic noise became relatively large compared to the impact signals which reduced the quality of data in the high-frequency range below acceptable levels. For example, consider Figs. 7.1 through 7.5 and 7.6 for a concrete pavement tested with a 4-oz (114 gm) hammer as the impact source. The distance between receivers was 0.5 ft (15 cm) and the source was 0.5 ft (15 cm) away from the first receiver. The frequency domain data usually start to deteriorate at about 30 KHz. The quality of data for an asphalt pavement site with the same source/receiver arrangement usually start to deteriorate at lower frequencies (about 20 KHz). The lack of energy above these frequencies results from an impedance mismatch between the hammer and the pavement system as well as the inability to generate sharp impacts with the hammer.

To sample material properties in the near-surface region of the pavement (say within the top 2 in. (5 cm) for concrete and asphalt concrete pavements, high-frequency signals (say to 50 KHz or above) are essential due to the fact that the effective sampling depth is inversely proportional to sampling frequency. Surface waves with high frequencies sample shallow depths while surface waves with low frequencies sample deeper depths. A hammer, depending on its size and shape as well as the pavement system being tested, can usually generate only a narrow

band of energy with a high energy level. Our experience has shown that larger hammers (more than about 8 oz (228 gm)) tend to generate energy at the low-frequency end of the energy spectrum (say below 10 KHz) while smaller hammers (about 4 oz (114 gm)) tend to generate energy containing slightly higher frequencies (up to 20 to 30 KHz). However, small hammers can not be depended upon to always generate frequencies up to 30 KHz.

8.2.2. "V" Meter As A Source

In search of a better high-frequency source (consistent energy up to 50 KHz), many different sizes and shapes of hammers have been tried. Instead of impacting the pavement surface directly with the hammer, chisels and metal plates have also been used as media to transmit hammer impacts. However, generation of high-frequency energy by these methods has not been successful. The "V" meter was found accidentally to be a good impulsive source which generates high-frequency signals. "V" meters have been commonly used to measure compression wave velocities of ultrasonic pulses traveling in solid material such as concrete blocks. This velocity is the typically correlated with density and elastic properties of the solid materials.

The "V" meter has two transducers (one source and one receiver) which consist of ceramic piezoelectric elements made of lead zirconate titanate (PZT-4). The elements are mounted in stainless steel cases. These elements are very tightly held onto the inside face of the case to provide efficient acoustic transmission. Only the source transducer was used in this work. By using different transducers, a variety of output frequencies ranging from 20 KHz to 500 KHz can be generated. The "V" meter used in this study is a model C-4899 meter with a model C-4898 transducer made by James Electronics, Inc of Chicago, Illinois. This type of transducer has a central ultrasonic output frequency of 54 KHz. However, energy spectra up to 100 KHz were successfully generated.

8.2.3. Performance of "V" Meter

To compare test results from using a hammer and a "V" meter as sources, SASW tests were performed at the BRC facility. Test locations include all locations shown in Fig. 3.2. PCB model 308B02 accelerometers were used for monitoring pavement surface motion. Typical time records, auto power spectra, phases of cross power spectra, and coherence functions are presented in Fig. 8.1 for the concrete pavement and Fig. 8.2 for the asphalt pavement. Testing of the concrete pavement was performed at location 2 (shown in Fig. 3.2) using parallel array 6. The spacing between receivers was 0.5 ft (15 cm), and source was 0.5 ft (15 cm) away from

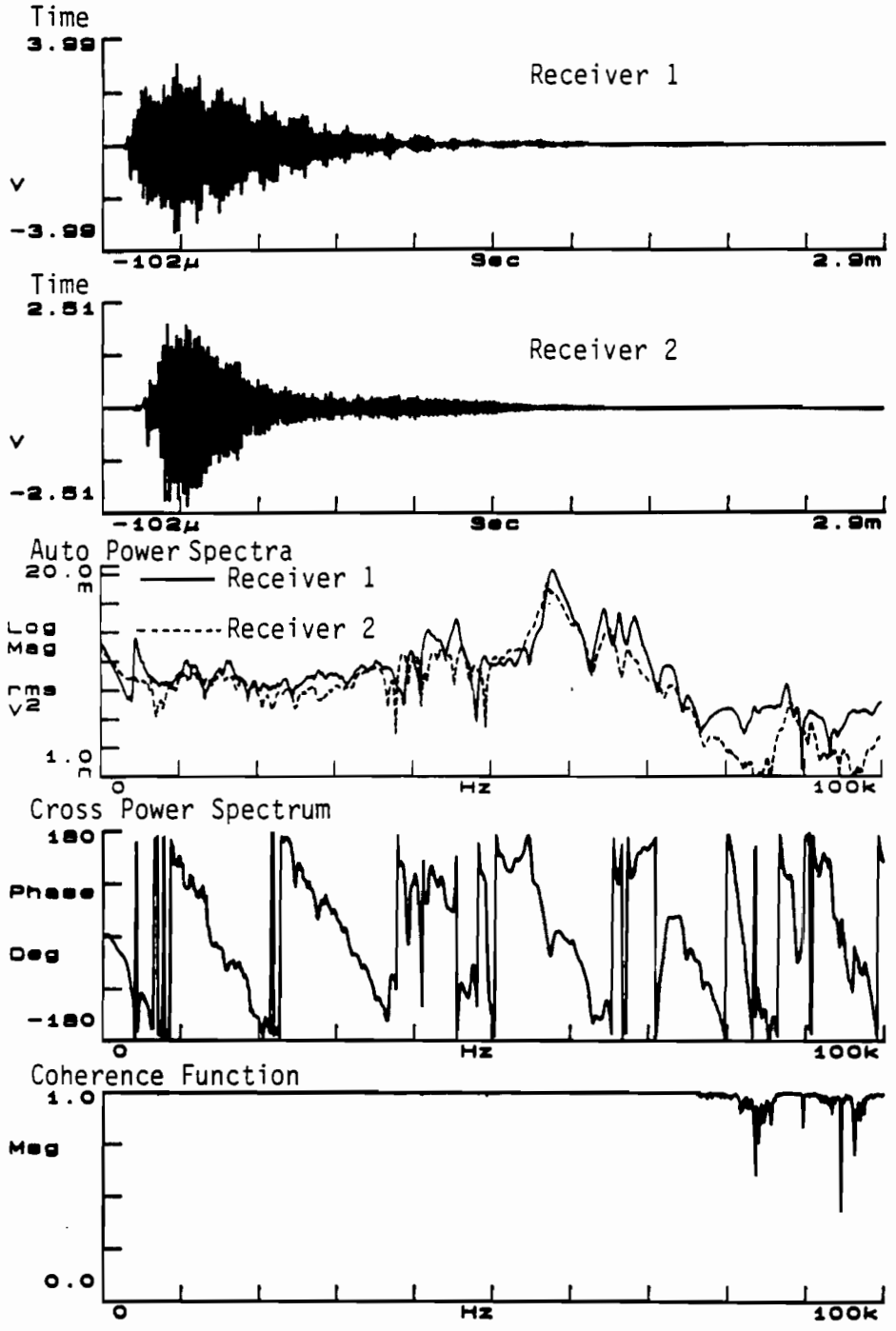

Fig. 8.1. Time Domain Signals and Corresponding Frequency Spectra from "V" Meter Source on Concrete Pavement.

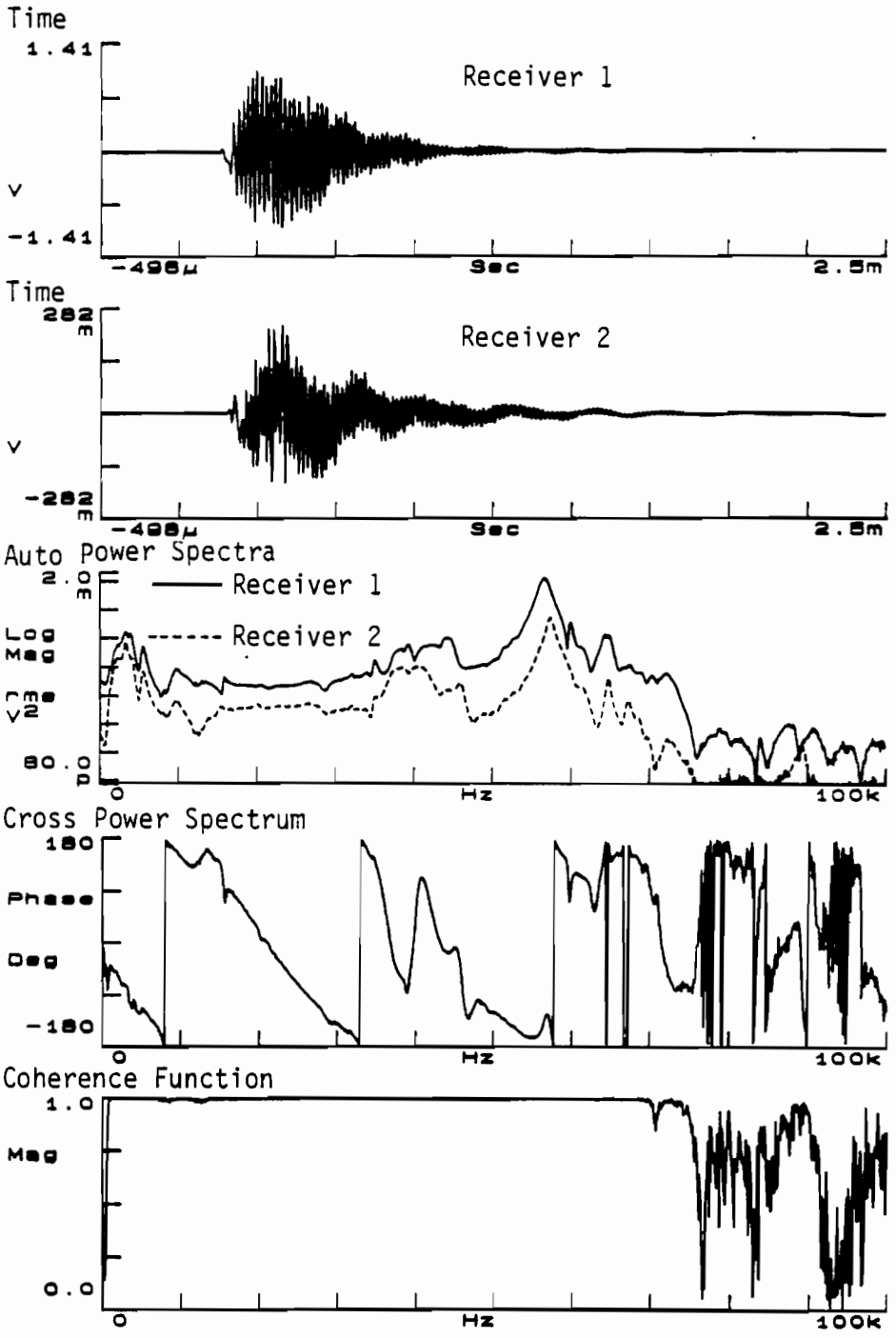

Fig. 8.2. Time Domain Signals and Corresponding Frequency Spectra from "V" Meter Source on Asphalt Pavement.

receiver 1. Testing of the asphalt pavement was performed (Fig. 8.2) at location 7 (shown in Fig. 3.2). The two receivers were 0.25 ft (7.6 cm) apart, and the source was 0.25 ft (7.6 cm) away from receiver 1 for the tests on asphalt.

The time records at both sites exhibit a lot of high frequency energy (Figs. 8.1 and 8.2). The auto power spectra in both figures show relatively good distribution of energy up to at least 75 KHz. At the concrete pavement (Fig. 8.1), the auto power spectrum of receiver 1 exhibits significant energy from 0 to about 75 KHz. The energy level then drops to a lower level over the rest of the spectrum. At receiver 2, the auto power spectrum shows an energy distribution similar to receiver 1 up to about 75 KHz. In the frequency range higher than 75 KHz, the auto power spectrum of receiver 2 shows some significant fluctuations. Whenever the energy level is low at receiver 2, the corresponding coherence function is low. Whenever the energy level is high at receiver 2, the corresponding coherence function is high. It seems that in the range of 0 to 75 KHz, damping which causes the energy level at receiver 2 to become significantly lower than the energy level at receiver 1 is quite uniform over these frequencies. But beyond 75 KHz, damping becomes selective at some frequencies but is generally increased.

The auto power spectra corresponding to receivers 1 and 2 for the asphalt pavement (Fig. 8.2) shows similar energy distribution up to about 75 KHz. Above 75 KHz, the energy level at receiver 1 seems to remain at a reasonable level, but the energy level at receiver 2 is very low. As a result, the coherence function for frequencies above 75 KHz is very low. The auto power spectra at the asphalt site indicate that damping at the asphalt site is much higher than at the concrete pavement. In addition, the two auto power spectra curves for the asphalt site are reasonably parallel to each other for frequencies less than 75 KHz. Since the spectra are plotted on a logarithmic scale, two parallel curves suggest that the ratios between the two curves are the same at all frequencies; that is, the amplitude of the auto power spectrum at receiver 1 is equal to the amplitude of the auto power spectrum at receiver 2 multiplied by a constant. As a result, this suggests that the damping factor (which lumps both geometrical damping and material damping together) seems to scale down the energy level at all frequencies with only one constant, and this constant does not change with respect to different energy levels (different amplitudes of velocity or acceleration). This finding provides a piece of valuable information for selecting A's (Eq. 3.11) in the modeling of the dispersion curves presented in Chapter Three.

At the concrete pavement (Fig. 8.1), the coherence function, which is an indication of the signal-to-noise ratio as well as an index of the quality of data collected, shows a value of almost 1.0 over the frequency span from zero to 80 KHz with the "V" meter as the source. This

coherence function is definitely better than any other coherence function generated with a hammer. The coherence function at the asphalt pavement site (Fig. 8.2) shows similar results except that it begins to degrade at about 75 KHz.

A comparison of dispersion curves for the concrete pavement (at location 3) acquired by using both hammer and "V" meter sources is presented in Fig. 8.3. PCB model 308B02 accelerometers were used as receivers. The spacing used between the two receivers was 1 ft (30 cm), and the source was 1 ft (30 cm) away from the first receiver. Both curves compare closely. (Similar results were found in other test locations.) The same experiment was performed for the asphalt pavement site (at location 7) except that the distances used for the source to receiver 1 and between the two receivers were 0.5 ft (15 cm). The comparison of dispersion curves for this asphalt site is shown in Fig. 8.4. Again, both dispersion curves follow each other closely. Notice that in Fig. 8.4, wavelengths in the dispersion curve with the "V" meter source are as short as about 0.08 ft (2.44 cm) while the curve for the hammer source has wavelengths no shorter than about 0.1 ft (3 cm). Although the difference is small, this example illustrates that the "V" meter is capable of sampling shallower depths than a hammer source. According to the writers' experience, the "V" meter usually delivers nearly the same dispersion curve as the hammer at a concrete pavement site, but the "V" meter is often capable of sampling shallower depths than the hammer at an asphalt pavement site. In addition, with the better signal-to-noise ratio as indicated by the coherence functions, the "V" meter should, theoretically, give more representative dispersion curves than a simple hammer since the signal-to-noise ratio is higher.

8.2.4. Additional Advantages and Drawbacks of "V" Meter

In addition to a relatively high energy output over a wide range of frequencies, the "V" meter also delivers very consistent energy levels which is a very desirable characteristic. To make accurate time domain measurements, the dynamic range of the spectral analyzer and the input energy level have to be compatible. For example, a 0.5-volt peak signal will be better measured by the analyzer set with a one-volt dynamic range rather than a 10-volt dynamic range because the accuracy of the measurement for the former will be several times better than for the higher sensitivity setting. Ideally, when a test is being performed, the dynamic range of the analyzer should be set to the lowest possible range but yet be large enough to avoid input overflow.

Control of the output energy level of a hammer swung by hand is virtually impossible even for an experienced operator. Sometimes the impact is too strong. Sometimes the impact is too soft. Hence, a compatible dynamic range of the analyzer is difficult to set. To cope with such

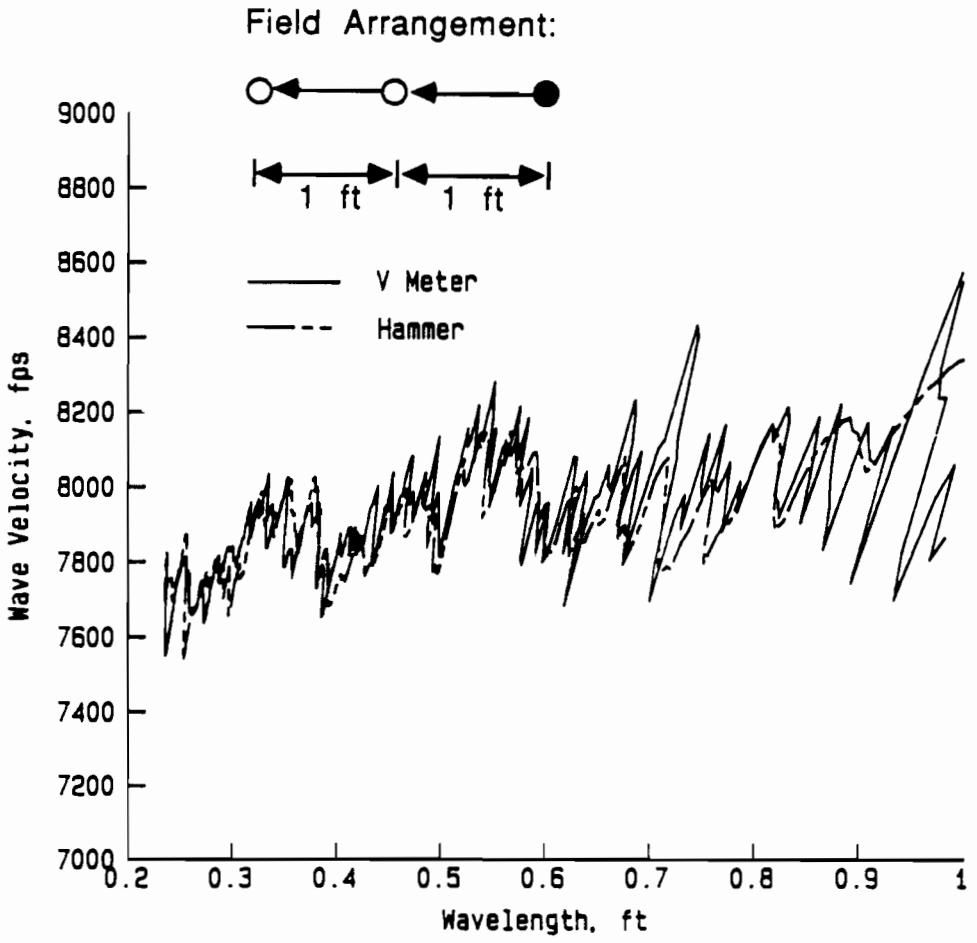

Fig. 8.3. Comparison of Dispersion Curves for Concrete Pavement from Hammer and "V" Meter Sources.

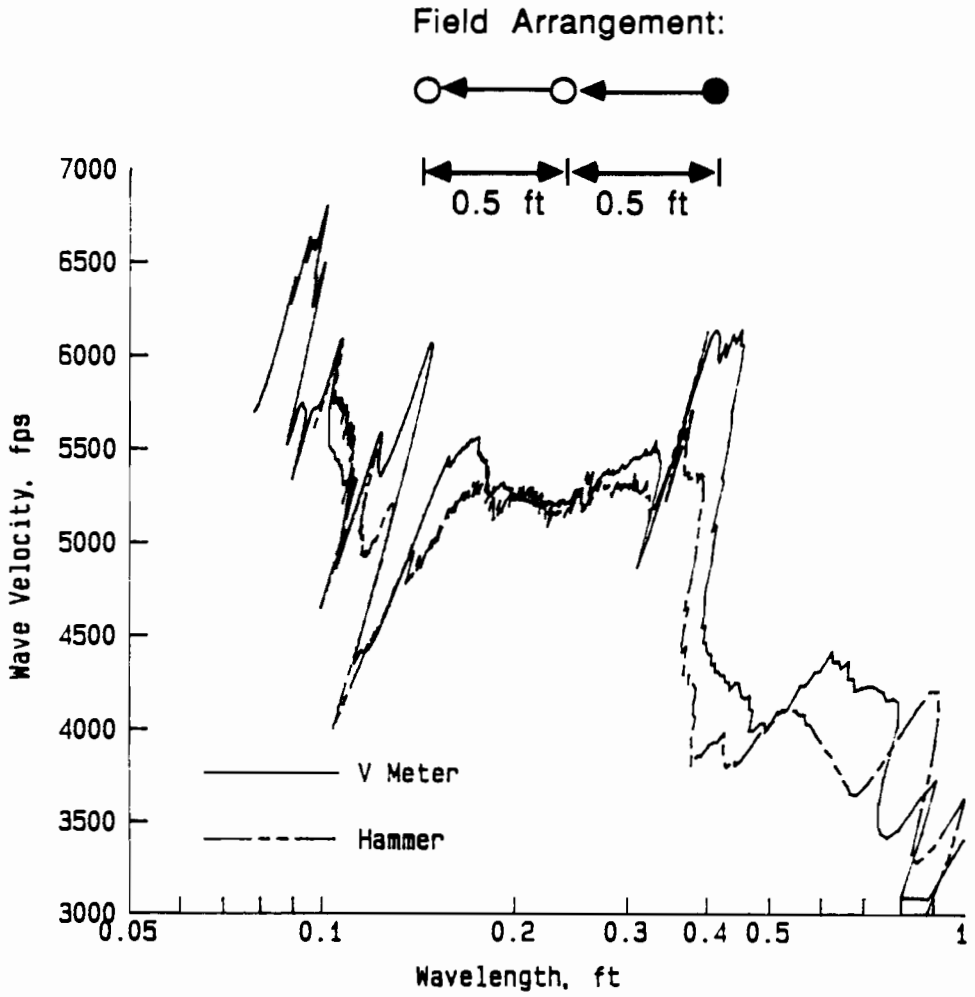

Fig. 8.4. Comparison of Dispersion Curves for Asphalt Pavement from Hammer and "V" Meter Sources.

a variety of energy levels, a relatively large dynamic range is usually selected with some sacrifice in measurement resolution. Since the output energy level from a "V" meter is relatively stable, it is very easy to have an optimum combination of the dynamic range of the analyzer and the energy level of the signal. In addition, the "V" meter is very easy to operate and could be one possible source in automation of the SASW method.

There are also several drawbacks with the use of the "V" meter. First, because the output energy level from a "V" meter is fixed, the distance between the source and receivers is limited to about 1.5 ft (46 cm). As the spacing between the source and receivers increases beyond this limit, low-quality data can be expected at both the high- and low-frequency ranges of the spectrum. This problem is illustrated in Fig. 8.5. Data from a test performed on the concrete pavement at location 2 (array 6) are shown in the figure. The spacing between the two receivers was 2 ft (61 cm), and source was 2 ft (61 cm) away from receiver 1. The quality of the phase of the cross power spectrum is very low as indicated by the corresponding low coherence function. Unless a more powerful "V" meter can be made, its application will be restricted to only shallow sampling depths.

To have good transmission of energy from the "V" meter into the pavement, especially in the high frequency range, a thin layer of silicon grease has to be applied between the piezoelectric transducer of the "V" meter and the surface of the pavement. If this is not done, much less energy is transmitted into the pavement system which further reduces the useful source-to-receiver distance and restricts the sampling depth. The extra work of applying the silicon grease may reduce the efficiency of the field work and should be considered as one of the drawbacks.

8.3. REPEATABILITY OF SASW TEST

All tests presented in this chapter and previous chapters were performed over a period of more than one year. By closely examining all records acquired, the surface wave velocity of the concrete pavement is always about 7800 fps. It is apparent that even though these tests were performed at different times, the dispersion curves are very consistent. The implications are that the properties of the concrete pavement did not change much in a period of one year and the SASW test is very repeatable and can be preformed on a regular basis without concern for instability in the test results. The SASW test is also quite fool proof, and very few things can go wrong if well-trained field personnel perform the test.

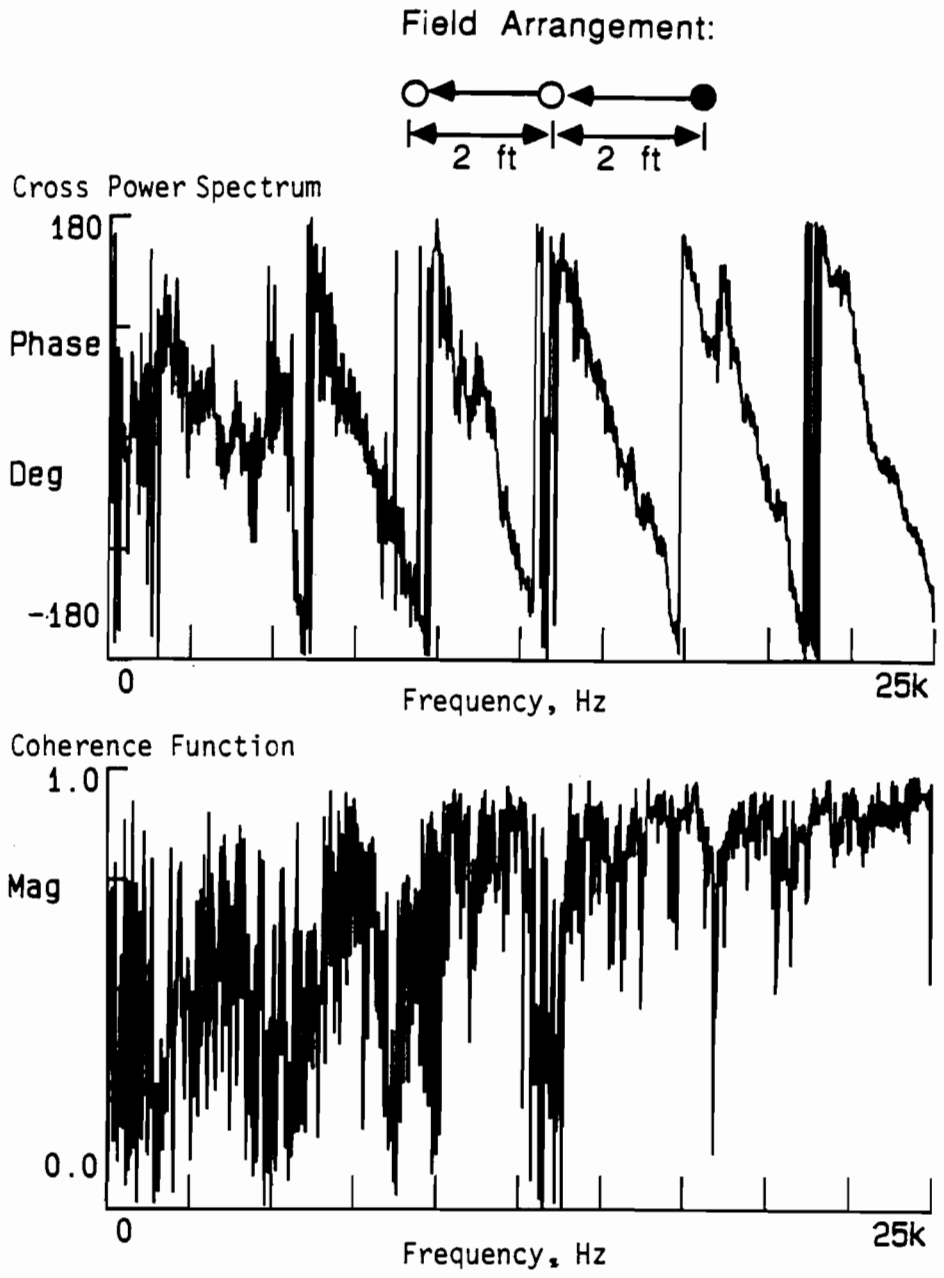

Fig. 8.5. Deteriorated Phase of the Cross Power Spectrum and Coherence Function on a Concrete Pavement Caused by a Large Spacing Between the "V" Meter and Receivers.

8.4. VARIABILITY OF CONCRETE STIFFNESS IN THE CONCRETE SLAB

Four trucks loads of concrete were poured to form the concrete pavement slab at the Balcones Research Center facility. The locations of concrete poured from each truck are shown in Fig. 8.6. The SASW test records at different locations have shown no velocities differences between these different pours. A composite plot of test results at locations 1, 2, 3, and 5 (shown in Fig. 3.1) is shown in Fig. 8.7. It is interesting to see that all dispersion curves are confined to a very narrow band in the wavelength range from 0.2 to 0.5 ft (6 to 15 cm). The small scatter in Fig. 8.7 suggests that the properties of the concrete used to build the concrete slab are very consistent and stable.

8.5. "QUICK AND EASY" METHOD TO ESTIMATE THE STIFFNESS OF THE PAVEMENT SURFACE LAYER

These studies at the concrete pavement have shown that wave velocity near the surface (in the top layer) is very consistent from one test to another and is hardly affected by reflections or improper bonding between the top layer and the second layer. Wave velocity in the pavement surface layer can be used to estimate Young's modulus of this layer quickly and easily in the field without complex computations (without inversion). The procedure is presented in Table 8.1 and is described as follows. Once the SASW test is performed, plot the dispersion curves so that the zone of constant apparent Rayleigh wave velocity can be determined The velocity ratio between Rayleigh and shear waves is a function of Poisson's ratio as given in Table 8.2. Values of Poisson's ratios used in the past have been 0.15 for concrete and 0.2 to 0.35 for asphalt. The accuracy of Poisson's ratio is rather unimportant because the wave velocity ratio only ranges from 0.87 to 0.96 for Poisson's ratio varying from 0.0 to 0.5, respectively. Therefore, a 10 percent error in the estimation of Poisson's ratio will cause only about a 0.6 percent error in estimation of the wave velocity ratio. Assume the unit weight of the concrete or asphalt is known, the shear modulus can then be calculated by:

$$G = \gamma V_S^2 / g \tag{8.1}$$

where

G = shear modulus,
V_S = shear wave velocity,
g = gravitational acceleration, and
γ = unit weight of tested material.

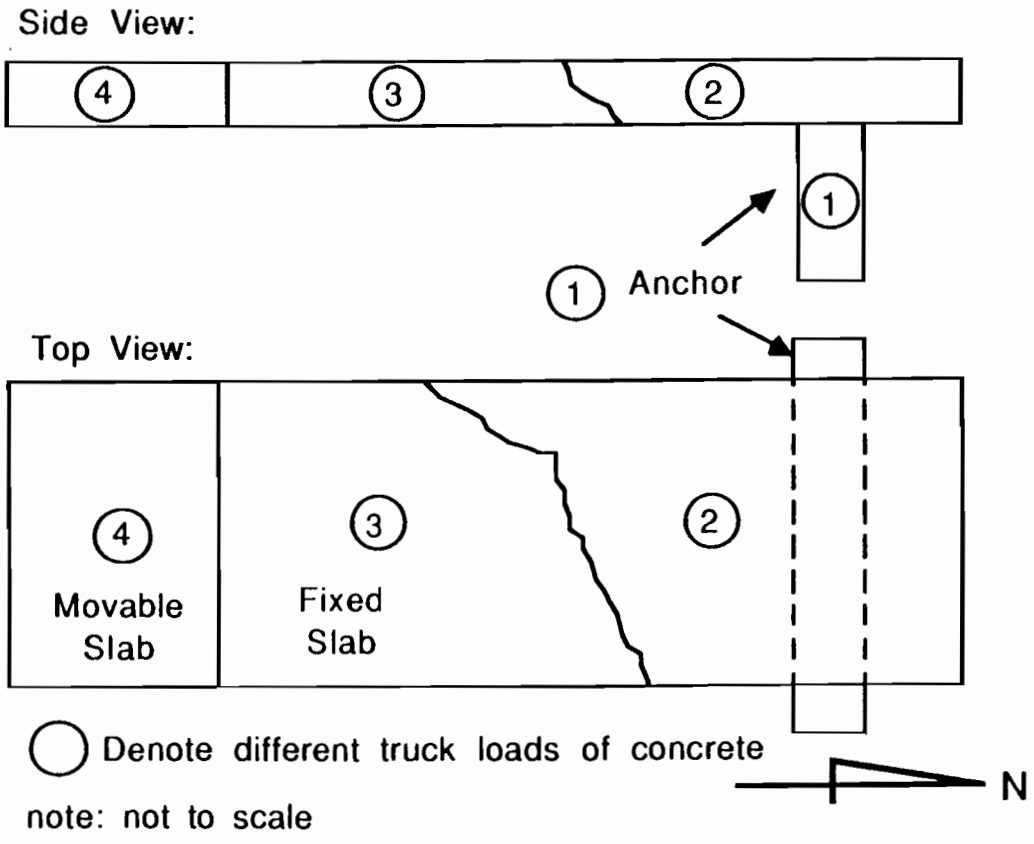

Fig. 8.6. Locations of Different Truck Loads of Concrete Used to Construct Pavement at BRC.

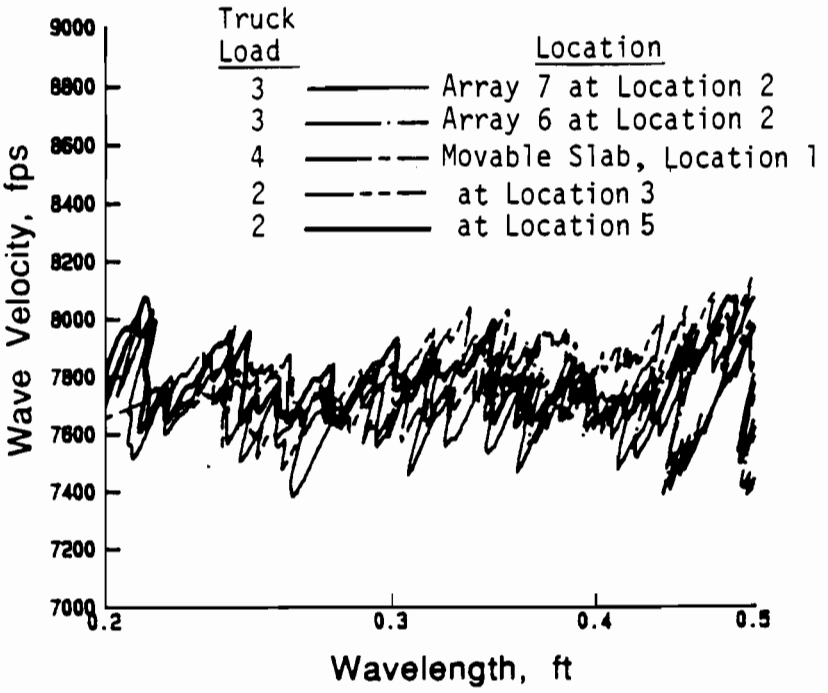

1.) From figure above, average $V_R = 7800$ ft/s.

2.) From theory of elasticity, $G = \rho V_S^2$,
$E = 2 (1 + \nu) G$, and
$E = 2 (1 + \nu) \gamma/g \ V_S^2$.

3.) For concrete, assume $\nu = 0.15$. Then $V_R = 0.9 V_S$.

4.) For concrete, assume $\gamma = 145$ lb/ft^3.

5.) The average value for the modulus of elasticity is:
$E = 5.6 \times 10^6$ psi.

Fig. 8.7. Variability in Concrete Stiffness at the BRC Facility.

TABLE 8.1. "QUICK AND EASY" METHOD FOR ACCESSING STIFFNESS OF THE TOP PAVEMENT LAYER

1. Select V_R from the field dispersion curve.

   $V_R = 7800$ ft/s (from Fig. 8.7)

2. Assume a value for Poisson's ratio.

   For concrete, $\nu = 0.15$.

3. Convert Rayleigh wave velocity to shear wave velocity.

   $V_R = 0.9\ V_S$

4. Assume a value for total unit weight.

   $\gamma = 145$ lb /ft^3

5. Calculate Young's modulus.

$$E = 2\,(1 + \nu)\,\frac{\gamma}{g}\,V_S^2$$

$$E = 5.6 \times 10^6 \text{ psi}$$

TABLE 8.2. RELATIONSHIP BETWEEN POISSON'S RATIO AND WAVE VELOCITY RATIO (V_R/V_S)

ν	V_R/V_S	ν	V_R/V_S
0.000	0.87403204889764	0.250	0.91940168676197
0.005	0.87500823020012	0.255	0.92022088242781
0.010	0.87598234472110	0.260	0.92103610350940
0.015	0.87695434116323	0.265	0.92184733117961
0.020	0.87792416847091	0.270	0.92265454747962
0.025	0.87889177585159	0.275	0.92345773531732
0.030	0.87985711279695	0.280	0.92425687846522
0.035	0.88082012910407	0.285	0.92505196155770
0.040	0.88178077489649	0.290	0.92584297008779
0.045	0.88273900064514	0.295	0.92662989040339
0.050	0.88369475718921	0.300	0.92741270970294
0.055	0.88464799575676	0.305	0.92819141603062
0.060	0.88559866798522	0.310	0.92896599827104
0.065	0.88654672594170	0.315	0.92973644614344
0.070	0.88749212214297	0.320	0.93050275019542
0.075	0.88843480957536	0.325	0.93126490179623
0.080	0.88937474171418	0.330	0.93202289312962
0.085	0.89031187254305	0.335	0.93277671718623
0.090	0.89124615657276	0.340	0.93352636775566
0.095	0.89217754885987	0.345	0.93427183941802
0.100	0.89310600502494	0.350	0.93501312753524
0.105	0.89403148127036	0.355	0.93575022824193
0.110	0.89495393439781	0.360	0.93648313843591
0.115	0.89587332182527	0.365	0.93721185576847
0.120	0.89678960160360	0.370	0.93793637863424
0.125	0.89770273243269	0.375	0.93865670616083
0.130	0.89861267367713	0.380	0.93937283819817
0.135	0.89951938538135	0.385	0.94008477530757
0.140	0.90042282828429	0.390	0.94079251875060
0.145	0.90132296383358	0.395	0.94149607047765
0.150	0.90221975419908	0.400	0.94219543311638
0.155	0.90311316228602	0.405	0.94289060995990
0.160	0.90400315174745	0.410	0.94358160495480
0.165	0.90488968699619	0.415	0.94426842268903
0.170	0.90577273321615	0.420	0.94495106837961
0.175	0.90665225637314	0.425	0.94562954786022
0.180	0.90752822322498	0.430	0.94630386756867
0.185	0.90840060133105	0.435	0.94697403453428
0.190	0.90926935906124	0.440	0.94764005636516
0.195	0.91013446560427	0.445	0.94830194123541
0.200	0.91099589097535	0.450	0.94895969787227
0.205	0.91185360602325	0.455	0.94961333554325
0.210	0.91270758243674	0.460	0.95026286404316
0.215	0.91355779275039	0.465	0.95090829368119
0.220	0.91440421034969	0.470	0.95154963526797
0.225	0.91524680947564	0.475	0.95218690010256
0.230	0.91608556522861	0.480	0.95282009995958
0.235	0.91692045357162	0.485	0.95344924707623
0.240	0.91775145133298	0.490	0.95407435413950
0.245	0.91857853620831	0.495	0.95469543427329
		0.500	0.95531250102563

The shear modulus, G, is converted to Young's modulus, E, by:

$$E = 2G(1+\nu) \tag{8.2}$$

This estimating process is easy and fast to perform and can readily be performed in the field with just a hand calculator.

8.6. POSSIBLE METHOD OF ESTIMATING MAXIMUM AGGREGATE SIZE

Either concrete or asphalt concrete is composed of aggregate with a wide range of sizes. Concrete or asphalt concrete can be considered homogeneous only when the aggregate size is relatively small compared to the wavelength used in SASW testing. In other words, the material being tested can not be considered homogeneous if the aggregate size is as big or bigger than the sampling wavelength.

It is known that wavelength is inversely proportional to frequency. When the frequency increases, wavelength decreases. As a result, there will be some cut-off frequency beyond which the corresponding wavelength is no longer "relatively large" compared to the aggregate size. For those (short) wavelengths, the material can no longer be considered homogeneous. It is difficult to imagine exactly what may happen in performing the SASW test when the system can no longer be classified as a homogeneous continuum, but an unrecognizable phase of the cross power spectrum and a low coherence function are expected.

By examining Figs. 8.1 and 8.2, the expected trends seem to exist. There is a cut-off frequency in both cases beyond which meaningful data can not be obtained. This cut-off frequency is about 80 KHz for the concrete pavement and about 75 KHz for the asphalt pavement. The cut-off frequencies correspond to about a 1-in. (2.54-cm) wavelength in the concrete pavement and also about a 1-in. (2.54-cm) wavelength in the asphalt pavement. According to the field inspector, aggregate size used for the concrete slab is mostly less than 1 in. (2.54 cm), with a maximum size of about 1.2 in. (3 cm). The maximum aggregate size for the asphalt pavement is less than 1 in. (2.54 cm). It appears that the shortest sampling wavelength is nearly similar to the maximum aggregate size. However, the energy level of the auto power spectra beyond these cut-off frequencies seem to be rather low even at receiver 1. Therefore, it is also possible that the "V" meter was unable to generate enough energy beyond these cut-off frequencies which complicates this matter. As such, this conclusion is tentative and more detailed investigations need to be done to further verify this point. However, this study provides a

possible nondestructive method of determining the maximum aggregate size used in both concrete and asphalt pavements.

8.7. SUMMARY

Use of the "V" meter as a high-frequency source was studied. It was found that the "V" meter provides very good signals in the high-frequency range, frequencies from 30 to 100 KHz. With a high-frequency source like the "V" meter, a quick and easy method of accessing material stiffness in the top pavement layer was developed. This method is shown to be useful and easy to apply. Another possible application of the SASW method at high frequencies is accessing the maximum aggregate size in an asphalt or concrete pavement. However, this application is somewhat crude and further studies are necessary.

CHAPTER NINE

APPLICATIONS OF SASW METHOD

9.1. INTRODUCTION

Intensive research on the SASW method has been conducted for the past few years at The University of Texas. Improvements in the method have been made in theoretical and experimental aspects. Most applications of the method have been at existing pavement sites and at soil sites. Two other types of applications are presented in this chapter. The first is use of the SASW method at the BRC facility which was constructed under carefully controlled conditions. The second application is use of the SASW method in observing the curing process of concrete. Two other applications have already been presented in Chapter Eight, quick stiffness measurements of the pavement surface layer and estimation of maximum aggregate size in the pavement surface layer.

9.2. STIFFNESS PROFILING AT THE RIGID PAVEMENT TEST FACILITY

Construction of the BRC facility (White et al, 1984) was based on the need for a fully instrumented concrete pavement test facility with which nondestructive testing equipment and methods such as the SASW , Dynaflect, and Falling Weight Deflectometer could be evaluated. The material profile at the test facility is shown in Fig. 9.1. The soil profile at the facility location before construction consisted of about 3 ft (91 cm) of natural soil (organic clay) underlaid by a thick strata of bedrock (limestone).

The facility was constructed in the following manner. The top 6 in. (15 cm) of natural soil was removed prior to placement of the embankment. This soil layer was mostly organic soil. Seven ft (213 cm) of embankment was then placed using readily available clayey fill from a nearby source at BRC. The natural soil surface at the site dipped slightly. Consequently, the actual height of the fill was varied to keep the top surface of the embankment level. (The variation in height of the fill causes the vertical distance between the surface of the embankment and the top of bedrock to vary at different locations which added some difficulty in SASW data interpretation.) The fill was placed and compacted in layers. The first 5 ft (152 cm) was compacted with a sheeps-foot roller. The last 2 ft (61 cm) was compacted by rolling with vehicular traffic. A 6-in. (15 cm) layer of crushed stone was then placed on top of the compacted

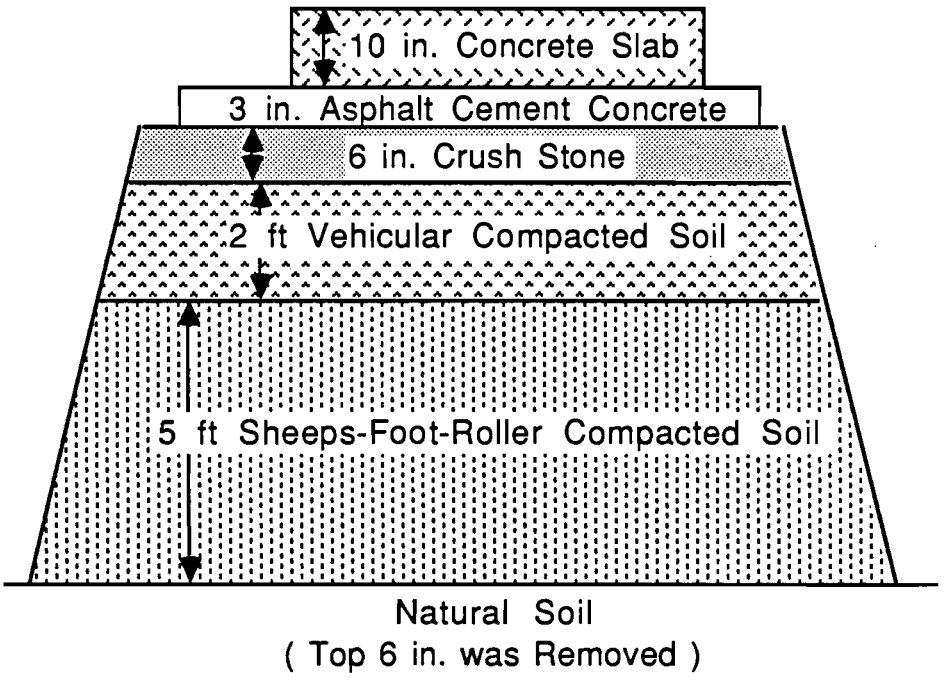

Fig. 9.1 Material Profile at the BRC Pavement Facility.

soil and compacted as the base. On top of this base, 3 in. (7.6 cm) of asphalt cement concrete was placed after which a 10-in. (25 cm) thick concrete slab was cast.

SASW tests were performed at various stages during construction to determine the stiffness profiles. One set of SASW tests was performed on February 12, 1984 when 2 ft (61 cm) of fill was placed. The locations of the SASW tests are shown in Fig. 9.2. Field dispersion curves, layering used for inversion, and inverted shear wave velocity profiles are shown in Figs. 9.3 and 9.4 for sites 1 and 2, respectively. Tabulated values including Young's moduli for sites 1 and 2 are listed in Tables 9.1 and 9.2. Note that the field dispersion curves shown in these figures are filtered dispersion curves. All low-quality data have been removed, and the data have been averaged. Also note that the scale used in the wavelength axis is three times as large as the scale used on the depth axis of the material profile. Before the inversion process was developed at The University of Texas, practicing engineers usually divided the wavelength axis by 3 to obtain the wave velocity profile. By comparing the field dispersion curve and the shear wave velocity profile from the inversion process, one can see that a reasonable estimate of the shear wave velocity profile can be acquired by dividing the wavelength axis by 3 in this case, although some error is introduced in the region where the change in shear wave velocity is quite significant (at a depth of about 7 ft (2 m)).

Dispersion curves from both sites are very similar. Consequently, the shear wave velocity profiles after inversion are very similar as shown in the figures. It seems that the soil properties are quite uniform at this site except that the bedrock surface dips somewhat which makes the top soil layer thinner at site 1 than at site 2. According to the SASW tests, stiffness profiles at these two sites indicate a 1-ft (30-cm) thick softer soil layer underlain by a 1-ft (30-cm) thick layer of relatively stiff compacted soil. Under the two layers is a 4-ft (2-m) thick layer of softer natural soil underlain by limestone. Although the thickness of the natural soil seems to be somewhat thicker than was stated earlier (3 ft (91 cm)), the profile still seems correct because of the inclined natural ground surface.

Another set of tests on the embankment was performed on August 12, 1984. At that time, the embankment was completed, and only the asphalt cement concrete and concrete slab were yet to be placed. Two SASW tests were performed at the same locations as the first two sets of test. Filtered dispersion curves, layering used for inversion, and the accompanying shear wave velocity profiles after inversion from this set of tests are presented in Figs. 9.5 and 9.6 for sites 1 and 2, respectively. Material property profiles are tabulated in Table 9.3 and 9.4. The field data at site 1 scattered greatly for unknown reason at wavelengths longer than about 15 ft (5 m) and

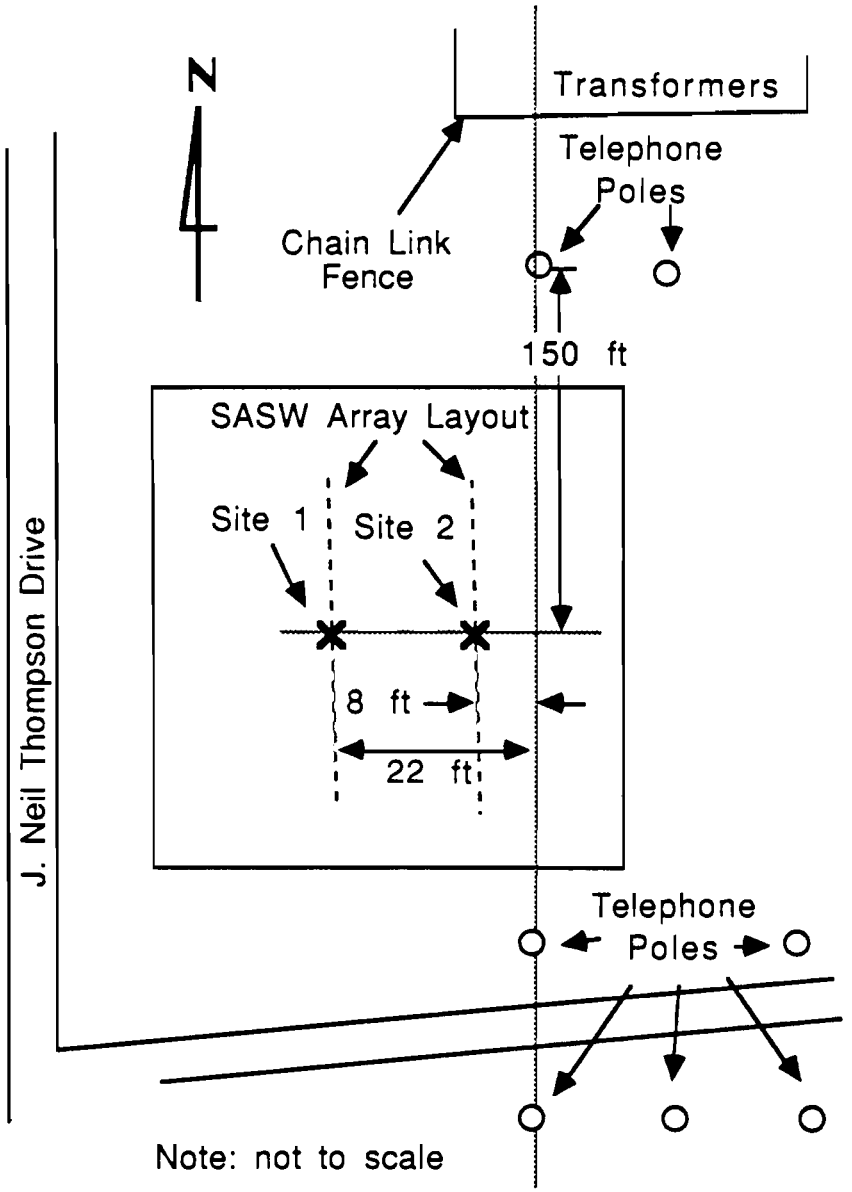

Fig. 9.2. Layout of SASW Arrays Used at the BRC Facility.

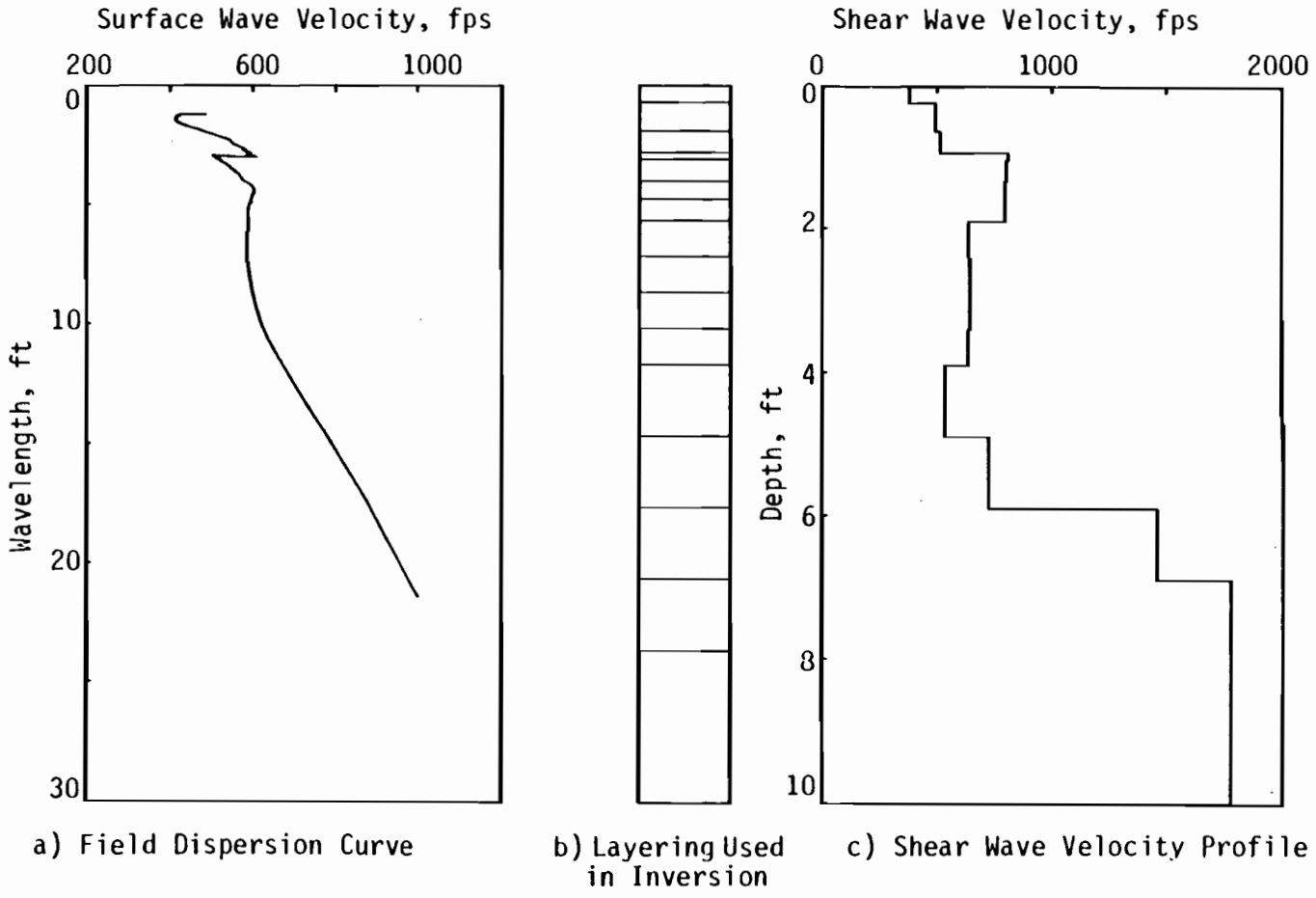

Fig. 9.3. Composite Profile at Site 1 on Embankment at BRC Facility: SASW Tests Performed on February 22, 1984.

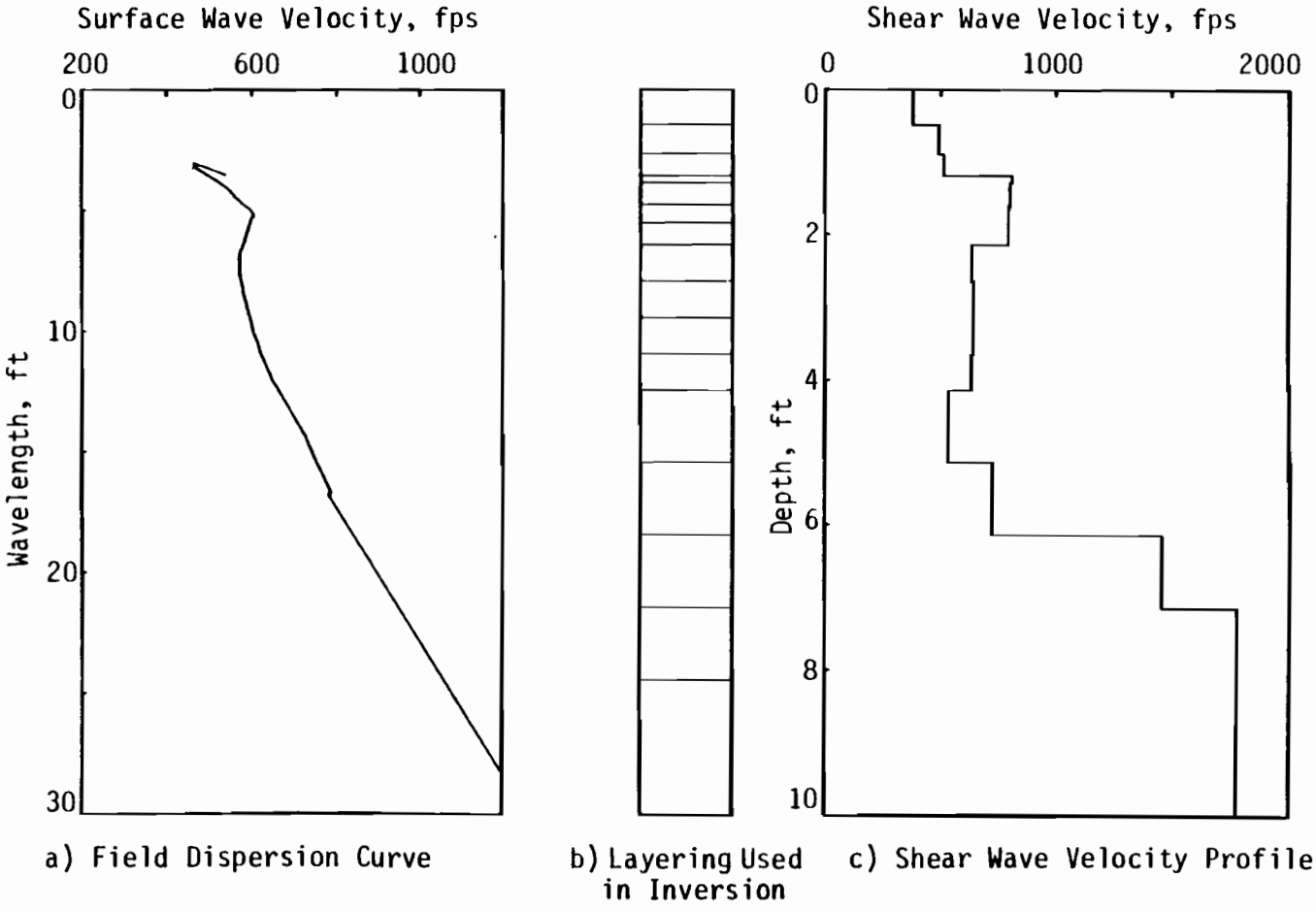

Fig. 9.4. Composite Profile at Site 2 on Embankment at BRC Facility: SASW Tests Performed on February 22, 1984.

TABLE 9.1. COMPOSITE PROFILE OF SITE 1 AT BRC FACILITY: Testing Performed on February 22, 1984

Layer No.	Layer Thickness (ft)	Mid-Layer Depth (ft)	Shear Velocity (fps)	Compression Velocity (fps)	Shear Modulus (psi)	Young's Modulus (psi)	Assumed Poisson's Ratio	Assumed Unit Weight (psf)
1	0.25	0.13	377.	705.	3372	8765	0.30	110.
2	0.40	0.45	492.	920.	5743	14930	0.30	110.
3	0.30	0.80	514.	960.	6268	16280	0.30	110.
4	0.10	1.00	809.	1510.	15530	40330	0.30	110.
5	0.30	1.20	800.	1497.	15180	39480	0.30	110.
6	0.25	1.48	793.	1481.	14920	38760	0.30	110.
7	0.30	1.75	793.	1481.	14920	38760	0.30	110.
8	0.50	2.15	634.	1186.	9536	24790	0.30	110.
9	0.50	2.65	640.	1198.	9717	25270	0.30	110.
10	0.50	3.15	640.	1198.	9717	25270	0.30	110.
11	0.50	3.65	631.	1180.	9446	24550	0.30	110.
12	1.00	4.40	531.	993.	6689	17390	0.30	110.
13	1.00	5.40	722.	1351.	12370	32160	0.30	110.
14	1.00	6.40	1454.	2720.	50150	130400	0.30	110.
15	1.00	7.40	1776.	3323.	74830	194600	0.30	110.

TABLE 9.2. COMPOSITE PROFILE OF SITE 2 AT BRC FACILITY: Testing Performed on February 22, 1984

Layer No.	Layer Thickness (ft)	Mid-Layer Depth (ft)	Shear Velocity (fps)	Compression Velocity (fps)	Shear Modulus (psi)	Young's Modulus (psi)	Assumed Poisson's Ratio	Assumed Unit Weight (psf)
1	0.50	0.25	377.	705.	3372	8765	0.30	110.
2	0.40	0.70	492.	920.	5743	14930	0.30	110.
3	0.30	1.05	514.	960.	6268	16280	0.30	110.
4	0.10	1.25	809.	1510.	15530	40330	0.30	110.
5	0.30	1.45	800.	1497.	15180	39480	0.30	110.
6	0.25	1.73	793.	1481.	14920	38760	0.30	110.
7	0.30	2.00	793.	1481.	14920	38760	0.30	110.
8	0.50	2.40	634.	1186.	9536	24790	0.30	110.
9	0.50	2.90	640.	1198.	9717	25270	0.30	110.
10	0.50	3.40	640.	1198.	9717	25270	0.30	110.
11	0.50	3.90	631.	1180.	9446	24550	0.30	110.
12	1.00	4.65	531.	999.	6689	17430	0.30	110.
13	1.00	5.65	722.	1351.	12370	32160	0.30	110.
14	1.00	6.65	1454.	2720.	50150	130400	0.30	110.
15	1.00	7.65	1776.	3322.	74830	194500	0.30	110.

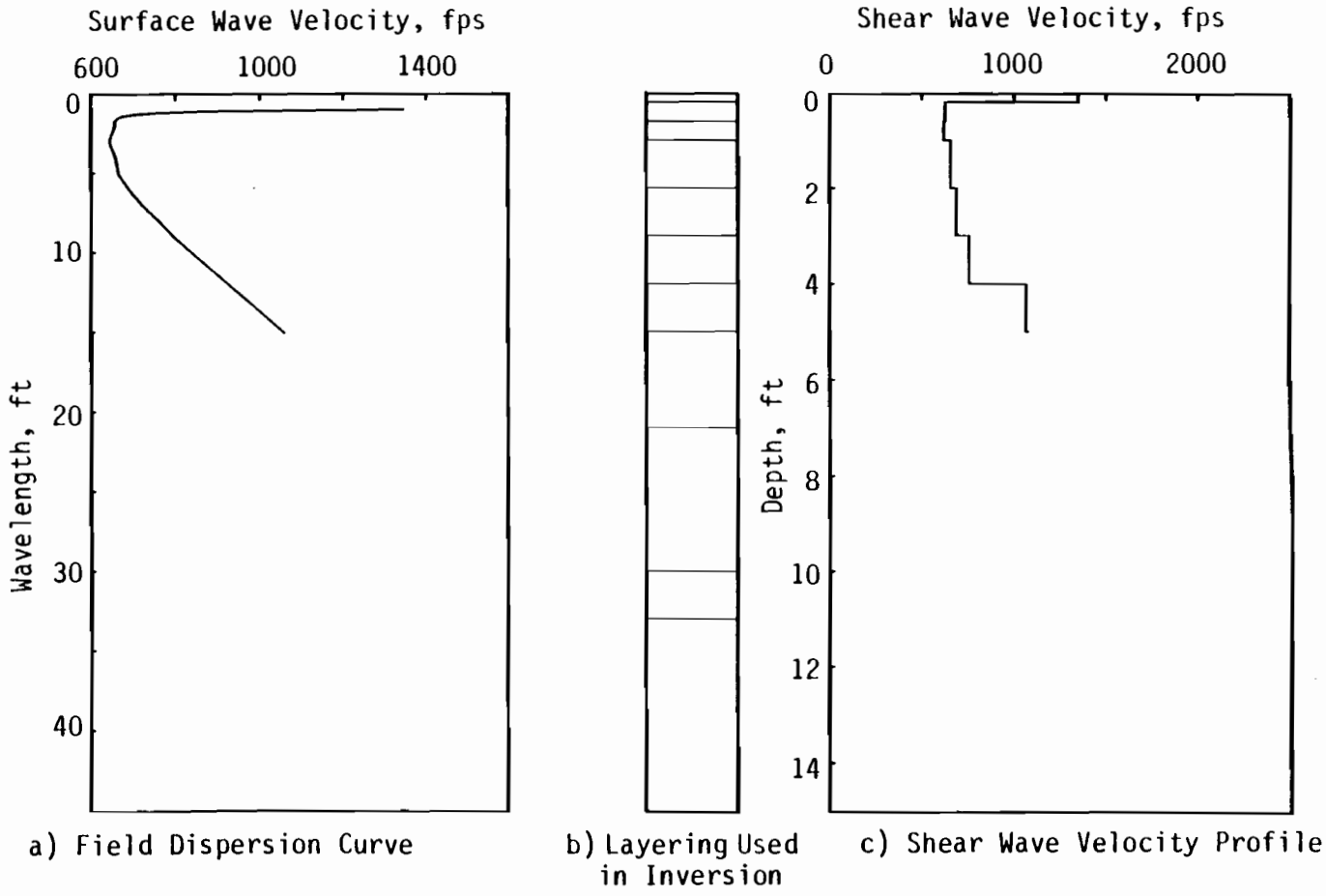

Fig. 9.5. Composite Profile at Site 1 on Embankment at BRC Facility: SASW Tests Performed on August 12, 1984.

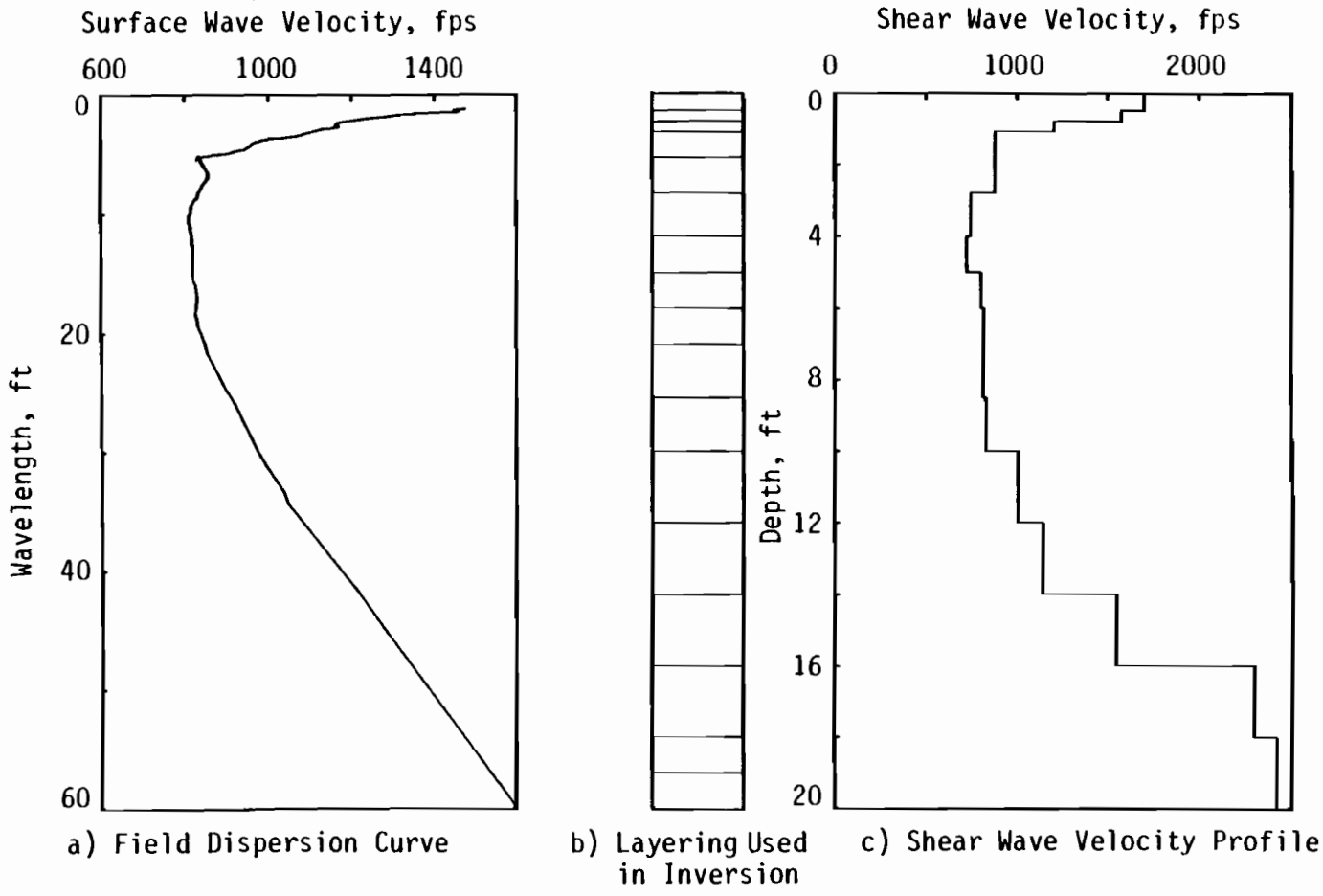

Fig. 9.6. Composite Profile at Site 2 on Embankment at BRC Facility: SASW Tests Performed on August 12, 1984.

TABLE 9.3. COMPOSITE PROFILE OF SITE 1 AT BRC FACILITY: Testing Performed on August 12, 1984

Layer No.	Layer Thickness (ft)	Mid-Layer Depth (ft)	Shear Velocity (fps)	Compression Velocity (fps)	Shear Modulus (psi)	Young's Modulus (psi)	Assumed Poisson's Ratio	Assumed Unit Weight (psf)
1	0.20	0.10	1346.	2518.	44930	116800	0.30	115.
2	0.40	0.40	624.	1167.	9237	24010	0.30	110.
3	0.40	0.80	616.	1152.	9002	23400	0.30	110.
4	1.00	1.50	657.	1229.	10240	26620	0.30	110.
5	1.00	2.50	687.	1285.	11200	29110	0.30	110.
6	1.00	3.50	758.	1418.	13630	35440	0.30	110.
7	1.00	4.50	1064.	1989.	26860	69800	0.30	110.

TABLE 9.4. COMPOSITE PROFILE OF SITE 2 AT BRC FACILITY: Testing Performed on August 12, 1984

Layer No.	Layer Thickness (ft)	Mid-Layer Depth (ft)	Shear Velocity (fps)	Compression Velocity (fps)	Shear Modulus (psi)	Young's Modulus (psi)	Assumed Poisson's Ratio	Assumed Unit Weight (psf)
1	0.50	0.25	1699.	3178.	71590	186100	.30	115.
2	0.30	0.65	1573.	2943.	58700	152600	.30	110.
3	0.30	0.95	1200.	2245.	34160	88820	.30	110.
4	0.70	1.45	875.	1637.	18160	47220	.30	110.
5	1.00	2.30	875.	1637.	18160	47220	.30	110.
6	1.20	3.40	742.	1389.	13060	33970	.30	110.
7	1.00	4.50	720.	1347.	12300	31980	.30	110.
8	1.00	5.50	800.	1496.	15180	39470	.30	110.
9	1.00	6.50	815.	1524.	15760	40960	.30	110.
10	1.50	7.75	813.	1520.	15680	40760	.30	110.
11	1.50	9.25	828.	1549.	16260	42290	.30	110.
12	2.00	11.00	1003.	1876.	23870	62040	.30	110.
13	2.00	13.00	1138.	2128.	30720	79860	.30	110.
14	2.00	15.00	1543.	2885.	56480	14680	.30	110.
15	2.00	17.00	2296.	4294.	125100	325100	.30	110.
16	1.00	18.50	2417.	4521.	138600	360300	.30	110.

was discarded for longer wavelengths. Field data at site 2 were very good. At site 2, the boundary between the base and compacted soil is not very clear. The profile shows about 0.5 ft (15 cm) of base over 2 ft (61 cm) of compacted soil with relatively high wave velocities ranging from 875 to 1200 fps (267 to 366 m/s). The 5 ft (32 cm) of roller compacted soil seems to break into two layers, about 2 ft (61 cm) of softer soil over about 3 ft (91 cm)of a little stiffer soil. The 4-ft (122 cm) thick layer of natural soil shows an increasing velocity from 813 to 1003 fps (248 to 306 m/s). The boundary between the natural soil and bedrock is not as clear as in the earlier tests, probably because it is deeper in these tests and long wavelengths were not generated.

Many SASW tests were performed after completion of the pavement. One set of tests performed on October 31, 1986 is presented in Fig. 9.7 and Table 9.5. The exact test location of the set of SASW tests could not be verified due to the fact that reference objects (telephone poles) had been removed. Therefore, the stiffness profile serves mainly as a general profile acquired from the top of the pavement on the embankment.

A composite plot of all wave velocity profiles and accompanying moduli profiles is shown in Fig. 9.8. These profiles have been adjusted for varying elevations at the testing time so that all profiles can be placed correctly on the same plot. It is interesting to see that the stiffness of the natural soil increased between tests performed on February 22, 1984 and August 12, 1984 after which time the stiffness remained. The increasing velocity might be caused by consolidation of the natural soil and/or by moisture changes as a result of wetting and drying. Generally speaking, the shear wave velocity profiles are quite consistent.

Since both concrete and asphalt free surfaces are available for testing by the "quick and easy" method discussed in Section 8.5, wave velocities acquired from inversion of the dispersion curves for concrete and asphalt were checked against the velocity by the "quick and easy" method. For the concrete, the average shear wave velocity from the quick method was found to be 8667 fps (2642 m/s) (Fig. 4.31) while a velocity of 8646 fps (2635 m/s) was found from inversion. For the asphalt, the wave velocity by the quick method was found to be 5775 fps (1760 m/s) (using Fig. 9.9 to find V_R = 5400 fps (1646 m/s) and assuming a Poisson's ratio of 0.35). The velocity from inversion is 5739 fps (1749 m/s). Wave velocities estimated by "quick and easy" method are very close to wave velocities calculated from the inversion process. However, the material thickness were known prior to the inversion process which helped to reduce the effort and improve the accuracy of the results. If one compared moduli, then the moduli of the concrete pavement are 5.402×10^6 psi (3.724×10^7 kPa) from the quick method and 5.376×10^6 psi (3.706×10^7 kPa) from inversion. For the asphalt pavement moduli are

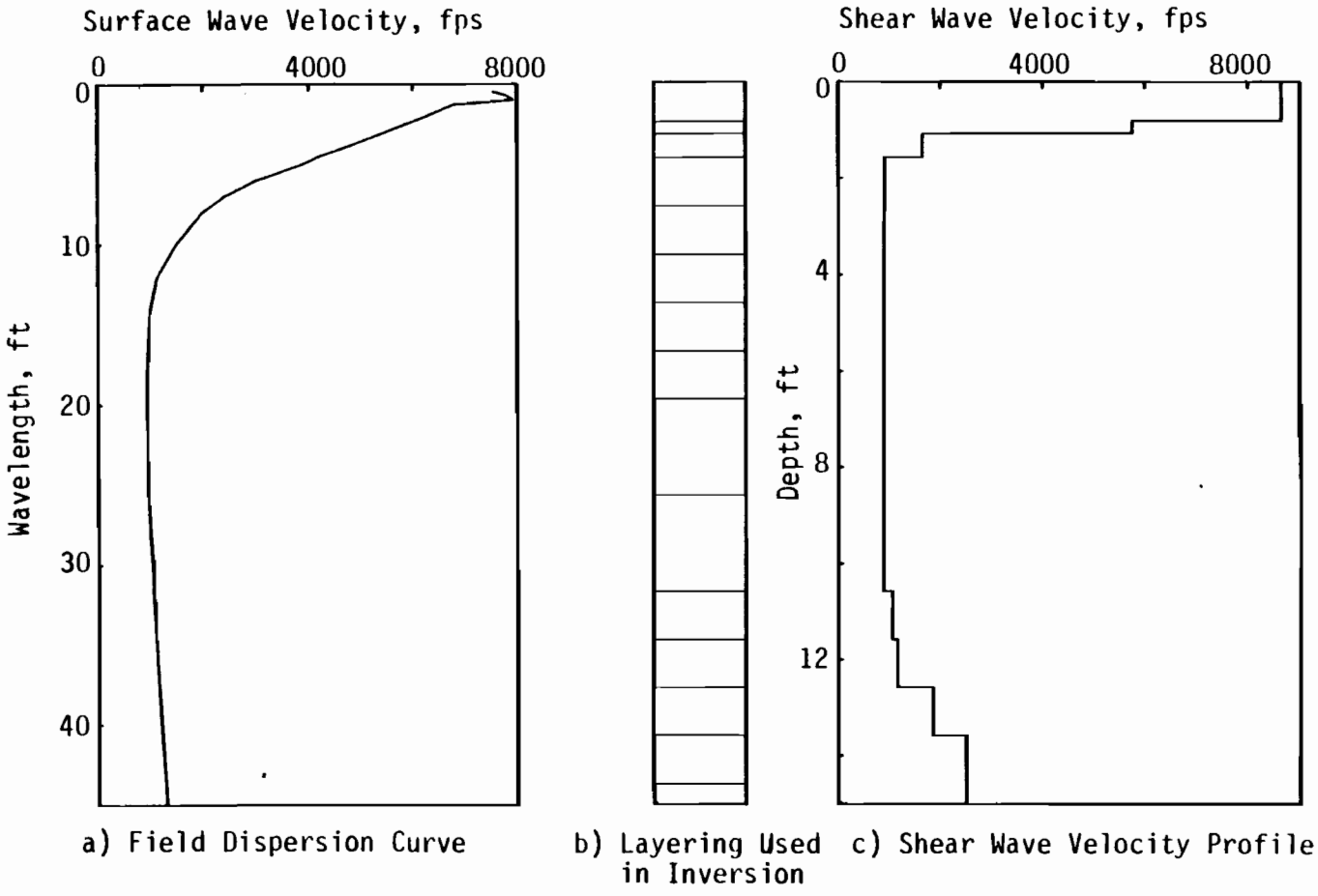

Fig. 9.7. Composite Profile on Embankment at BRC Facility: SASW Tests Performed on October 31, 1986.

TABLE 9.5. COMPOSITE PROFILE FOR BRC FACILITY AFTER THE COMPLETION OF CONSTRUCTION (Testing Performed on October 31, 1986)

Layer No.	Layer Thickness (ft)	Mid-Layer Depth (ft)	Shear Velocity (fps)	Compression Velocity (fps)	Shear Modulus (psi)	Young's Modulus (psi)	Assumed Poisson's Ratio	Assumed Unit Weight (psf)
1	0.83	0.41	8646.	13473.	2338000	5376000	0.15	145.
2	0.25	0.95	5739.	10739.	958900	2493000	0.30	135.
3	0.50	1.33	1635.	3059.	66300	172400	0.30	115.
4	1.00	2.08	894.	1673.	18960	49300	0.30	110.
5	1.00	3.08	884.	1657.	18540	48240	0.30	110.
6	1.00	4.08	871.	1630.	18000	46800	0.30	110.
7	1.00	5.08	871.	1630.	18000	46800	0.30	110.
8	1.00	6.08	871.	1630.	18000	46800	0.30	110.
9	2.00	7.58	871.	1630.	18000	46800	0.30	110.
10	2.00	9.58	871.	1630.	18000	46800	0.30	110.
11	1.00	11.08	1048.	1961.	26060	67750	0.30	110.
12	1.00	12.08	1152.	2157.	31480	81890	0.30	110.
13	1.00	13.08	1854.	3467.	81540	212000	0.30	110.
14	1.00	14.08	2500.	4673.	148300	385400	0.30	110.

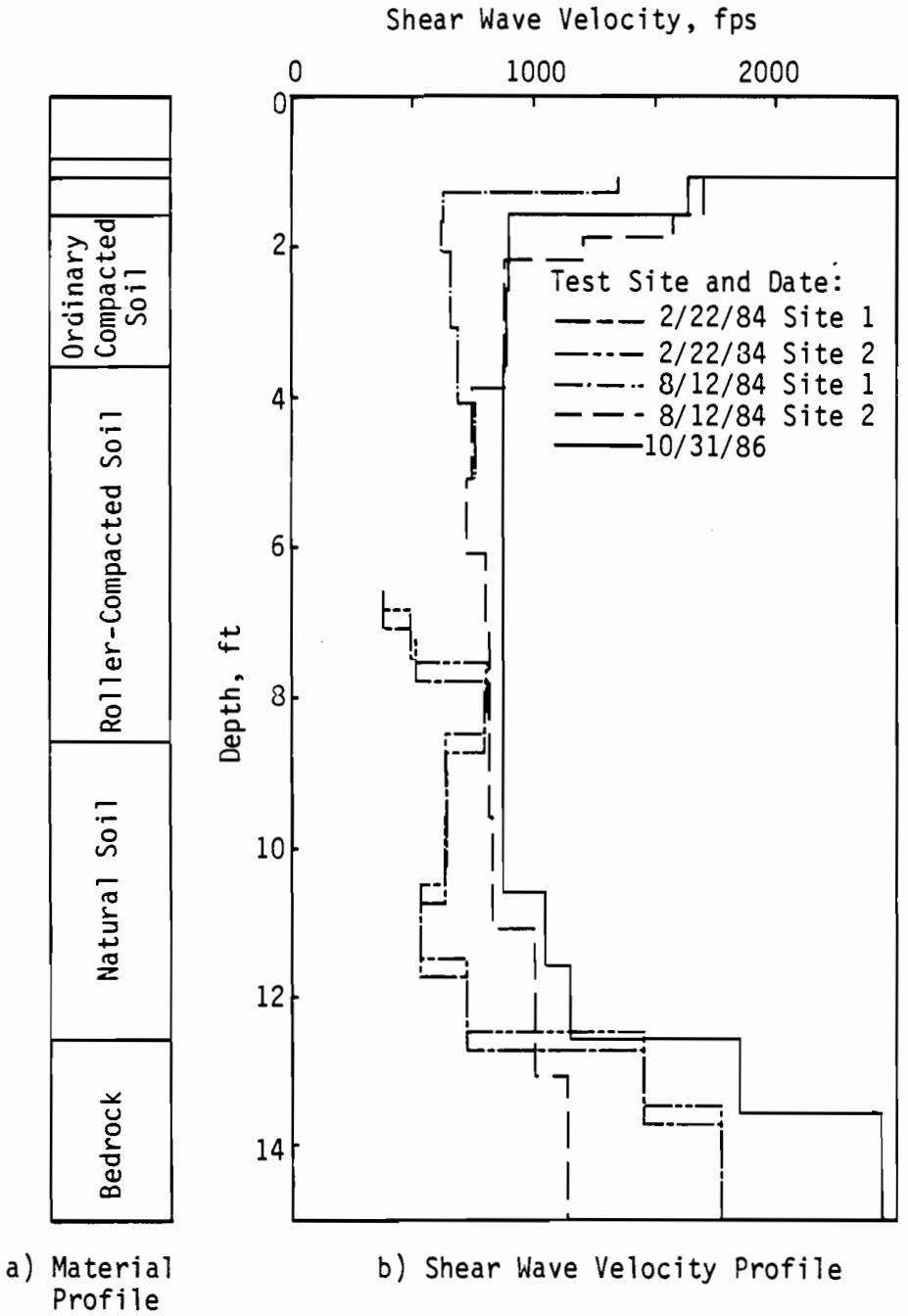

Fig. 9.8. Composite Shear Wave Velocity Profile from Different Tests and Material Layering at BRC Facility.

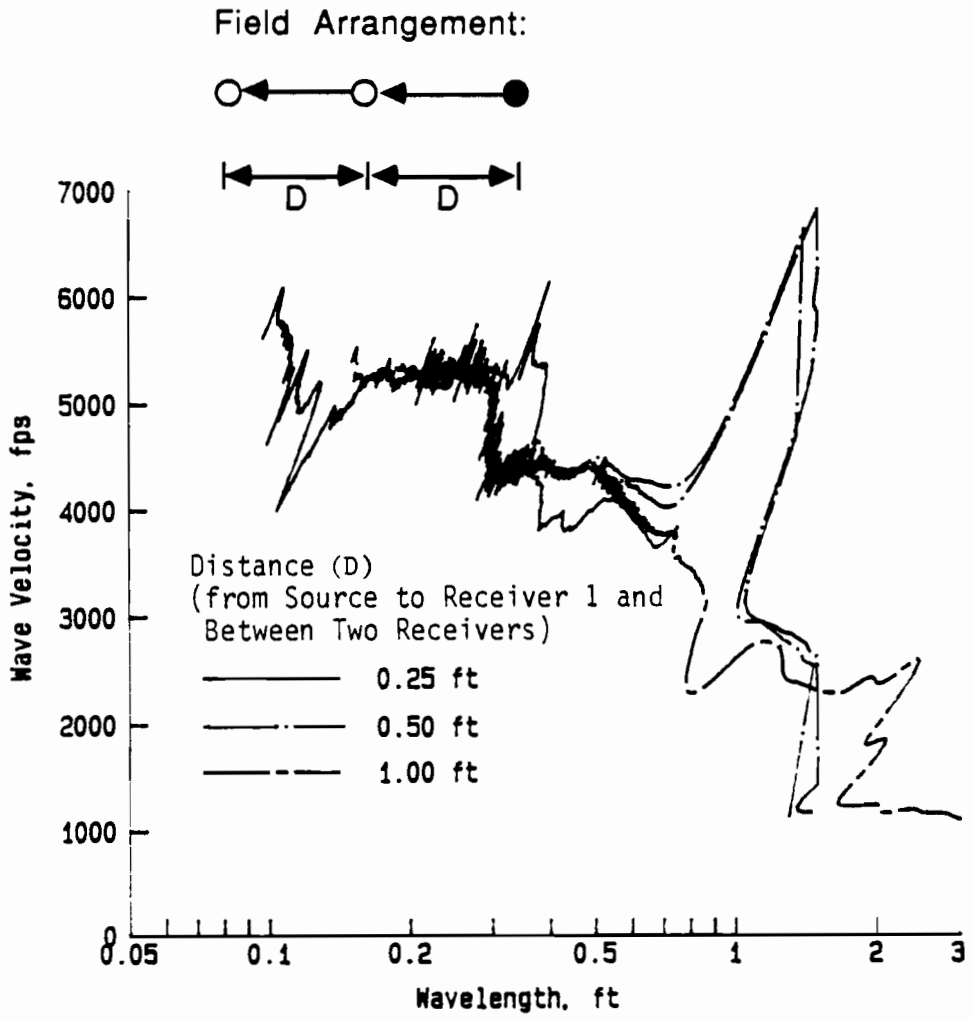

Fig. 9.9. Typical Composite Dispersion Curves for the Asphalt Pavement at BRC Facility.

2.524 x 10^6 psi (1.740 x 10^7 kPa) and 2.493 x 10^6 psi (1.719 x 10^7 kPa) for the quick method and inversion, respectively.

9.3. MONITORING CURING OF CONCRETE

One of the most desirable features of the SASW method is its nondestructive character. As such, it is possible to apply this method to observe stiffness changes of solid materials with respect to temperature, time , or other effects without damaging the material during testing. One example of this use is observation of stiffness changes of concrete during the curing process. This work was undertaken to see if one can determine how surface covering agents on concrete pavements affect the curing process.

In these preliminary tests, the concrete pavement was modeled in the laboratory by a concrete beam. As a result of previous studies (Chapters Four and Five), the beam size was designed specifically to reduce the effects of reflected waves. A beam 12-ft (366-cm) long, 4-in. (10 cm) wide, and 10-in. (25 cm) deep was used. The source/receiver array was placed at one end of the beam, with the source placed between the receivers and end of the beam so that reflected surface waves created by the near end of the beam would be traveling in the same direction as the direct surface waves (Chapter Four). This test arrangement is shown in Fig. 9.10. To minimize the effect of the reflecting boundary oriented parallel to the test array (Chapter Four), the k value (ratio between source/receiver spacing and distance to the boundary nearest to the test array, see Fig. 4.34) should be smaller than 0.2 or greater than 3. To keep the size of the beam as small as possible for easy handling, the width of the beam was selected on the narrow side (to make k smaller than 0.2 rather than bigger than 3). It was decided to use the same spacing between the source and receiver 1 as between the two receivers. Two different spacings were selected: 0.5 and 1 ft (15 and 30 cm). Based on the spacings and a value of $k < 0.2$, a 4-in. (10 cm) width was selected for the beam. This width is, in fact, too wide for the 0.5-ft (15 cm) source/receiver spacing. However, a mold narrower than 4 in. (10 cm) wide would be very difficult to cast and test. Therefore, the quality of the data from the 0.5-ft spacing was compromised.

A "V" meter was used as the impulsive source. The transducers of the "V" meter were placed directly on the fresh concrete surface. PCB model 308B02 accelerometers were used to monitor the surface motion. These accelerometers were mounted on 0.75-in (2 cm) long screws buried in the concrete. The screws helped to support the accelerometers and to provide good

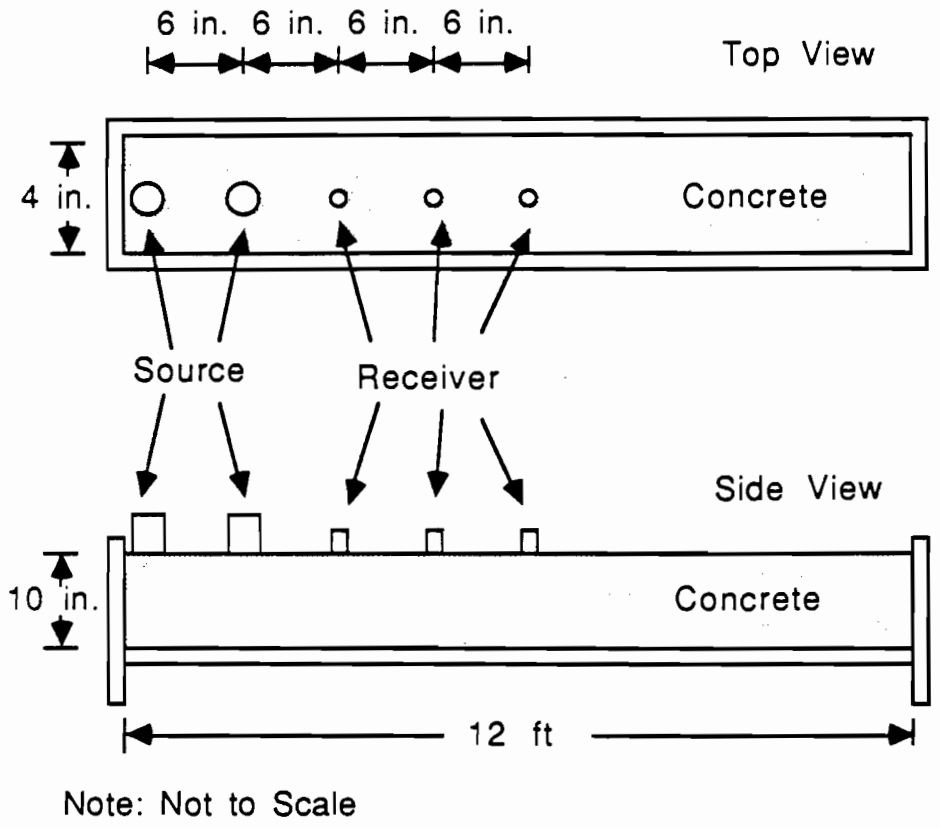

Fig.9.10. Experiment Arrangement Used to Monitor Stiffness Changes in Concrete During Curing.

contact between the concrete surface and accelerometers when the concrete was still in a semi-fluid state.

The first measurement was taken 2 hours after the concrete was mixed and poured. Before 2 hours, the concrete was so soft that no useful data could be collected due to the tremendous damping in the system (which made the impulse signal too small to be measured). As a matter of fact, at this stage (2 hours after mixing) the concrete was still too soft to be tested with the 1-ft source/receiver spacing. Even at the 0-5 ft (15 cm) source/receiver spacing, significant averaging was necessary (usually over 100 averages) to obtain good data.

Figure 9.11 shows the phase of the cross power spectrum and the coherence function determined 216 minutes after mixing the concrete. The resulting dispersion curve is shown in Fig. 9.12. Because the beam is only 10-in. (25 cm) deep, any data with wavelengths longer than 0.5 ft (15 cm) (about half of the beam depth) were disregarded. The raw dispersion curve was fit with a smooth curve, and wave velocities at wavelengths of 0.1, 0.2, 0.3, 0.4, and 0.5 ft (3, 6, 9, 12, and 15 cm) were determined. By repeating the process outlined above at each different curing stage, surface wave velocities at different curing times were measured.

Wave velocities corresponding to different wavelengths at each measurement time are shown in Figs. 9.13 through 9.17. One can see that data in the short-wavelength range (say 0.1 and 0.2 ft (3 and 6 cm)) were not generated in the first test (Figs. 9.17 and 9.16) because high-frequency data which corresponds to these short-wavelengths could not be collected due to damping present in the system at this early curing stage.

The increase in wave velocities with time clearly reflects the increasing stiffness of the concrete with curing time. This behavior can be observed at all wavelengths. One interesting point is that the wave velocities measured with the 1-ft spacing are almost always slightly smaller than the velocities measured with the 0.5-ft (15-cm) spacing. The cause of this discrepancy is unknown but is minor.

It is interesting to observe changes in the dispersion curves with curing time. At the start, the dispersion curves are relatively flat and typically look like the curve shown in Fig. 9.12 for 216 minutes after mixing the concrete. The "flatness" of the curve implies that the concrete beam has a relatively uniform stiffness throughout the depth of the beam. However, after a few more hours, the beam no longer has a uniform wave velocity profile as shown in Fig. 9.18 for 361 minutes after mixing. At this time, wave velocities at shallower depths are higher than at deeper depths. This type of wave velocity profile lasted for some time. After about 800 minutes, interpretation of the data become either very difficult or impossible because phases of cross power

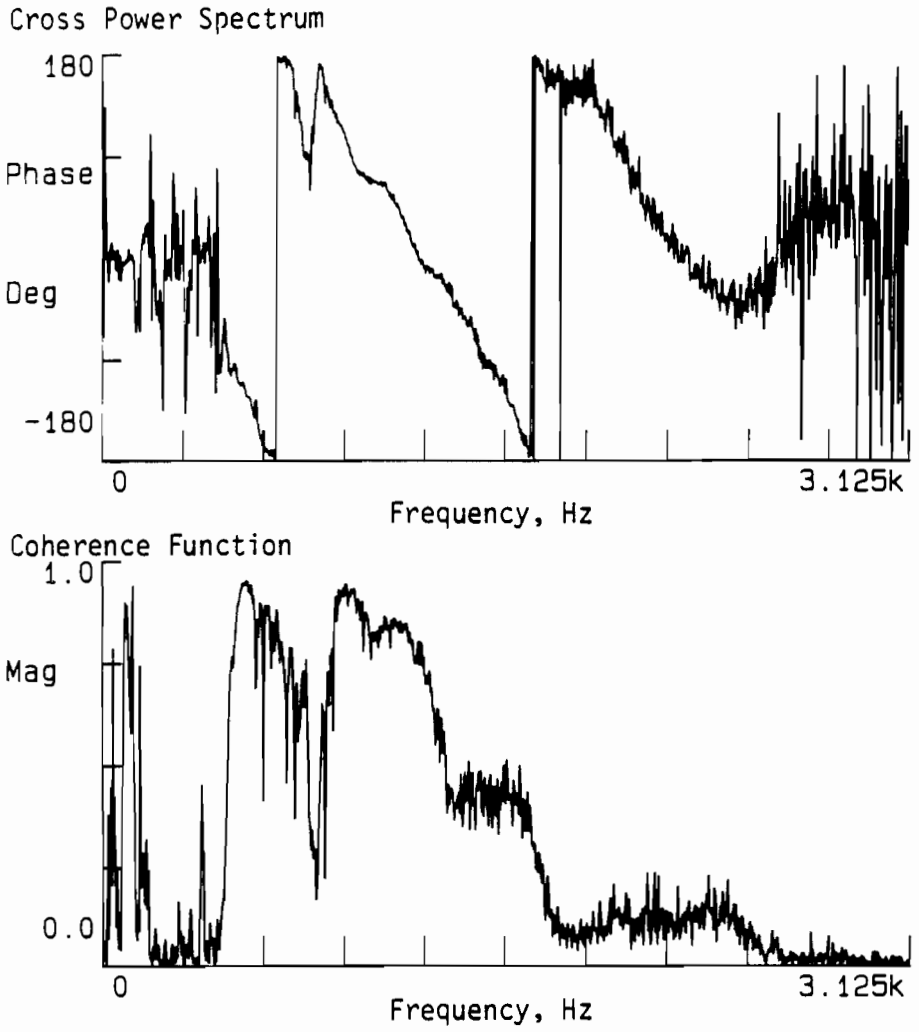

Fig. 9.11. Phase of Cross Power Spectrum and Coherence Function for Concrete Beam at 216 Minutes After Mixing: 0.5-ft Source/Receiver Distances.

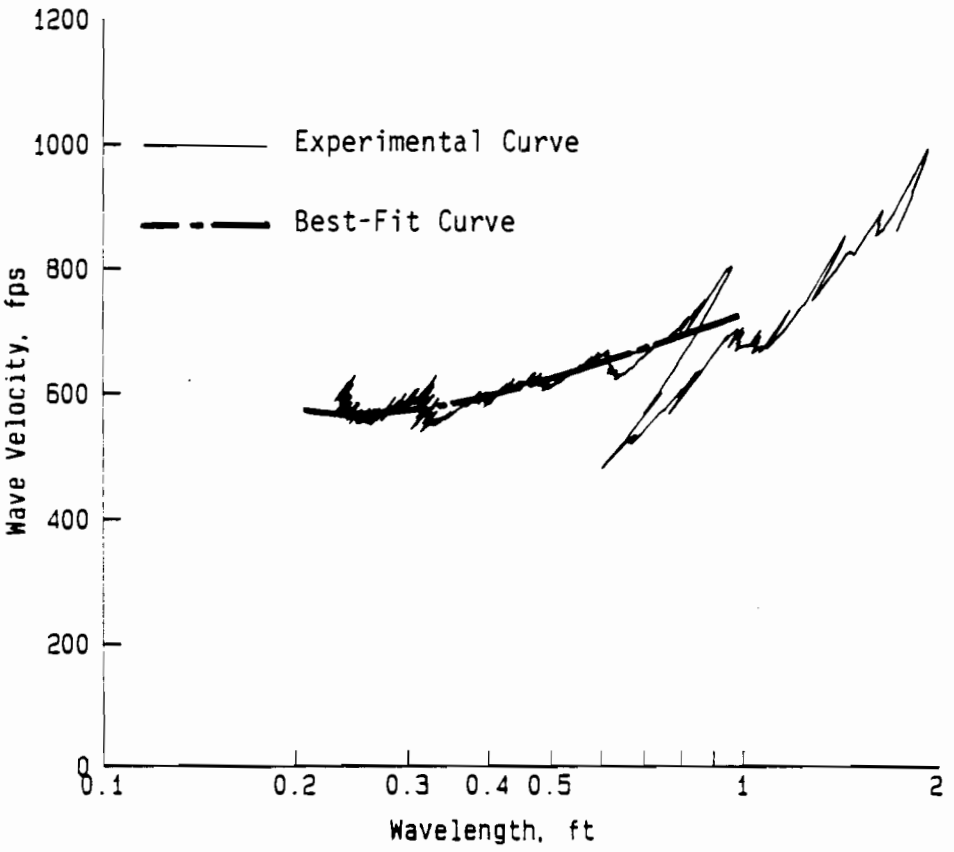

Fig. 9.12. Experimental and Best-Fit Dispersion Curves for Concrete Beam at 216 Minutes After Mixing Concrete: 0.5-ft Source/Receiver Distances.

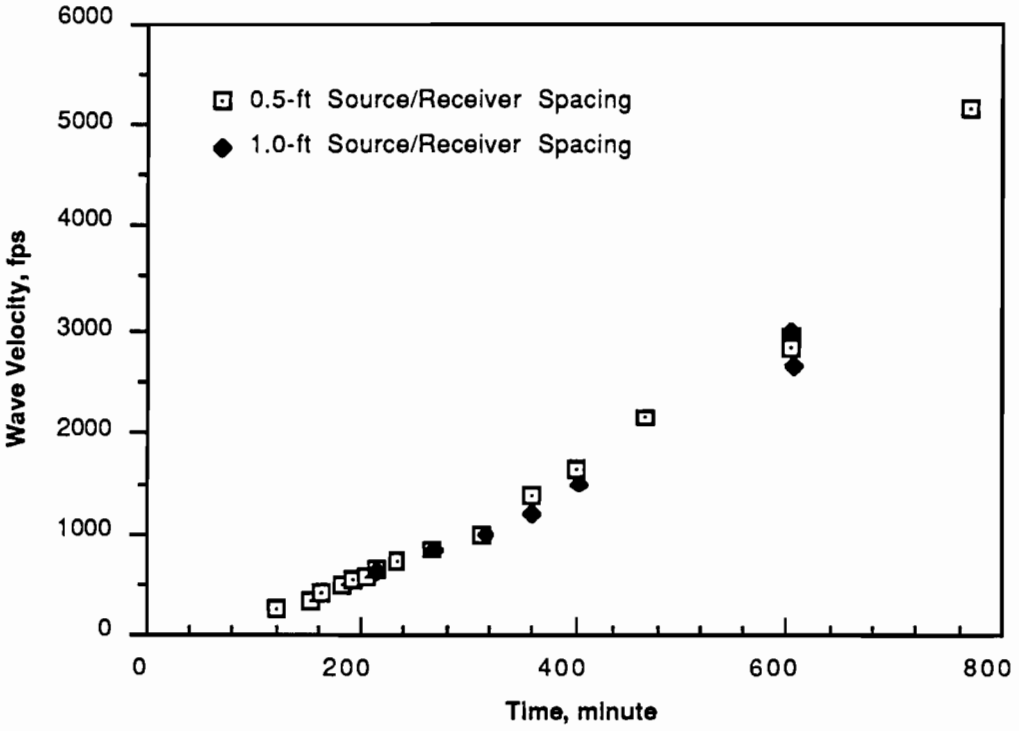

Fig. 9.13. Variation in Surface Wave Velocity with Curing Time for 0.5-ft Wavelength.

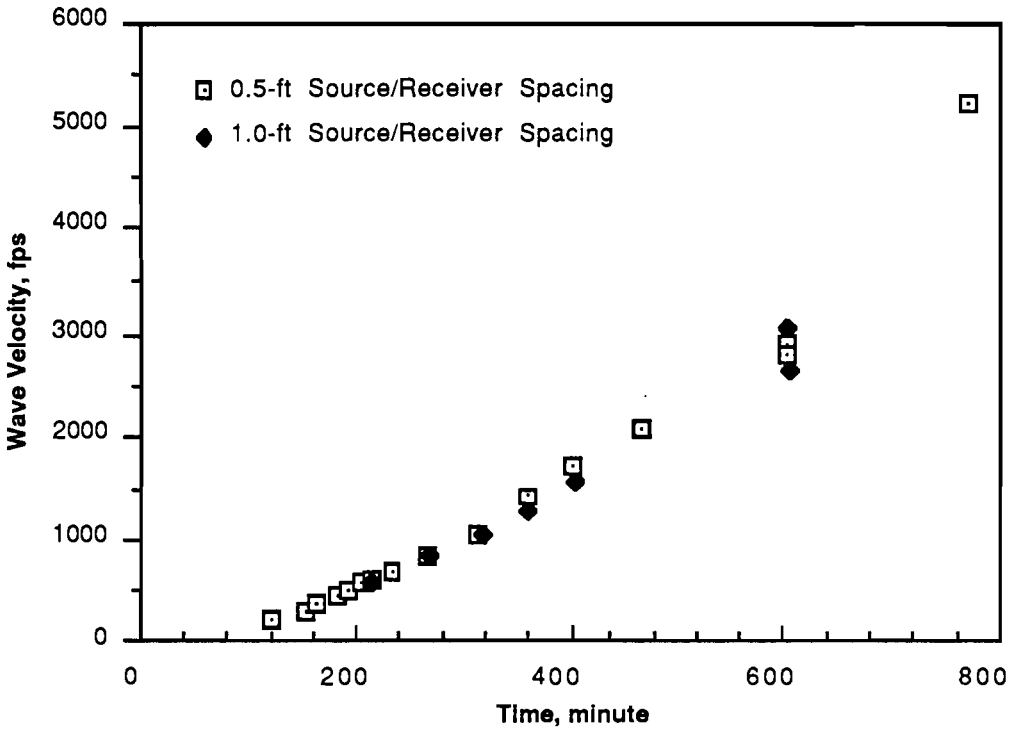

Fig. 9.14. Variation in Surface Wave Velocity with Curing Time for 0.4-ft Wavelength.

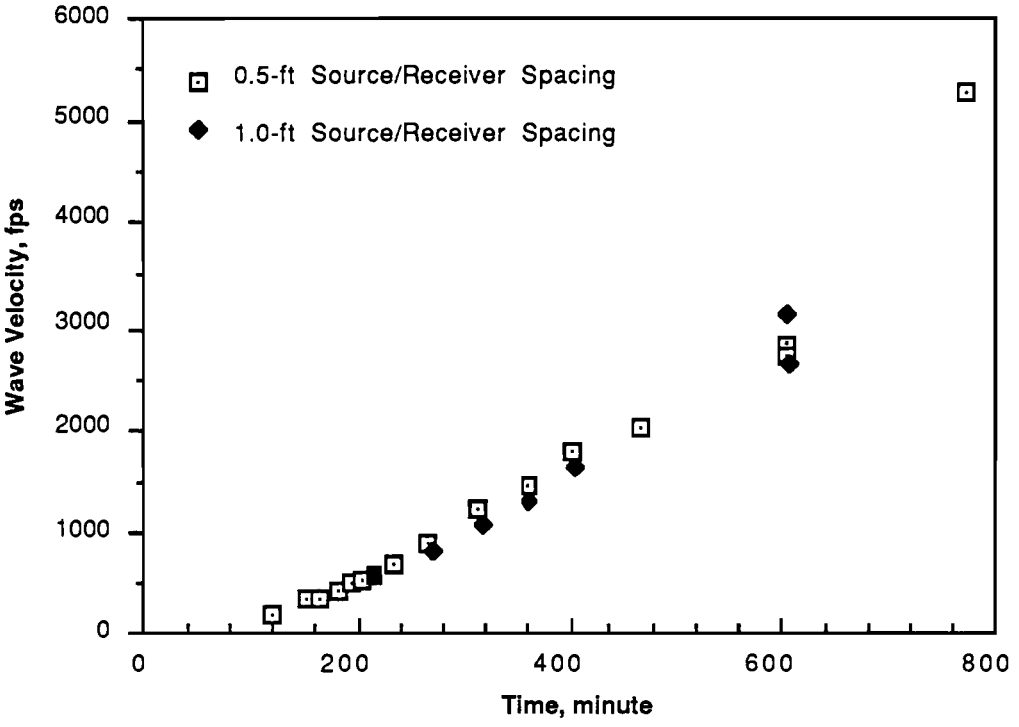

Fig. 9.15. Variation in Surface Wave Velocity with Curing Time for 0.3-ft Wavelength.

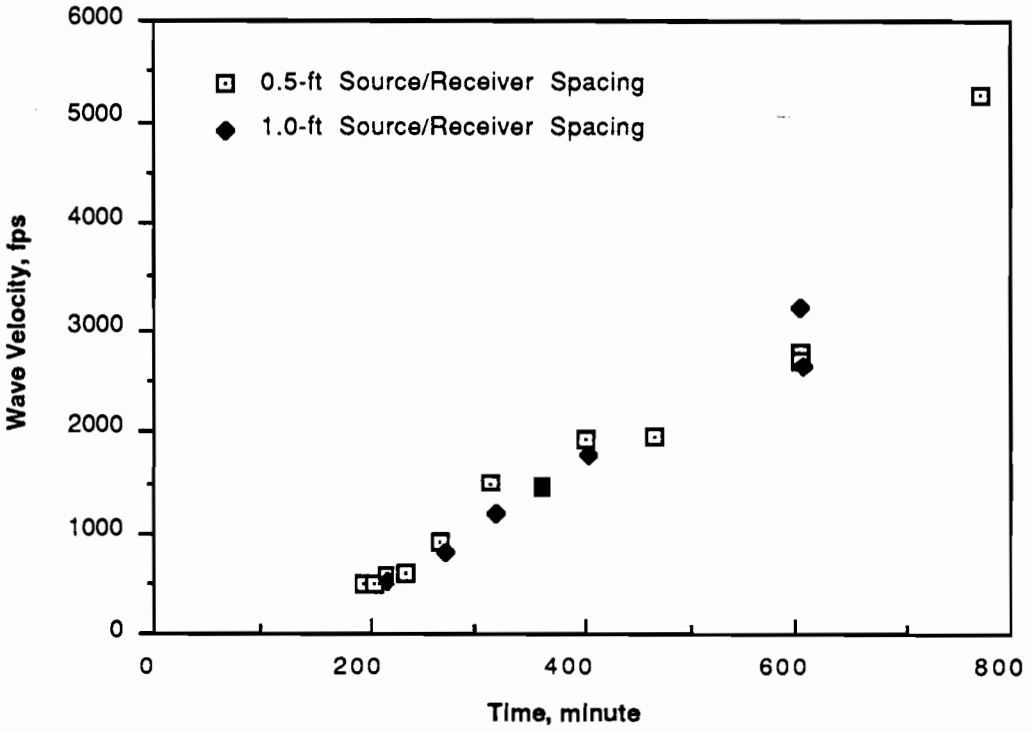

Fig. 9.16. Variation in Surface Wave Velocity with Curing Time for 0.2-ft Wavelength.

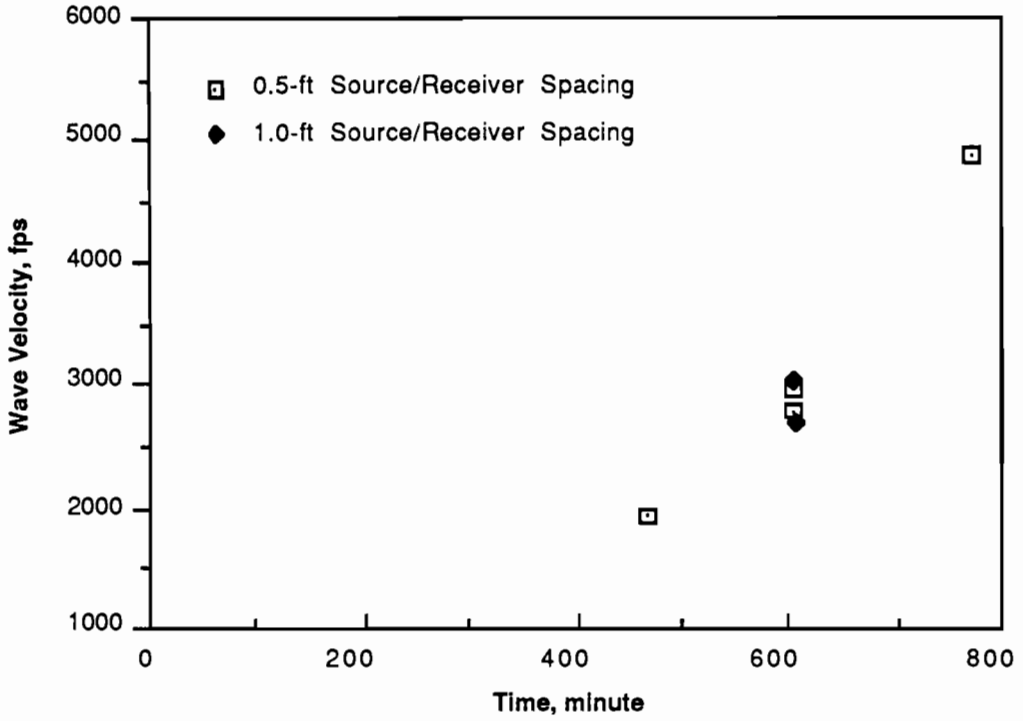

Fig. 9.17. Variation in Surface Wave Velocity with Curing Time for 0.1-ft Wavelength.

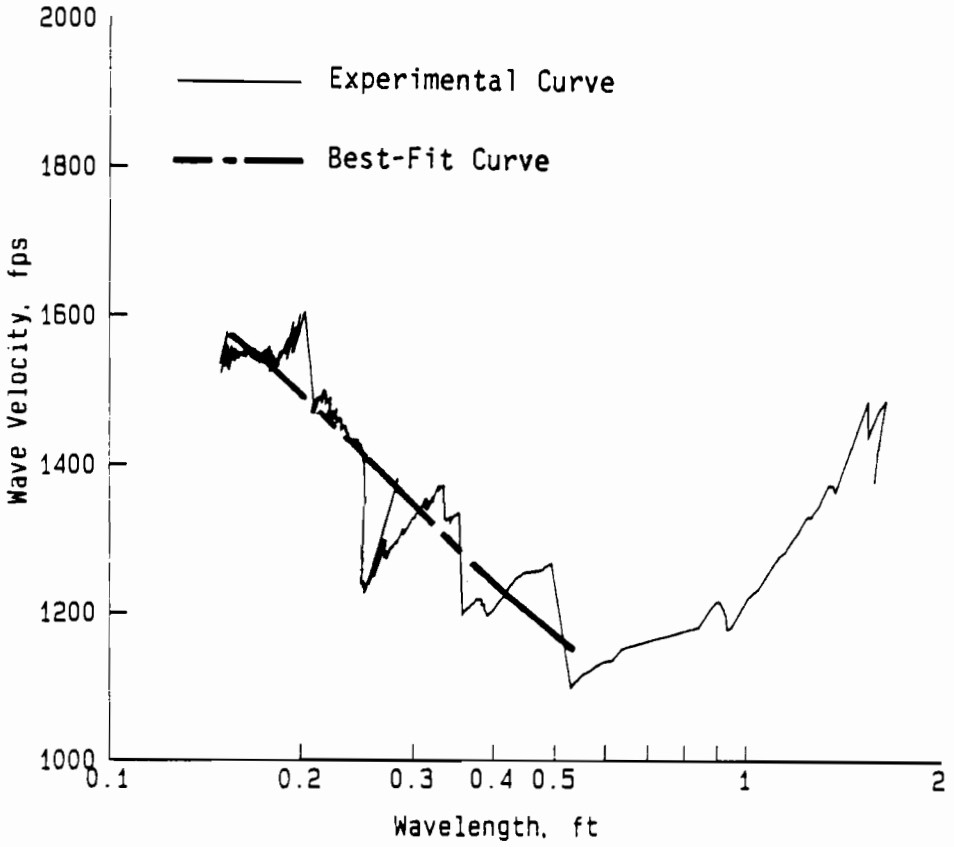

Fig. 9.18. Experimental and Best-Fit Dispersion Curves for Concrete Beam at 361 Minutes After Mixing Concrete: 0.5-ft Source/Receiver Distances.

spectra become very complex. The reason or reasons for this occurrence are unknown. Since reflected surface waves from both ends and from the sides of the beam were effectively controlled, this complex phase might have been caused by reflected body waves from the bottom face of the beam. However, this preliminary study does demonstrate the capability of the SASW method in observing the material properties nondestructively. Although measurements were not successfully made after about 800 minutes due to unknown causes, this work still provides a good starting point for further research on these kinds of applications.

9.4. SUMMARY

Two applications of the SASW method are presented in this chapter. The first one is at the BRC facility where an embankment was built under controlled conditions. SASW tests performed at different stages during construction show how stiffness changes in the material profile can be followed during construction.

The second application of the SASW method was to observe the curing process in concrete. A concrete beam was constructed. The beam was designed to model the top layer in a concrete pavement. The stiffness of the concrete (in terms of shear wave velocity) was clearly monitored over a period of about 8 hours during which time the stiffness changed by a factor of about 100 (velocity changed by a factor of about 10).

CHAPTER TEN

USE OF MASSCOMP MINICOMPUTER WITH THE SASW METHOD

10.1. INTRODUCTION

The SASW method has the potential to be one of the most powerful nondestructive seismic methods. For advances to be made in the basic understanding and uses of this method, multi-channel high-speed data acquisition equipment is required in the field. This equipment must also have the capability of handling extensive computer programs for intensive numerical manipulation of the raw data. Ideal instrumentation for the SASW method is instrumentation that is capable of: 1. recording multiple data channels simultaneously (up to 24 channels) with high-frequency resolution (up to 100 KHz per channel) on a limited number of channels, 2. being programmable so that data can be manipulated and analyzed in the time and frequency domains as the data are being acquired, 3. displaying, plotting and/or printing the raw and analyzed data, and 4. performing analytical studies (such as inversion or forward modeling) on the data in real time in the field.

During the early stages (1983-1984) in the general research with the SASW method, an equipment research grant was obtained from the Air Force Office of Scientific Research (AFOSR) at Bolling Air Force Base in Washington, D.C. This equipment grant was used to purchase a MASSCOMP minicomputer and associated data acquisition equipment for use with the SASW method as outlined above. In addition, the Civil Engineering Department and the College Engineering at the University of Texas contributed funds to develop a mobile field van for SASW testing. Selection, purchase and implementation of this equipment in SASW testing has formed a portion of this project, especially work with the minicomputer. Therefore, the basis for selecting this equipment, the status of the equipment, and future uses are described in this chapter.

10.2. STATE-OF-THE-ART IN 1983-1984

In 1983-1984, the state-of-the-art in data collection and processing in the field involved recording seismic signals with waveform analyzers and storing the data on magnetic cartridge tapes or floppy disks at the test sites. The stored records were then brought back to the laboratory, and data were dumped to computers for additional processing. The waveform analyzers used were the Hewlett Packard 5423A Structural Dynamics Analyzer and/or the Hewlett

Packard 3562A Dynamic Signal Analyzer. [These analyzers are still used in this fashion today (1987).] The dual cyber mainframe computers at The University of Texas at Austin were then used for additional data processing.

This way of handling seismic data has several drawbacks. The first drawback is that it is tedious and time consuming to transfer data from one machine to another. In addition, more transfer processes lead to a higher possibility of data loss and data errors which in turn require more time and resources to recover.

The second drawback to this approach in handling SASW testing is that it precludes the possibility of examining semi-processed and processed data right at the test site. At present, all data collected in the field are raw time domain and raw frequency domain data, since the data manipulation capability is limited by the equipment (the spectral analyzers), it is only possible to examine the quality of raw time domain and raw frequency domain data at the site. In general, phases of cross power spectra, the basis on which dispersion curves are constructed, are important data collected in the field, and coherence functions are used for data quality control. However, the quality of frequency domain data (phase of cross power spectra and coherence functions) sometimes reflects the quality of dispersion curves only in a very transparent fashion. As a result, some data collected in the field may later be found to be of low quality (as discussed in Chapter Two). One may even find a lack of the data during the in-house data reduction stage. Yet, at this stage, options for improving the data quality are very limited.

Another drawback is that most waveform analyzers currently available in the market (1983-1984) have only two sampling channels. Therefore, only two receivers can be used at a time. Seismic testing is better performed with multiple receivers (from 6 to 24), hence multiple channels. If a waveform analyzer could be equipped with enough sampling channels (6 or more) so that signals from a series of receivers could be recorded at one time and frequency analysis could be performed between any selected channels, much less time would be required to perform the tests and much more accuracy would result.

All of these facts point to the need for field equipment that is capable of: doing multi-channel data acquisition at very high speeds, performing intensive numerical computations rapidly on captured waveforms, and having the graphical capabilities which can display the results immediately. Review of the technology in 1983-1984 suggested that a minicomputer suited those needs the best. As a result, a MASSCOMP model MC5500 minicomputer was selected and installed as the heart of this instrumentation.

In this chapter, the capacity, software, and hardware configurations of this computer are briefly outlined. The present operating level and software development are discussed, Immediate and final goals of software development and use are also presented as a conclusion.

10.3. GENERAL BACKGROUND OF MASSCOMP MINICOMPUTER

MASSCOMP (Massachusetts Computer Corporation) is a Massachusetts based computer manufacturer with six years of history (since 1982) which produces mainly minicomputers for different scientific and business applications. The model MC5500 was designed specifically for scientific applications and integrates both data acquisition and numerical computation capabilities into one unit; the key reason for selecting this unit. With such integrated capability, it is possible to use this computer for sampling and analyzing seismic data in the field efficiently and effectively.

The MC5500 computer was installed in April, 1984. Since then, both the software and the hardware have gone through several revisions. The hardware was finally fully operational in December, 1984. However, system software bugs (errors) appeared frequently from the beginning of its operation and posed a significant hurdle to software development. The system performance was finally stabilized with the installation of the most recently released version of the operating systems which become available in June, 1986 and was installed in December of the same year.

A software supporting contract was not purchased in any stage of the software development process because of lack of funds. As a result, it has been a significant task for the program designer to develop programs because the only way to revolve system problems was by trial and error. A great deal of effort has been expended due to the lack of a software supporting contract. Fortunately, even with a lot of hardware and software problems associated with the computer system throughout the first three years of operation, there are quite a few accomplishments which allow the Model MC5500 to be used for seismic data processing.

10.4. COMPUTER ARCHITECTURE

The MASSCOMP MC5500 computer achieves balanced performance without bottlenecks by off-loading many functions from the central processors. Co-processors carry the burden of graphics, data acquisition, floating point arithmetic, and vector arithmetic. Due to the presence of a physical cache, most memory accesses involve no-wait states. The MC5500 computer uses the

triple bus design shown in Fig. 10.1. Three buses are used for information transfer. They are a memory interconnected (MI) Bus, a multibus, and a STD+ bus.

The MI Bus operates at 8 Mbytes/sec and supports up to 8 Mbytes of error checking and correcting memory. The central processing unit (CPU) module accesses system memory through the use of this high-bandwidth bus. Both the FP-501 floating point accelerator and the AP-501 vector processor operate on this MI bus .

The Multibus is the system peripheral bus. It operates at 3 Mbytes/sec. Peripherals include a MASSCOMP data acquisition and control processor (DACP), an independent graphic system, a disk controller, and a tape controller. The separation of the memory bus and the peripheral bus helps prevent a bottleneck that would otherwise constrain the system throughput. The CPU module interfaces to the multibus through a hardware multibus adaptor designed for high speed-direct memory access (DMA) transfers.

The STD+ Bus is an enhanced version of the industrial standard STD bus. This bus operates at 2 Mbytes/sec and is connected to the Multibus through the DACP. It is designed as the combination of two STD buses side-by-side with shared address lines and separate data paths. All MASSCOMP-supplied data acquisition modules, as well as commercially available STD devices, are supported by this bus. Digital-to-analog (D/A) convertors, analog-to-digital (A/D) convertors, and a general purpose interface bus (GPIB) are currently connected to the STD+ bus.

10.5. HARDWARE CONFIGURATION OF THE MC5500 MINICOMPUTER

10.5.1 Basic Hardware

The MC5500 is a 32-bit computer system incorporating very large scale integration (VLSI) technology from a variety of vendors through the system. The CPU module includes a Motorola MC68010 processor and a Motorola MC68000 processor working in tandem at 10 MHz. Substantial hardware is used to support a demand-paged, virtual operating system with 4 Kbyte pages. There are 16 Mbytes of user virtual address space. A 1024-entry translation buffer stores the most recently used addresses, thereby minimizing average address translation time. A user can override certain memory management mechanisms, for example, by locking programs into physical memory to prevent swapping and paging which is a critical feature for real-time programming in the UNIX environment. It is also possible to map multibus addresses, such as a device register, directly into the virtual address space.

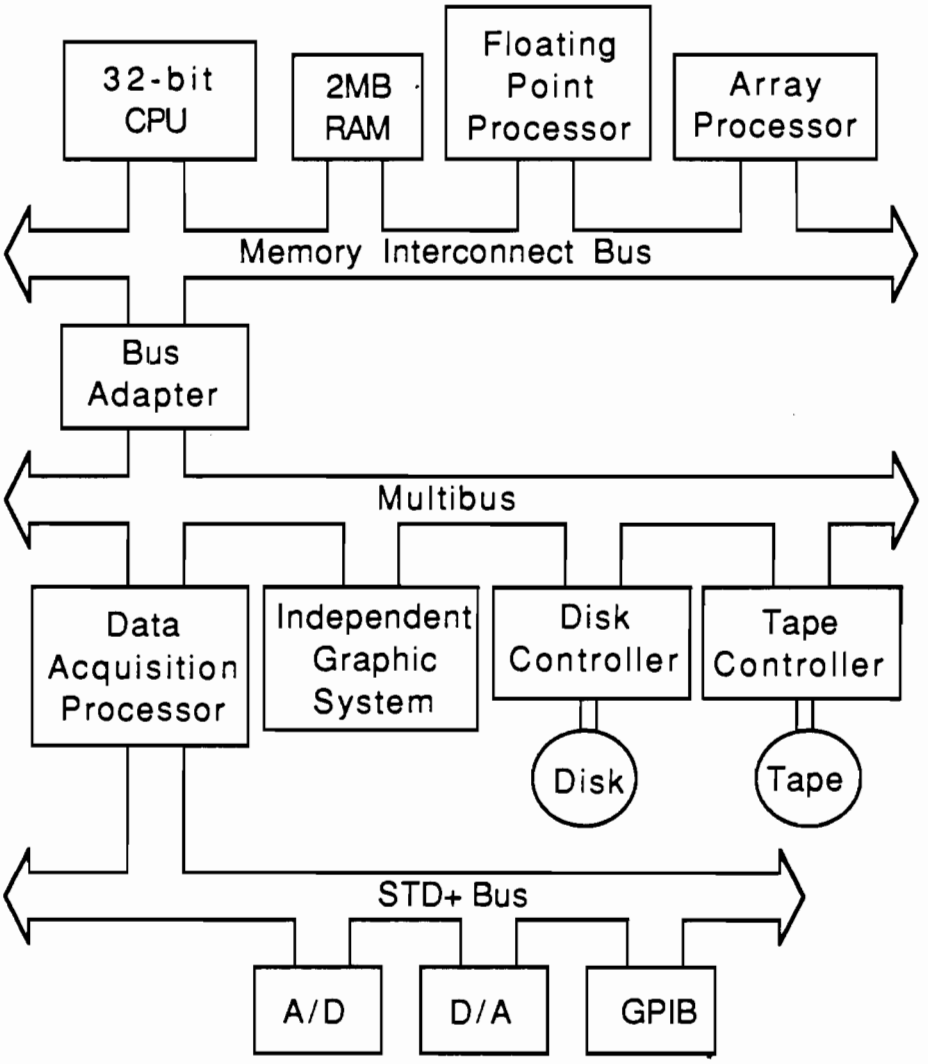

Fig. 10.1. Architecture of MASSCOMP MC5500 Computer.

The MC5500 uses a 4-Kbyte, one-way-associate cache which operates on physical addresses, and eliminates most of the need for wait states. By taking advantage of normally unused CPU cycles, the cache anticipates the instructional needs of the processor and "reads ahead". For common applications, 90 percent of all instruction and data fetches come from the cache. Since there are no processor wait states when reading from the cache, this represents a substantial performance gain. Physical memory consists of 64-Kbit dynamic random access memories (RAMs) on 1-Mbyte boards that communicate through the MI bus. The memory can detect multiple-bit faults and correct single-bit faults. Total physical memory is expendable to 8 Mbytes. Two Mbytes of physical memory are currently installed in the system.

10.5.2 Enhanced Hardware

An FP-501 floating point accelerator and an AP-501 vector processor are currently installed in the system. The floating point accelerator can increase the floating point performance to 924,000 Whetstones/sec. It features 24 sets of 32/64-bit registers. Data types supported are 32-bit integer, 32-bit real, and 64-bit real. The AP-501 vector processor enhances the performance for many scientific applications involving vector and array calculations. It handles single-precision floating point computation. Both the FP-501 and AP-501 operate on the high-speed MI bus with direct access to system memory and greatly increase the system efficiency.

The MC5500 supports an independent graphics processor (IGP). The IGP consists of a separate MC68000 processor with 256 Kbytes of graphics software memory, 2 frame buffers, and 6-plane raster image memory. A 13-in. (33 cm) color monitor with 640x480 pixel resolution is currently installed. An optical mouse and 117-key keyboard are also in use.

Mass storage of the system includes a 27-Mbyte, 5 1/4 in. (13 cm) hard disk, an 80-Mbyte 8-in. (20 cm) hard disk, a 1-Mbyte floppy disk driver and a 1/4-in. (0.635 cm) cartridge tape driver with a capacity of 50 Mbytes of storage per tape. These devices provide ample room for smooth system operation as well as convenient data exchange with other computer systems.

The data acquisition and control processor (DACP) is a 125 ns/cycle bit-slice processor operating on the multibus. The input data transfer rate is 2 Mbytes/sec. It also can make real-time data dependent decisions. Special operating system features make it possible for acquired data to be written to disk at very high speeds.

The analog-to-digital (A/D) convertor has a 1 MHz transfer rate with 12-bit resolution. The maximum number of channels that can be sampled is 64 single-ended or 32 differential channels.

An 8-channel digital-to-analog (D/A) convertor is also available in the system. It operates at a maximum frequency of 500 KHz with 12-bit resolution.

A general purpose interface bus (GPIB, also known as HPIB, IB-488 or IEEE-488) is installed in the system to provide convenient communication among a variety of instruments and computers. The GPIB is a bit-parallel, byte-serial, standard interface bus with a maximum data transfer rate of 500 Kbytes/sec. This interface bus enables the MC5500 to control all devices with the GPIB interface and is vital to computer-aided laboratory testing. Three, RS-232 serial ports are available for the connection of terminals, printers, plotters, modems and other peripherals with the same serial ports.

10.6. SYSTEM SUPPORTED SOFTWARE

The MC5500 uses a real-time UNIX operating system. This is a modified version of the UNIX operating system. The modification is necessary because UNIX is a time sharing operating system, but data acquisition and control of other laboratory instruments are real-time jobs. To prevent all real-time jobs from being interrupted, MASSCOMP modified the existing UNIX operating system. The real-time enhancements include a provision for special real-time program properties such as system calls that lock programs in primary memory, asynchronous system traps (AST) for extremely fast and error free interprocess communication and contiguous files to allow high-speed disk access.

MASSCOMP supports a complete graphic library, data acquisition library, array processor library and other necessary libraries for software development. The present system supports both FORTRAN77 and C compilers.

For the purpose of digital signal analysis, a software library, the interactive laboratory system (ILS), was purchased from Signal Technology Inc. in 1985. This library provides a full line of interactive programs for signal processes such as Fast Fourier Transformation (FFT), spectral analysis functions, design and application of filters, etc. A digital signal processing library edited by the Institute of Electrical and Electronic Engineers (IEEE) is available in the system, too. These software packages are very important to the SASW system development because they reduce the load on the system software designer so that he or she can concentrate on algorithm development rather than routine program coding.

10.7. CURRENT OPERATING LEVEL

For the purpose of field data sampling, several multi-channel data acquisition programs were developed based on different data transfer techniques. It is possible to sample different numbers of channels at desired frequencies. A major problem unsolved at present is the triggering problem. An external trigger which needs some hard-wiring can be implemented without too much difficulty, but the internal trigger and pre-trigger modes, which are necessary for SASW tests, need intensive programming and are yet to be implemented.

The use of the GPIB interface has been very successful. Several programs which are used to communicate with other instruments through this GPIB were developed. A GPIB Debugger manufactured by National Instruments Corporation was purchased for decoding and debugging any GPIB interface problems. With the help of this GPIB Debugger, it is even easier to make use of the GPIB interface.

Several data processing programs dedicated to SASW testing were developed. These programs include transferring data from and to a waveform analyzer, disk driver, or other computer and necessary instruments, field data filtering, averaging, and plotting. An inversion program for SASW which resides in the mainframe computer at The University of Texas at Austin is available on the MC5500 after some modifications. Post data process programs such as tabulating and plotting end results are also available in the system.

10.8. ADDITIONAL EQUIPMENT PURCHASES

To automate fully the SASW method in the field, a self-contained field vehicle equipped with all necessary support equipment is needed. The Civil Engineering Department and College of Engineering at The University of Texas at Austin have contributed funds for the development of this field vehicle. The vehicle, shown in Fig. 10.2, is a 1-ton (9-KN) Ford E350 Cutaway truck body with a 15-ft (457 cm) Utilimaster van body mounted on the frame. The van body has been divided into two areas by a partition as illustrated in Fig. 10.3. The area contigious with the cab of the truck is the instrumentation room. This room houses all data acquisition and reduction equipment and is designed to be kept "clean". This area is also equipped with a Coleman 1-ton air conditioning/heating system on the roof.

The second area in the van body is located at the back of the van. Access to this area is only from the rear of the vehicle. This area houses two, 6.5 KVa Onan electrical generators and two Topaz power filters. This second area is designed to be a "dirty" area. Field gear is stored in

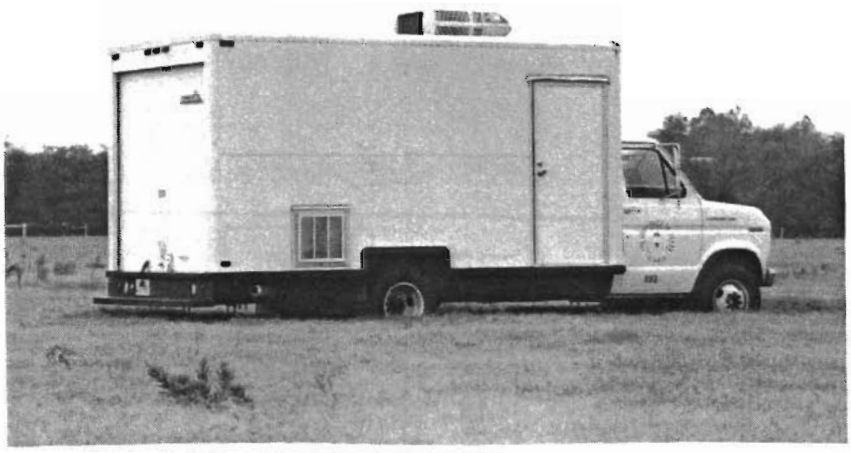

a.) Side View of Vehicle Showing Door into Instrumentation Room

b.) Rear View of Vehicle Showing Equipment Room

Fig. 10.2. Photographs of Field Seismic Vehicle.

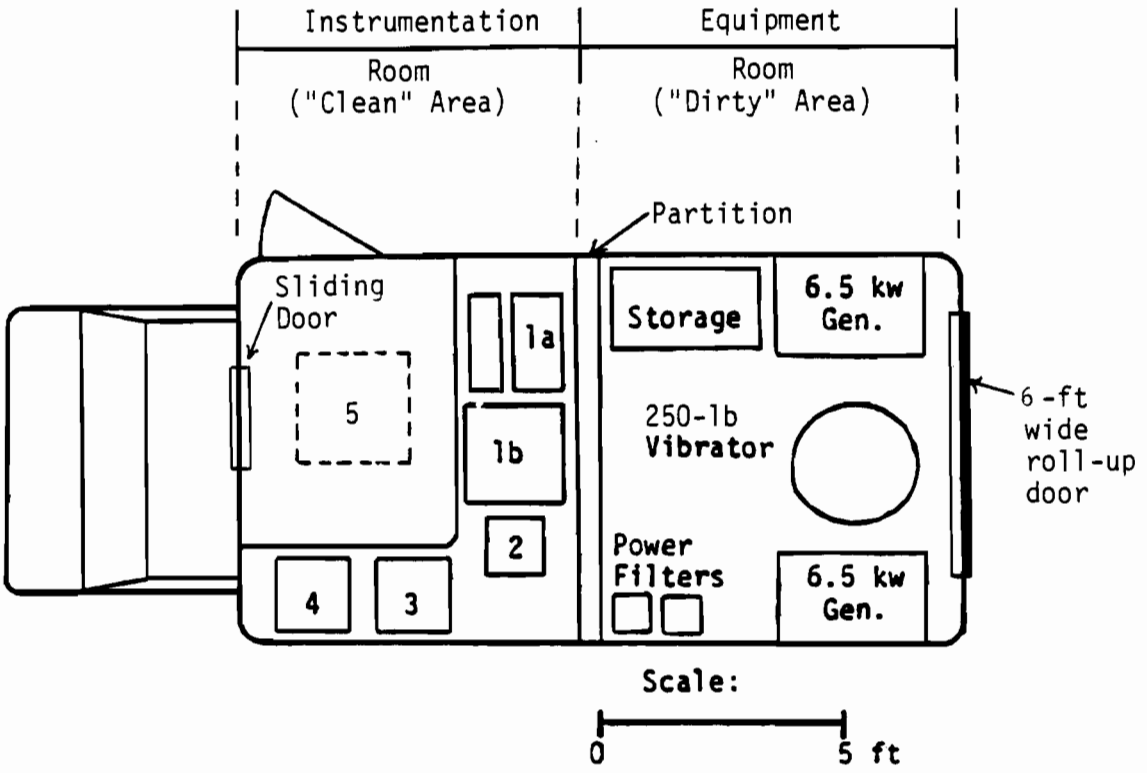

Data Acquisition and Reduction Equipment:

1. MASSCOMP Minicomputer
2. Pinter/Plotter
3. Waveform Analyzer
4. Additional Support Electronics

Additional Support Equipment:

5. Air Conditioner/Heater on Roof
6. Two, 6.5-kw Onan Electric Generators
7. Two, Topaz Power Filters
8. 250-lb Programmable Vibrator

Fig. 10.3. Plan View of Field Seismic Vehicle.

this area so that one does not have to worry about dirt on this equipment contaminating the minicomputer and other data acquisition equipment. Air conditioning is not supplied to this area.

In addition to the equipment listed above, a 250-lb electro-mechanical vibrator is being permanently installed in the rear of the vehicle. The vibrator will be used to generate seismic waves with known frequencies and will increase the quality of data obtained in the field.

With this field vehicle, the MC5500 minicomputer can be housed in a constant temperature environment and supplied with properly conditioned electrical power. The complete system is then rapidly deployable in the field.

10.9. IMMEDIATE AND FUTURE DEVELOPMENT GOALS FOR THE MC5500

The MC5500 has an excellent graphic capability which was not employed due to the complex nature of its graphic system and software bugs. The newest operating system and graphic library (installed in December, 1986) seem to have considerably fewer bugs. It will be delightful to have this powerful graphic system fully developed which should be accomplished within the next year.

Field spectral analyses is a critical part of SASW testing. As a result, a data acquisition program integrated with the spectral analyses and graphic display functions is needed. A present, this type of program is not available in the system and is an immediate goal for software development.

The final goal is a mobile field system with the capability of graphically displaying properties profiles during testing at the test site. This system requires integration into one program or the combination of a series of programs of: data acquisition, spectral analyses, graphic display, data filtering, inversion, and post data processing. All of these tasks can be done solely by the MC5500 and will be implemented in the near future. The mobility of the system will come from integrating the MC5500 and supporting electronics into the field vehicle described in Section 10.8. This task will hopefully be accomplished by the summer of 1988.

CHAPTER ELEVEN

SUMMARY, CONCLUSIONS AND RECOMMENDATIONS FOR FUTURE RESEARCH

11.1. SUMMARY

Use of seismic wave propagation methods for assessing material properties , such as the SASW, crosshole, and seismic reflection methods, has been proven through years of varied applications. The nondestructive and easy-to-apply nature of the SASW method has made this technique attractive to engineers. Significant theoretical and practical advances in the SASW method have occurred in the past few years, and this method is rapidly becoming an important method for nondestructive testing of pavement systems.

In this study, much effort has been devoted to investigating the adverse effects of reflected surface waves and direct and reflected body waves on field dispersion curves. A simplified mathematical model to account for these effects is presented. Field measurements were also performed at the rigid pavement facility at Balcones Research Center to compare with the model. The usefulness of the model is confirmed by the good agreement between modeled and field dispersion curves. It is found that field dispersion curves are basically smooth curves once the adverse effects of unwanted waves (reflected surface and body waves) are removed. For a typical pavement site, the dispersion curve is very close to a straight line in the short-wavelength range (for wavelengths less than about the thickness of the surface layer). The material properties in the surface layer can easily be determined from this part of the dispersion curve. The study also demonstrates that the effect of body waves is secondary to the effect of reflected surface waves and can be neglected in most instances. Recommendations for reducing the adverse effect of reflected surface waves based on both model and experimental studies are presented.

Field SASW testing procedures are also investigated in the study. The effects of the impact stress level, variability of time domain signals, and natural frequencies of the accelerometers and coupled accelerometer/pavement system were studied. In addition, a source which is capable of generating energy at high frequencies, the "V" meter, was found. With the "V" meter, surface waves with frequencies of about 50 kHz can be generated. A "quick and easy" method to access the near-surface material properties for any solid material by incorporating this "V" meter with accelerometers was developed. This development represents a significant

advance in the use of the SASW method. This method also bears the potential of estimating the size of the largest aggregate used in the material being tested.

The need exists to accelerate and automate the data acquisition and processing parts of the SASW method. It is obvious that a minicomputer is a suitable device for this need. The installation of a MASSCOMP MC5500 computer is the first step toward this goal. The capacity, current operating level, and suggested future software enhancements are presented.

11.2. CONCLUSIONS

Much effort in this research was devoted to the development of a comprehensive set of field results (dispersion curves) with which variables affecting SASW testing could be evaluated. The bulk of the experimental tests were performed at the BRC rigid pavement facility. This facility is composed of a jointed concrete pavement which is 10-in. (25-cm) thick. The concrete pavement is underlain by a 3-in. (7.6-cm) thick asphalt layer, a 10-in. (15-cm) thick granular base, and subgrade. The general configuration and material properties of this pavement facility should be kept in mind when considering the following conclusions. None of the conclusions should, however, be considered as only being site specific. The conclusions are quite generic in nature.

1. The following conclusions were found from model and field tests with reflected surface waves created by vertical reflecting boundaries,
   a. When the reflecting boundary is oriented perpendicularly to the test array, the source should be placed between the reflecting boundary and receivers so that reflected surface waves propagate in the same direction as the direct waves. This arrangement essentially eliminates any problems with reflected surface waves because the direct and reflected waves exhibit essentially the same phase shifts between receivers.
   b. When the reflecting boundary is oriented parallel to the test array, the distance between the array and boundary should either be very small or quite large. In the case of a standard SASW test arrangement in which the distance from the source to receiver 1 is the same as the distance between the two receivers, the distance between the array and boundary should be less than 0.2 or more than 3 times the distance between the source and receiver 1. In the case of the short distance to the boundary, the direct and reflected surface waves exhibit essentially the same phase shifts between receivers. In the case of the large distance to the boundary, the

reflected surface waves have attenuated significantly so that their amplitudes are small enough to only slightly affect the measurements.

c. The simplified mathematical model presented in Chapter Three is very helpful in identifying the effect of reflected surface waves and can explain the cause of most of the major fluctuations in measured dispersion curves of pavement systems. Most of these fluctuations are the result of reflections in the pavement surface layer.

2. The following conclusions were found from model and field tests with direct and reflected body waves, compression and shear waves. (The direct waves propagated along the pavement surface, and the reflected waves were considered to occur as a result of reflections from the bottom of the top pavement layer.)
   a. The effect of direct and reflected body waves simulated by the simplified model appears only slightly in the field data. This result may occur because the amplitudes of body waves in the field are much smaller than those used in the model studies or the model may be too simple to simulate the effect of body waves. However, the study does show that the effect of body waves on the field dispersion curve is secondary to the effect of reflected surface waves.
   b. The least important body waves is the direct compression wave which has essentially no effect on the field dispersion curve in typical SASW testing.
   c. The most important contributor from all direct and reflected body waves is the reflected shear (SV) wave; that is, the shear wave reflected once or twice from the bottom of the pavement surface layer. This wave imposes additional fluctuations on the dispersion curve, especially at longer wavelengths.
3. When the effects of undesired waves (any wave arrivals other than direct surface waves arrivals) on the dispersion curve are removed, the dispersion curve is basically a smooth curve for short wavelengths. For a typical pavement site, this curve is nearly a horizontal line in the range of frequencies corresponding to sampling of the top layer of the system. The stiffness of the pavement surface layer can then be readily calculated from this curve. This approach is introduced herein as the "quick and easy" method iin Chapter Eight.
4. The dispersion curve measured by using a hammer as the impact source is insensitive to impact stress level and impact method. Therefore, a great deal of time does not have to be spent in the field in trying to select identical time records from one impact

blow to the next. As long as the frequency range of concern is generated by the impact, one should simply collect data as rapidly as possible.

5. Natural frequencies of accelerometers themselves do not affect the phase measurement in SASW testing. However, the resonant frequency of the coupled accelerometer/pavement system can alter the phase measurement in the test. It is essential to use a pair of matched accelerometers, and these accelerometers should be attached to the pavement surface by the same mechanism so that the coupled responses are similar for both receivers. Any adverse effects will then be minimized. However, erroneous phase shifts will still be measured near the resonant frequencies and care must be taken when interpreting this data. The auto power spectra are very helpful in this regard because peaks in the spectra can be used to identify resonances.
6. The influence of the "near-field" effect was evaluated in this study. The results suggest that this influence on dispersion curves is secondary to that of reflected surface waves. For the standard SAW test arrangement in which the source-to-receiver-1 and receiver-1-to-receiver-2 distances are equal, wavelengths as long as 2 times the source-to-receiver-1 distance seem to be safe to use.
7. High-frequency SASW measurements using the "V" meter are found to be very useful. By using the "V" meter as a source, a "quick and easy" method for accessing the material properties in the near-surface region of any solid material was developed. This method is extremely useful for measuring the stiffness of the top layer of asphalt or concrete pavements. Since this method is nondestructive, some special measurements such as the stiffness change of the material with respect to changes of time, temperature and other factors become very possible.
8. Field data on the concrete pavement at the BRC research facility show that the SASW method provides very consistent and repeatable measurements, a most desirable characteristic for any experimental procedure.

Finally a minicomputer is an ideal device for automating the SASW method. A MASSCOMP minicomputer was selected for this use and initial work was begun on installing the minicomputer in a field vehicle so that in the future data acquisition and reduction can be performed in the field. A field vehicle was also purchased and work commenced on making this system operational. The ultimate goal of this effort is to develop the stiffness profiles at the site in real time.

11.3. RECOMMENDATIONS FOR FUTURE RESEARCH

1. It was found that good receiver/pavement coupling is critical to the measurement of phases of cross power spectra. The current method of gluing holders on the tested surface is very effective but is too time consuming. It is necessary to develop a better method which can provide good receiver/ground coupling and easy deployment. Use of "bees wax" seems possible and should be studied.
2. The process of filtering out low-quality data needs more refinement. Use of the exponential window seems to allow one to partly reduce the problem of reflected waves, but it also introduces some other errors. It is necessary to develop a more sophisticated method for eliminating low-quality data and problems associated with reflected waves.
3. The "quick and easy" method to evaluate the stiffness of the pavement surface layer is still not fully developed. Problems sometimes arise in generating and collecting data in the very high frequency range (more than 80 kHz). This problem is usually more pronounced at asphalt sites, especially at elevated temperatures. More studies need to be conducted to further improve this valuable method.
4. Proper software to utilize fully the MASSCOMP minicomputer is needed and should be developed. With the MASSCOMP it is possible to fully automate the SASW method. Such automation would represent a significant advance in nondestructive testing of pavements.
5. Proper coupling of the receiver/pavement system is not fully understood, and a more rigorous theoretical analysis is needed to further understand this problem. The use of measuring devices which require no contact with the measured system, such as laser vibrometers, deserve more attention. At this time, the high cost seems to be the biggest hurdle.

REFERENCES

1. Ballard, R. F., Jr. (1964), "Determination of Soil Shear Moduli at Depth by In Situ Vibratory Techniques," Miscellaneous Paper No. 4-691, U.S. Army Engineer Waterways Experiment Station, Vicksburg, Mississippi.
2. Ballard, R. F., Jr. and Casagrande, D. R. (1967), "Dynamic Foundation Investigations, TAA-2A Radar Site, Cape Kennedy, Florida," Miscellaneous Paper No. 4-878, U.S. Army Engineer Waterways Experiment Station, Vicksburg, Mississippi.
3. Ballard, R. F., Jr. and Chang, F. K. (1973), "Rapid Subsurface Exploration; Review of Selected Geophysical Techniques," Miscellaneous Paper No. S-69-30, U.S. Army Engineer Waterways Experiment Station, Vicksburg, Mississippi.
4. Cunny, R. W. and Fry, Z.B. (1973), "Vibratory In Situ and Laboratory Soil Moduli Compared," Journal of the Soil Mechanics and Foundations Division, ASCE Vol. 99, SM12, pp 1055-1076.
5. Fry, Z. B. (1965), "Dynamic Soils Investigations Project Buggy, Buckboard Mesa Nevada Test Site, Mercury, Nevada," Miscellaneous Paper No. 4-666, U.S. Army Engineer Waterways Experiment Station, Vicksburg, Mississippi.
6. Haskell, N. A. (1953), "The Dispersion of Surface Waves in Multilayered Media," Bulletin of the Seismological Society of America, Vol 43, pp 17-34.
7. Heisey, J. S. (1982), "Determination of In Situ Shear Wave Velocity from Spectral-Analysis-of-Surface-Waves," Master's Thesis, The University of Texas, Department of Civil Engineering, Austin, Texas, 300 pp.
8. Heisey, S., Stokoe, K. H., II, Hudson, W.R., and Meyer, A.H., "Determination of In Situ Shear Wave Velocities from Spectral Analysis of Surface Waves," Research Report 256-2, Center for Transportation Research, The University of Texas at Austin, 292 pp.
9. Heukelom, W. and Klomp, J. G. (1962), "Dynamic Testing as a Means of Controlling Pavements During and After Construction," Proceedings, International Conference on Structural Design of Asphalt Pavements," Ann Arbor, Michigan, pp 495-510.
10. IMSL Library, FORTRAN Subroutines for Mathematics and Statistics User Manual, Chapter E, Subroutine ICSSCU.
11. Jones, R., (1962), "Surface Wave Technique for Measuring the Elastic Properties and Thickness of Roads: Theoretical Development," British Journal of Applied Physics, Vol 13, pp 21-29.

12. Krohn, C. E., (1984), "Geophone Ground Coupling", Geophysics, Vol 49, No. 6, June, pp 722-731.
13. Krohn, C. E., (1985), "Geophone Ground Coupling", Geophysics, Vol 50, No. 4, April, pp 56-60.
14. Maxwell, A. A. and Fry, F. B. (1967), "A Procedure for Determining Elastic Moduli of In Situ Soils by Dynamic Techniques," Proceedings, International Symposium on Wave Propagation and Dynamic Properties of Earth Materials, Albuquerque, New Mexico, pp 913-920.
15. Nazarian, S. and Stokoe, K. H., II, (1983), "Use of Spectral-Analysis-of-Surface-Waves Method for Determination of Moduli and Thicknesses of Pavement Systems," Transportation Research Record, No. 930, Washington, D.C.
16. Nazarian, S. (1984), "In Situ Determination of Elastic Moduli of Soil Deposits and Pavement Systems by Spectral-Analysis-of-Surface-Waves Method," Ph.D. Dissertation, The University of Texas, Department of Civil Engineering, Austin, Texas, 446 pp.
17. Nazarian, S. and Stokoe, K. H., II, (1985), "In Situ Determination of Elastic Moduli of Pavement Systems by Spectral-Analysis-of-Surface-Waves Method (Practical Aspects)," Research Report 368-1F, Center for Transportation Research, The University of Texas, Austin, Texas, 161 pp.
18. Nazarian, S. and Stokoe, K. H., II, (1986), "In Situ Determination of Elastic Moduli of Pavement Systems by Spectral-Analysis-of-Surface-Waves Method (Theoretical Aspects)," Research Report 437-2, Center for Transportation Research, The University of Texas, Austin, Texas, 114 pp.
19. Rayleigh, L. (1887), "On Waves Propagated Along the Plane Surface of an Elastic Solid," Proceedings, London Mathematical Society, Vol. 17, pp 4-11.
20. Richart, F. E., Jr., Hall, J. R. Jr., and Woods, R. D. (1970), Vibrations of Soils and Foundations, Prentice-Hall, Inc., New Jersey.
21. Robinson, E. A. and Treitel, S. (1980), Geophysical Signal Analysis, Prentice-Hall, Inc., New Jersey.
22. Sanchez-Salinero, I. (1987), "Analytical Investigation of Seismic Method Used for Engineering Application," Ph.D. Dissertation, The University of Texas, Department of Civil Engineering, Austin, Texas.

23. Sanchez-Salinero, I., Roesset, J. M., and Stokoe, K. H., II (1987), "Analytical Investigation of the Spectral-Analysis-of-Surface-Waves Method," Research Report 1123-2, Center for Transportation Research, The Unversity of Texas at Austin, (in press).
24. Thomson, W. T. (1950), "Transmission of Elastic Waves Through a Stratified Solid," Journal of Applied Physics, Vol 21, pp. 89-93.
25. Thornhill, J. and Smith, C.C. (1980), Fourier and Spectral Analysis, A Short Course, Craig C. Smith and R. Joe Thornhill, p 138.
26. White, R., Hudson, W. R., Meyer, A. H., and Stokoe, K. H. II, (1984), "Design and Construction of a Rigid Pavement Research Facility," Research Report 355-1, Center for Transportation Research, The University of Texas, Austin, Texas, 122 pp.

APPENDICES

APPENDIX A

FIELD DISPERSION CURVES FOR SURFACE WAVES REFLECTED FROM A VERTICAL BOUNDARY ORIENTED PERPENDICULARLY TO TEST ARRAY

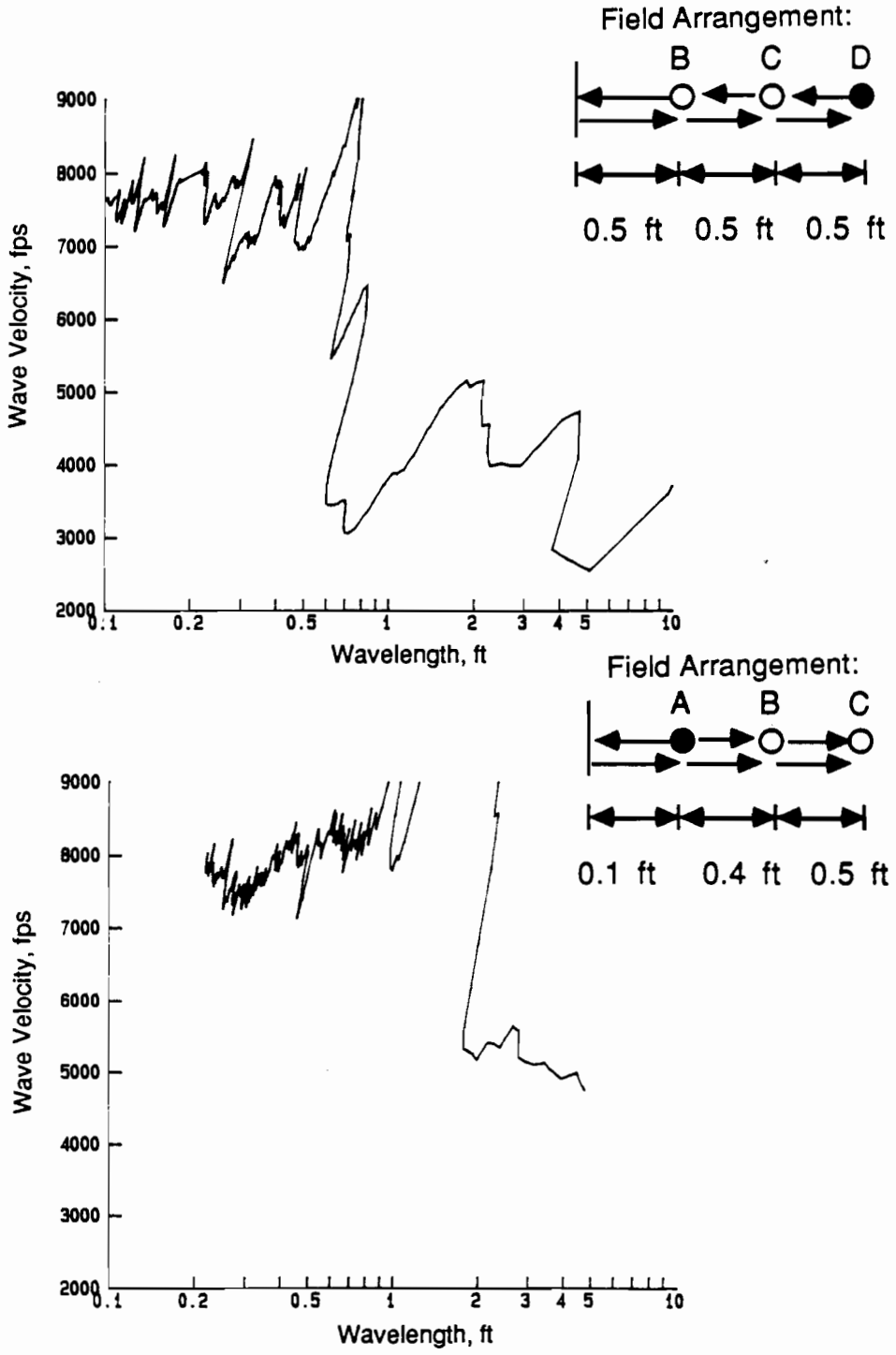

Fig. A-1. Comparison of the Effect on Dispersion Curves of Source Location with Respect to Locations of Receivers and Reflecting Boundary: Receivers at Locations B and C.

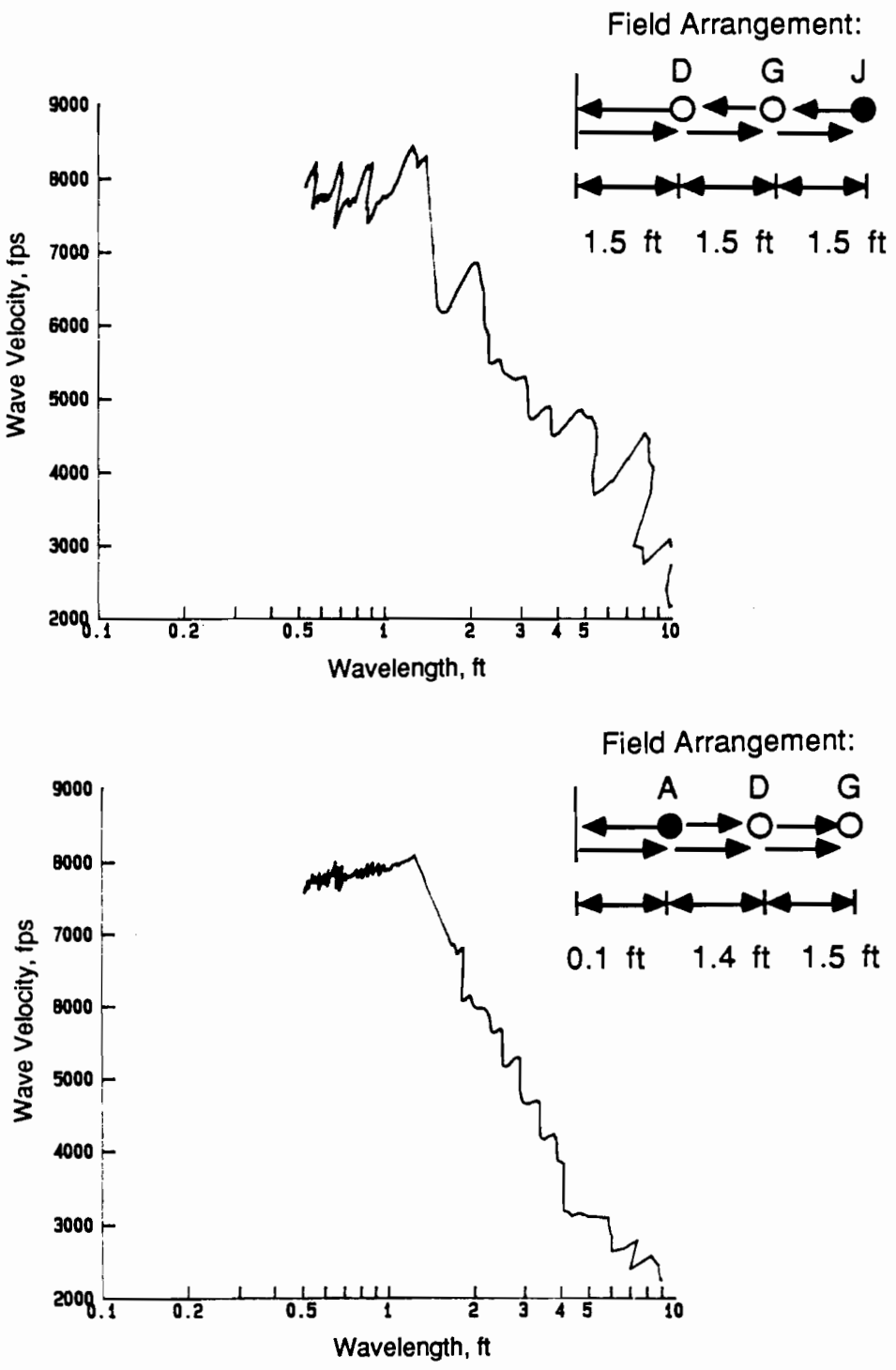

Fig. A-2. Comparison of the Effect on Dispersion Curves of Source Location with Respect to Locations of Receivers and Reflecting Boundary: Receivers at Locations D and G.

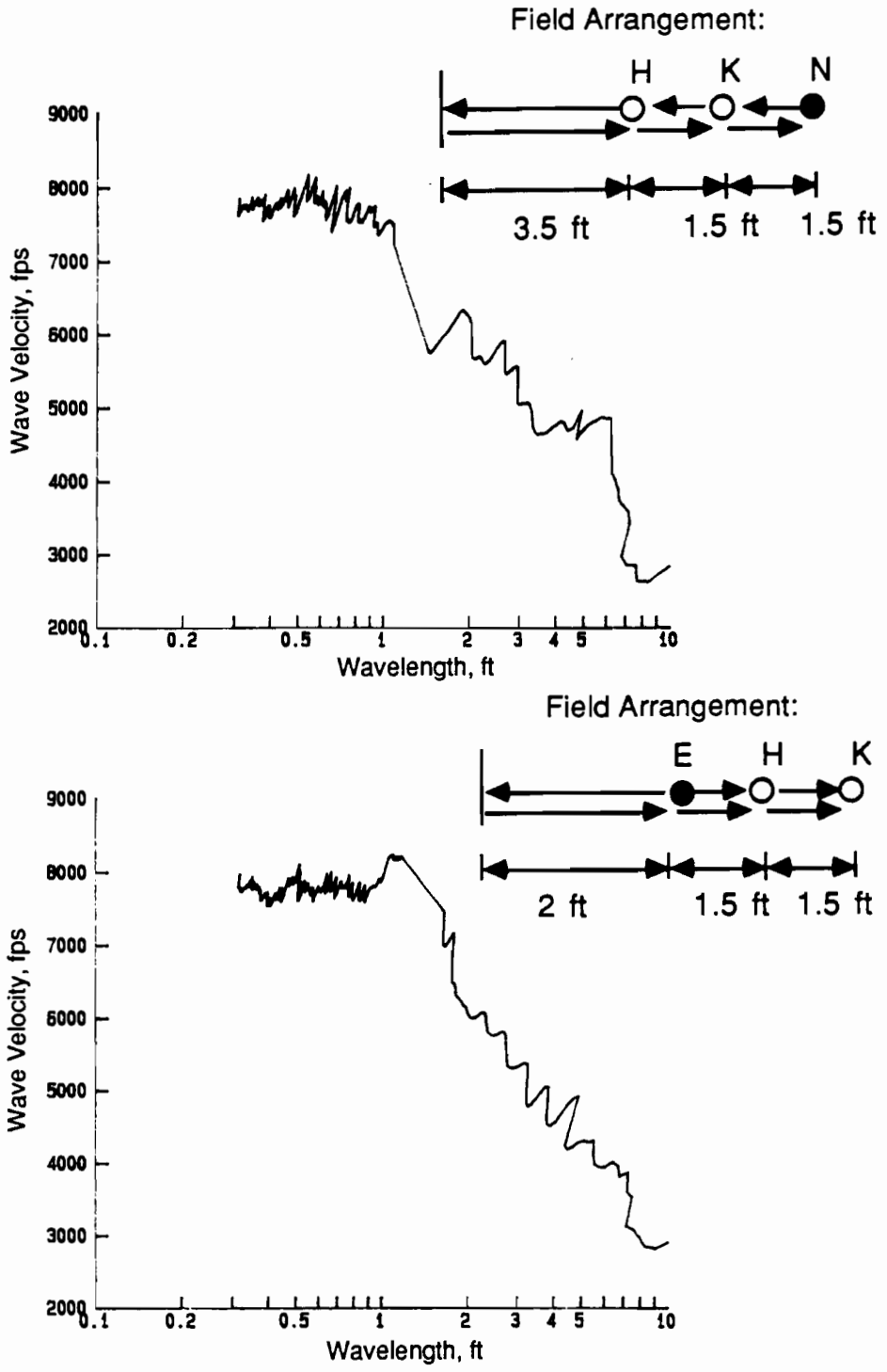

Fig. A-3. Comparison of the Effect on Dispersion Curves of Source Location with Respect to Locations of Receivers and Reflecting Boundary: Receivers at Locations H and K.

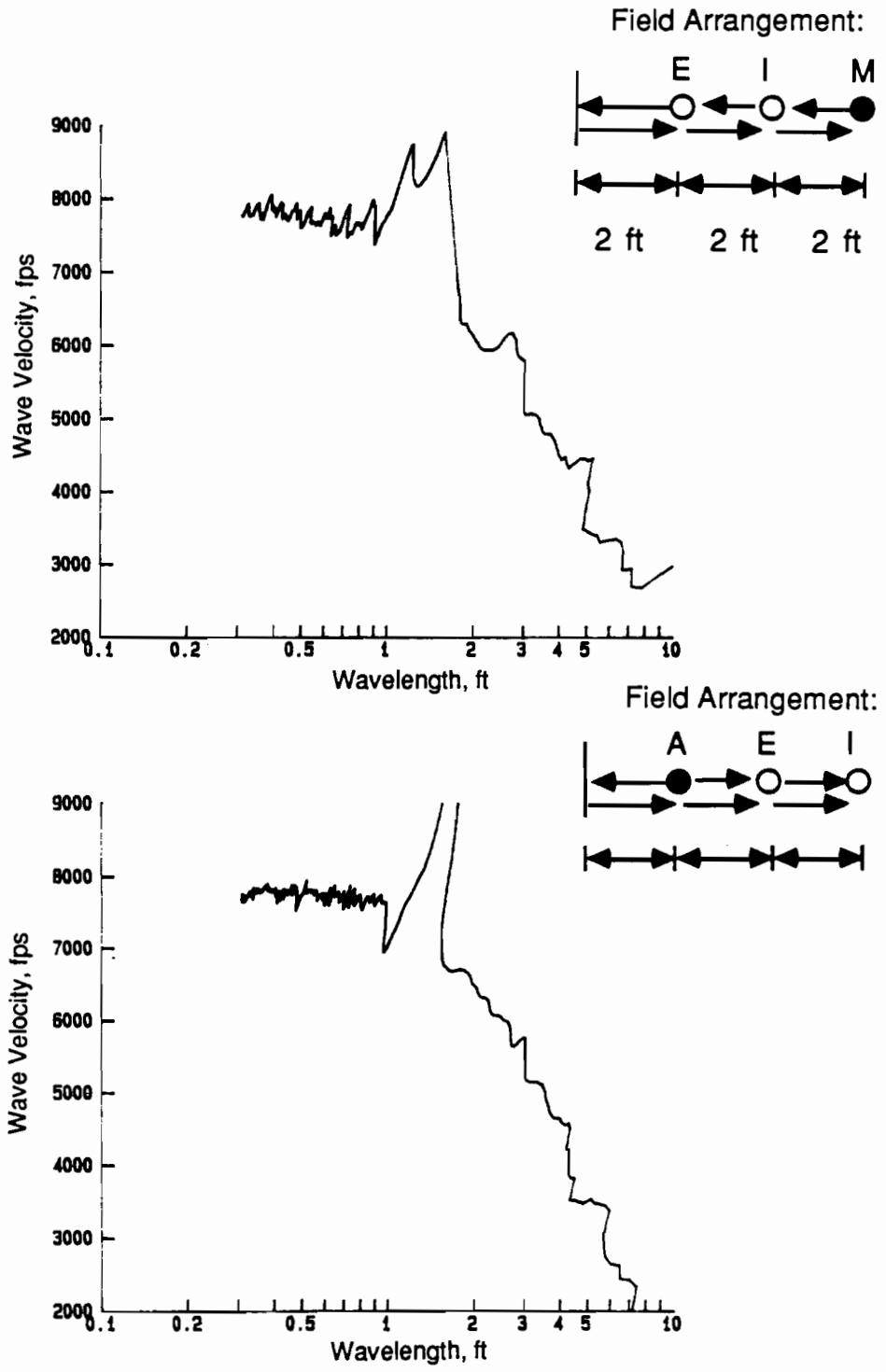

Fig. A-4. Comparison of the Effect on Dispersion Curves of Source Location with Respect to Locations of Receivers and Reflecting Boundary: Receivers at Locations E and I.

APPENDIX B

FIELD AND MODELED DISPERSION CURVES FOR SURFACE WAVES REFLECTED FROM A VERTICAL, PARALLEL BOUNDARY FOR A CONSTANT SOURCE/RECEIVER SPACING OF 2 FT

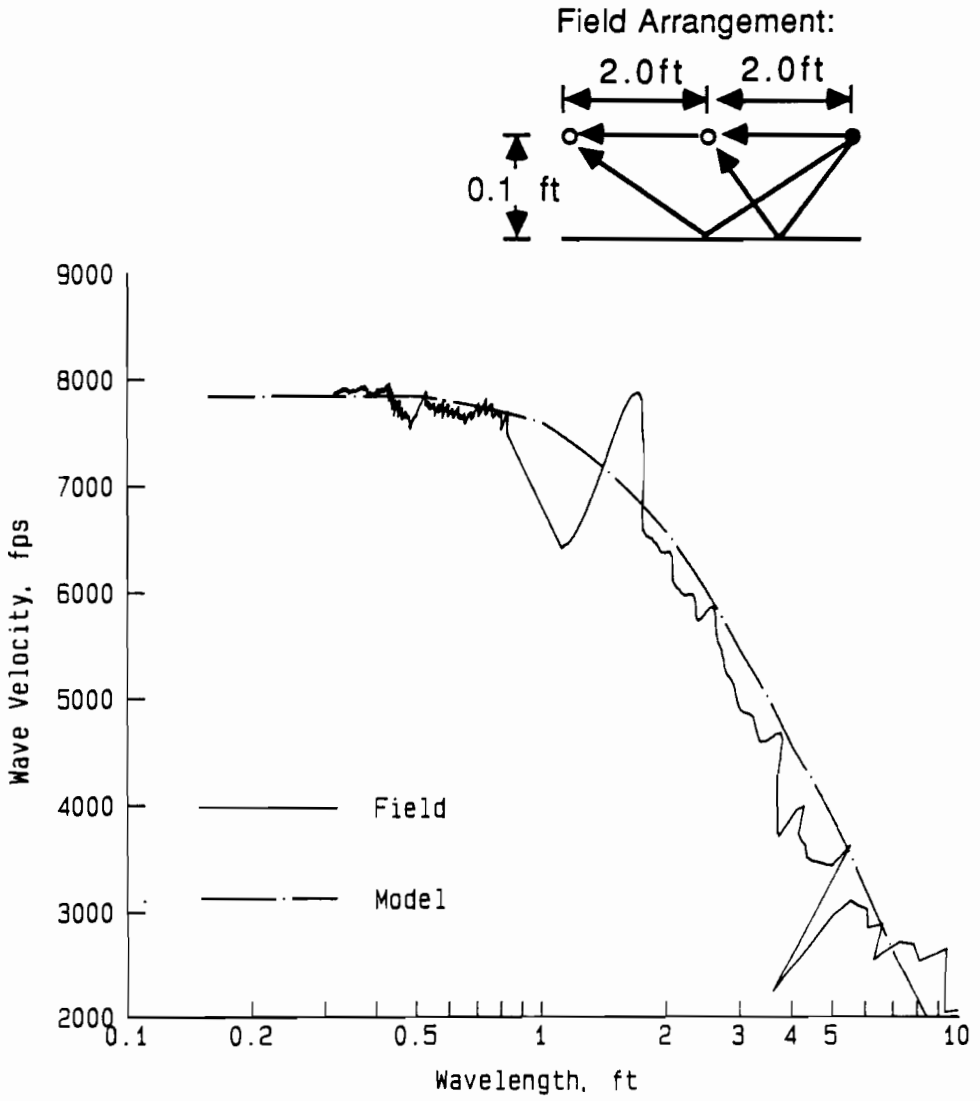

Fig. B-1. Comparison of Field and Modeled Dispersion Curves for Surface Waves Reflected from a Vertical Boundary: Test Array 1 Oriented Parallel to Reflecting Boundary.

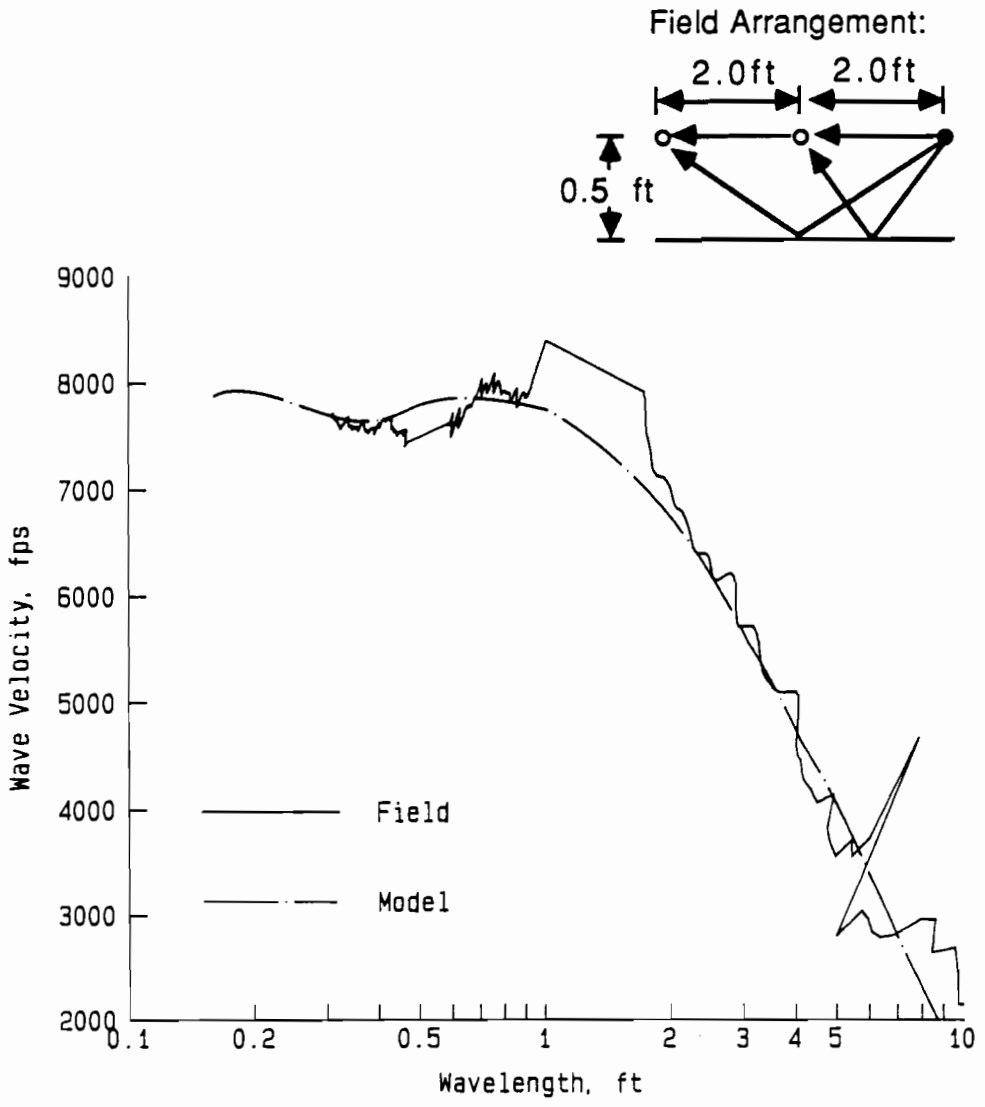

Fig. B-2. Comparison of Field and Modeled Dispersion Curves for Surface Waves Reflected from a Vertical Boundary: Test Array 2 Oriented Parallel to Reflecting Boundary.

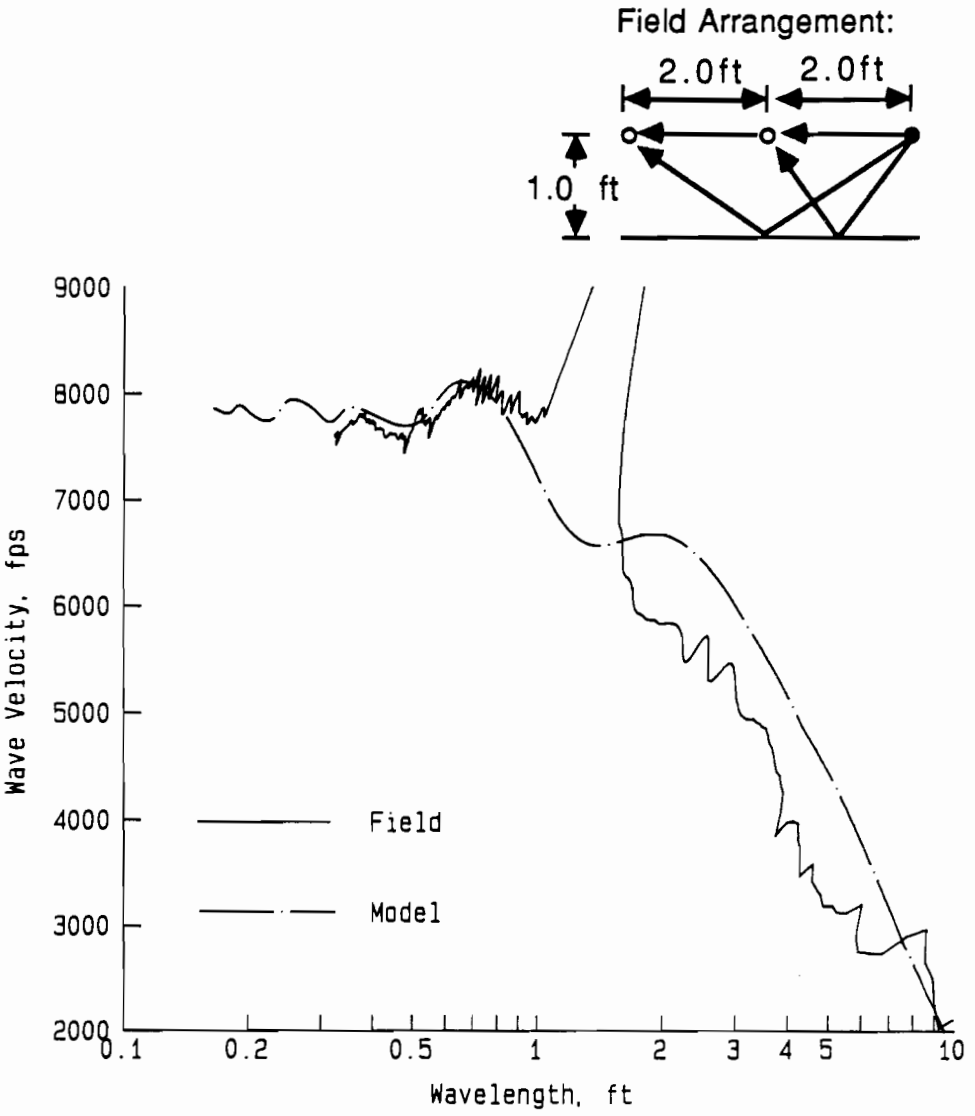

Fig. B-3. Comparison of Field and Modeled Dispersion Curves for Surface Waves Reflected from a Vertical Boundary: Test Array 3 Oriented Parallel to Reflecting Boundary.

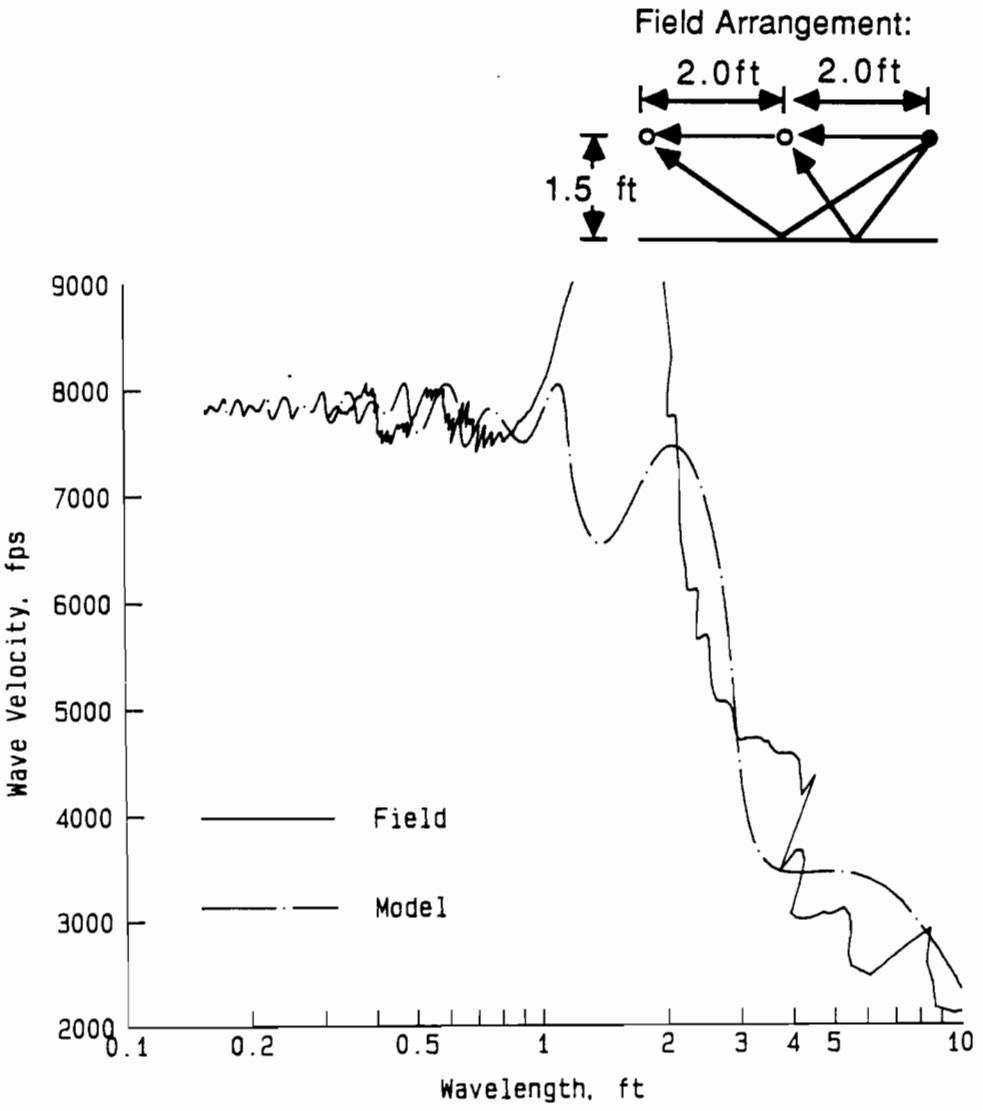

Fig. B-4. Comparison of Field and Modeled Dispersion Curves for Surface Waves Reflected from a Vertical Boundary: Test Array 4 Oriented Parallel to Reflecting Boundary.

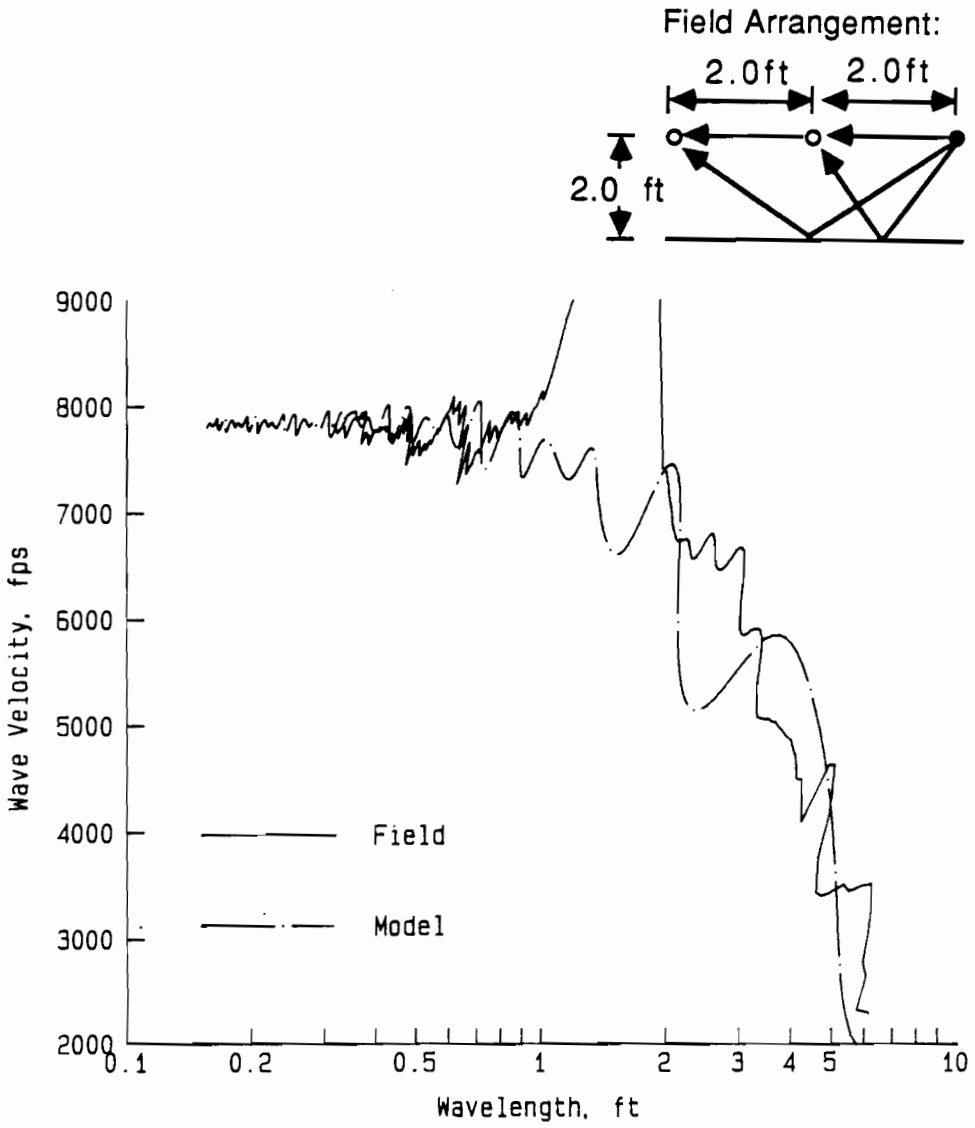

Fig. B-5. Comparison of Field and Modeled Dispersion Curves for Surface Waves Reflected from a Vertical Boundary: Test Array 5 Oriented Parallel to Reflecting Boundary.

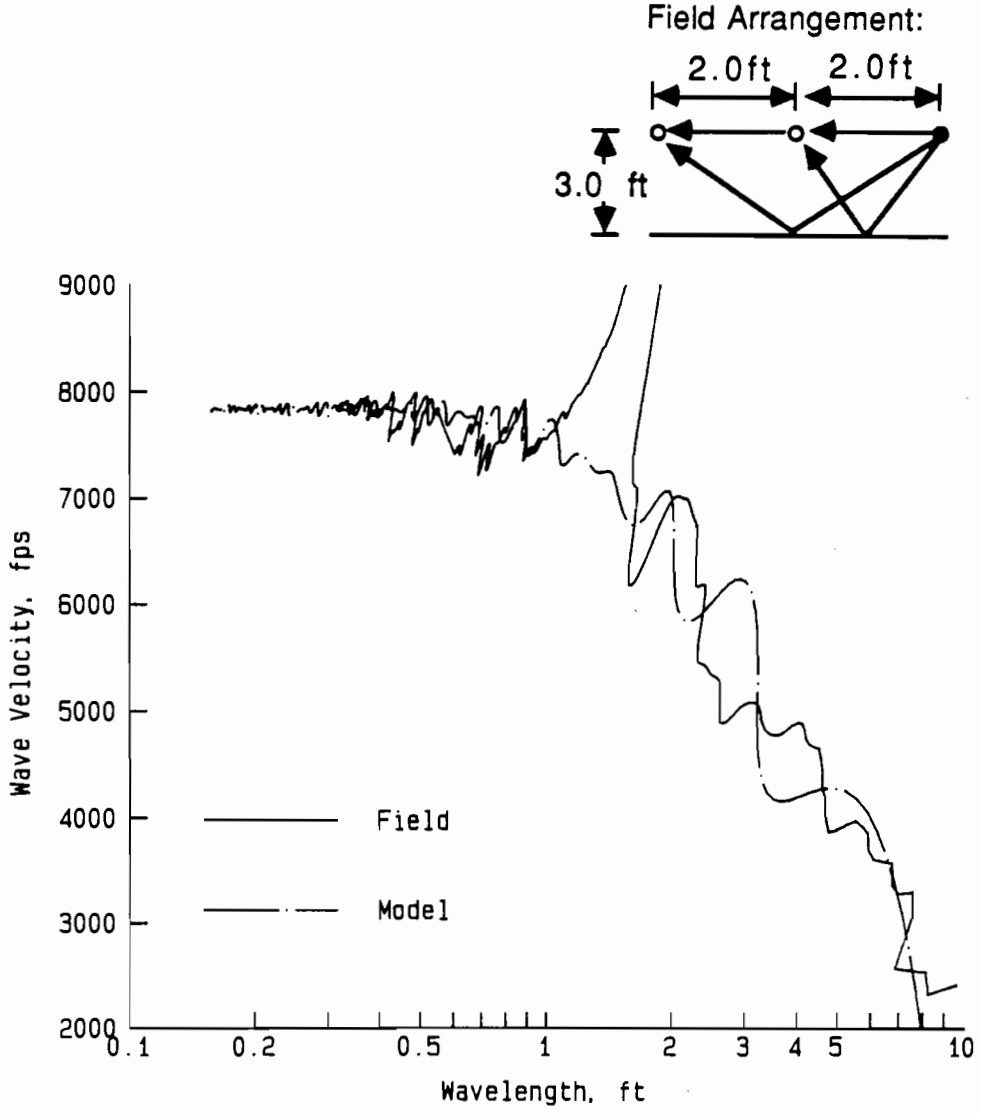

Fig. B-6. Comparison of Field and Modeled Dispersion Curves for Surface Waves Reflected from a Vertical Boundary: Test Array 6 Oriented Parallel to Reflecting Boundary.

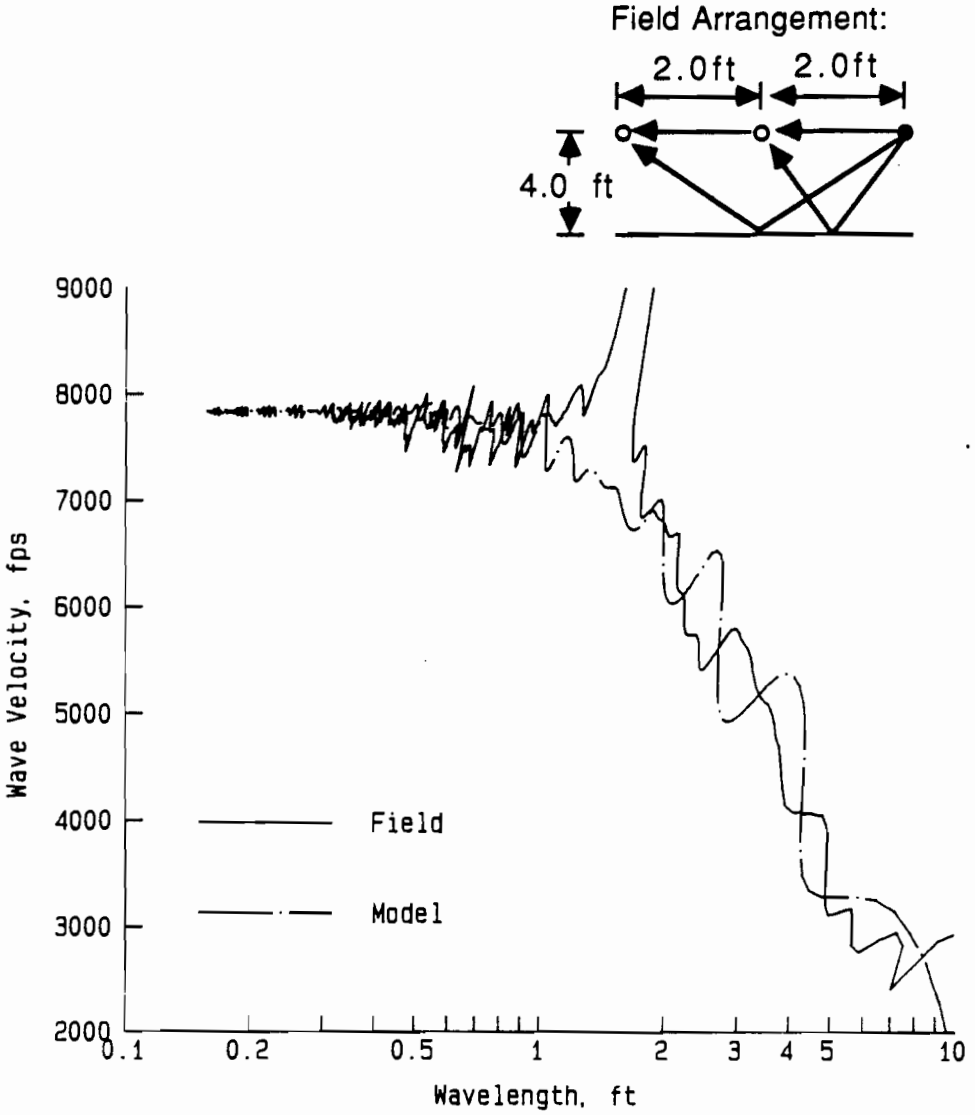

Fig. B-7. Comparison of Field and Modeled Dispersion Curves for Surface Waves Reflected from a Vertical Boundary: Test Array 7 Oriented Parallel to Reflecting Boundary.